Study of Drugs and Biologically Active Fluorophores in Different Biomimetic Systems

A THESIS

Submitted in partial fulfillment of the requirements for the award of the degree

of

DOCTOR OF PHILOSOPHY

by

Raina Thakur

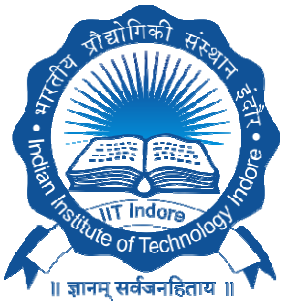

DISCIPLINE OF CHEMISTRY

INDIAN INSTITUTE OF TECHNOLOGY INDORE

May 2014

INDIAN INSTITUTE OF TECHNOLOGY INDORE

CANDIDATE'S DECLARATION

I hereby certify that the work which is being presented in the thesis entitled **"Study of Drugs and Biologically Active Fluorophores in Different Biomimetic Systems"** in the partial fulfillment of the requirements for the award of the degree of **DOCTOR OF PHILOSOPHY** and submitted in the **DISCIPLINE OF CHEMISTRY, Indian Institute of Technology Indore**, is an authentic record of my own work carried out during the time period from August 2010 to May 2014 submission under the supervision of Dr. Anjan Chakraborty, Assistant Professor, Indian Institute of Technology Indore.

The matter presented in this thesis has not been submitted by me for the award of any other degree of this or any other institute.

(Raina Thakur)

This is to certify that the above statement made by the candidate is correct to the best of my/our knowledge.

(Dr. Anjan Chakraborty)

Raina Thakur has successfully given her Ph.D. Oral Examination held on **……..**

Signature of Thesis Supervisor
Date:

Convener, DPGC
Date:

Signature of PSPC Member
Date:

Signature of PSPC Member
Date:

Signature of External Examiner
Date:

ACKNOWLEDGEMENTS

"Acknowledgements are never written by ink, they are always written by heart"

First and foremost, I would like to express my profound gratitude and deep regards for my mentor Dr. Anjan Chakraborty for his exemplary guidance, monitoring and constant encouragement throughout this journey & making my Ph.D. experience productive & stimulating. It has been an honor to be his first Ph.D. student. His joy & enthusiasm for research always kept me motivated during tough times in Ph.D. pursuit. I also take this opportunity to express a deep sense of gratitude towards our Director, Prof Pradeep Mathur for constantly motivating us for research and providing various facilities, which helped us to remain, focused.

I would also like to acknowledge all our collaborators, mainly Dr. Arbinda Mallik and Dr. Kalyan Sundar Gosh for their significant contributions.

I am very grateful towards my PSPC committee members Dr. Tushar Kanti Mukherjee and Dr. Sarika Jalan for their valuable suggestions. I am obliged to SIC (sophisticated Instrument Center), all the faculty members and staff members of discipline of chemistry for their constant help and support. Especially, Mr. Kinney Pandey, for helping in obtaining various results.

I am grateful to Mr. Anupam Das for his moral support, brother hood and constant help in all my tedious experiments. I would also like to thank Mr. Chandan Adhikari for extending his co-operation during my research.I would also like to thank all my friends, especially Tamalika for her encouragement, care and continuous support, Rajendar , Bhagwati, Bhaushaheb, Dnyanesh, Indrajeet, Anuradha, Prabhat, Manideepa, Anvita, Sonam, Veenu, Shivendra, Debashish, Thaksen, Ramesh, Rekha, Maruti, Surajeet, Roopali, Mriganka, Arpan, Rohit, Deepika, Ambikesh, Somen, Manoj, Sagar, Sagnik, Kavita, Indrani, my roommates Aradhna, Ankita and Smriti for their constant support and motivation.

Finally, I would like to dedicate it to my parents, parent-in-laws, husband, brother, Eesha bhabhi, Sister-in-laws & will always remain indebted for their constant encouragement, love and prayers, without which it would not have been possible to achieve & celebrate this.

There are many more people who have contributed in their own ways, I hope I could thank all of them, but time, space and conscience compel me to stop here.

Raina Thakur,
IIT Indore

Dedicated

to

My Family

ABSTRACT

1.1 Introduction:

In the past decades, there is burgeoning interest in understanding the properties of systems that arise out of the interactions of biomolecules. Thus the importance of organized assemblies which act as biomimetic systems in biological and photophysical/photochemical processes, have been considerably recognized. Reactants confined in molecular assemblies such as micelles, reverse micelles, microemulsion and vesicles etc. offer a greater degree of organization compared to their geometries in homogeneous solution. They can mimic reactions in biosystems and also have great potential to act as a host system for several organic molecules which includes important drug molecules. Since the local properties e.g. polarity, viscosity, and pH in such a nanoenvironment are vastly different from those in a bulk medium, the structure, dynamics, and reactivity of biomolecules at an interface differ markedly from those observed in the bulk. Interestingly, most natural and biological processes occur at such interfaces or in confined systems, e.g., proteins, biomembranes, and vesicles. Therefore, chemistry, in organized assemblies, mimics the extremely efficient chemical processes occurring in the natural systems. The wide range of functions performed by biological membranes and membrane proteins have motivated the researchers to look for simple model systems that can mimic, at least in part, the physicochemical properties of the membrane architecture. Because of the widespread interest, the study of different kinds of organized assemblies has grown enormously over the last decade and it has become virtually impossible to summarize all the new results in a single article.

Studies on the supramolecular interactions of drugs with various biological targets, are of immense importance for the perception of structural and functional features of biomacromolecules, so as to simulate the biophysical processes. This leads to a widespread interest in studying the spectroscopic and photophysical properties of

fluorescent molecules in different organized media for a better understanding of the solubilization site and interaction in true biological systems. Therefore, we have undertaken entrapment of various fluorophores in different biomimetic systems and studied the photodynamical and photophysical behavior of those complexes. The various biomimetic systems studied in this thesis are bile salt aggregates, reverse micelles, liposome-bile salt aggregates, proteins and liposomes-proteins complex. We used two fluoroquinolone drug molecules namely Norfloxacin and Ofloxacin and an anticancer drug molecule namely Ellipticine and exploited their photophysical properties to understand their interaction with biological systems.

1.2 Objectives:

The objective of this thesis is to explore the interaction of drug molecules with different biomimetic systems, which would help in development of various drug delivery systems (DDS), for those drugs that are insoluble or poorly soluble in water. The present study would also help to increase the bioavailability of such poorly soluble drugs. For this purpose, we have selected two widely used Fluoroquinolone (Norfloxacin and Ofloxacin) and an anti cancer agent Ellipticine along with a membrane probe PRODAN and explored their entrapment, bio-distribution, dynamics and photophysical properties with the help of steady state and time resolved fluorescence spectroscopy. Interestingly, fluoroquinolone molecules are well soluble in water while Ellipticine is sparingly soluble. All these drug molecules are reported to exist in different prototropic species in aqueous solution. Entrapment of these drugs into various biomimetic systems would help us to achieve the given objective. For the formulation of the facts to achieve the above goal following aims are clarified in this thesis:

1. How different prototropic species of Fluoroquinolone and Ellipticine bind with amphiphilic biosurfactants such as bile salts? How do conjugated and non-conjugated bile salts differ in interaction with Fluoroquinolone and Ellipticine? Do the bile salts act as multisite drug carrier because of their ability to hold the

cationic and neutral species of Ellipticine in hydrophilic and hydrophobic surface?

2. What would be the photophyscial behavior of Ellipticine inside aqueous and methanolic reverse micelles?
3. Since Ellipticine is poorly soluble in aqueous medium, so; we would like to see if a reasonable amount of Ellipticine could be encapsulated in different liposomes for a successful drug delivery. Then we would address if it is possible to release the encapsulated drug molecules by adding external bio-surfactant such as bile salts. We would also address whether the release of drug molecules depend on the nature of bile salts.
4. So far in the literature there is no study on binding of Ellipticine with protein albumin and globulin. Since Ellipticine exists in two prototropic species (neutral and cationic) we would like to know what would be the binding strategy of different prototropic species of Ellipticine towards those serum proteins. Do the experimental binding results corroborate with the theoretical study? We undertook the docking studies to answer this question.
5. As Ellipticine is entrapped in liposomes and binds with proteins, so; it can be used to unravel the liposome-protein interaction using Ellipticine as a probe molecule. Thus human serum albumin (HSA) and Ellipticine encapsulated liposomes of different phase transition temperatures were used to see the nature of interactions. Therefore, the obvious question to be addressed is that what kind of interaction takes place between liposomes and proteins? Whether it is electrostatic and hydrophobic in nature or both? What would be the fate of Ellipticine when HSA interacts with liposomes? Is it possible to transport this kind of drug molecules through HSA after removing from the liposomes?
6. How can we probe the interaction of serum albumin with conjugated and unconjugated liposomes differing widely in their phase transition temperatures using a membrane probe?

Summary of the Work Done

(a) Photophysical and Photodynamical Study of Fluoroquinolones and Drug Molecules in Bile Salt Aggregates:

Photophysical properties of two widely used antibiotic fluoroquinolone drugs, namely Norfloxcacin (NOR) and Ofloxacin (OFL) have been investigated in biomimicking environments formed by bile salts. We have chosen three bile salts namely Sodium deoxycholate (NaDC), Sodium taurocholate (NaTC) and Sodium glycodeoxycholate (NaGDC), to study the photophysics of Norfloxacin and Ofloxacin. Our experimental results demonstrate that, photophysical enhancement and fall of a particular prototropic species are sensitive to the excitation wavelength in bile salt aggregates. Excitation at shorter wavelengths (305 nm and 325 nm) reveals quenching of fluorescence of these fluroquinolones with addition of NaDC, NaTC and NaGDC. On the contrary, we observe a steady increase in the fluorescence intensity with a continuous red shift upon excitation at longer wavelengths (350 and 375 nm). We found that, with addition of bile salt at physiological pH (~ 7.40) the neutral and zwitterionic fluoroquinolone turns into cationic species. The cationic species which is formed from neutral or zwitterionic species in presence of bile salt, is selectively excited at longer wavelength and is entrapped by the hydrophilic face of bile salt. Consequently, the emission intensity increases upon excitation at longer wavelength. We found that, NaGDC and NaTC are more effective in converting neutral species into cationic species than NaDC, because NaGDC and NaTC possess conjugated head groups. On the other hand zwitterionic/neutral species which decrease with addition of bile salt, are excited at shorter wavelength and thus leads to quenching. The induced non-polarity upon addition of bile salt is also responsible for the observed quenching. And this is evident from the fact that quenching order is in accordance with hydrophobicity indices of bile salts.

(b) Dynamics of Prototropic Species of an Anticancer Drug Ellipticine in Bile Salt Aggregates of Different Head Groups and Hydrophobic Skeleton: A Photophysical Study to Probe Bile Salt as Multisite Drug Carrier:

We investigated the entrapment of neutral and cationic species of an anticancer drug namely Ellipticine and its dynamic features in different bile salt aggregates for the first time using steady state and time-resolved fluorescence spectroscopy. Because Ellipticine exists in two different prototropic forms in physiological condition, we performed a comparative photophysical and dynamical studies of these prototropic species in different bile salts varying their head groups and hydrophobic skeletons.

Ellipticine shows two bands around 440 nm and 540 nm at physiological condition (pH~ 7.40). We assigned the bands at 440 and 540 nm wavelengths to neutral and cationic species respectively. Addition of bile salts to aqueous solution of Ellipticine enhances the intensity at 540 nm as well as at 440 nm. The rise in intensity at 540 nm indicates the binding of cationic species with bile salts head groups. On the other hand increase in intensity at 440 nm indicates that the neutral species are entrapped in the hydrophobic pocket of bile salt. We found that the initial interaction between Ellipticine and bile salt is governed by the electrostatic forces where cationic Ellipticine is anchored to the head groups of bile salts. This is evident from the plot of $\phi_{cationic}/\phi_{neutral}$ as a function of concentration of different bile salts. It is revealed that $\phi_{cationic}/\phi_{neutral}$ initially increases, reaches a maximum and then decreases for all the bile salts except NaTC. The rise in $\phi_{cationic}/\phi_{neutral}$ signifies that a strong interaction between Ellipticine and bile salt is dominated by electrostatic forces where the cationic Ellipticine species are anchored to the negatively charged head groups of bile salts. Bile salts of conjugated head groups were found to be better candidates to capture the cationic species as compared to the bile salts having non-conjugated head groups. The hydrophobic interaction

dominates at higher concentration of bile salt due to formation of aggregates which results in entrapment of neutral Ellipticine in the hydrophobic cavity of aggregates. The neutral species of the drug molecules were found to be partitioned according to the hydrophobicity indices of bile salts. Cationic Ellipticine exhibits a faster rotational relaxation in the tri-hydroxy bile salt aggregates than in di-hydroxy bile salts. We interpreted this observation by the fact that tri-hydroxy bile salt hold more number of water molecules in their hydrophilic surface offering a less viscous environment for Ellipticine compared to di-hydroxy bile salts.

(c) Fate of anticancer drug Ellipticine in reverse micelles in aqueous and methanolic environment: a photophysical approach:

The present investigation explored a detailed photophysics of Ellipticine in AOT reverse micelle using steady state and time resolved spectroscopy. Steady state absorption and emission spectra indicates that Ellipticines are entrapped as a cationic species in AOT/hexane system. We found that two contradictory phenomena take place upon addition of water and methanol to AOT/hydrocarbon system. Increase in water content in reverse micelles, entraps more number of cationic species while increase in methanol content causes switch over of cationic Ellipticine to a neutral species. The absorbance was found to increase further with at 352 and 425 nm bands with increase in water content. The increment in the absorbance at 425 nm confirms that neutral Ellipticine molecules are converted into the cationic species because this band has a close resemblance with the excitation spectra in acidic condition (pH~2). On the other hand, we found a decrement in absorbance at 425 nm when methanol is added to AOT/hydrocarbon system and thus cationic species are converted into neutral. The conversion of neutral species into the cationic species with increment in water content and reverse phenomenon with increment of methanol content are also confirmed by emission spectra. In hexane, the emission maximum appears at 385 nm. With addition of 0.1 M AOT to this solution the emission band shifts to 500 nm. With

increase in the water content, the emission spectra are found to be red shifted followed by a decrease in the quantum yield. On the other hand, the emission intensity at 500 nm decreases and increases at 425 nm with increase in methanol content. The observation suggests that cationic species are converted into the neutral species with increase methanol in content. Interestingly, even at highest methanol content, any solvent assisted proton transfer was not observed. This fact is attributed to the lack of bulk methanol in an AOT/hydrocarbon/ methanol system. Moreover, methanol mostly binds to AOT head group region. Therefore, these methanol molecules are unable to donate a proton to Ellipticine as well as do not facilitate solvent assisted proton transfer. This fact is responsible for the observed decrease in fluorescence at longer wavelength in AOT/hydrocarbon/ methanol system.

(d) Photophysical and photodynamical study of Ellipticine: an anticancer drug molecule in bile salt modulated in vitro created liposome:

We studied entrapment of anticancer drug Ellipticine in *1,2-dipalmitoyl-sn-glycero-3-phosphocholine* (DPPC) liposome and its release by addition of three different bile salts namely Sodium deoxycholate, cholate and taurocholate. It was revealed from this study that Ellipticine is entrapped in the liposome in a substantial amount. The partition coefficient (K_p) of Ellipticine in lipid phase calculated from steady state and time resolved measurement was found to be 4×10^4 and this implies that more 90% drug molecules are captured in liposomes. Addition of bile salt causes a quenching at 435 nm while there is an increase at 540 nm implying that drug molecules are released from liposomes. We found that the degree of release of the drug from liposome depends on the degree of penetration of bile salts. Among the three bile salts, deoxycholate was most effective in releasing the drug from hydrocarbon core of liposome because of its highest insertion ability owing to its maximum hydrophobicity. The possible reasons for the decrease in intensity could be due to the

removal of drug molecules from liposomes as well as the change in the fluidity of liposome due to the insertion of bile salt. Bile salts hydrate the hydrocarbon core of liposome by carrying hydrogen bonded water and cause expulsion of drug molecules. Since penetration of deoxycholate is higher as compared to other bile salt, so; this causes maximum quenching. The time resolved studies revealed that after expulsion from the liposome, Ellipticine molecules were entrapped in interfacial region of liposomes by electrostatic interaction. This led to an increase in the shorter lifetime component. On the other hand the longer lifetime component decreased due to wetness of the liposome as well as increase in fluidity.

(e) Interaction of anticancer agent Ellipticine with major transport proteins in their native and denatured states:

Study of interaction of Ellipticine with various transport protein is essential to gain insight upon solubility and transport of Ellipticine in physiological conditions. Interactions of Ellipticine with two prominent serum proteins i.e. Human Serum Albumin (HSA) and Immunoglobulin G (IgG) in their native and denatured states have been studied by molecular docking, circular dichroism (CD), steady state and time resolved fluorescence spectroscopy. From ANS and Warfarin displacement experiments it was confirmed that Ellipticine binds with sudlow site II of HSA. The binding constant was found to be around 2.5×10^5 M^{-1}. We observed a weak energy transfer between tryptophan 214 and Ellipticine leading to apparent distance of 31 Å between Trp214 and Ellipticine. This experimental finding corroborates well with the docking study which also substantiate the fact that Ellipticine binds with Sudlow site II of HSA. In the time resolved study, the average life time of neutral species of Ellipticine increases and very long component is generated which also confirm that neutral species are entrapped in the hydrophobic pocket of HSA.

Unlike HSA, IgG does not bind with the neutral species in its native state while it binds appreciably with cationic Ellipticine. The fact implies that the hydrophobic pocket of IgG is inaccessible in its native

state. However, in the denatured state of IgG, we observe a significant increase in binding of neutral species. This fact indicates that the hydrophobic pockets of IgG are exposed upon heat and acid denaturation. Molecular docking experiment proves that Ellipticine binds with F_{ab} and F_c sites to different extent. The lifetime measurements reveal that there are two components with shorter and longer lifetime. The species with increasing longer lifetime has been assigned as IgG bound species whose population increases with increase in IgG concentration. From CD measurements it is evident that Ellipticine interact with both the proteins in their native and denatured states. Upon interaction with HSA in denatured state Ellipticine help in resuming α-helical content. Similarly in IgG after addition of Ellipticine to denatured protein reduction in percentage of random coils was observed. So; we can infer that Ellipticine help in stabilization of both the proteins. Thus binding of Ellipticine with two major proteins may help in increasing the bioavailability of this sparingly water soluble drug.

(f) The fate of anticancer drug, Ellipticine in DPPC and DMPC liposomes upon interaction with HSA: A photophysical approach:

Interaction of human serum albumin (HSA) with two liposomes namely and 1,2-dipalmitoyl-*sn*-glycero-3-phosphocholine (DPPC) and 1,2-dimyristoyl-*sn*-glycero-3-phosphocholine (DMPC) has been probed by anticancer drug Ellipticine using steady state and time resolved fluorescence spectroscopy. The entrapment of drug molecules in liposomes was confirmed by estimating partition coefficients. The values of partition coefficient are 1.1×10^4 and 2.1×10^4 for DPPC and DMPC respectively. The higher value of partition coefficient in DMPC is due to its lower phase transition temperature. It was observed that HSA penetrates into the liposomes through hydrophobic interaction which reduces the packing order of the lipid bilayer and leads to a quenching in fluorescence intensity of Ellipticine. Since DPPC is more hydrophobic than DMPC due to longer aliphatic chain in DPPC, so; HSA penetrates more into DPPC which results in higher quenching in

DPPC ($k_q = 3.580 \times 10^{11}$ $M^{-1}S^{-1}$) compared to that in DMPC ($k_q = 1.210 \times 10^{11}$ $M^{-1}S^{-1}$). Moreover, DPPC is less prehydrated due to its higher phase transition temperature (42º C) as compared to that of DMPC (23º C) at room temperature. Therefore, HSA exhibits more affinity towards DPPC than it does towards DMPC. The time resolved fluorescence measurements revealed that penetration of HSA into liposomes results in release of Ellipticine from the liposome which is followed by a migration to the hydrophobic pocket of HSA. We plotted the shorter component (τ_1) and the longer component (τ_2) of Ellipticine in native HSA and in liposomes as a function of concentration of HSA. It is revealed that there is a break point at around 1 μM HSA concentration which indicates that Ellipticine molecules are migrated to the hydrophobic pocket of HSA from liposomes. We found an increment in rotational relaxation time with incorporation of HSA and this suggests the penetrative interaction as well as formation of a bigger complex.

(g) Interaction of human serum albumin with liposomes of saturated and unsaturated lipids with different phase transition temperatures: a spectroscopic investigation by membrane probe PRODAN:

The interaction of HSA with liposomes made of saturated and unsaturated phosphocholines having distinctly different phase transition temperatures has been studied using membrane probe PRODAN (6-Propionyl-2-Dimethylaminonaphthalene). We used DPPC, DMPC as saturated lipids and *1,2-dioleoyl-sn-glycero-3-phosphocholine* (DOPC), *2-oleoyl-1-palmitoyl-sn-glycero-3-phosphocholine* (POPC) as unsaturated lipids to prepare liposomes. DPPC and DMPC possess saturated carbon chains with phase transition temperature around 42^0 C and 23^0 C respectively. On the other hand DOPC and POPC have the phase transition temperature around -20^0 C and -2^0 C respectively. The partition coefficient is least for DPPC and highest for DMPC. Addition of HSA to PRODAN impregnated liposomes causes a quenching in the fluorescence intensity of PRODAN. The continuous decrease in the intensity with

addition of HSA to PRODAN impregnated liposomes indicates that HSA interacts with the liposomes. We plotted ϕ_0/ϕ as a function of concentration of HSA in different liposomes. Maximum quenching takes place in DPPC liposome and minimum in DOPC and POPC liposomes. The quenching can be rationalized by the fact that HSA partially penetrates in the liposomes due to hydrophobic interaction and destabilizes the packing order of lipid bilayer leading to leakage of the probe molecules from the liposome. It was found that HSA preferably penetrates into the liposomes, which are less prehydrated at room temperature. Thus penetration is higher in DPPC and DMPC liposomes as these liposomes are less prehydrated due to higher phase temperature. On the other hand HSA has less penetration in DOPC and POPC liposomes because these liposomes are more hydrated owing to lower phase transition temperature. The time resolved fluorescence measurements revealed the change in lifetime component particularly longer component takes place in the decreasing order of phase transition temperatures. The change in the amplitudes indicates that penetration of HSA into liposomes brings in release of PRODAN molecules. Incorporation of HSA in all the liposomes results in significant increase in the rotational relaxation time of PRODAN. This fact confirms that HSA penetrates into the liposome and forms bigger complex.

List of Publications:

1. Thakur R., Mallik A., Chakraborty A. (2012), Photophysical and Photodynamical Study of Fluoroquinolone Drug Molecule in Bile Salt Aggregates, *Photochem. Photobiol.,* 88, 1248-1255 (DOI: 10.1111/j.1751-1097.2012.01175.x).

2. Thakur R., Das A., Chakraboty A. (2012), Photophysical and photodynamical study of Ellipticine: an anticancer drug molecule in bile salt modulated in vitro created liposome, *Phys. Chem. Chem. Phys.,* 14, 15369-15378 (DOI: 10.1039/C2CP41708A).

3. Thakur R., Das A., Chakraborty A. (2013), Fate of anticancer drug Ellipticine in reverse micelles in aqueous and methanolic environment: A photophysical approach, *Chem. Phys. Lett.,* 563, 37-42 (DOI: S0009261413001358).

4. Thakur R., Das A., Chakraborty A. (2014), The fate of anticancer drug, Ellipticine in DPPC and DMPC liposomes upon interaction with HSA: A photophysical approach, *J. Photochem. & Photobiol. B. Biol.,* 130, 122–131 (http://dx.doi.org/10.1016/ j.jphotobiol. 2013.10.016).

5. Thakur R., Das A., Chakraborty A. (2014), Interaction of human serum albumin with liposomes of saturated and unsaturated lipids with different phase transition temperatures: a spectroscopic investigation by membrane probe PRODAN, *Rsc Adv.,* 4, 14335-14347 (DOI: 10.1039/c4ra01214c).

6. Thakur R., Das A., Adhikari C., Chakraborty A. (2014), Dynamics of Prototropic Species of an Anticancer Drug Ellipticine in Bile Salt Aggregates of Different Head Groups and Hydrophobic Skeleton: A Phtophysical Study to Probe Bile Salt as Multisite Drug Carrier, (accepted manuscript *Phys. Chem. Chem. Phys*. DOI:10.1039/C4CP01308E)..

7. Thakur R., Das A., Adhikari C., Chakraborty A., Gosh K. S. (2014), Binding of an anticaner alkaloid with HSA and IgG proteins: A spectroscopic and molecular modeling study, (*To be communicated*).

8. Das A., Thakur R., Chakraborty A. (2013), A steady-state and time-resolved fluorescence study on liposome-calf thymus DNA interaction: probed by an anticancer drug Ellipticine, *RSc Adv.,* 3, 19572-19581 (DOI: 10.1039/c3ra43037e).

9. Das A., Thakur R., Dagar A., Chakraborty A. (2014), A spectroscopic investigation and molecular docking study on the interaction of hen egg white lysozyme with liposomes of saturated and unsaturated phosphocholines probed by an anticancer drug Ellipticine, *Phys. Chem. Chem. Phys.,* 16, 5368-5381 (10.1039/ C3CP54247E).

[#] (8 and 9 are not included in this thesis)

TABLE OF CONTENT

LIST OF FIGURES

LIST OF TABLES

Chapter 6 : Binding of an anticaner alkaloid with HSA and IgG proteins: A spectroscopic and molecular modeling study

Chapter 7 : The fate of anticancer drug, Ellipticine in DPPC and DMPC liposomes upon interaction with HSA: A photophysical approach.

Chapter 8 : Interaction of human serum albumin with liposomes of saturated and unsaturated lipids with different phase transition temperatures: a spectroscopic investigation by membrane probe PRODAN

NOMENCLATURE

α	Alpha
β	Beta
γ	Gamma
τ	Lifetime
□	Quantum Yield
Å	Angstrom
λ	Wavelength
μ	micro
χ	Chi
π	Pi
Σ	Summation
nm	Nanometer
ns	Nanosecond
mM	Milli Molar
μM	Micromole
a_i	amplitude
η	Viscosity
K_{sv}	Stern Volmer Quenching Constant
K_p	Partition Coefficient
η^1N	Imine Nitrogen.
N	Amine Nitrogen
ε^2N	Nitrogen of amide group.
ε^1O	Oxygen of amide group.
γO	Oxygen of Carboxyl group.

ACRONYMS

ANS	8-Anilinonaphthalene-1-sulfonic acid
AOT	Dioctyl sodium sulfosuccinate
Arg	Arginine
ASA	Accessible Surface Area
Asp	Aspartic Acid
CASTp	Computed Atlas of Surface Topography of proteins
CD	Circular Dichroism
DMPC	1,2-dimyristoyl-*sn*-glycero-3-phosphocholine
DPPC	1,2-dipalmitoyl-sn-glycero-3-phosphocholine
DOPC	1,2-dioleoyl-sn-glycero-3-phosphocholine
Glu	Glutamic Acid
HSA	Human Serum Albumin
IgG	Immunoglobulin G
Lys	Lysine
NaC	Sodium Cholate
NaDC	Sodium Deoxy Cholate
NaGDC	Sodium Glycodeoxy Cholate

NaTC	Sodium Taurocholate
NaTDC	Sodium Taurodeoxy Cholate
NOR	Norfloxacin
OFL	Ofloxacin
POPC	2-oleoyl-1-palmitoyl-sn-glycero-3-phosphocholine
PRODAN	6-Propionyl-2-Dimethylaminonaphthalene
Pro	Proline
Ser	Serine
Thr	Threonine
Trp	Trptophan
Val	Valine
cps	cycles per second
ps	Picosecond

Chapter 1

Introduction to biologically relevant organized assemblies: An overview of various biomimetic systems

1.1. Introduction:

There are various organized assemblies of biological relevance. Self organization is a process by which several components of a system interact and become ordered in space. This is a process of construction "in which atoms, molecules, aggregates of molecules and components arrange themselves in ordered fashion. After self organization the whole system has characteristic that differ qualitatively from those of component parts *[1,2]*. There is increasing interest in understanding the properties of the systems that arise out of the interactions of biomolecules. Understanding the principles underlying self-organization in biology will require a biomimetic system i.e. self-assembly mimicking biology. "Biomimetics is the study of biological structures, their function, and their synthetic pathways, in order to stimulate and develop these ideas into synthetic systems similar to those found in biological systems *[3,4]*." Therefore in the present thesis entrapment of various fluorophore drugs in different biomimetic systems and the photophysical behavior of those complexes were studied. The brief description of various biomimetic systems related to this thesis are given below.

1.2. Description of various biomimetic system:

1.2.1. Micelles:

Surfactant molecules, which are made up of polar, ionic, or nonionic head groups and extended apolar, organic residues, in aqueous solution self-assemble to form spherical or non spherical aggregates commonly known as micelles, at concentrations above the so-called critical

micelle concentration (CMC) and specific temperature known as Kraft temperature *[5,6]*. The criterion to form micelle is the amphiphilicity, i.e., presence of both polar and non polar group in the same molecule. A typical micelle in aqueous solution forms an aggregate with the hydrophilic "head" regions in contact with surrounding solvent, sequestering the hydrophobic single-tail regions in the micelle centre *[7,8]*. In aqueous solution these monomers aggregates in such a way that hydrophobic groups are removed from water and forms the dry core of the micelles. The hydrophilic part remains in water. The dry 'core' of the micelles is surrounded by the polar 'Stern' layer for ionic micelles and 'palisade' layer for neutral micelles. The polar headgroups, bound counterions and water molecules are present in this layer. A diffusive layer exists between Stern (or palisade) layer and bulk water, called Guoy-Chapman (GC) layer containing free counter ions and bound water molecules. Conventional micelles are fluid aggregates of surfactants with shape and size decided by packing of individual surfactant *[9]*.

These micelles are stabilized by hydrophobic forces and head group repulsion (electrostatic and steric) *[10,11,12]*. The study of photophysical properties, such as fluorescence excitation and emission spectra, their shifts and excited states lifetimes of probe has provided significant information on the micellar structure at molecular level *[13,14]*. Critical micellar concentration (CMC) is one of the most thoroughly studied properties in the micellization process *[15,16,17]*. Micelles are spherical or nearly spherical in structure. The size of the micellar aggregates is usually 1-10 nm and the aggregation number, i.e., the number of surfactant molecules per micelles, ranges from 20 to 200. The thickness of the Stern layer is 6-9 Å for cationic and anionic sodium micelles. For neutral micelles the Palisade layer is about 20 Å thick and radius of dry hydrophobic core is 25-27 Å. Thus cationic and anionic micelles overall radii are 50 Å and 30 Å, respectively *[18,19,20]*. In biological system, bile salts are important surfactants from the chemical and biological point of view.

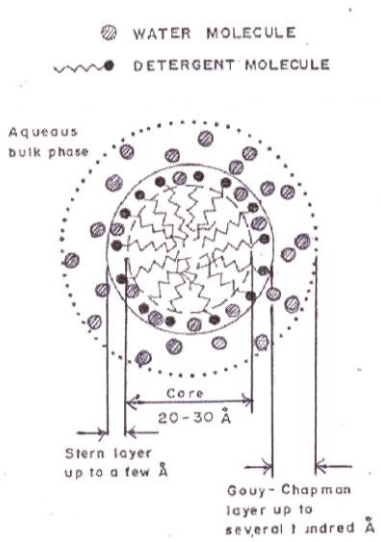

Figure 1.1. *Structure of micelle*

1.2.2. Bile salt aggregates:

Bile salts are available in the bile. They are biosynthesized from cholesterol in the liver and stored in the gall bladder. Bile salts are the main products of cholesterol metabolism and, biologically, the most important detergent-like molecules commonly known as biosurfactant *[21,22,]*. They are amphipathic molecules, possessing hydrophobic and hydrophilic regions. Bile salts posses a large, rigid, and planar hydrophobic moiety of a steroid nucleus with two or three hydroxyl groups on α face and a short aliphatic side chain on β face. Unlike other small molecules, bile salts are noticeably assorted in structural sense. Bile salts usually differ in three respects: (i) side chain structure (ii) stereochemistry of rings (iii) the distribution and number of hydroxyl groups in the steroid nucleus. They are surface active molecules and in aqueous environments bile salts self associate to form aggregates which are commonly known as micelles depending on the number and position of the hydroxyl groups, concentration, pH, ionic strength, etc. *[23,24]*. According to Bohne and co-workers, they accommodate various kind of guest within these aggregates. Small changes such as the introduction of short alkyl chains or the inclusion of hydroxyl groups can lead to significant changes in the accessibility

of guest to the aggregate as well as changes in the residence time of the guest inside the aggregate *[25,26,]*. The facial amphiphilicity enables them to aggregate in aqueous media. Aggregation is largely driven by hydrophobic association of apolar β faces of steroid backbone, whereas further aggregation occurs by hydrogen bonding interactions. Pegylated bile acids can form spherical aggregates that are capable of encapsulating hydrophobic compounds in aqueous solutions, encapsulation efficiency depends on the length and number of attached PEG chains *[27]*. Bile salts are more adaptable than rigid host systems and therefore capable of solubilizing photo chromic compounds with very low solubility *[28]*.

Their amphiphilic nature and unique aggregation pattern, account for their solubilization of both hydrophobic and hydrophilic solutes. They have a remarkable ability to transform lamellar arrays of lipids into mixed micelles *[29]*. They transport lipid by solubilization and have secretory and regulatory properties. They operate as steroidal detergents, which together with lipids/fats/cholesterol form mixed micelles in the intestine to enable fat digestion and absorption through the intestinal wall *[30]*. The exceptional properties of bile salts have recommended for taking advantage of these properties for pharmaceutical application *[31]*. According to Miranda and co-workers, within the available hydrophobic microenvironments, steroidal framework of bile salts constitutes a promising strategy to introduce a drug or any flourescent probe within primary and secondary cholic acid aggregates *[32,33,34,]*. Bile salts help in solubilization and absorption of various insoluble drugs. Bile salts also affect the drug absorption either by involving membrane permeability or by altering normal gastric emptying rates. Bile salts–drug mixed micelles can be used in formulations for liver associated problems and also as cholesterol depressing agents *[35,36,37,38,39]*. Drugs have been associated with bile acids ensuring improved absorption from the intestine of poorly absorbed or non-absorbed drug combined with increased metabolic stability and extended period of influence *[40,41]*.

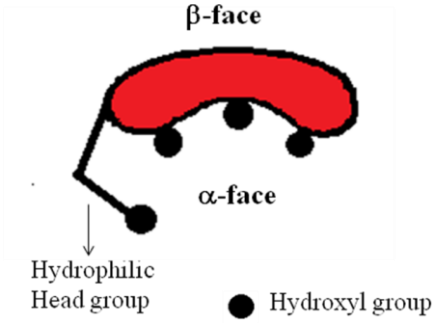

Figure 1.2. *Cartoon representation of bile salt*

1.2.3. Reverse Micelles:

Reverse micelles are one of the most interesting models for biomembranes among the different organized media. These are formed by the aggregation of the surfactant molecules in non-polar solvents. In water containing reverse micelle the surfactant molecules are pointing with their hydrophilic head groups towards the micellar water core, with their tails dissolved in the oil, so that the surfactant forms a soft shell that separates both liquids *[42,43,44]*. Often used as templates for nanoparticles and as microreactor for heterogeneous chemistry *[45,46]*. Depending upon the use of co-solvents (water or polar organic solvents) the reverse micelles are termed as aqueous or non aqueous reverse micelles *[47,48,49]*. For a given surfactant concentration the size of the water core increases linearly with increasing water content *[50]*. In biological systems sometimes, water is trapped between biomolecules in small pores and nearly all of the water is in contact with a surface. In this case, water might be expected to behave quite differently than bulk water since almost all water molecules are in contact with a surface. The presence of the interface plays an important role in the dynamics of all the confined water. To understand the transition between the mostly bulk and interfacial regimes, it is useful to explore a model system that can be tuned through this entire range *[51,52,53]*. So; for the study of the confined water, the reverse micelles offer the information about the important parameters like the degree of confinement and probably also the hardness of the

confinement *[54]*. Reverse micelles formed by anionic surfactant AOT (sodium bis [ethylhexyl] sulfosuccinate) has proven to be a very useful model system for studying confined water and water near an interface. AOT is a surfactant that has an anionic sulfonate head group and sodium counter ion, which preferentially partition into the aqueous phase and branched, bulky alkyl tails that prefer a nonpolar phase. AOT forms well characterized, reverse micelles (spherical water pools) over a wide range of sizes with water nanopools ranging from radii of less than 1 nm up to tens of nanometers. AOT solubilizes approximately 50 water molecules per molecule of surfactant. Reverse micelles can be characterized by the parameter w_0, the number of water molecules per surfactant molecule,

$$w_0 = [H2O] / [AOT].$$

Where w_0 is defined as water/surfactant molar ratio. The structure of AOT reverse micelle was determined by dynamic light scattering, small angle neutron scattering, ultrasound velocity measurement and FT-IR studies. There exist three types of water molecules in reverse micelles which is proved using FT-IR spectroscopy. The water molecules near the polar head group of the surfactant are called bound water. The free water molecules are near the central region of the water pool and the trapped water molecules are between the surfactants *[55]*. All the water molecules in a microemulsion, except the approximately six most tightly held freezes at -50^0 C *[56]*.

Apart from water, confinement of other polar solvents, such as acetonitrile, alcohol *[57,58]*, formamide, dimethylformamide, ethylene glycol *[58,59,60]* etc. have been reported in AOT reverse micelles. Costa and co-workers characterized the glycerol reverse micelles *[60,61]* and recently Levinger and co-workers proposed that methanol/AOT/ hydrocarbon system are continous system *[62]*. Several nonionic or neutral surfactants, e.g., Triton X-100 and poly (oxyethylene) lauryl ether (Brij-30) have also been reported to form reverse micelles in pure and mixed hydrocarbon solvents *[63,64]*.

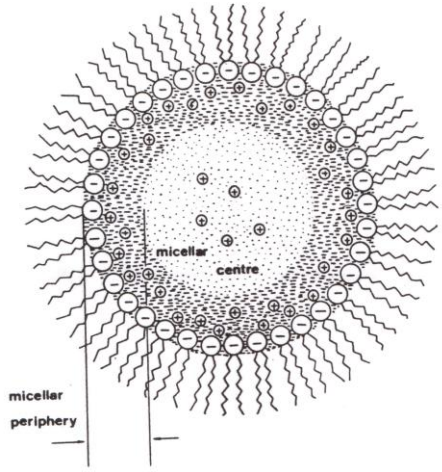

Figure 1.3. *Structure of reverse micelle*

1.2.4. Liposomes:

Biomimetic liposomes are self-assembling structures in a lipid dispersion in water and a useful tool for drug delivery. They are used as a container for the storage, transfer, and controllable release of agents *[65]*. Bangham et al. for the first time prepared liposomes *[66]*. Liposomes are composed of natural or synthetic lipids which form a spherical self closed aqueous core having one or more lipid layers *[67,68]*. Lipid is the predominant building block of biological membranes, as well as liposomes. Liposomes composed of natural phospholipids are biologically inert and weakly immunogenic, and they possess low intrinsic toxicity *[69,70,71]*. Liposomes serve as model systems for cell membranes and help in the study of basic mechanism and function of membranes, liposomes display some unique pharmacokinetic characteristics *[72]*. Some pioneer workers established that liposomes could entrap drugs and be used as drug delivery system *[73,74]*. They have been investigated for many years as parenteral drug carrier systems, particularly for the selective delivery of anticancer, antibiotic and antifungal agents. It is also accomplished that liposomes could change the in vivo distribution of entrapped drugs *[75,76]*. Their significance lies in their composition, which makes them biocompatible and biodegradable *[65,66]*.

Liposomes are also evaluated as a potential vehicle for the oral delivery of bioactive proteins *[77]*. Phospholipid vesicles are also used in encapsulation and controlled release of pharmaceuticals *[78,79]*, cosmetics *[80]*, and food production *[81,82]*. Recently, liposomes have been used to deliver flavors and nutrients within foods *[83]* and have also been investigated for their ability to incorporate food antimicrobials *[84]*. Liposomes can be classified according to their size, as SUV, LUV and MLV which mainly depends upon the preparation method*[85]*.

(i) The small unilamellar vesicles (SUV) size ranges from 0.03 – 0.2 µm.
(ii) The large unilamellar vesicles (LUV) size is greater than 0.5 µm.
(iii) The multi lamellar vesicle (MLV) size range is from 1- 3 µm.

Altering the content of the liposome bilayer, in particular by incorporation of cholesterol was shown to 'tighten' fluid bilayers and reduce the leakage of contents from liposomes *[86,87]*. Insertion of cholesterol also changes the fluidity of bilayer *[88,89]*. pH-sensitive liposomes, provides a significant mechanisms that can mediate delivery of the liposomal contents into the cytosol within endocytic compartments, after release from vesicle *[90]*. Physical characteristics of drugs make them amenable to retention in liposomes and help in controlling the release rate of entrapped substances *[91,92]*. Similar to biological membranes, model membranes such as liposomes have low permeability to hydrophilic drugs and high permeability to hydrophobic drugs *[93,94]*. Hof and coworkers used various fluorescent probes within the lipid bilayer for studying solvation and photophysical properties of these probes within model membranes *[95,96,97,98]*. The addition of an adequate amount of biosurfactants can solubilize vesicles and terminate their roles as drug carriers causing release of entrapped drug *[99]*. Bile salts are the popular biosurfactant known for solubilization and disintegration of vesicles in to mixed micellar structures. Slolubilization of liposomes by bile salts is three step process *[100,101,102]*.

(i) First is vesicular stage when the concentration of surfactant is low and surfactant is partitioned between aqueous solution and lipid bilayer.

(ii) When the concentration of surfactant is further increased, vesicle micelle co-exist and solubilization starts taking place.

(iii) In the last stage surfactants are at their CMC and disrupt the bilayer into mixed micelles. Thus complete solubilization of vesicle takes place.

At physiological concentrations, the bile present in the gallbladder, bile ducts, and intestinal lumens are associated with phospholipids and cholesterol in mixed micellar structures *[103]*.

Plasma components also influence the role of liposomes as drug carrier. It has been found that plasma proteins partially penetrate and deform the lipid bilayer *[104,105]*. Interaction of blood proteins with phospholipid vesicles have been studied by various workers *[106,107,108, 109]*. Plasma proteins Human Serum Albumin (HSA) and Immunoglobulin G (IgG) are found to cause vesicle leakage and release of entrapped drug. Castanho and co-workers had studied interaction of vesicles with different peptide and proteins *[110,111,112,113,114]*.

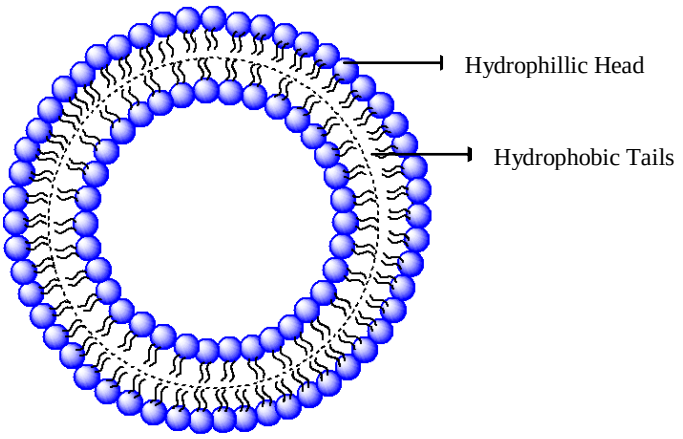

Figure 1.4. *Structure of liposome*

1.2.5. **Proteins:**

Various proteins are found in plasma, major proteins of blood plasma are albumin and globulin. The normal serum protein level is 6 to 8 g/dl. Albumin makes up 3.5 to 5.0 g/dl, and the remainder is the total globulins *[115]*. Albumin is the most abundant protein in human plasma about 600 µM *[116,117]*. Albumin, which is synthesized in the liver, is a soluble, monomeric, globular protein *[118]*. HSA has an exceptional binding capacity for a wide variety of hydrophobic ligands and plays a key role in the transport of fatty acids, amino acids, metals such as Cu^{2+} and Zn^{2+}, metabolites such as bilirubin, and pharmaceutical drug compounds *[119]*. Human serum albumin (HSA) is circulating in plasma and it's also a major component of most extracellular fluids, including interstitial fluid and lymph *[120]*. Its diverse functions include maintenance of colloid osmotic pressure and sequestration of toxins and oxidants *[121,122,123]*. The protein binds a wide variety of endogenous and exogenous ligands in multiple binding sites. The most essential physiological role of the HSA carrier protein is therefore thought to be the transport of such water-insoluble solutes and various drugs in the bloodstream to target organs such as the liver, intestine, kidney, and brain *[124]*. Crystal structure of HSA was reveled by Carter and co-workers in 1992 *[125]*. The molecular weight of HSA is about 66 kDa, it consist of single polypeptide of 585 amino acid residue. Its amino acid sequence consist of 1 tryptophan (Trp214), 18 tyrosine, 6 methionines, 17 disulphide bridges, and only one free thiol (Cys 34). The unglycosylated protein is composed of three structurally similar, though asymmetrical, repeating domains-I (residues 1-195), II (196-383), and III (384-585)-each of which are divided into two subdomains, A and B. This series of six helical subdomains assembles to form a heart-shaped molecule. Each domain posses common structural motifs. Domains I and II are almost perpendicular to each other in which the tail of subdomain IIA is attached to the interface region between subdomains IA and IB by hydrophobic interactions and hydrogen bonds. Conversely, domain III projects out from subdomain IIB at a 45º angle to form a Y-shaped

configuration for domains II and III. Thus, domain III only interacts with subdomain IIB. The HSA protein has been found to be very flexible in different conditions and can easily change its shape when participating in binding interactions due to the relative motions of the domain structures. The relative arrangements of the three domains are largely changed when fatty acid chains bind to the protein. During complex formation, the domains largely retain their conformation; however, the two C-terminal helices in domain III move toward the outside of the molecule.

The main regions of ligand interaction are located in hydrophobic pockets at sub domain IIA and IIIA *[114,126,127,128]*. X-rays have revealed sites for several endogenous and several exogenous ligands. Two distinct primary drug binding sites, Sudlow's drug sites I and II, are identified and characterized for their ability to reversibly bind drugs such as warfarin and phenylbutazone. Many ligands bind specifically either to subdomain IIA (Sudlow site I) or to subdomain IIIA (Sudlow site II) of HSA *[129,130]*. Various ligands are transported to different tissues by binding at either of the sites. Generally, HSA has a greater affinity for small, negatively charged hydrophobic molecules. Evidence has shown that HSA contains six dominant areas of ligand association. There are two high affinity binding sites for small heterocyclic or aromatic compounds (located on subdomains IIA and IIIA). At similar positions in their structures, subdomains IIA and IIIA contain deep pockets lined with hydrophobic side chains. The entrance to the pocket in both IIA and IIIA is surrounded by positively charged amino acid residues. Residues Trp 214, Lys 199, and Tyr 411 are strategically located in the hydrophobic pockets of IIA and IIIA and are supposed to be crucial to the binding process. Each HSA molecule can carry up to seven fatty acid molecules. Subdomains IIA and IIIA are the locations for the primary fatty-acid and bilirubin-binding sites. On subdomains IB and IIIB two to three dominant long-chain fatty acid binding sites are located, and two distinct metal-binding sites, one involving Cys-34 and the other on

the N terminus. The crystal structure of HSA shows that domains II and III share a common interface, therefore ligands bound to domain III affect conformational changes and binding affinities in domain II. Unlike IIA and IIIA, subdomain IA does not have a pocket near its hydrophobic core thus IA is not an active ligand binding site. Crystal structures with compounds bound in drug sites I and II, such as warfarin and phenylbutazone are particularly useful for our current studies *[117,131,132,133,134,135,136]*. Albumin binding may be desirable in helping to solubilize drugs that would otherwise aggregate and be poorly distributed.

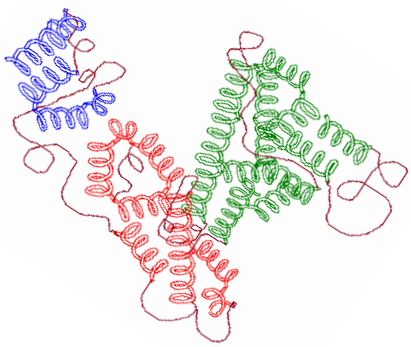

Figure 1.5. *Structure of Human Serum Albumin.*

Along with albumins the major components of serum proteins also include globulins. Globulin constitute about 36% of plasma proteins. The serum globulins are classified as α, β and γ globulins, and γ Globulins are major among these and play crucial role in defense mechanism and are commonly known as immunoglobulin *[115]*. Immunoglobulins are glycoprotein molecules that are produced by plasma cells in response to an immunogen and which function as antibodies *[137]*. This is the second most copious circulating protein and contains long-standing defensive antibodies against several infectious agents. Each immunoglobulin actually binds to a specific antigenic determinant. Antigen binding by antibodies is the primary function of antibodies and can result in protection of the host *[115,116,117]*. Immunoglobulins comprise of five major classes: immunoglobulin G (IgG), IgA, IgM, IgD and IgE. Each is composed

of two identical heavy chains (H) and two identical light chains (L). The main immunoglobulin (Ig) in human blood is IgG. IgG molecular weight is about 150 kDa two heavy chains (50 kDa), and two light chains (25 kDa). The serene of four polypeptide chains, two heavy and two light are cross linked by disulphide bonds in to the Y-shaped structure. The two heavy chains are held together by inter-chain disulfide bonds and by non-covalent interactions. The number of inter-chain disulfide bonds varies among different immunoglobulin molecules. Within each of the polypeptide chains there are also intra-chain disulfide bonds. Amino acid sequence of both heavy and light chains of an IgG characterizes two distinct regions of the chains based on variability of the amino acid sequence, known as 'variable' (V) and 'constant' (C) regions. Variable and constant region of light chains are designated as VL and CL respectively. Similarly, heavy chains are denoted as VH and VL. The amino acid sequence of the variable region forms the N-terminal ends of the chains and determine antigenic specificity of the IgG. Constant regions are the same for each specific class of IgG and carry the effector sites. The variable region makes up half of the entire light chain and the constant region the remaining half. the variable region makes up a quarter of the entire heavy chain while ¾ of the remaining chain is the constant region *[138,139,140,141]*. The hinge region is the area of the IgG where the arms of the antibody form a 'Y'. This is the region that links the two important regions of IgG i.e. F_c and F_{ab} portions. Hinge region allows independent movement of the two F_{ab} arms, it is a flexible region. The two arms of the Y end in regions that vary between different antibody molecules, the V regions. The amino-terminal variable or V domains of the heavy and light chains (VH and VL, respectively) together make up the V region of the antibody and confer on it the ability to bind specific antigen, These are involved in antigen binding, whereas the stem of the Y, or the C region, is far less variable and is the part that interacts with effector cells and molecules. While the constant domains (C domains) of the heavy and light chains (CH and CL, respectively) make up the C region. Carbohydrates are attached to the CH_2 domain lying between

the 2 H chains in most immunoglobulins. However, in some cases carbohydrates may also be attached at other locations*[142,143,144]*.

This Y-shaped structure is characterized by three fragments (two F_{ab} and one F_c). Specific amino acid sequence in F_{ab} of an IgG determines its ability to selectively bind to a particular antigen. These molecules have domains that are structurally independent *[145,146,147]*. The typical IgG is highly soluble at physiological conditions. A prime attribute of these proteins is that non-polar residues are sequestered in a core, where they avoid contact with water. The disclosure of these hydrophobic residue crop up upon heat and acid treatment *[148,149,150,151]*. It is anticipated that partial denaturation of IgG would lead to an increase in exposed hydrophobic surface which results in enhanced binding with ANS. It is believed that IgG acquire chemo attractant activity after exposure of hydrophobic sites. According to several reports hydrophobic domains are located at F_{ab} and F_c region of IgG. DSC measurements propose that F_{ab} domains are mostly affected by heating at 63º C due to lower melting temperature compared with Fc. IgG at low pH provides highly denatured and more hydrophobic conformation. F_c and F_{ab} denature individually of each other, upon decreasing the pH F_c fragment is primarily affected and is denatured *[152,153,154]*. Further, circular dichroic and infrared spectroscopic analyses of rabbit and human IgG have suggested the presence of a β-sheet structure *[155,156]*.Amino acid sequencing and limited enzymatic proteolysis studies have led to the proposal that the immuno-globulin molecule exists in a series of compact domains with the central feature of each being the intrachain disulfide linkage. The studies reported in this communication were directed toward assessing the solution conformation of isolated immunoglobulin chains before and after cleavage of the intrachain disulfide linkage *[157,158,159,160]*. The macro class of proteins, serum globulins includes diversity of carrier proteins some of which could perform metal transport. reaction abilities of the drug cisplatin to different proteins follows the order : hemoglobin > albumin > immunoglobulin

[161]. Thus the present study is done to acquire appropriate insight on interaction of drug with proteins in their native and denatured state.

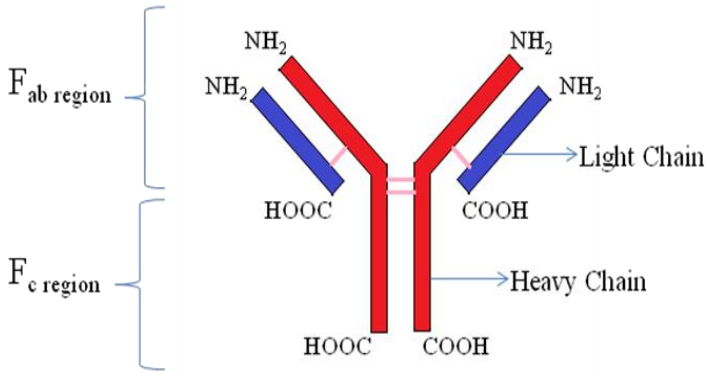

Figure 1.6. *Structure of Immunoglobulin G*

1.3. Organization of thesis:

Chapter 2: In this chapter, we briefly discuss the different instruments used for the experiments and the procedures for sample preparations.

Chapter 3: In this chapter, we have explored the photophysical properties of two widely used antibiotic fluoroquinolone drugs Norfloxcacin (NOR) and Ofloxacin (OFL) and an anticancer drug Ellipticine in biomimicking environments formed by bile salts using both steady state and time resolved fluorescence quenching measurement**.**

Chapter 4: In this chapter, a detailed photophysics of an anticancer agent Ellipticine, in Sodium bis (2-ethylhexyl) sulfosuccinate (AOT) reverse micelle (RM) have been investigated using steady state and time resolved spectroscopy.

Chapter 5: In this chapter, entrapment of anticancer drug Ellipticine in *1,2-dipalmitoyl-sn-glycero-3-phosphocholine* (DPPC) liposome and its release by addition of three different bile salts namely Sodium deoxycholate (NaDC), cholate (NaC) and taurocholate (NaTC) have been studied by steady state and time resolved fluorescence spectroscopy.

Chapter 6: In this chapter, interactions of different prototropic species of Ellipticine with two prominent serum proteins i.e. Human Serum Albumin (HSA) and Immunoglobulin G (IgG) in their native and denatured states have been studied by molecular docking, circular dichroism (CD), steady state and time resolved fluorescence spectroscopy.

Chapter 7: In this chapter, anticancer drug, Ellipticine is encapsulated within two liposomes namely 1,2-dipalmitoyl-*sn*-glycero-3-phosphocholine (DPPC) and 1,2-dimyristoyl-*sn*-glycero-3-phosphocholine (DMPC) and release of this encapsulated drug from these two liposomes upon addition of HSA have been studied by steady state and time resolved fluorescence spectroscopy.

Chapter 8: In this chapter, interaction of human serum albumin (HSA) with liposomes made of saturated and unsaturated phosphocholines having distinctly different phase transition temperatures has been studied using circular dichroism (CD), steady state and time resolved fluorescence spectroscopic techniques.

1.4. References:

1. Breen T. L., Tien J, Oliver S. R, Hadzic T, Whitesides G. M. (1999), Design and self-Assembly of open, regular, 3D mesostructures, *Science*, 284, 948-951.(DOI: 10.1126/science.284.5416.948).
2. Atkinson I. M., Lindoy L. F., Stoddart J. F. (2000), Self Assembly in Supramolecular Systems, Royal Society of Chemistry, Cambridge U.K., pp. 1-6 (ISBN-10: 0854045120).
3. Check E. (2005), Synthetic biology: Designs on life, *Nature*, 438, 417-18 (DOI: 10.1038/438417a).
4. Dillow A., Lowman A. (2002), Biomimetic Materials And Design: Biointerfacial Strategies, Tissue Engineering And Targeted Drug Delivery, first edition, CRC Press, New York, pp. 54-57 (ISBN: 0-8247-0791-5).
5. Atwood D., Florence A. T. (1983), Surfactant Systems: their chemistry, pharmacy and biology, Chapman and Hall, London, pp. 87-108 (ISBN: 13:978-94-009-5777-0).
6. Blandamer M. J., Cullis P. M., Soldi L. G., Engberts J. B. F. N., Kacperska A., Vanos N. M., Subha M. C. S. (1995), Thermodynamics of micellar systems: Comparison of mass action and phase equilibrium models for the calculation of standard Gibbs energies of micelle formation, *AdV. Colloid Interfaces*, 58,171–209 (DOI: 10.1016/0001-8686(95)00252-l).
7. Wettig S. D., Verrall R. E. J. (2001), Thermodynamic Studies of Aqueous m–s–m Gemini Surfactant Systems, *Colloid Interface Sci.*, 235, 310-316 (DOI: 10.1006/jcis.2000.7348).
8. Amato M. E., Caponetti E., Martin, D. C., Pedone L. (2003), ^{1}H and ^{19}F NMR Investigation on Mixed Hydrocarbon− Fluorocarbon Micelles *J. Phys. Chem. B*, 107, 10048–10056 (DOI: 10.1021/ jp022697b).

9. Schubert B. A., Kaler E. W., Wagner N. J. (2003), The microstructure and rheology of mixed cationic/anionic wormlike micelles, *Langmuir*, 19, 4079-4089 (DOI: 10.1021/la020821c).

10. Seddon J. M., Templer R. H. (1995), Structure and Dynamics of Membranes: I. From Cells to Vesicles. In: Lipowsky R., Sackmann (ed) Polymorphism of Lipid-Water Systems, Vol. 1, Elsevier Science B.V., Amsterdam, (ISBN 0-444-81975-4).

11. Baeurle S. A., Kroener J. (2004), Modeling effective interactions of micellar aggregates of ionic surfactants with the Gauss-Core potential, *J. Math. Chem.* 36, 409–421 (DOI: 10.1023/b:jomc. 0000044526. 22457.bb).

12. Fuhrhop J. H., Helfrich W. (1993), Fluid and solid fibers made of lipid molecular bilayers, *Chem. Rev.*, 93, 1565-1582 (DOI: 10.1021/ cr00020a008).

13. Salkar R. A., Hassan P. A., Samant S. D., Valaulikar B. S., Kuma R. V. V., Kern F., Candau S. J., Manohar C. (1996), A thermally reversible vesicle to micelle transition driven by a surface solid–fluid transition *Chem. Comm.*,1223-1224 (DOI: 10.1039/CC9960001223).

14. Manohar C. (1999), Structure and Dynamics of Materials in Mesoscopic Domain. In Lal, M., Mashelkar, R. A., Kulkarni, B. D. and Naik, V. M. (ed.) Imperial College Press, London, pp. 252-258 (ISBN: 10: 1860941907).

15. Gehlen M. H., De Schryver F. C. (1993), Time-resolved fluorescence quenching in micellar assemblies, *Chem. Rev*. 93, 199-221 (DOI: 10.1021/cr00017a010).

16. Magid L. J., Triolo R., Jr. Johnson J. S. (1984), Small-angle neutron-scattering study of critical phenomena in aqueous solutions of C12E8, an nonionic amphiphile, *J. Phys. Chem.* 88, 5730-5734 (DOI: 10.1021/j150667a054).

17. Corti M., Deghiorghio V. (1980) In “Light Scattering in Liquids and Macromolecule solutions”, Deghiorghio V., Corti M., Gigilio M., (Eds.) pp. 111, Plenum Press, New York. (ISBN: 978-1-4615-9187-0).
18. Paradies H. H. (1980), Shape and size of a nonionic surfactant micelle. Triton X-100 in aqueous solution, *J. Phys. Chem.* 84, 599-607 (DOI: 10.1021/j100443a008).
19. Berr S. S. (1987), Solvent isotope effects on alkytrimethylammonium bromide micelles as a function of alkyl chain length, *J. Phys. Chem.*, 91, 4760-4765 (DOI: 10.1021/j100302a024).
20. Berr S. S., Caponetti E., Johnson J. S., Jr. Jones R. R. M., Magid L. J. (1986), Small-angle neutron scattering from hexadecyltrimethy-lammonium bromide micelles in aqueous solutions, *J. Phys. Chem.*, 90, 5766-5770 (DOI: 10.1021/j100280a059).
21. Small D. M. (1971), The Bile Acids: Chemistry, Physiology and Metabolism, Nair, P.P., Kritchevsky, D. (Eds.), vol. 1, Plenum Press, New York, pp. 249-356 (ISBN: 10: 0306371316).
22. Danielsson, H. (1973), In The Bile Acids: Chemistry, Physiology and Metabolism (eds Nair, P. P. and Kritchevsky, D.), Plenum Press, New York, 1973, vol. 3, pp. 5–32 (ISBN-10: 1461575656).
23. Mukhopadhyay S., Maitra U. (2004), Chemistry and biology of bile acids, *Current Science,* 87, 1666-1683.
24. Hofmann A. F. (2000), In Bile Acids and Hepatobiliary Disease, Northfield, T., Zentler-Munro, P. L., Jazrawi, R. P. (Eds.), Kluwer, Boston, pp. 303–332 (ISBN-10: 0792387554).
25. Li R., Carpentier E., Newell E. D., Olague L. M., Heafey E., Yihwa C., Bohne C. (2009), Effect of the Structure of Bile Salt Aggregates on the Binding of Aromatic Guests and the Accessibility of Anions, *Langmuir,* 25, 13800-13808.(DOI: 10.1021/la901826y).

26. Yihwa C., Bohne C. (2007), Effect of Solvent Polarity and Viscosity on the Guest Binding Dynamics with Bile Salt Aggregates, *Photochem. Photobiol.*, 83, 494-502 (DOI: 10.1562/2006-09-17-RA-1043).

27. Le Dévédec F., Fuentealba D., Strandman S., Bohne C., Zhu X. X. (2012), Aggregation Behavior of Pegylated Bile Acid Derivatives, *Langmuir*, 28, 13431-13440 (DOI: 10.1021/la303218q).

28. Li R., Santos C. S., Norsten T. B., Morimitsu K., Bohne C. (2010), Aqueous Solubilization of Photochromic Compounds by Bile Salt Aggregates, *Chem Commun*, 46, 1941 – 1943 (DOI: 10.1039/B926351A).

29. Kawamura H., Murata Y., Yamaguchi T., Igimi H., Tanaka M., Sugihara G., Kratohvil J. P. (1989), Spin-label studies of bile salt micelles, *J. Phys. Chem.*, 93, 3321–3326 (DOI: 10.1021/j100345a087).

30. Haslewood G. A. D. (1964), The biological significance of chemical differences in bile salts, *Biol. Rev.*, 39, 537-574 (DOI: 10.1111/j.1469-185X.1964.tb01170.x).

31. Mendoza M. G., Nuin E., Andreu I., Marin M. L., Miranda M. A. (2012), Photophysical Probes To Assess the Potential of Cholic Acid Aggregates as Drug Carriers, *J. Phys. Chem. B*, 116, 10213–10218 (DOI: 10.1021/jp304708y).

32. Cuquerella M. C., Rohacova J., Marin M. L., Miranda M. A. (2010), Stereodifferentiation in fluorescence quenching within cholic acid aggregates, *ChemComm*, 46, 4965–4967 (DOI: 10.1039/ C0CC00176G).

33. Rohacova J., Sastre G., Marin M. L., Miranda M. A. (2011), Dansyl Labeling To Modulate the Relative Affinity of Bile Acids for the Binding Sites of Human Serum Albumin, *J. Phys. Chem. B*, 115, 10518–10524 (DOI: 10.1021/jp201788d).

34. Mendoza M. G., Marin M. L., Miranda M. A. (2011), Dansyl Derivatives of Cholic Acid as Tools to Build Speciation Diagrams for Sodium Cholate Aggregation, *J. Phys. Chem. Lett.*, 2, 782–785 (DOI: 10.1021/jz200178r).
35. Mueller K. (1981), Structural dimorphism of bile salt/lecithin mixed micelles: A possible regulatory mechanism for cholesterol solubility in bile? X-ray structural analysis, *Biochemistry,* 20, 404-414 (DOI: 10.1021/bi00505a028).
36. Haslewood, G. A. D. (1978), The biological importance of bile salts , North Holland Publishing Co, Amsterdam (ISBN-10: 0720406625).
37. Carey, M. C. (1983), In Phospholipids and Atherosclerosis, Avogaro P. (ed.), Raven Press, New York, pp. 33-63 (ISBN-10: 0890048428).
38. Kramer W., Wess G. (1996), Bile acid transport systems as pharmaceutical targets, *Eur. J. Clin. Invest.*, 26, 715–732 (DOI: 10.1111/j.1365-2362.1996.tb02383.x).
39. Kramer W., Glombik H. (2006), Bile acid reabsorption inhibitors (BARI): novel hypolipidemic drugs, *Curr. Med. Chem.*, 13, 997-1016 (DOI: 10.2174/092986706776361003).
40. Enhsen A., Kramer W., Wess G. **(**1998), Bile acids in drug discovery, *Drug Discovery Today,* 3, 409-418 (DOI: 10.1016/S1359-6446(96)10046-5).
41. Tamminen J., Kolehmainen E. (2001), Bile Acids as Building Blocks of Supramolecular Hosts, *Molecules,* 6, 2-46 (DOI:10.3390/ 60100021).
42. M. P. Pileni (1990), Structure and Reactivity in Reverse Micelles, first ed. Elsevier, Amsterdam, (ISBN-10: 0444881662).
43. P. L. Luisi, B. E. Straube (1984), Reverse Micelles, Plenum Press, New York.

44. Van Dijk M., Joosten J., Levine Y., Bedeaux D. (1989), Dielectric study of temperature dependent aerosol OT/water/isooctane microemulsion structure, *J. Phys. Chem.*, 93, 2506-2512 (DOI: 10.1021/j100343a054).

45. De T. K., Maitra A. (1995), Solution behaviour of Aerosol OT in non-polar solvents, *Adv. Colloid Interface Sci.*, 59, 95-193 (DOI:10.1016/0001-8686(95)80005-N).

46. Jones M. N., Chapman D. (1995), Micelles, Monolayers, and Biomembranes, John Wiley and Sons, New York, (ASIN: B004EC9N1W).

47. Zhang J., Bright F. V. (1992), Steady-state and time-resolved fluorescence studies of bis (2-ethylhexyl) sodium succinate (AOT) reserve micelles in supercritical ethane, *J. Phys. Chem.*, 96, 5633-5641 (DOI: 10.1021/j100192a080).

48. Gale R. W., Fulton J. L., Smith R. D. (1987), Organized molecular assemblies in the gas phase: reverse micelles and microemulsions in supercritical fluids, *J. Am. Chem. Soc.*, 109, 920-921 (DOI: 10.1021/ ja00237a059).

49. Niemeyer E. D., Bright F. V. (1998), The pH within PFPE Reverse Micelles Formed in Supercritical CO_2, *J. Phys. Chem. B*, 102, 1474-1478 (DOI: 10.1021/jp973157v).

50. Van Dijk M. A., Joosten J. G. H., Levine Y. K., Bedeaux D. (1989), Dielectric study of temperature-dependent aerosol OT/water/ isooctane microemulsion structure, *J. Phys. Chem.*, 93, 2506-2512 (DOI: 10.1021/j100343a054).

51. Zulauf M., Eicke H. F. (1979), Inverted micelles and microemulsions in the ternary system water/aerosol-OT/isooctane as studied by photon correlation spectroscopy, *J. Phys. Chem.* 83, 480-486 (DOI: 10.1021/j100467a011).

52. Kinugasa T., Kondo A., Nishimura S., Miyauchi Y., Nishii Y., Watanabe K., Takeuchi H. (2002), Estimation for size of reverse micelles formed by AOT and SDEHP based on viscosity measurement, *Colloids Surf., A,* 204, 193-199 (DOI:10.1016/S0927-7757(01) 01132-3).

53. Eicke H. F., Rehak J. (1976), On the Formation of Water/Oil-Microemulsions, *Helv. Chim. Acta,* 59, 2883-2891 (DOI: 10.1002/hlca.19760590825).

54. Meier W. (1997), Kerr Effect Measurements on a Poly(oxyethylene) Containing Water-in-Oil Microemulsion, *J. Phys. Chem. B,* 101, 919-921 (DOI: 10.1021/jp963410b).

55. Moulik S. P., Pal B. K. (1998), Structure, dynamics and transport properties of microemulsions, *Adv. Colloid Interface Sci.,* 78, 99-195 (DOI:10.1016/S0001-8686(98)00063-3).

56. Hauser H., Haering G., Pande A., Luisi P. L. (1989), Interaction of water with sodium bis(2-ethyl-1-hexyl) sulfosuccinate in reversed micelles, *J. Phys. Chem.,* 93, 7869-7876 (DOI: 10.1021/ j100360a029).

57. Shirota H., Horie K. (1999), Solvation Dynamics in Nonaqueous Reverse Micelles, *J. Phys. Chem. B,* 103, 1437-1443 (DOI: 10.1021/jp983605e).

58. Riter R. E., Kimmel J. R., Undiks E. P., Levinger N. E. (1997), Novel Reverse Micelles Partitioning Nonaqueous Polar Solvents in a Hydrocarbon Continuous Phase, *J. Phys. Chem. B,* 101, 8292-8297 (DOI: 10.1021/jp971732p).

59. Roy S., Moulik S. P. (1994), Dynamics and Thermodynamics of Aerosol OT-Aided Nonaqueous Microemulsions, *Langmuir,* 10, 2511-2515 (DOI: 10.1021/la00020a005).

60. Laia C. A. T., Brown W., Almgren M., Costa S. M. B. (2000), Temperature and Composition Dependence of the Structure of Isooctane/AOT Microemulsion L2 Phases with Glycerol and Formamide: A Light Scattering Study, *Langmuir,* 16, 8763-8770 (DOI: 10.1021/la000527p).

61. Laia C. A. T., Brown W., Almgren M., Costa S. M. B. (1998), Dynamic Light Scattering Study of AOT Microemulsions with Nonaqueous Polar Additives in an Oil Continuous Phase, *Langmuir,* 14, 3531-3537 (DOI: 10.1021/la9709047).

62. Correa N. M., Silber J. J., Riter R. E., Levinger N. E. (2012), Nonaqueous Polar Solvents in Reverse Micelle Systems, *Chem. Rev.*, 112, 4569-4602 (DOI: 10.1021/cr200254q).

63. Zhu D. M., Feng K. I., Schelly Z. A. (1992), Reverse micelles of Triton X-100 in cyclohexane: effects of temperature, water content, and salinity on the aggregation behavior, *J. Phys. Chem.*, 96, 2382-2385 (DOI: 10.1021/j100184a068).

64. Caldararu H., Caragheorgheopol A., Vasilescu M., Dragutan I., Lemmetyinen H. (1994), Structure of the Polar Core in Reverse Micelles of Nonionic Poly(oxyethylene) Surfactants, As Studied by Spin Probe and Fluorescence Probe Techniques, *J. Phys. Chem.*, 98, 5320-5331 (DOI: 10.1021/j100071a024).

65. Lavan D. A., Terry McGuire T., Langer R. (2003), Small-scale systems for in vivo drug delivery, *Nature Biotechnology,* 21, 1184-1191 (DOI:10.1038/nbt876).

66. Bangham A. D., Standish M. M., Watkins J. C. (1965), Diffusion of univalent ions across the lamellae of swollen phospholipids, *J. Mol. Biol.*, 13, 238-242 (DOI:10.1016/S0022-2836(65)80093-6).

67. Allen T. M., Hansen C., Martin F., Redemann C., Yau-Young A. (1991), Liposomes containing synthetic lipid derivatives of poly(ethylene glycol) show prolonged circulation half-lives in vivo, *Biochim. Biophys. Acta,* 1066, 29-36 (DOI:10.1016/0005-2736(91) 90246-5).

68. Torchilin V. P. (2005), Recent advances with liposomes as pharmaceutical carriers, *Nature Reviews Drug Discovery,* 4, 145-160 (DOI:10.1038/nrd1632).

69. Sharma A., Mayhew E., Bolcsak L., Cavanaugh C., Harmon P., Janoff A., Bernacki R. J. (1997), Activity of paclitaxel liposome formulations against human ovarian tumor xenografts, *Int. J. Cancer,* 71, 103-107 (DOI:10.1002/(SICI)1097-0215(19970328) 71:1<103:: AID-IJC17>3.0.CO;2-J).

70. Sharma A., Mayhew E., Straubinger R. M. (1993), Antitumor effect of taxol-containing liposomes in a taxol-resistant murine tumor model, *Cancer Res.*, 53, 5877- 5881.

71. Sharma A., Sharma U. S., Straubinger R. M. (1996), Paclitaxel-liposomes for local treatment of intraperitoneal P388 leukemia, *Cancer lett.*, 107, 265-272 (DOI:10.1016/0304-3835(96)04380-7).

72. Charrois G. J. R., Allen T. M. (2004), Drug release rate influences the pharmacokinetics, biodistribution, therapeutic activity, and toxicity of pegylated liposomal doxorubicin formulations in murine breast cancer, *Biochim. Biophys. Acta,* 1663, 167-177 (DOI:10.1016/ j.bbamem.2004.03.006).

73. Gregoriadis G., Ryman B. E. (1971), Liposomes as carriers of enzymes or drugs: a new approach to the treatment of storage diseases, *Biochem. J.*, 124, 58.

74. Gregoriadis G. (1973), Drug entrapment in liposomes, *FEBS Lett.*, 36, 292-296 (DOI:10.1016/0014-5793(73)80394-1).

75. Allen T. M., Cullis P. R. (2004), Drug delivery systems entering the mainstream, *Science,* 303, 1818-1822 (DOI: 10.1126/ science.1095833).

76. Pantos A., Tsiourvas D., Paleos C. M., Nounesis G. (2005), Enhanced Drug Transport from Unilamellar to Multilamellar Liposomes Induced by Molecular Recognition of Their Lipid Membranes, *Langmuir,* 21, 6696-6702 (DOI: 10.1021/ la050211n).

77. Smith A. M., Jaime-Fonseca M. R., Grover L. M., Bakalis S. (2010), Alginate-Loaded Liposomes Can Protect Encapsulated Alkaline Phosphatase Functionality When Exposed to Gastric pH, *J. Agric. Food Chem.*, 58, 4719-4724 (DOI: 10.1021/jf904466p).

78. Choi M. J., Maibach H. I., (2005), Liposomes and niosomes as topical drug delivery systems, *Skin Pharmacol. Physiol*, 18, 209-219 (DOI:10.1159/000086666).

79. Tanaka T., Taneda K., Kobayashi H., Okumura K., Muranishi S., Sezaki, H. (1975), Biopharmaceutical studies on parenteral preparations 10 Application of liposomes to pharmaceutical modification of distribution characteristics of drugs in rat, *Chem. Pharm. Bull.*, 23, 3069-3074 (DOI:10.1248/cpb.23.3069).

80. Vanlerberghe G., (1996), Liposomes in cosmetics how and why? In: Lasic, D., Barenholz, Y. (Eds.), Handbook of Nonmedical Applications of Liposomes, CRC Press, Boca Raton, pp. 77 (ISBN-10: 0849340128).

81. Dufour P., Laloy E., Vuillemard J. C., Simard R. (1996), Liposomes in cheesemaking. In: Lasic, D., Barenholz, Y.(Eds.), Handbook of Nonmedical Applications of Liposomes; CRC Press: Boca Raton, pp 158-164 (ISBN-10: 084934011X).

82. Picon A., Gaya P., Medina M., Nunez, M. (1997), Proteinases encapsulated in stimulated release liposomes for cheese ripening, *Biotechnol. Lett.,* 19, 345-348.

83. Taylor T. M., Davidson P. M., Bruce B. D., Weiss, J. (2005), Liposomal nanocapsules in food science and agriculture. *Crit. Rev. Food Sci. Nutr.*, 45, 587-605.

84. Were L. M., Bruce B. D., Davidson P. M., Weiss, J. (2003), Size, stability, and entrapment efficiency of phospholipid nanocapsules containing polypeptide antimicrobials, *J. Agric. Food. Chem.*, 51, 8073-8079 (DOI: 10.1021/jf0348368).

85. Sharma A., Sharma U. S. (1997), Liposomes in drug delivery: progress and limitations, *Int J. Pharma.*, 154, 123-140 (DOI: 10.1016/S0378-5173(97)00135-X).

86. Allen T. M., Cleland L. G. (1980), Serum-induced leakage of liposome contents, *Biochim. Biophys. Acta*, 597, 418-426 (DOI: 10.1016/0005-2736(80)90118-2).

87. Cullis P. R. (1976), Lateral diffusion rates of phosphatidylcholine in vesicle membranes: effects of cholesterol and hydrocarbon phase transitions, *FEBS Lett.*, 70, 223-228 (DOI: 10.1016/0014-5793(76)80762-4).

88. Subuddhi U., Haldar S., Sankararaman S., Mishra A. K. (2008), Unusual fluorescence spectral response of 1-(4-N, N-dimethy-laminophenylethynyl) pyrene towards the thermotropic phase change in lipid bilayer membranes, *J. Photochem. Photobiol., A*, 200, 381-387 (DOI:10.1016/j.jphotochem.2008.09.001).

89. Sankaram M. B., Thompson T. E. (1990), Modulation of phospholipid acyl chain order by cholesterol. A solid-state deuterium nuclear magnetic resonance study, *Biochemistry*, 29, 10676-10684 (DOI: 10.1021/bi00499a015).

90. Lee K. D., Oh Y. K., Portnoy D. A., Swanson J. A. (1996), Delivery of Macromolecules into Cytosol Using Liposomes Containing Hemolysin from Listeria monocytogenes, *The J. Biol. Chem.*, 271, 7249-7252 (DOI:10.1074/jbc.271.13.7249).

91. Zucker D., Marcus D., Barenholz Y., Goldblum A. (2009), Liposome drugs' loading efficiency: a working model based on loading conditions and drug's physicochemical properties, *J. Controlled Release*, 139, 73-80 (DOI:10.1016/j.jconrel. 2009.05.036).

92. Wang T., Yang S., Petrenko V. A., Torchilin V. P. (2010), Cytoplasmic Delivery of Liposomes into MCF-7 Breast Cancer Cells Mediated by Cell-Specific Phage Fusion Coat Protein, *Molecular Pharmaceutics*, 7, 1149-1158 (DOI: 10.1021/ mp1000229).

93. Xu Q., Tanaka Y., Czernuszka J. T. (2007), Encapsulation and release of a hydrophobic drug from hydroxyapatite coated liposomes, *Biomaterials,* 28, 2687-2694 (DOI: S0142961207001469).

94. Xu Q., Czernuszka J. T. (2008), Controlled release of amoxicillin from hydroxyapatite-coated poly(lactic-co-glycolic acid) microspheres, *J. Controlled Release,* 127, 146-153 (DOI: S0168365908000722).

95. Jurkiewicz P., Olzùynska A., Langner M., Hof M. (2006), Headgroup Hydration and Mobility of DOTAP/DOPC Bilayers: A Fluorescence Solvent Relaxation Study, *Langmuir,* 22, 8741-8749 (DOI: 10.1021/la061597k).

96. Sÿachl R., Sÿtepanek M., Prochazka K., Humpolíčková J., Hof M. (2008), Fluorescence Study of the Solvation of Fluorescent Probes Prodan and Laurdan in Poly (E-caprolactone)-block-poly(ethylene oxide) Vesicles in Aqueous Solutions with Tetrahydrofurane, *Langmuir,* 24, 288-295 (DOI:10.1021/ la702277t).

97. Cwiklik L., Aquino A. J. A.,Vazdar M., Jurkiewicz P., Pittner J., Hof M., Lischka H. (2011), Absorption and Fluorescence of PRODAN in Phospholipid Bilayers: A Combined Quantum Mechanics and Classical Molecular Dynamics Study, *J. Phys. Chem. A,* 115, 11428-11437 (DOI:10.1021/jp205966b).

98 . Hutterer R., Schneider F. W., Sprinz H., Hof M. (1996), Binding and Relaxation Behaviour of Prodan and Patman in Phospholipid Vesicles: A Fluorescence and 1H NMR Study, *Biophys. Chem.,* 61, 151-60 (DOI: 10.1016/s0301-4622(96)02185-0).

99. Lin C. M., Chang G. P., Tsao H. K., Sheng Y. J. (2011), Solubilization mechanism of vesicles by surfactants: Effect of hydrophobicity, *J. Chem. Phys.,* 135, 045102-045110 (DOI: http://dx.doi.org/10.1063/1.3615540).

100. Jackson M. L., Schmidt C. F., Lichtenberg D., Litman B. J., Albert A. D. (1982), Solubilization of phosphatidylcholine bilayers by octyl glucoside, *Biochemistry*, 21, 4576-4582 (DOI:10.1021/ bi00262a010).
101. Lichtenberg D., Robson R. J., Dennis E. A., (1983), Solubilization of phospholipids by detergents structural and kinetic aspects, *Biochim. Biophys. Acta*, 737, 285-304 (DOI: 0304415783900047).
102. Kragh-Hansen U., Maire M. le., Moller J. V. (1998), The Mechanism of Detergent Solubilization of Liposomes and Protein-Containing Membranes, *Biophys. J.*, 75, 2932-2946 (DOI: S0006349598777355).
103. Donovan J. M., Timofeyeva N., Carey C. M. (1991), Influence of total lipid concentration, bile salt:lecithin ratio, and cholesterol content on inter-mixed micellar/vesicular (non-lecithin-associated) bile salt concentrations in model bile, *J. Lipid Res.*, 32, 1501-1512.
104. Toimila P., Prieto G., Mi~nones J. Jr, Trillo J. M., Sarmiento F. (2012), Monolayer and brewster angle microscopy study of human serum albumin-dipalmitoyl phosphatidyl choline mixtures at the air–water interface, *Colloids Surf. B: Biointerfaces*, 92, 64-73 (DOI: S0927776511006813).
105. Hoekstra D., Scherphoft G. (1979), Effect of fetal calf serum and serum protein fractions on the uptake of liposomal phosphatidylcholine by rat hepatocytes in primary monolayer culture, *Biochim. Biophys. Acta*, 551,109-121 (DOI: 0005273679903572).
106. Sabín J., Prieto G., Ruso J. M., Messina P. V., Salgado F. J., Nogueira M., Costas M., Sarmiento F. (2009), Interactions between DMPC Liposomes and the Serum Blood Proteins HSA and IgG, *J. Phys. Chem. B*, 113, 1655-1661 (DOI:10.1021/jp804641e).

107. Toimil P., Prieto G., Miñones J. Jr., Sarmiento F. (2010), A comparative study of F-DPPC/DPPC mixed monolayers. Influence of subphase temperature on F-DPPC and DPPC monolayers, *Phys. Chem. Chem. Phys.*, 12, 13323-13332 (DOI:10.1039/C0CP00506A).

108. Toimil P., Prieto G., Miñones J. Jr., Trillo J. M., Sarmiento F. (2012), Interaction of human serum albumin with monofluorinated phospholipid monolayers, *J. Colloid Int. Sci.*, 388, 162-169 (DOI: S0021979712009460).

109. Martinez-Landeira P., Ruso J. M., Prieto G., Sarmiento F., Jones M. N., (2002), The Interaction of Human Serum Albumin with Dioctanoylphosphatidylcholine in Aqueous Solutions, *Langmuir*, 18, 3300-3305 (DOI:10.1021/la011681u).

110 . Melo M. N., Castanho M. A. R. B. (2012), The Mechanism of Action of Antimicrobial Peptides: Lipid Vesicles vs. Bacteria, Front Immunol., 3, 236-239 (DOI: 10.3389/fimmu.2012.00236).

111. Henriques S. T., Huang Y. H., Rosengren, K. J., Franquelim H. G., Carvalho F. A., Johnson A., Sonza S., Tachedjian G., Castanho, M.A.R.B., Daly N. L., Craik D. J. (2011), Decoding the Membrane Activity of the Cyclotide Kalata B1. The Importance of Phosphatidiletanolamine Phospholipids and Lipid Organization on Hemolytic and anti-HIV Activities, *J. Biol. Chem.*, 286, 24231-24241 (DOI: 10.1074/jbc.M111.253393).

112. Freire J. M., Veiga A. S., de la Torre B. G., Andreu D., Castanho M.A.R.B. (2013), Quantifying molecular partition of cell-penetrating peptides-cargo supramolecular complexes into lipid membranes: optimizing peptide-based drug delivery systems, *J. Pep. Sci.*, 19, 182-189 (doi.org/10.1002/psc.2477).

113. Carvalho F. A., Carneiro F. A., Martins I. C., Assunção-Miranda I, Faustino A. F., Pereira R. M., Bozza P. T., Castanho M. A. R. B., Mohana-Borges R, Da Poian A. T., Santos N. C. (2012),Dengue virus capsid protein binding to hepatic lipid droplets (LD) is potassium ion dependent and is mediated by LD

surface proteins, *J Virol.*, 86, 2096-2108 (doi.org/10.1128/jvi.06796-11).

114. Freire J. M., Domingues M. M., Matos J., Melo M. N., Veiga A. S., Santos N. C., Castanho M. A. R. B. (2011),Using Zeta-potential Measurements to Quantify Peptide Partition to Lipid Membranes, *Eur Biophys J.,* 40, 481-487 (DOI: 10.1007/s00249-010-0661-4).
115. Busher, J. T., (1990), The History, Physical, and Laboratory Examinations. In: Walker, H. K., Hall, W. D., Hurst, J. W. (Eds.), Clinical Methods 3rd ed, Butterworths : Boston, 497-499 (ISBN-10: 040990077X).
116. He X. M., Carter D. C. (1992), Atomic structure and chemistry of human serum albumin, *Nature*, 358, 209-215 (DOI:358209a0).
117. Carballal S., Radi R., Kirk M. C., Barnes S., Freeman B. A., Alvarez, B. (2003), Sulfenic Acid Formation in Human Serum Albumin by Hydrogen Peroxide and Peroxynitrite, *Biochemistry*, 42, 9906-9914 (DOI:10.1021/bi027434m).
118. Peters T. Jr., (1977), Serum albumin: recent progress in the understanding of its structure and biosynthesis, *Clinical Chemistry*, 23, 15-12.
119. Sugio S., Kashima A., Mochizuki S., Noda M., Kobayashi K. (1999), Crystal structure of human serum albumin at 2.5 Å resolution, *Prot. Engg.,* 12, 439-446 (DOI:10.1093/protein/ 12.6.439).
120. Kragh-Hansen U. (1981), Molecular aspects of ligand binding to serum albumin, *Pharmacol. Rev.* 33, 17-53.
121. Curry S. (2002), Beyond Expansion: Structural studies on the transport roles of human serum albumin, *Vox Sang.* 83, 315-319 (DOI:10.1111/j.1423-0410.2002.tb05326.x).

122. Curry S., Mandelkow H., Brick P., Franks N. (1998), Crystal structure of human serum albumin complexed with fatty acid reveals an asymmetric distribution of binding sites, *Nature Struc. Mol Biol.*, 5, 827-835 (DOI:1869).

123. Ghuman J., Zunszain P. A., Petitpas I., Bhattacharya A. A., Otagiri M., Curry S. (2005), Structural Basis of the Drug-binding Specificity of Human Serum Albumin, *J. Mol. Biol.*, 353, 38-52 (DOI:S0022283605008855).

124. Bhattacharya A. A., Grune T., Curry S. (2000), Crystallographic analysis reveals common modes of binding of medium and long-chain fatty acids to human serum albumin, *J. Mol. Biol.*, 303, 721-732 (DOI:S0022283600941585).

125. Carter D. C., Ho J. X. (1994), Structure of serum albumin, *Adv Prot. Chem,* 45, 153-203 (http://dx.doi.org/10.1016/s0065-3233(08) 60640-3).

126. Carter D. C., He X. M., Munson S. H., Twigg P. D., Gernert K. M., Broom M. B., Miller T. Y. (1989), Three-dimensional structure of human serum albumin, *Science,* 244, 1195-1198 (http://dx.doi.org/10.1126/science.2727704).

127. Dockal M., Carter D. C., Ruker F. (1999), The three recombinant domains of human serum albumin: structural characterization and ligand binding properties, *The J. Biol. Chem.,* 274, 29303-29310 (http://dx.doi.org/10.1074/jbc.274.41.29303).

128. Wardell M., Wang Z., Ho J. X., Robert J., Ruker F., Ruble J., Carter D. C. (2002), The Atomic Structure of Human Methemalbumin at 1.9 Å, *Biochem. Biophys. Res. Comm.*, 291, 813-819 (DOI: S0006291X0296540X).

129. Sudlow G., Birkett D. J., Wade D. N. (1976), Further Characterization of Specific Drug Binding Sites on Human Serum Albumin, *Mol. Pharm.*, 12, 1052-1061.

130. Petitpas I., Bhattacharya A. A., Twine S., East M., Curry S. (2001), Crystal Structure Analysis of Warfarin Binding to Human Serum Albumin: Anatomy of Drug Site I, *The J. Biol. Chem.*, 276, 22804-22809 (DOI: 10.1074/jbc.M100575200).
131. Choi J. K., Ho J., Curry S., Qin D., Bittman R., Hamilton J. A. (2002), Interactions of very long-chain saturated fatty acids with serum albumin, *J. Lipid Res.*, 43, 1000-1010 (DOI:10.1194/jlr. M200041-JLR200).
132. Bhattacharya A. A., Curry S., Franks N. P. (2000), Binding of the General Anesthetics Propofol and Halothane to Human Serum Albumin, *The J. Biol. Chem.*, 275, 38731–38738 (http://dx.doi.org/10.1074/jbc.m005460200).
133. Fasano M., Curry S., Terreno E., Galliano M., Fanali1 G., Narciso P., Notari S., Ascenzi P. (2005), The Extraordinary Ligand Binding Properties of Human Serum Albumin, *IUBMB Life*, 57, 787 – 796 (DOI:WQ428PW07QLU4258).
134. Fehske K. J., Muller W. E., Wollert U. (1981), The location of drug binding sites in human serum albumin, *Biochem. Pharmacol*, 30, 687-692 (DOI: 0006295281901519).
135. Kragh-Hansen U., (1990), Structure and ligand binding properties of human serum albumin, Dan Med Bull, 37, 57-84.
136. Kratochwil N. A., Huber W., Muller F., Kansy M., Gerber P. R. (2002), Predicting plasma protein binding of drugs: a new approach, *Biochem Pharmacol*, 64, 1355-1374 (DOI:S0006295202010742).
137. Kindt, T. J., Goldsby, B. A., Osborne, B. A., Kuby, J. (2006), Kuby Immunology, sixth ed. W. H. Freeman, New York, pp. 76-110 (ISBN-10: 1429202114).
138. Buxbaum, E. (2007), Fundamentals of Protein Structure and Function, Springer Science. New York, pp. 137-158 (ISBN-10: 079237858X).

139. Cohn M., Deutsch H. F., Wetter L. R. (1950), Biophysical Studies of Blood Plasma Proteins. XIII: Analysis of Immunological Heterogeneity of Human Gamma Globulin Fractions, *J Immunol,* 64, 381-395.

140. Judith, A., Owen, J. P., Stranford S. A. (2013), Kuby Immunology, seventh ed. W. H. Freeman, New York, pp. 59-105 (ISBN-10: 142921919X).

141. Alt F. W. (2011), Advances in Immunology. Pavri R., Nussenzweig M. C. (ed), Academic Press, London, pp. 2-18 (ISBN-10: 012387663X).

142. Nezlin R., (1998), General characteristics of Immunoglobulin molecules. In: The Immunoglobulins structure and function, Academic press, London, pp. 1-62 (ASIN: B00CLW8LDI).

143. Janeway, C. A. Jr, Travers, P., Walport, M., Shlomchik M. (2004), The immune system in health and disease. In: Immunobilogy sixth ed, Garland Science, New York, pp 154-164 (ISBN-10: 0815341016).

144. Harris L. J., Skaletsky E., McPherson A. (1998), Crystallographic Structure of an Intact IgG1 Monoclonal Antibody, *J. Mol. Biol.*, 275, 861-872 (DOI: S0022283697915084).

145. Schaller, J., Gerber, S., Kaempfer, U., Lejon, S., Trachsel, C, (2008), The Immune System. In: Human Blood Plasma Proteins: Structure and Function, Wiley, Singapore, pp. 195-209 (ISBN: 10: 0470016744).

146. Harris L. J., Larson S. B., Hasel K. W., Day, J., Greenwood A., McPherson A. (1992), The three-dimensional structure of an intact monoclonal antibody of canine lymphoma, *Nature***,** 360, 369-372 (DOI:360369a0).

147. Saphire E. O., Parren P. W., Pantophlet R., Zwick M. B., Morris G. M., Rudd P. M., Dwek R. A., Stanfield R. L., Burton D. R., Wilson, I. A. (2003), Glycobiology and Medicine, Axford J. S. (ed), Plenum Press, New York, pp. 55-56 (978-1-4613-4908-2).

148. Chothia C., Novotny J., Bruccoleri R., Karplus M. (1985), Domain association in immunoglobulin molecules, *J. Mol. Biol.*, 186, 651 (DOI:0022283685901378).

149. Amze, L. M., Poljak R. J. (1979), Three-Dimensional Structure of Immunoglobulins, *Annu. Rev. Biochem.,* 48, 961 (DOI:10.1146/ annurev.bi.48.070179.004525).

150. Relkin P., Kamyshny A., Magdassi S. (2000), Changes in Calorimetric Parameters and Solvent Accessibility of Hydrophobic Groups in Native and Chemically Modified Immunoglobulin G, *J. Phys. Chem. B,* 104, 4980-4985 (DOI: 10.1021/jp993350k).

151. Rispens T., Lakemond C. M. M., Derksen N. I. L., Aalberse R. C. (2008), Detection of conformational changes in immunoglobulin G using isothermal titration calorimetry with low-molecular-weight probes, *Anal. Biochem.,* 380, 303 (DOI:S0003269708003734).

152. Parker C. W., Osterland C. K. (1970), Hydrophobic binding sites on immunoglobulins, *Biochemistry.,* 9, 1074 (DOI:10.1021/ bi00807a004).

153. Taves, C. J., Kusumi, A., Winkethake, J. L. (1984), Human aglycosyl-IgG exhibits increased hydrophobicity: Binding/ fluorescence studies with 8-anilinonaphthalene-1-sulfonic acid (ANS), *Biochem. Biophys. Res .Comm.* 1984, 124, 605 (DOI:0006291X84915973).

154. Vermeer A. W. P., Norde W. (2000), The Thermal Stability of Immunoglobulin: Unfolding and Aggregation of a Multi-Domain Protein, *Biophys., J.,* 78, 394 (DOI:S0006349500766021).

155. Ross D. L., Jirgensons B. (1968), The Far Ultraviolet Optical Rotatory Dispersion, Circular Dichroism, and Absorption Spectra of a Myeloma Immunoglobulin, Immunoglobulin G, *J. Biol. Chem.*, 243, 2829.

156. Cathou R. E., Kulczycki A., Haber E., (1968), Structural features of γ-immunoglobulin, antibody and their fragments. Circular dichroism studies, *Biochemistry*., 7, 3958 (DOI:10.1021/bi00851a024).

157. Edelman, G. M., Gall W. E. (1969), The Antibody Problem, *Annu. Rev. Biochem.*, 38, 415 (DOI:10.1146/annurev.bi.38. 070169.002215).

158. Frangione B., Milstein C., Franklin E. C. (1971), Interchain and Intrachain Disulfide Bridges of a Human Immunoglobulin M: Detection of a Unique Fragment, *Proc. Nat. Acad. Sci.*, 68, 1547-1551 (doi.org/10.1073/ pnas.68.7.1547).

159. Frangione B., Milstein C. (1971), Disulphide bridges of the heavy chain of human immunoglobulin G1, *Nature*, 216, 939-941 (DOI: 216939b0).

160. Litman G. W., Good R. A., Frommel D., Rosenberg A. (1970), Conformational Significance of the Intrachain Disulfide Linkages in Immunoglobulins, *Proc. Nat. Acad. Sci.*, 67, 1085 (DOI: http://dx.doi.org/10.1073/pnas.67.3.1085).

161. Takada K., Kawamura T., Inai M., Masuda S., Oka T., Yoshikawa Y., Shibata N., Yoshikawa H., Ike O., Wada H., Hitomi S. (1999), Pharmacokinetics of cisplatin in analbuminemic rats, *Biopharm. Drug Dispos.*, 20, 421 (DOI: 10.1002/1099-081X(199912)20:9<421::AID-BDD206> 3.0.CO;2-9).

Chapter 2

Instrumentation and Materials

In this section we briefly discuss the different instruments used for the experiments and the procedures for sample preparations.

2.1 Steady State Absorption and Emission Spectra:

Steady state absorption spectra were taken in a Varian UV-Vis spectrometer (Model: Cary 100). Emission spectra were taken in a Fluoromax-4p fluorimeter from Horiba Jobin Yovon (Model: FM-100). The fluorescence spectra were corrected for the spectral sensitivity of the instrument.

2.2. Measurements of Fluorescence Decays:

TCSPC (Time Correlated Single Photon Counting) Setup: For the time-resolved studies, we used a TCSPC system from Horiba Yovin (Model: Fluorocube-01-NL). The samples were excited at 375 nm using a picosecond diode laser (Model: Pico Brite-375L). The repetition rate was 5 MHz. The signals were collected at magic angle (54.70) polarization using a photomultiplier tube (TBX-07C) as detector, which has a dark counts less than 20 cps. The instrument response function of our setup is 140 ps. A block diagram of our setup is shown below (Figure 2.1).

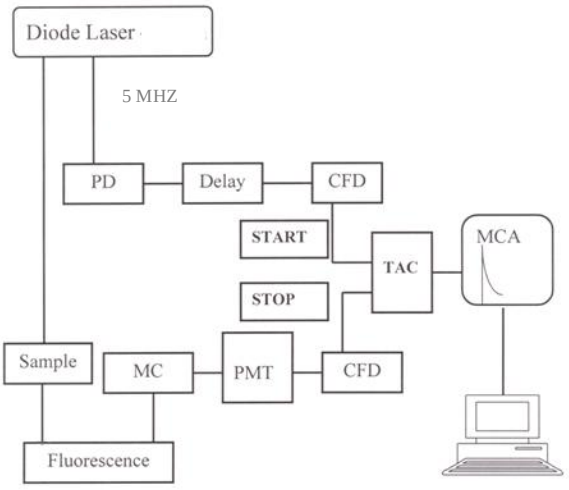

Figure 2.1. *Schematic diagram of TCSPC*

2.2.1. TCSPC Technique:

TCSPC techniques *[1,2,3]* is based on the concept that the probability distribution for emission of a single photon after an excitation event yields the actual intensity versus time distribution of all the photons emitted as a result of the excitation. By statistically sampling, the single photon emission following a large number of excitation events, the experiment constructs the probability distributions *[1]*. The most important part of a TCSPC system is time-to-amplitude converter (TAC). It measures the elapsed time between the initial rise in intensity of the pulse light source and the detection of an emitted photon from the sample *[4]*. In operation, an electrical pulse is generated at a time exactly correlated with the time of generation of the optical pulse by the trigger. After receiving the trigger pulse, the TAC then initiates the charging of a capacitor plate, which is routed to the TAC start input via a discriminator. The same optical pulse (which triggers the TAC) excites the fluorescent sample. Now only one stop photon is detected for every 100-200 excitations. The signal resulting from the detected photon stops the charging ramp in the TAC, which transmits a pulse. The amplitudes of this pulse is proportional to the charge in the capacitor, and hence to the time difference between the start and stop pulses. The TAC output pulse is given a numerical value within the analog-to-digital converter (ADC) and a count is stored in the data storage in an address corresponding to that number. Excitation and data storage are repeated again and again in this way until the histogram of the number of counts against address numbers (channel number) in the storage devise represents, to some required precision, the decay curve of the sample.

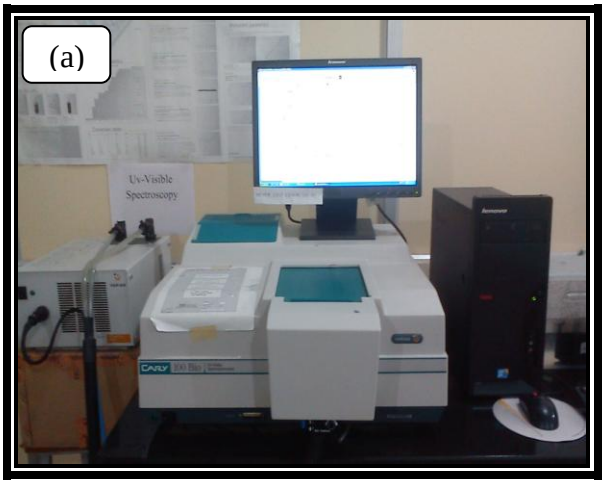

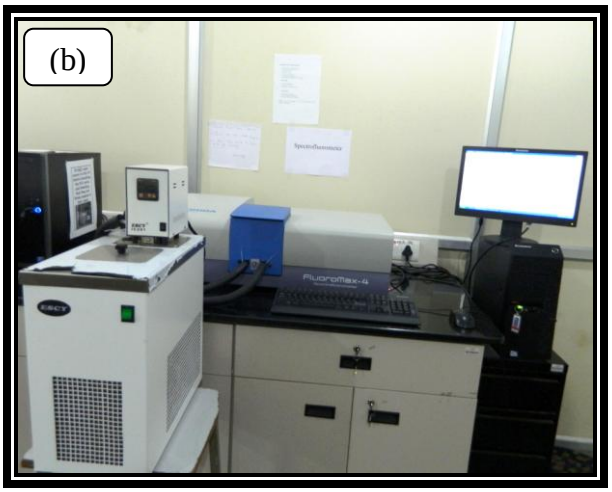

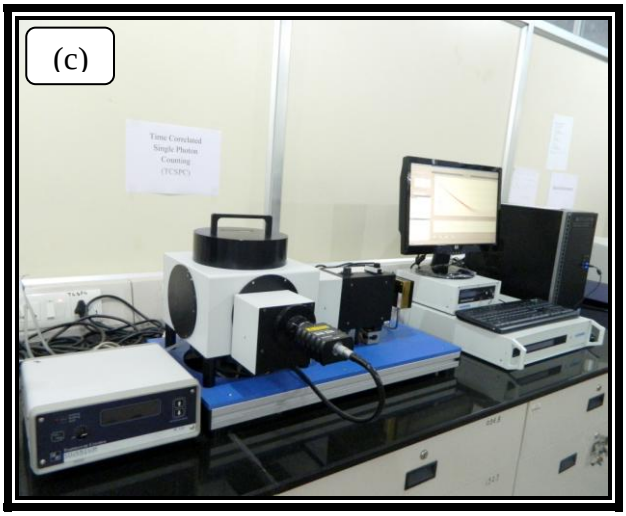

Photographs of Instruments Used: (a) UV-Vis Spectrpphotometer (b) Fluorimeter (c) Time Corelated Single Photon Counting System

2.2.2. Deconvolution Procedure:

Simple time domain decay profiles arise only if the sample is excited with a δ-function (infinitely short) pulse of light. But most real situations involve the excitation pulses that are on the same timescale as the fluorescence process. Now the fluorescence response is convolution of the measured instrumental prompt response *P(t)* and the theoretical fluorescence response function F(t) of the form:

$$R(t) = \int_0^t P(t')F(t-t')dt' \qquad (2.1)$$

where t' defines the variable time delays (in practice, channel numbers) of the infinitesimally small widths dt' (i.e, channel widths) of which *P(t)* is composed.

Numerous method exist to obtain *P(t)* from *R(t)*. But most commonly use method is least-square method in concert with an iterative reconvolution scheme. The convolution integral is then calculated using the test model

$$F(t) = \sum_i \alpha_i e^{t/\tau_i} \qquad (2.2)$$

and using initial set of α_i and τ_i values and the measured instrument response function. The calculated data is compared to observed data and α_i and τ_i terms are adjusted until a best fit is obtained. The quality of the fit is judged by chi-squared (χ^2) test:

$$\chi^2 = \sum_{i=1}^{n} \omega_i [R(t) - R_c(t)]^2 \qquad (2.3)$$

where $R_c(t)$ is calculated values by assuming the functional form of *F(t)* (equation 2.2), ω_i is the weighting factor ($\omega_I = 1/R(t)$), *i* is the number of data points in the decay file. ω_i is follows the Poisson statistics *[1,5]*.

2.2.3. Analysis of Fluorescence Decays:

The data analysis was performed using IBH DAS (version 6, HORIBA Scientific, Edison, NJ) decay analysis software.

2.3. Time Resolved Fluorescence Anisotropy:

2.3.1. An Overview:

Time dependent decays of anisotropy provide considerable additional information about the diffusive motions of the fluorophore *[2, 3]*. These data can reveal whether a fluorophore is free to rotate over all angles, or if the environment surrounding the fluorophore restricts its angular displacement. Fluorescence anisotropy is widely used to study the dynamics in micelles *[6]*, reverse micelles *[7,8]* and lipid bilayers *[9]*.

In the time domain, the sample is excited with a brief pulse of polarized light and the time dependent parallel ($I_{//}(t)$) and perpendicular ($I_{\perp}(t)$) components of the fluorescence are used to form the time-resolved fluorescence anisotropy, $r(t)$:

$$r(t) = \frac{I_{||}(t) - I_{\perp}(t)}{I_{||}(t) + 2I_{\perp}(t)} \qquad (2.4)$$

To compensate the polarization biased of the detection system and monochromator efficiency, the above equation is modified to,

$$r(t) = \frac{I_{||}(t) - GI_{\perp}(t)}{I_{||}(t) + 2GI_{\perp}(t)} \qquad (2.5)$$

Where G is the correction factor introduced for the polarization sensitivity of the detection system and monochromator.

For a simple isotropic rotor, $r(t)$ decays with a single rotational correlation time (τ_r) *[2]*,

$$r(t) = r_0 \exp(-t/\tau_r) \qquad (2.6)$$

For more complicated systems, *r(t)* takes the form of a sum of exponentials:

$$r(t) = r_0 \sum \beta_i \exp(-t/\tau_{r_i}) \qquad (2.7)$$

where β_i and τ_{r_i} are the fractional contribution of total depolarization and rotational correlation times attributed to reorientational motion i, respectively.

In terms of Stokes-Einstein theory, τ_r is related to the medium by,

$$\tau_r = \frac{\eta V}{kT} = \frac{1}{6D} \qquad (2.8)$$

where η is the viscosity of the medium, V is the molecular volume, k is the Boltzmann's constant, T is the absolute temperature, and D is the diffusion coefficient.

Immediately following photoexcitation, the fluorophore has yet to reorient, and the observed anisotropy should be equal to r_0 (the fundamental anisotropy). As time passes, the molecules reorient and the anisotropy decays towards zero. The r_0 value depends on the relative angular orientation between the absorption and emission transition moments. If the rotational motion is hindered or otherwise restricted, one would see that the anisotropy does not decay to zero at longer time. In this case, the fluorescence is said to have a limiting anisotropy, r_∞ and the decay can be represented as

$$r(t) = (r_0 - r_\infty)e^{-t/\tau_r} + r_\infty \qquad (2.9)$$

2.3.2 Methods for Measuring Anisotropy Decays:

The time resolved anisotropy measurements are done by toggling method using time correlated single photon counting technique and exciting the sample by 375 nm using a picosecond diode laser (Model: Pico Brite-375L). In toggling method, a motorized polarizer was used in the emission side. This polariser toggles between parallel and

perpendicular orientations and the emission intensities at parallel ($I_{//}(t)$) and perpendicular ($I_{\perp}(t)$) polarization was collected alternatively for 30 seconds until a certain peak difference between parallel ($I_{//}(t)$) and perpendicular ($I_{\perp}(t)$) decay is reached. The peak difference depends on the tail matching of the parallel ($I_{//}(t)$) and perpendicular ($I_{\perp}(t)$) decay. For typical anisotropy decay the difference between the peak counts at parallel and perpendicular polarization are kept at 2500. The *G* factor is measured by taking two additional decay measurements ($I_{HV}(t)$ and $I_{HH}(t)$) of the same sample with the excitation polariser set to perpendicular or horizontal position, because *G* factor is given by, $G = I_{HV}(t)/I_{HH}(t)$, where $I_{HV}(t)$ and $I_{HH}(t)$ denote the fluorescence decay kinetics of the sample measured using horizontally or perpendicularly (*H*) polarized exciting light and detecting the emission components polarized vertically (*V*) and horizontally (*H*), respectively.

2.3.3. Analysis Technique:

We have analyzed our data by direct analysis method. This method makes use of the decay curves, $I_{//}(t)$ and $I_{\perp}(t)$, together with the *G* factor, to calculate the anisotropy decay curve directly, point by point:

$$r(t) = \frac{I_{||}(t) - GI_{\perp}(t)}{I_{||}(t) + 2GI_{\perp}(t)} = \frac{I_D(t)}{I_T(t)} \qquad (2.10)$$

This method does not use reconvolution analysis and therefore does not require measurements of decay of lamp profiles at parallel and perpendicular orientations of the emission polarizer. The $r(t)$ curve obtained can then be analyzed using any of the experimental fitting programs, in terms of a number of exponential decay components, superimposed on a static anisotropy, r_{∞}. The general form of the fitting equation is,

$$r(t) = A + \sum_i B_i \exp^{-t/\tau_{r^i}} \qquad (2.11)$$

Here, A is related to the residual or static anisotropy, r_∞ and B is related to contribution of the each component of rotational correlation time (τ_r).

2.4. Other Instruments:

2.4.1. Circular Dichroism (CD):

CD is a sensitive technique to monitor the conformational changes in proteins. CD spectra of HSA and its lipid complexes were recorded with a Jasco J-815 spectrometer (Jasco, Tokyo, Japan). For measurements in the near UV region (200-270), a quartz cell with a path length of 0.1 cm (Hellma, Muellheim/Baden, Germany) was used in nitrogen atmosphere. The protein concentration was 10µm for HSA and 2µm for IgG. An accumulation of five scans with a scan speed of 20 nm/min was performed data were collected for each sample from 200 to 270 nm. The sample temperature was maintained at 25ºC using Escy temperature controller circulating water bath connected to the water-jacketed quartz cuvettes. Spectra were corrected for buffer signal.

2.4.2. Transmission Electron Microscope (TEM):

A 10µl sample of lipid was loaded onto Formvar-coated, copper grids and was dried for 1 minute. Excess fluid was removed from the grids and then a 10µl of 1% sodium phosphotungstate was applied on the same grid, after which the excess stain was similarly removed from the grids. The sample-containing grid was air dried and then examined by a Philips CM200 TEM microscope.

Principle: In TEM the wavelength of illumination is produced by an energized beam of electrons which increases greatly the resolving capabilities of image. So, the main use of this technique is to examine the submicroscopic details of the specimen. Using an electron microscope offers the advantage of increasing both the magnification of an object and the resolution over other imaging tools. Deflection in TEM is due to the electromagnetic properties of the lens which are

defined by electromagnetic plates that are able to deviate the electrons in the trajectory of the electrons from a point source which causes them to converge at a single focal point. By this way, the electron beam is focused precisely.

There are essentially three types of lenses used to form the final image in the TEM. These are the condenser, objective, and projector lenses. The function of the condenser lens is to concentrate and focus the beam of electrons coming off of the filament onto the sample to give a uniformly illuminated sample. The objective lens forms the initial enlarged image of the illuminated portion of the specimen in a plane that is suitable for further enlargement by the projector lens.

Those electrons that pass through the sample go on to form the image, while those that are stopped or deflected do not contribute in image formation. In this way a black and white image is formed. The smaller aperture is used to prevent the flow of scatter electrons. The projector lens is used to project the final magnified image onto the phosphor screen or photographic emulsion. Thus total magnification is a product of the objective and projector magnifications.

Another important element of the TEM is the vacuum system. Vacuum system avoids collisions between electrons of the beam and stray molecules. Which results in a spreading or diffusing of the beam in volatization event if the molecule is organic in nature.

For a conventional TEM analysis, a specimen has to be reasonably dried and thin to ensure the proper imaging *[10]*.

2.4.3. Atomic Force Microscope:

For atomic force microscopy image, Images were recorded in an AIST-NT instrument; model No. smart SPM 1000 in soft tapping-mode.

Principle: AFM provides a 3D profile of the surface, on a nanoscale by measuring force between a sharp probe (<10 nm) and surface at very short distance (0.2-10 nm probe sample separation). The probe is

supported on a flexible cantilever. The AFM tip gently touches the surface and records the small force between the probe and the surface. In AFM, mechanical force interactions acting between a sharp probe and a sample are used for surface imaging. The probe, which represents a micromachined cantilever with a sharp tip at one end, is brought into interaction with the sample surface. The interaction level between the tip apex and the sample is determined through precise measurements of the cantilever displacements amplified to generate height images, which reflect surface corrugations. The height image, in which brighter contrast is assigned to elevated surface locations, represent the vertical translations of the piezo-scanner needed to eliminate the error signal when the probe is moved from one sample location to the other. *[11]*.

2.5. Molecular Docking:

The crystal structure of HSA, F_{ab} and F_c fragments of IgG were downloaded from Protein Data Bank (PDB entry 1AO6, 1N0X and 4BYH respectively). The energy minimized conformation of Ellipticine was generated by using a web-server known as *FROG [12]* (Frog2 version), which generates energy-minimized conformations using *AMMOS [13]*. This conformation of ligand was used further for docking with the protein. Preparation of the target proteins for docking using Autodock tools involved removal of all water molecules from PDB files, addition of polar hydrogen atoms and assigning Gasteiger charges to the proteins. Docking was carried out with Autodock 4.2 Lamarckian Genetic Algorithm. A grid size of 56 x 40 x 58 $Å^3$ with a grid spacing of 0.375 Å for HSA, grid size of 120 x 124 x 90 $Å^3$ with a grid spacing of 0.642 Å for F_{ab} fragment of IgG and grid size of 124 x 70 x 60 $Å^3$ with a grid spacing of 0.625 A° for F_c fragment of IgG were used respectively. All other docking parameters were kept as default. *PyMol* was used for visualization and measurement of distances between the atoms of ligand and the residues of protein.

The solvent accessible surface area (ASA) of all the amino acid residues in uncomplexed proteins and in protein-Ellipticine docked complexes of three proteins HSA, F_{ab} and F_c regions of IgG were calculated using *NACCESS [14]*. The best docked conformation of the ligand in each case of docking was selected and composite coordinates were generated to form the docked complex. The change in ASA (ΔASA) for a particular residue of a protein due to interaction with ligand was calculated as a difference between the ASA of the residue before and after interaction. If ASA of a residue lost significantly on interaction with the ligand, it was considered as being involved in interaction.

2.6. Materials:

2.6.1. Different Fluorophores:

Fluoroquinolone (Norfloxacin and Ofloxacin), Ellipticine and PRODAN (Fig 2.2) were purchased from Sigma Aldrich and were used as received.

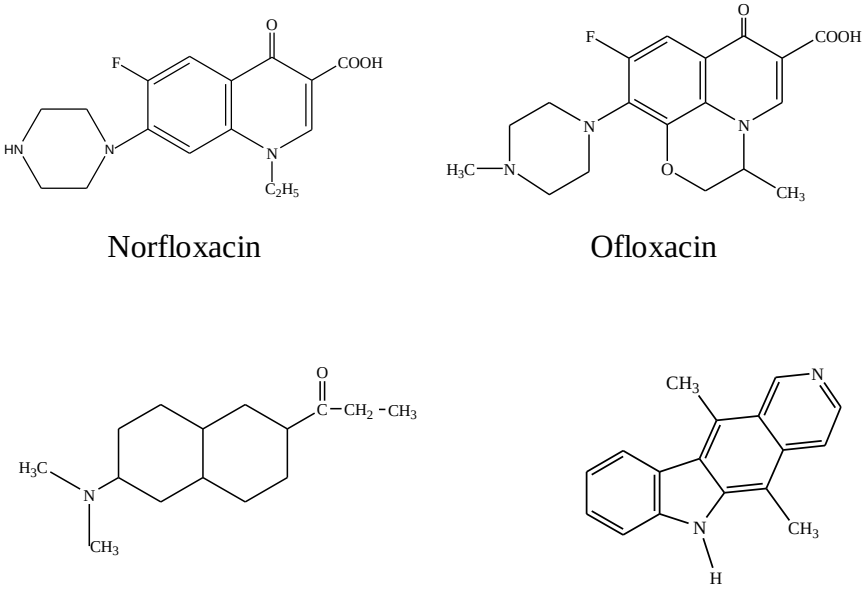

Figure 2.2. *Structures of Various Fluorophores.*

2.6.2. Photophysical relevance of various fluorophores:

(a) Fluoroquinolone: Fluoroquinolones are the class of important antibacterial agents, which display a broad spectrum of antibacterial activity and are used to treat bacterial urinary tract infections, sexually transmitted diseases such as prostatitis, selected pneumonias and skin infections *[15,16,17,18,19]*. Fluoroquinolone molecules, such as NOR and OFL contain a carboxyl group and at 7-carbon atom a piperazinyl group. Consequently, acid–base behavior and antibacterial response of fluoroquinolones depends on the physiochemical properties of solvent *[20,21,22,23,24]*. The degree of ionization of fluoroquinolone molecules depends on the pH of the system *[25,26]*. It is found that fluoroquinolone molecules have proton binding sites at carboxylic acid group and terminal nitrogen atom of piperazinyl ring. Thus, fluoroquinolone molecules exhibit two protolytic equilibria with two different pK_a values. The $pK_{a1}$and pK_{a2} of OFL and NOR are 6.10, 8.28 and 6.23, 8.55, respectively *[27,28]*. Therefore, depending upon the pH of the solvents, fluoroquinolone molecules take different forms. It is already reported that fluoroquinolone molecules exist in four different forms at physiological pH *[18,19]*. Several groups reported the spectroscopic details of the individual species. The photophysical and photochemical properties of fluoroquinolone molecules have been well characterized in conventional solvents and solvent mixtures. However, the modulation of prototropic equilibrium and biodistribution of this kind of molecules in different biomimetic environment are not well known. In the excited state, fluoroquinolone molecules undergo a twisted intramolecular charge transfer (TICT) and fluorescence spectra exhibit a reverse solvatochromism in the mixed solvents *[24,25]*. As NOR and OFL are good TICT molecules in the excited state and show better antibacterial activity so; photophysical properties of these molecules are examined in biomimetic systems *[18]*. Recently, Sortino reported photochemical study of some fluoroquinolones in sodium dodecyl sulfate (SDS) micelles at physiological pH *[29,30]*. It was proposed in their study that at

micellar surface fluoroquinolone molecule takes a cationic form and thus attracted to the anionic surfactant.

(b) Ellipticine: Ellipticine is a pyridocarbazole-type plant alkaloid, which exhibits cytotoxic activity against various tumor cells *[31]*. These pyridocarbazoles interact with DNA and actively treat solid tumors like breast cancer cells, renal carcinoma and lung cancer cells *[32,33]*. The biological action of these pyridocarbazoles result in direct binding to DNA *[34]*. They induce protein associated DNA strand break by trapping Topoisomerase II. The cytotoxicity of Ellipticine is believed to be primarily related to two modes of action: (i) intercalation in to DNA and (ii) inhibition of Topoisomerase II activity *[35,36,37,38,39]*.Recently, Ellipticine was reported to have application in the treatment of obesity and tested for human pre-AIDS treatment in association with other drugs *[40]*. A substantial research work has been devoted to understand the biological activity, sequence selectivity, and metabolism of Ellipticine for several years *[41,42,43,44,45,46,47,48,49,50,51]*. Fung et al. reported photophysical properties of Ellipticine in different solvents varying the polarity and hydrogen bonding *[52]*. The authors found a large Stokes shift (10,000 cm^{-1}) in polar solvents compared to that (8900 cm^{-1}) in non-polar solvents. Miskolczy et al. suggested that in methanol photoinduced protonation by the solvent, instead of 'quinoid-like' tautomerization, takes place *[53,54]*. Very recently Samanta and co-workers *[55]* reported that in methanol, the second emission band occurs due to an excited state reaction. The study suggests that an excited state reaction involves solvent reorganization around Ellipticine to form a ''cyclic'' solvated species, which facilitates a rapid proton transfer and the two emission bands arise from the normal and tautomeric forms. Ellipticine exists as protonated or deprotonated species in aqueous medium depending on the pH *[56,57,58]*. At pH value below 7.4, due to protonation of pyridine like nitrogen cationic species are prevalent*[56]*. Studies in living cells have revealed that Ellipticine exists both in neutral and protonated forms in aqueous cytoplasm, but

only in its protonated form in the nucleus *[58]*. The major shortcomings in usage of neutral Ellipticine as pharmaceuticals are its toxicity and low solubility in water but cationic Ellipticine is relatively more soluble in water than neutral Ellipticine. To surmount the trouble of low solubility of Ellipticine in aqueous media, the drug was attached to polymers, peptides, micelles and liposomes *[59,60,61,62]*. Therefore, such amphiphilic systems are desired which can modulate the different prototropic species of Ellipticine.

(c) PRODAN: PRODAN (6-propionyl 1,2-dimethylamino-naphthalene) is chosen as a probe primarily to study the environment inside the liposomes and various proteins. PRODAN is very sensitive towards environmental polarity and the origin of its solvatochromatic nature have been debated *[63,64,65,66,67]*. When it is attached to membranes it shows large spectral shifts *[68,69,70]*. PRODAN emits at around 390 nm in cyclohexane whereas its emission in water is around 520 nm. This sensitivity towards polarity is attributed to a large difference between the dipole moments in its ground (S_0) and excited (S_1) states *[71,72]*. According to various calculations, difference in dipole moment of PRODAN from 5.50 to 10.20 D causes a shift in the $S_0 \rightarrow S_1$ transition*[73]*. Recently Samanta and co-workers *[74]* have suggested this value to be 4.4-5.0 D based on transient dielectric loss measurements. In RPODAN, locally excited (LE) and twisted internal charge transfer (TICT) states simultaneously exist *[75,76,77]*. This amazing feature of PRODAN makes it a useful probe to study structure, function and dynamics of proteins and membranes *[78,79,80,81,82]*. The probe has widely been used to study the dynamics inside a reverse micelles. It was reported that in reverse micelle with sufficient water content the PRODAN molecules are distributed in three regions, according to the polarity of that particular region *[83,84,85,86,87,88,89]*. PRODAN is having higher water solubility and is loosely anchored to the bilayer *[90,91]*. Hof and co-workers studied solvent relaxation of various probes including PRODAN in phosphocholine vesicles *[92,93,94]*. The emission

maximum of PRODAN depends upon the phase state of phospholipids. It usually emits at 440 nm in gel and at 490 nm in liquid crystalline phase. The shift in emission band from gel to liquid crystalline phase takes place due to dipolar relaxation in liquid crystalline phase of phospholipid but not in gel phase. This dipolar relaxation originates due to a few water molecules present in bilayer at the glycerol backbone where fluorescence moiety of PRODAN actually resides *[95,96]*. The complex character of emission peak of PRODAN in the lipid bilayer can be explained assuming that both twisted and planar configuration emit in the bilayer *[94]*. As emission of PRODAN is highly sensitive, it has been used to study different protein molecules *[97,98,99,100,101,102]*. Hydration dynamics studies of HSA using PRODAN as probe reveals that hydration level of different domains is different and they have different time scales for hydration *[103,104]*. The free thiol group allows site specific labeling of protein with chromophoric or fluorescent probes *[105,106]*.

2.6.3. <u>Different Surfactants, Proteins, and Lipids:</u> Sodium deoxycholate (NaDC), Sodium taurocholate (NaTC), Sodium cholate (NaC), Sodium glycodeoxy cholate (NaGDC), Sodium taurodeoxy cholate (NaTDC), dioctylsulphosuccinate sodium salt (AOT), 1,2-dipalmitoyl-sn-glycero-3-phosphocholine (DPPC), 1,2-dimyristoyl-sn-glycero-3-phosphocholine (DMPC), 1,2-dioleoyl-sn-glycero-3-phosphocholine (DOPC), 2-oleoyl-1-palmitoyl-sn-glycero-3-phosphocholine (POPC), Human Serum Albumin (HSA), Immunoglobulin G (IgG).

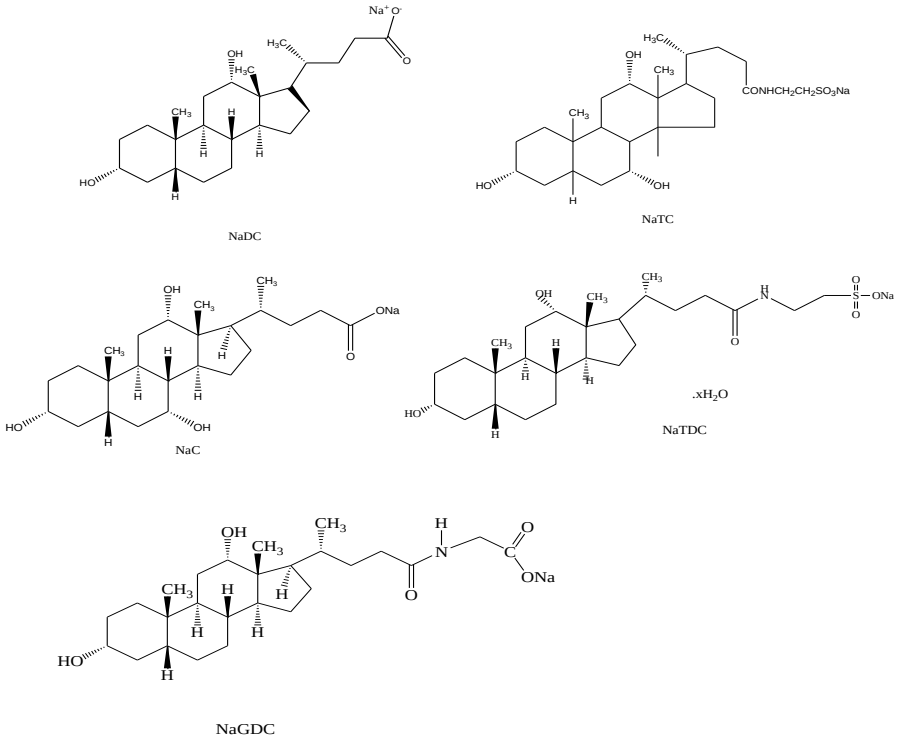

Figure 2.3. *Structure of various bile salts*

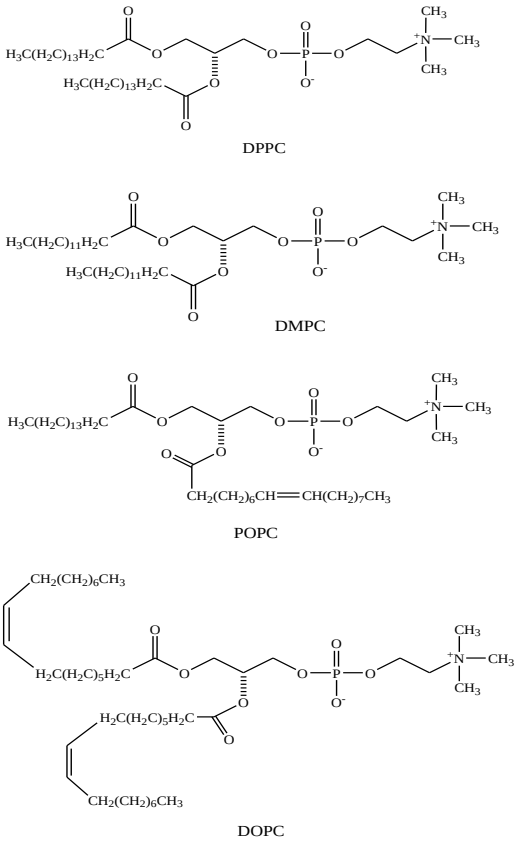

Figure 2. 4. *Structures of various lipids.*

2.7. Preparation of Solution:

2.7.1 Preparation of Buffer Solution:

The phosphate buffer was prepared using NaH_2PO_4 and Na_2HPO_4 purchased from Merck chemicals. Tris HCl was purchased from Rankem India. Buffer solutions were prepared in Rankem HPLC grade water and Milli Q water. The pH of buffer solutions was adjusted at 7.4 using a Eutech pH Tutor.

2.7.2 Preparation of fluorophore Solution:

Solutions of various fluorophores were prepared using either of these buffer solutions. These aqueous fuorophore solutions were sonicated for almost 60 minutes to ensure the complete solubility. We passed argon gas to remove the dissolved oxygen from the buffer solution prior to any experimental measurements.

2.7.3 Preparation of water and methanol reverse micelles:

AOT (bis-2-ethyl hexyl sulfosuccinate sodium salt, Aldrich) was dried under high vacuum for 48 hours and was used without purification. n-Hexane spectroscopic grade (Sigma Aldrich) was used to create water reverse micelles and methanol reverse micelles respectively. These solvents were freshly distilled over calcium hydride (Sigma Aldrich) before use. The water content and methanol content inside the reverse micellar pool are defined as

$$w_0 = \frac{[water]}{[AOT]} \text{ and } w_m = \frac{[methanol]}{[AOT]}.$$

The concentration of probe molecules maintained in all the measurements is 5×10^{-7} M and that of AOT is 0.09 M.

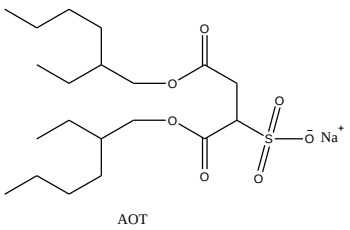

AOT

Figure 2.5 *Structure of AOT*

2.6.4. Preparation of small unilamellar vesicles:

The stock solution of lipid was prepared in ethanol. The desired amount of ethanolic lipid solution was injected rapidly into the aqueous solution of Ellipticine at temperature above the phase transition temperatures of respective lipids (DPPC 50°C, DMPC 23°C, DOPC -20°C, POPC -2°C). This solution was then equilibrated for 60 minutes. The concentration of lipid in the solution was 0.4 mM and the percentage of ethanol was less than 1% (v/v). The molar ratio of Ellipticine to lipid was around 1: 200 (v/v).

2.6.5 Preparation of Protein solution:

All the protein solutions were freshly prepared on the day of experiment. For heat denaturation experiment proteins were dissolved in appropriate buffer and was heated on a water bath at 70ºC for15 minutes and then were cooled at room temperature. For acid denaturation proteins were dissolved in phosphate buffer of pH 3.5. All the protein solutions were incubated for an hour before the experiment.

2.6.6 Estimation of Quantum yeild:

Quantum yield of any compound can be estimated using the following equation:

$$\phi_S = \phi_R \left(\frac{n_S^2}{n_R^2} \right) \left(\frac{I_S}{I_R} \right) \left(\frac{1-10^{-0.5A_R}}{1-10^{-0.5A_S}} \right) \qquad (2.12)$$

We used Quinine sulphate dihydrate in 0·05 M H_2SO_4 as reference (ϕ_R = 0·508). In equation 2.12, n_S and n_R represent refractive index of the sample (S) and reference solution (R) respectively, I is the integrated emission intensity, and A the absorbance.

2.8. References:

1. Conor D. V. O, Philips D. (1984), Time Correlated Single Photon Counting, Academic Press, London, pp. 36-51 (ISBN-10: 0124122310).
2. Lakowicz J. R., (1999), Principles of Fluorescence Spectroscopy, second ed. Plenum Press, New York, pp. 103-154 (ISBN:978-1-4757-3063-0).
3. Fleming G. R., (1986), Chemical Applications of Ultrafast Spectroscopy, Oxford University Press, New York (ISBN-10: 0195036441).
4. Bright F. V., Betts T. A., Litwiler K. S. (1990), Advances in Multifrequency Phase and Modulation Fluorescence Analysis, *CRC Crit. Rev. Anal. Chem.*, 21, 389-405 (DOI: 10.1080/10408349008051635).
5. Lakowicz J. R. (2006), Principles of Fluorescence Spectroscopy, third ed. Kluwer Academic Plenum Publisher, New York , pp. 3-23 (ISBN-10: 0387312781).
6. Quitevis E. L., Marcus A. H., Fayer M. D. (1993), Dynamics of ionic lipophilic probes in micelles: picosecond fluorescence depolarization measurements, *J. Phys. Chem.*, 97, 5762-5769 (DOI: 10.1021/j100123a049).
7. Heitz M. P., Bright F. V. (1996), Rotational Dynamics of Aerosol-OT Reverse Micelles in Compressible Fluids, *Appl. Spectrosc.*, 50, 732-739 (DOI:0003-7028(19960601)50: 6L.732;1-).
8. Heitz M. P., Bright F. V. (1995), Rotational Reorientation Dynamics of Xanthene Dyes within the Interior of Aerosol-OT Reversed Micelles, *Appl. Spectrosc.*, 49, 20-30 (DOI:0003-7028(19950101)49:1L.20;1-).
9. Grieser F., Dummond C. J. (1988), The physicochemical properties of self-assembled surfactant aggregates as determined by some molecular spectroscopic probe techniques, *J. Phys. Chem.*, 92, 5580-5593 (DOI: 10.1021/j100331a012).

10. Watt I. M., (1997), The Principles and Practice of Electron Microscopy, second ed. Cambridge University Press, New York, pp. 1-60 (ISBN -0521- 43591).
11. Moris, P., (2014), Biomedical Imaging Application and Advances, Woodhead Publishing Ltd., Kidlington UK, pp. 41-62 (ISBN 978-0-85709-127-7).
12. Miteva M. A., Guyon F., Tufféry P. (2010), Frog2: Efficient 3D conformation ensemble generator for small compounds, *Nucleic Acids Res.*, 38, W622-W627 (doi.org/10.1093/nar/gkq325).
13. Pencheva T., Lagorce D., Pajeva I., Villoutreix B. O., Miteva M. A. (2008), AMMOS: Automated Molecular Mechanics Optimization tool for in silico Screening, *BMC Bioinformatics*, 9, 438-445 (DOI:10.1186/1471-2105-9-438).
14. Hubbard S. J., Thornton J. M. (1993), 'NACCESS'. Computer Program, Department of Biochemistry and Molecular Biology, University College London.
15 . Hooper D. C. (1999), Mode of action of fluoroquinolones, *Drugs*, 58, 6-10 (10.2165/00003495-199958002-00002).
16. Zhang T., Li J. L., Ma X. C., Xin J., Tu Z. H. (2003), Reliability of phototoxic test of fluoroquinolones in vitro. *Acta Pharmacol. Sin.* 24, 453-459.
17. Appelbaum P. C., Hunter P. A. (2000), The fluoroquinolone antibacterials: Past, present and future perspectives, *Int. J. Antimicrob. Agents*, 16, 5-15 (http://dx.doi.org/10.1016/S0924-8579(00)00192-8).
18. Ball P. (2000), Quinolone generations: Natural history or natural selection? *J. Antimicrob. Chemother.* 46, 17-24 (doi.org/10.1093/oxfordjournals.jac.a020889).
19. Stahlmann R., Lode H. (1999), Toxicity of quinolones, *Drugs* 58, 37-42 (10.2165/00003495-199958002-00007).

20. Snaz-Nebot V., Valls I., Barber D., Barbosa J. (1997), Acid-base behavior of quinolones in aqueous acetonitrile mixtures, *Acta Chem. Scand.,* 51, 896-903 (DOI:10.3891/acta.chem.scand.51-0896).

21. Park H. R., Lee H. C, Lee J. K., Yang K., Bark K. M. (2000), Spectroscopic properties of fluoroquinolone antibiotics and nanosecond solvation dynamics in Aerosol-OT reverse micelles, *Photochem. Photobiol.,* 71, 281–293 (DOI:10.1562/0031-8655(2000)0710281SPOFAA2.0.CO2).

22. Park, H. R., T. H. Kim and K. M. Bark (2002), Physicochemical properties of quinolone antibiotics in various environment. *Eur. J. Med. Chem.* 37, 443–460 (DOI: 10.1562/0031-8655(2000) 0710281SPOFAA2.0.CO2).

23. Bilski P., Martinez L. J., Koker E. B., Chingell C. F. (1996), Photosensitization by Norfloxacin is a function of pH, *Photochem. Photobiol.,* 64, 496-500 (DOI:10.1111/j.1751-1097.1996.tb03096.x).

24. Sortino S., Guidi G. D., Giuffrida S., Monti S., Velardita A. (1998), Spectroscopic and photochemical behavior of Enoxacin: A steady-state and time-resolved study, *Photochem. Photobiol.,* 67, 167–173.

25. Albini A., Monti S. (2003), Photophysics and photochemistry of fluoroquinolones, *Chem. Soc. Rev.,* 32, 238-250 (DOI:10.1039/ B209220B).

26. Monti, S., Sortino S. (2002), Laser flash photolysis study of photoionization in fluoroquinolones, *Photochem. Photobiol. Sci.,* 1, 877-881 (DOI:10.1039/B206750A).

27. Park H. R., Oh C. H., Lee H. C., Lee J. K.,Yang K., Bark K. M. (2002), Spectroscopic properties of fluoroquinolone antibiotics in water-methanol and water-acetonitrile mixed solvents, *Photochem. Photobiol.* 75, 237-248 (doi.org/10.1562/0031-8655(2002)075<0237:spofai> 2.0.co;2).

28. Park H. R., Lee H. C., Lim S. R., Yang K., Bark K. M. (2004), Spectroscopic properties of various quinolone antibiotics in aqueous-organic solvent mixtures, *Photochem. Photobiol.*, 80, 554-564 (http://dx.doi.org/10.1562/2004-04-23-ra-14.1).
29. Sortino S., (2006), Selective entrapment of the cationic form of Norfloxacin within anionic sodium dodecyl sulfate micelles at physiological pH and its effect on the drug photodecomposition, *Photochem. Photobiol.*, 82, 64-70 (DOI:10.1562/2005-06-01-RA-560).
30. Sortino S., Guidi G. D., Giuffrida S. (2001), Drastic photochemical stabilization of Lomefloxacin through selective and efficient self-incorporation of its cationic form in anionic sodium dodecyl sulfate (SDS) micelles, *New J. Chem.*, 25, 197-199 (DOI:10.1039/B008257K).
31. Rivalle C., Wendling F., Tambourin P., Lhoste J.M., Bisagni E., Chermann J.C. (1983), Structure-activity studies on the N-terminal region of growth hormone releasing factor, *J. Med. Chem.*, 28, 181-185 (DOI:10.1021/jm00356a012).
32. Cordell G. A., Brossi A. (1994), The Alkaloid Chemistry and Pharmacology, Academic Press, San Diego, CA, pp. 39–42 (ASIN: B001F7B3LC).
33. Arteaga C. L., Kisner D. L., Goodman A., Von Hoff D. D. (1987), Elliptinium, a DNA intercalating agent with broad antitumor activity in a human tumor cloning system, *Eur J. Cancer Clin. Oncol.*, 23, 1621-1626 (DOI:0277537987904408).
34. Garbett N. C., Graves D. E. (2004), Extending nature's leads: the anticancer agent Ellipticine, *Curr. Med. Chem.: Anticancer Agents*, 4, 149-72 (DOI: 10.2174/1568011043482070).
35. Le Pecq J. -B., Xuong N. -D., Gosse C., Paoletti C. (1974), A New Antitumoral Agent: 9-HydroxyEllipticine. Possibility of a Rational Design of Anticancerous Drugs in the Series of DNA Intercalating Drugs, Proc. *Natl. Acad. Sci. U.S.A.*, 71, 5078-5082 (http://dx.doi.org/10.1073/pnas.71.12.5078).

36. Garbett N. C., Graves D. E. (2004), Extending nature's leads: the anticancer agent Ellipticine, *Curr. Med. Chem.*, 4, 149-172 (DOI: 10.2174/1568011043482070).

37. Goodwin S., Smith A. F., Horning E. C. (1959), Alkaloids of Ochrosia elliptica Labill, *J. Am. Chem. Soc.*, 81, 1903-1908 (DOI: 10.1021/ja01517a031).

38. Zwelling A., Michales S., Kerrigan D., Pommier Y., Kohn K. W. (1982), Protein-associated deoxyribonucleic acid strand breaks produced in mouse leukemia L1210 cells by Ellipticine and 2-methyl-9-hydroxyellipticinium, *Biochem. Pharmacol.*, 31, 3261-3267 (http://dx.doi.org/10.1016/0006-2952(82)90560-3).

39. Ohashi M., Oki T. (1996), Overview Oncologic, Endocrine & Metabolic: Oncologic, Endocrine & Metabolic :Ellipticine and related anticancer agents, *Expert Opin. Ther. Pat.*, 6, 1285-1294 (DOI: 10.1517/13543776.6.12.1285).

40. Mathe G., Hallard M., Pontiggia P. (1996), Lymphangiographic study of pelvic adenopathy regression in a phase II trial of methyl-hydroxy-Ellipticine in HIV1-AIDS complex, *Biomed Pharmacother*, 50, 510-511 (DOI: S0753332297892840).

41. Behravan G., Leijon M., Selhlstedt U., Vallberg H., Bergamn J., Grauslund A. (1994), The interaction of Ellipticine derivatives with nucleic acids studied by optical and 1H-nmr spectroscopy: Effect of size of the heterocyclic ring system, *Biopolymers*, 34, 599-609. (DOI: 10.1002/bip.360340503).

42. Canals A., Purciolas M., Aymami J., Coll M. (2005), The anticancer agent Ellipticine unwinds DNA by intercalative binding in an orientation parallel to base pairs, *Acta Crystallogr.*, 61, 1009-1012 (DOI: S0907444905015404).

43. Dodin G., Schwaller M. A., Aubard J., Paoletti C. (1988), Binding of Ellipticine base and ellipticinium cation to calf-thymus DNA, *Eur. J. Biochem.*, 176, 371-376 (DOI: 10.1111/j.1432-1033.1988.tb14291.x).

44. Kohn K. W., Waring M. J., Glaubiger D., Friedman A. (1975), Intercalative binding of Ellipticine to DNA, *Cancer Res.,* 35, 71-76.

45. Jain S. C., Bhandary K. K., Sobell H. M. (1979), Visualization of drug-nucleic acid interactions at atomic resolution: VI. Structure of two drug-dinucleoside monophosphate crystalline complexes, Ellipticine-5-iodocytidylyl (3′–5′) guanosine and 3,5,6,8-tetramethyl-n-methyl phenanthrolinium-5-iodocytidylyl (3′–5′) guanosine, *J. Mol. Biol.,* 135, 813-840, (http://dx.doi.org/ 10.1016/0022-2836(79)90514-X) .

46. Elcock A. H., Rodger A., Richards W. G. (1996), Theoretical studies of the intercalation of 9-hydroxyEllipticine in DNA, *Biopolymers,* 39, 309-326 (DOI: 10.1002/(SICI)1097-0282(199609)39:3<309::AID-BIP4>3.0.CO;2-S).

47. El Hage Chahine J. M., Bertigny J. P., Schwaller M. A. (1989), Kinetics and thermodynamics of the formation of inclusion complexes between cyclodextrins and DNA-intercalating agents. Inclusion of Ellipticine in γ-cyclodextrin, *J. Chem. Soc., Perkin Trans. 2,* 629-633 (DOI: 10.1039/P29890000629).

48. Auclair A., Arch C. (1987), Multimodal action of antitumor agents on DNA: The Ellipticine series, *Biochem. Biophys.* 259, 1-14 (http://dx.doi.org/10.1016/0003-9861(87)90463-2).

49. Bailly C., Ohuigin C., Rivalle C., Bisagni E., Waring M. J. (1990), Sequence-selective binding of an Ellipticine derivative to DNA, *Nucleic Acids Res.,* 18, 6283-6291.

50. Reha D., Kabelac M., Ryjacek F., Sponer J., Sponer J. E., Elstner M., Suhai S., Hobza P. (2002), Intercalators. 1. Nature of Stacking Interactions between Intercalators (Ethidium, Daunomycin, Ellipticine, and 4‘,6-Diaminide-2-phenylindole) and DNA Base Pairs. Ab Initio Quantum Chemical, Density Functional Theory, and Empirical Potential Study, *J. Am. Chem. Soc.,* 124, 3366-3376 (DOI: 10.1021/ja011490d).

51. Ammon S. J. F., Marcia W. P., Osheroff N., Thompson R. B. (1995), Topoisomerase II Binds to Ellipticine in the Absence or Presence of DNA.Characterization of Enzyme, Drug Interactions by Fluorescence Spectroscopy, *J. Biol. Chem.*, 270, 14998-15004.

52. Fung S. Y., Duhamel J., Chen P. (2006), Solvent Effect on the Photophysical Properties of the Anticancer Agent Ellipticine, *J. Phys. Chem. A*, 110, 11446-11454 (DOI: 10.1021/jp062778y).

53. Miskolczy Z., Biczok L., Jablonkai I. (2006), Effect of hydroxylic compounds on the photophysical properties of Ellipticine and its 6-methyl derivative: The origin of dual fluorescence, *Chem. Phys. Lett.*, 427, 76-81 (http://dx.doi.org/10.1016/j.cplett.2006.06.045).

54. Miskolezy Z., Biczok L. (2006), Fluorescent properties of hydrogen-bonded Ellipticine: A special effect of fluoride anion, *J. Photochem. Photobio A.* 182, 82-87 (DOI: S1010603006000360).

55. Banerjee S., Pabbathi A., Chandra Sekhar M., Samanta A. (2011), Dual Fluorescence of Ellipticine: Excited State Proton Transfer from Solvent versus Solvent Mediated Intramolecular Proton Transfer, *J. Phys. Chem. A,* 115, 9217-9225 (DOI: 10.1021/jp206232b).

56. Sbai M., Ait Lyazidi S., Lerner D. A., Castillo B. del., Martin M. A. (1996), Stoichiometry and association constants of the inclusion complexes of Ellipticine with modified β-cyclodextrin, *The Analyst*, 121, 1561-1564 (DOI: 10.1039/AN9962101561).

57. Sbai M., Lyazidi S. A., Lerner D. A., Castillo B. del., Martin M. A. (1995), Modified β-cylclodextrins as enhancers of fluorescence emission of carbazole alkaloid derivatives, *Anal. Chim. Acta.*, 303, 47-55 (http://dx.doi.org/10.1016/0003-2670(94)00475-2).

58. Schwaller M. Allard B. (1994),Protonation Equilibrium of Ellipticine Bound to the Energy-Transducing Membrane of Mitochondria, *J. Phys. Chem.*, 98, 4209-4211 (DOI: 10.1021/ j100067a002).

59. Fung S., Yang H., Bhola P. T, Sadatmousavi P., Muzar E., Liu M., Chen P. (2009), Self-Assembling Peptide as a Potential Carrier for Hydrophobic Anticancer Drug Ellipticine: Complexation, Release and In Vitro Delivery, *Adv. Funct. Mater.,* 19, 74-83 (DOI: 10.1002/adfm.200800860).

60. Liu J., Xiao Y., Allen C. (2004), Polymer-drug compatibility: a guide to the development of delivery systems for the anticancer agent, Ellipticine, *J. Pharm. Sci.*, 93, 132-143 (doi.org/10.1002/ jps.10533).

61. Moody T. W., Czerwinski G., Tarasova N. I., Moody D. L., Michejda C. J. (2004), The development of VIP-Ellipticine conjugates, *Regul Pept,* 123, 187-192 (doi: 10.1016/ j.regpep.2004.03.021).

62. Moody T. W., Czerwinski G., Tarasova N. I., Michejda C. J. (2002), VIP-Ellipticine derivatives inhibit the growth of breast cancer cells, *Life Sci.*, 71, 1005-1014 (doi: 10.1016/S0024-3205(02)01741-1).

63. Parusel A. (1998), Semiempirical studies of solvent effects on the intramolecular charge transfer of the fluorescence probe PRODAN, *J. Chem. Soc., Faraday Trans.*, 94, 2923-2927 (DOI: 10.1039/A804841J).

64. Parusel A. B. J., Nowak W., Grimme S. (1998), Comparative Theoretical Study on Charge-Transfer Fluorescence Probes: 6-Propanoyl-2-(N,N-dimethylamino)naphthalene and Derivatives, *J. Phys. Chem. A*, 102, 7149-7156 (DOI: 10.1021/jp981540+).

65. Nowak W., Adamczak P., Balter A., Sygula A. (1986), On the Possibility of Fluorescence from Twisted Intramolecular Charge Transfer States of 2-Dimethylamino-6-Acylnaphthalenes. A Quantum-Chemical Study, *J. Mol. Struct.: THEOCHEM*, 139, 13-23 (http://dx.doi.org/10.1016/0166-1280(86)80103-8).

66. Harianawala A. I., Bogner R. H.(1998), Sensitivity and selectivity of p-(N-dimethylamino cinnamylidene) malononitrile, 6-propionyl-2-(dimethylamino) naphthalene (PRODAN) and fluorescein, *J. Lumin.*, 79, 97-105 (http://dx.doi.org/10.1016/S0022-2313(98)00034-9).

67. Marks D., Prosposito P., Zhang H., Glasbeek M. (1998), Femtosecond laser selective intramolecular double-proton transfer in [2,2′-bipyridyl]-3,3′-diol, *Chem. Phys. Lett.*, 289, 535-540 (http://dx.doi.org/10.1016/S0009-2614(98)00426-6).

68. Guha S., Sahu K., Roy D., Mondal S. K., Roy S., Bhattacharyya K. (2005), Slow Solvation Dynamics at the Active Site of an Enzyme: Implications for Catalysis, *Biochemistry*, 44, 8940-8947 (DOI: 10.1021/bi0473915).

69. Krasnowska E. K., Bagatolli L. A., Gratton E., Parasassi T. (2001), Surface properties of cholesterol-containing membranes detected by Prodan fluorescence, *Biochim. Biophys. Acta*, 1151, 330-340.

70. Bondar O. P., Rowe E. S. (1999), Preferential interactions of fluorescent probe Prodan with cholesterol, *Biophys. J.*, 76, 956-962 (DOI:0006-3495/99/02/956/07).

71. Macgregor R. B., Weber G. (1986), Estimation of the polarity of the protein interior by optical spectroscopy, *Nature*, 319, 70-73 (DOI: 319070a0).

72. Balter A., Nowak W., Pawelkiewicz W. (1988), Some remarks on the interpretation of the spectral properties of PRODAN, *Chem. Phys. Lett.*, 143, 565-570 (http://dx.doi.org/10.1016/0009-2614(88)87067-2).

73. Bunker C. E., Bowen T. L., Sun Y. P. (1993), A Photophysical Study of Solvatochromic Probe 6-Propionyl-Z(*N*,*N*-Dimethylamino) Napthalene (PRODAN) in Solution, *Photochem. Photobiol.,* 58, 499-505 (DOI: 10.1111/j.1751-1097.1993.tb04921.x).

74. Samanta A., Fessenden R. W. (2000), Excited State Dipole Moment of PRODAN as Determined from Transient Dielectric Loss Measurements, *J. Phys. Chem. A,* 104, 8972-8975 (DOI: 10.1021/jp0009960).

75. Pal S. K., Mandal D., Bhattacharyya K. (1998), Photophysical Processes of Ethidium Bromide in Micelles and Reverse Micelles, *J. Phys. Chem. B,* 102, 11017-11023 (DOI: 10.1021/jp982126c).

76. Lobo B. C., Abelt C. J. (2003), Does PRODAN Possess a Planar or Twisted Charge-Transfer Excited State? Photophysical Properties of Two PRODAN Derivatives, *J. Phys. Chem. A*, 107, 10938 - 10943 (DOI: 10.1021/jp036013r).

77. Mennucci B., Caricato M., Ingrosso F., Cappelli C., Cammi R., Tomasi J., Scalmani G., Frisch M. J. (2008), How the Environment Controls Absorption and Fluorescence Spectra of PRODAN: A Quantum-Mechanical Study in Homogeneous and Heterogeneous Media, *J. Phys. Chem. B,* 112, 414-423 (DOI: 10.1021/jp076138m).

78. Rottenberg H. (1992), Probing the interactions of alcohols with biological membranes with the fluorescent probe PRODAN, *Biochemistry,* 31, 9473-9481 (DOI: 10.1021/bi00154a021).

79. Bondar O. P., Rowe E. S. (1999), Probing the interactions of alcohols with biological membranes with the fluorescent probe PRODAN, *Biophys. J.,* 71, 1440-9481 (DOI: 10.1021/ bi00154a021).

80. Sommer A., Paltauf F., Hermetter A. (1990), Dipolar solvent relaxation on a nanosecond time scale in ether phospholipid membranes as determined by multifrequency phase and modulation fluorometry, *Biochemistry*, 29, 11134-11140 (DOI: 10.1021/bi00502a017).s
81. Krasnowska E. K., Gratton E., Parasassi T. (1998), Prodan as a Membrane Surface Fluorescence Probe: Partitioning between Water and Phospholipid Phases, *Biophys. J.*, 74, 1984-1993 (http://dx.doi.org/10.1016/S0006-3495(98)77905-6).
82. Zeng J., Chong P. L. G. (1991), Interactions between pressure and ethanol on the formation of interdigitated DPPC liposomes: a study with Prodan fluorescence, *Biochemistry*, 30, 9485-9491 (DOI: 10.1021/bi00103a014).
83. Sengupta B., Guharay J., Sengupta P. K. (2000), Characterization of the fluorescence emission properties of prodan in different reverse micellar environments, *Spectrochim. Acta Part A*, 56, 1433- 1441 (http://dx.doi.org/10.1016/S1386-1425(00)00245-6).
84. Agazzi F. M., Rodriguez J., Falcone R. D., Silber J. J., Correa N. M. (2013), PRODAN Dual Emission Feature To Monitor BHDC Interfacial Properties Changes with the External Organic Solvent Composition, *Langmuir*, 29, 3556-3566 (DOI: 10.1021/ la304951f).
85. Novaira M., Moyano F., Biasutti M. A., Silber J. J., Correa N. M. (2008), An Example of How to Use AOT Reverse Micelle Interfaces to Control a Photoinduced Intramolecular Charge-Transfer Process, *Langmuir*, 24, 4637-4646 (DOI: 10.1021/la704004m).
86. Novaira M., Biasutti M. A., Silber J. J., Correa N. M. (2007), New Insights on the Photophysical Behavior of PRODAN in Anionic and Cationic Reverse Micelles: From Which State or States Does It Emit, *J. Phys. Chem. B*, 111, 748-759 (DOI: 10.1021/jp065528q).

87. Quintana S. S., Falcone R. D., Silber J. J., Correa N. M. (2012), Comparison between Two Anionic Reverse Micelle Interfaces: The Role of Water–Surfactant Interactions in Interfacial Properties, *Chem. Phys. Chem.*, 13, 115-123 (DOI: 10.1002/cphc.201100638).

88. Durantini A. M., Falcone R. D., Silber J. J., Correa N. M. (2009), Effect of the Constrained Environment on the Interactions between the Surfactant and Different Polar Solvents Encapsulated within AOT Reverse Micelles, *Chem. Phys. Chem.*, 10, 2034-2040 (DOI: 10.1002/cphc.200900130).

89. Adhikary R., Barnes C. A., Petrich J. W. (2009), Solvation Dynamics of the Fluorescent Probe PRODAN in Heterogeneous Environments: Contributions from the Locally Excited and Charge-Transferred States, *J. Phys. Chem. B*, 113, 11999-12004 (DOI: 10.1021/jp905139n).

90. Chong P. L. G. (1988), Effects of hydrostatic pressure on the location of PRODAN in lipid bilayers and cellular membranes, *Biochemistry*, 27, 399-404 (DOI: 10.1021/bi00401a060).

91. de Vequi-Suplicy C. C., Benatti C. R., Lamy M. T. (2006), Laurdan in Fluid Bilayers: Position and Structural Sensitivity, *J. Fluoresc.*, 16, 431-439 (DOI:10.1007/s10895-005-0059-3).

92. Sykora J., Kapusta P., Fidler V., Hof M. (2002), On What Time Scale Does Solvent Relaxation in Phospholipid Bilayers Happen?, *Langmuir*, 18, 571-574 (DOI: 10.1021/la011337x).

93. Jurkiewicz P.,Olzuynska A., Langner M., Hof M. (2006), Headgroup Hydration and Mobility of DOTAP/DOPC Bilayers: A Fluorescence Solvent Relaxation Study, *Langmuir*, 22, 8741-8749 (DOI: 10.1021/la061597k).

94. Cwiklik L., Aquino A. J. A., Vazdar M., Jurkiewicz P., Pittner J., Hof M., Lischka H. (2011), Absorption and Fluorescence of PRODAN in Phospholipid Bilayers: A Combined Quantum Mechanics and Classical Molecular Dynamics Study, *J. Phys. Chem. A*, 115, 11428-11437 (DOI: 10.1021/jp205966b).

95. Parasassi T., De Stasio G., Ubaldo A., Gratton E. (1990), Quantitation of lipid phases in phospholipid vesicles by the generalized polarization of Laurdan fluorescence, *Biophys. J.*, 57, 179-189 (http://dx.doi.org/10.1016/S0006-3495(91)82041-0).

96. Parasassi T., Krasnowska E. K., Bagatolli L., Gratton E. (1998), Laurdan and Prodan as Polarity-Sensitive Fluorescent Membrane Probes, *J. Fluoresc.*, 8, 365-373 (10.1023/A:1020528716621).

97. Krishnakumar S. S., Panda D. (2002),Spatial Relationship between the Prodan Site, Trp-214, and Cys-34 Residues in Human Serum Albumin and Loss of Structure through Incremental Unfolding, *Biochemistry*, 41, 7443-7452 (DOI: 10.1021/bi025699v).

98. Basak S., Debnath D., Haque H., Ray S., Chakrabarti A., Structural perturbation of proteins in low denaturant concentration, *Indian J. Biochem. Biophys.,* 2001, 38, 84-89.

99. Abbyad P., Schi X., Childs W., McAnaney T. B., Cohen B. E., Boxer S. G. (2007), Measurement of Solvation Responses at Multiple Sites in a Globular Protein, *J. Phys. Chem. B*, 111, 8269-8276 (DOI: 10.1021/jp0709104).

100. Chakrabarti A. (1996), Fluorescence of Spectrin-Bound Prodan, *Biochem. Biophys. Res. Commun.*, 226, 495-497 (http://dx.doi.org/10.1006/bbrc.1996.1383).

101. Chakrabarti A., Kelkar D. A., Chattopadhyay A. (2006), Spectrin Organization and Dynamics: *New Insights, Biosci. Rep.*, 26, 386-369 (DOI 10.1007/s10540-006-9024-x).

102. Chattopadhyay A., Rawat S. S., Kelkar D. A., Ray S., Chakrabarti A. (2003), Organization and dynamics of tryptophan residues in erythroid spectrin: Novel structural features of denatured spectrin revealed by the wavelength-selective fluorescence approach, *Protein Sci.*, 12, 2389-2403 (DOI: 10.1110/ps.03302003).

103. Zhong D., Douhal A., Zewail A. H. (2000), Femtosecond studies of protein–ligand hydrophobic binding and dynamics: Human serum albumin, *Proc. Natl. Acad. Sci. U. S. A.*, 97, 14056-14061 (DOI:10.1073ypnas.250491297).

104. Kamal J. K. A., Zhao L., Zewail A. H. (2004), Ultrafast hydration dynamics in protein unfolding: Human serum albumin, *Proc. Natl. Acad. Sci. U. S. A.*, 101, 13411-13416 (doi/10.1073/ pnas.0405724101).

105. Nerli B., Romanini D., Pico G. (1997), Structural specificity requirements in the binding of beta lactam antibiotics to human serum albumin, *Chem.-Biol. Interact.*, 104, 179-202 (http://dx.doi.org/10.1016/S0009-2797(97)00024-0).

106. Moreno F., Cortijo M., Jimenez J. G. (1999), The Fluorescent Probe Prodan Characterizes the Warfarin Binding Site on Human Serum Albumin, *Photochem. Photobiol.*, 69, 8-15 (DOI: 10.1111/j.1751-1097.1999.tb05299.x).

Chapter 3

Photophysical and Photodynamical Study of Fluoroquinolone and Ellipticine Drug Molecules in Bile Salt Aggregates

In this chapter, we have explored the photophysical properties of two widely used antibiotic fluoroquinolone drugs Norfloxcacin (NOR) and Ofloxacin (OFL) and an anticancer drug Ellipticine in biomimicking environments formed by bile salts using both steady state and time resolved fluorescence quenching measurement**.**

The first part of this chapter demonstrates the photophysical enhancement and fall of a particular prototropic species of antibiotic fluoroquinolone drugs, namely NOR and OFL which are sensitive to the excitation wavelength in bile salt aggregates. With addition of sodium deoxycholate (NaDC), sodium taurocholate (NaTC) and sodium glycodeoxycholate (NaGDC) and excitation at shorter wavelengths resulted in quenching of fluorescence of these fluoroquinolone. On the contrary, we observed a steady increase in the fluorescence intensity with a continuous red shift upon excitation at longer wavelength. The experimental results were rationalized in terms of the fact that, neutral and zwitterionic species of fluoroquinolone molecules in bile salt aggregates are selectively excited at shorter wavelength while the cationic form of fluoroquinolone molecules are excited at longer wavelength. We found that NaGDC and NaTC because of the conjugate head group are more effective in converting the neutral species of fluoroquinolones into a cationic species than NaDC. The quenching order is in accordance with hydrophobicity indices of bile salt.

In the second part of the chapter entrapment of neutral and cationic species of Ellipticine in different bile salt aggregates has been investigated. As Ellipticine exists in various prototropic forms in

aqueous solutions, a comparative study of entrapment of these prototropic species in different bile salts varying the head groups and hydrophobic skeleton was performed. The cationic species bind with the negatively charged head groups of bile salt through electrostatic interaction. On the other hand neutral species of Ellipticine are entrapped in the hydrophobic site of bile salt and the partition of neutral species in bile salt aggregates takes place according to the hydrophobicity indicies of bile salt.

(A) Photophysical and Photodynamical Study of Fluoroquinolone and Drug Molecules in Bile Salt Aggregates:

3.1. Perspective of the Present Study:

Fluroquinolones are considered as important antibacterial agents which exhibit a extensive range of antibacterial activity and are used to treat various infections *[1,2,3,4,5]*. The degree of ionization of fluroquinolone molecules depends on the pH of the system *[6,7]*. Fluoroquinolone molecules exhibit two protolytic equilibria with two different pK_a values. Several groups reported the spectroscopic details of the individual species *[7,6,8]*. However, the modulation of prototropic equilibrium and bio-distribution of this kind of drug molecules in different biomimetic environment are not well known. As Norfloxacin and Ofloxacin show better antibacterial activity so; binding of these molecules are examined in biomimetic systems *[8]*. Recently, Sortino et al reported that at micellar surface of Sodium dodecyl sulphate (SDS) at physiological pH fluroquinolone molecule takes a cationic form and thus get attracted to the anionic surfactant *[9,10]*. In the present study, we would like to explore the possible prototropic forms of Norfloxacin and Ofloxacin in bile salt aggregates by their photophysics and the nature of binding between different prototropic forms of these fluoroquinolones with bile salts.

Micelles formed by bile salts are simple model for complex biological system. Bile salts are surface active molecules and most prominent

biosurfactant. Bile salts consist of hydrophobic steroidal backbone with one to three hydroxyl groups and a carboxyl side chain lying along in the same plane of hydroxyl groups [*11,12]*.The polar hydroxyl groups are oriented towards the concave side of the steroid ring. So; the concave side is hydrophilic while the convex side is hydrophobic. They self aggregate in aqueous environments to form micelles *[13,14,15,16,17]*.

Previously some important photophysical and photodynamical studies have been carried out in bile salt aggregates by several groups *[18,19,20]*. Bohne and co-workers studied binding of various guest molecules with bile salts and effect of aggregation of bile salts on this binding *[21,22]*. Marinda and co-workers also studied aggregation and binding of various guest molecules to bile salts *[23,24]*. The present study involves three bile salts namely Sodium deoxycholate Soidum taurocholate, Sodium glycodeoxycholate (Figure 2.3 pp. 52) to explore the photophysics of Norfloxacin and Ofloxacin. As these drugs contain carbonyl group, the acid base behavior will be influenced by the physiochemical properties of the medium *[6-10]*. We have chosen deoxycholate taurocholate and glycodeoxycholate because of several reasons. The hydrophobic and hydrophilic skeleton of deoxycholate and glycodeoxycholate salts are akin but they contain different head groups. Deoxycholate contains an unconjugated head group ($-COO^-$) while glycodeoxycholate has a conjugated head group ($-CO-NH-CH_2-CO_2^-$). On the other hand taurocholate contains an extra hydroxyl group in their hydrophilic surface and the head group of taurocholate ($-CO-NH-CH_2-SO_3^-$) is also different from the other two bile salts. Thus by varying the head group and hydrophilic skeleton we tuned the photophysics of the fluoroquinolone molecules. The present study would also focus on the confinement of fluoroquinolone molecules in the hydrophilic and hydrophobic skeleton of different bile salts.

3.2. Results and Discussion:

3.2.1. Steady State Absorption and Emission Spectra:

The absorption spectrum of NOR in aqueous solution shows bands at around 270 nm and 325 nm and that of OFL shows bands at around 290 nm and at 332 nm. Upon addition of bile salts to aqueous buffer solution of NOR, the band at 270 nm is red shifted to 274 nm with increase in absorbance. On the other hand, absorbance decreases at 325 nm band. We observed that addition of bile salts yields two isobestic points at 315 nm and 350 nm in absorption spectra of NOR. With addition of bile salt a tail appears with significant absorbance at longer wavelength (beyond 350 nm). Interestingly, similar changes in absorption spectra of NOR in aqueous buffer solution is observed when pH is changed from 7.4 to 3.5. This fact indicates that in presence of bile salt NOR predominantly exists as a cationic species. Figure 3.1 illustrates the absorption spectra of NOR at different concentration of bile salts. The absorption spectra of NOR in aqueous buffer solution at different pH are inset of Figure 3.1.

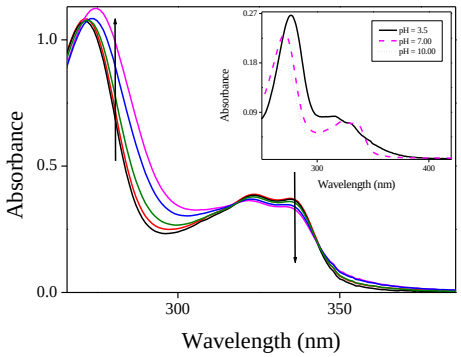

Figure 3.1. *Absorption spectra of NOR at different concentration of NaDC. In the inset absorption spectra of NOR in aqueous buffer solution at different pH are shown. The downward arrow illustrates that absorption decreases at 325-335 nm band while upward arrow illustrates the absorption increases at 270-275 nm band.*

Our result are in well agreement with that of Sortino and co-workers *[8,9,10]*. In case of OFL, the change in the absorption spectra with addition of bile salts is similar to that of NOR. However, we did not

observe any isobestic point for OFL. We took emission spectra of NOR and OFL exciting at 325 nm wavelength over a range of pH from 10.50 to 3.50. The corresponding emission spectra of NOR at different pH are shown in Figure 3.2a. It is revealed from Figure 3.2a that the change in pH from 10.50 to 3.50 in aqueous buffer solution results in red shift of the emission spectra and significant increase in quantum yield. The quantum yields of NOR and OFL at different pH are summarized in Table 3.1 (pp. 81) After taking the emission spectra over a range of pH, we took emission spectra of NOR and OFL exciting at 305, 325, 350, 365 and 375 nm wavelengths at physiological pH ~ 7.40. The normalized emission spectra of NOR obtained by exciting at different wavelength are shown in Figure 3.2b. It is revealed from Figure 3.2b that the emission spectra are continuously red shifted as the excitation wavelength moves towards longer wavelengths. At pH ~ 7.40 excitation at 305-350 nm wavelength yields emission maxima of NOR at around 410-415 nm. On the other hand excitation at 365-375 nm wavelength yields the emission maxima of NOR at 435 and 440 nm respectively.

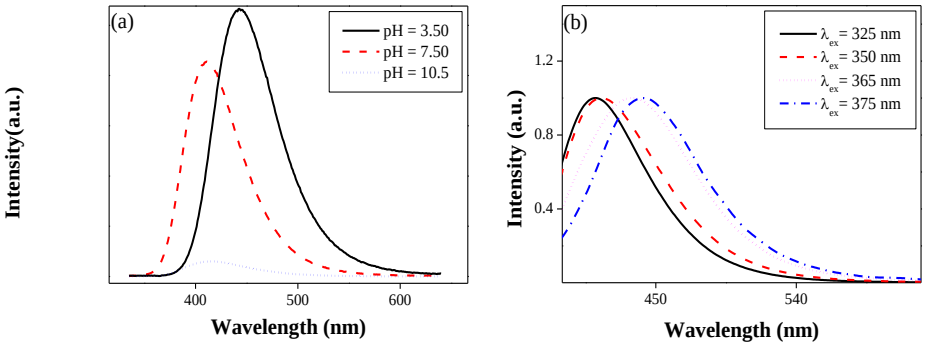

Figure 3.2. (a) *Emission spectra of NOR at pH 3.5, 7.4 and 10.5 at* λ_{ex} *= 325 nm.* ***(b)*** *Normalized emission spectra of NOR at pH 7.40 at* λ_{ex} *= 325, 350, 365 and 375 nm.*

Similarly a red shift is observed in case of OFL from 460 nm to 472 nm with excitation at longer wavelength. The red shift for NOR and OFL upon excitation at longer wavelength at a particular pH confirms that cationic species of fluoroquinolone are selectively excited at longer wavelength.

After perfoming studies in aqueous solutions we proceed to study photophysics of NOR and OFL in bile salt aggregates. NOR and OFL upon excitation at 305, 325, 350, and 365 nm wavelengths in bile salt aggregates fabricate interesting results. Increasing bile salt concentration, while exciting at 305 and 325 nm quenches the intensity of NOR. But excitation of NOR at 350 and 365 nm leads to an increase in quantum yield. The quantum yield of NOR in aqueous buffer solution is around 0.075 and in the presence of 40 mM NaDC, NaTC and NaGDC the quantum yield increases up to 0.095, 0.150 and 0.165 respectively. The emission spectra of NOR in presence of NaDC by excitation at 325 nm and 350 nm are illustrated in Figure 3.3a and Figure 3.3b respectively.

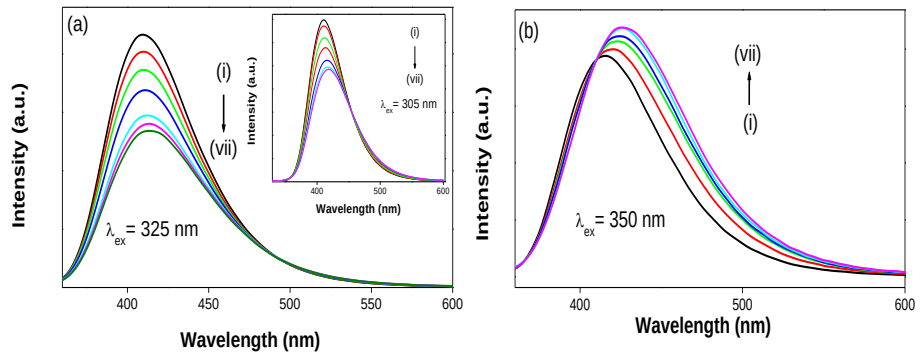

Figure 3.3*. The emission spectra of NOR with increasing concentration of NaDC (0 mM to 20 mM).* ***(a)*** *λ_{ex} = 325 nm. In the inset emission spectra of NOR at λ_{ex} = 305 nm. The downward arrow indicates that emission intensity decreases with addition of bile salt.* ***(b)*** *λ_{ex} = 350 nm. The upward arrow indicates that emission intensity increases with addition of bile salt.*

In case of OFL the results were quite similar; we observe that quenching takes place when OFL is excited at 305, 325 and 350 nm. Excitation at 365 and 375 nm leads to increase in the quantum yield with increasing bile salt concentration. However, NaDC is an exception from this trend. OFL exhibits a quenching in NaDC aggregates irrespective of excitation wavelength. The quantum yield of OFL in aqueous buffer solution is around 0.11 and in presence of 40

mM NaDC, NaTC and NaGDC the quantum yield becomes 0.110, 0.180 and 0.270 respectively. We have summarized the results in Table 3.1 (pp. 81). The variation in the emission intensity (fall and enhancement) as a function of bile salt concentration is shown in Figure 3.4. For the quenching process, we estimated Stern-Volmer constants using the following equation.

$$\frac{I_0}{I} = 1 + K_{SV}[Q] \qquad (3.1)$$

where I_0 and I are the initial and final intensity. Q is the concentration of the quencher. Thus the Stern-Volmer constants of NOR were estimated to be 26.35 M^{-1}, 8.00 M^{-1} and 24.00 M^{-1} in NaDC, NaTC and NaGDC aggregates respectively. On the other hand Stern-Volmer constants of OFL were estimated to be 8.0 M^{-1}, 4.5 M^{-1} and 8.0 M^{-1} for NaDC, NaTC and NaGDC aggregates respectively.

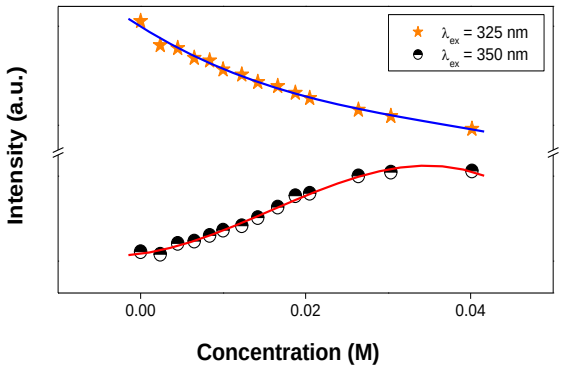

Figure 3.4. *Emission intensity of NOR at different concentration of bile salt for excitation wavelengths 350 nm and 325 nm for NaTC aggregates. A polynomial regression fit is drawn to show the change of measured values.*

To discover the possible reasons for the observed fluorimetric variation i.e. enhancement and fall in emission intensity of fluoroquinolone molecules upon excitation at different wavelengths. We took different prototropic structures of NOR and OFL along with structural aspects of bile salt aggregation in account. Earlier Sortino et al. reported that SDS micellar surface makes the abundant cationic form of NOR *[9,10]*. This assumption seems to be applicable in case of bile salt aggregates

for the observed enhancement in emission intensity at longer wavelength excitation (350 and 365 nm). Because of excess hydronium ion in micellar phase, the piperazinyl ring of NOR and OFL takes up a proton and switches over to a cationic form. The cationic species are selectively excited at the longer wavelengths and are trapped in the hydrophilic face of the bile salt which leads to an enhancement in the emission intensity. The binding mode consist of a positively charged piperazinyl group anchored to the negatively charged head group and remaining part is attached to the -OH groups of bile salt. We found that quantum yield is maximum in NaGDC aggregates and least in NaDC aggregates. Interestingly the hydrophobic skeleton of NaGDC and NaDC are akin but their head groups are different. NaDC has a $-COO^-$ head group while in NaGDC the head group is $-CO-NH-CH_2-COO^-$. As the conjugated head group is more efficient to protonate the fluoroquinolone molecules, so; it is justified that quantum yield would be higher in NaGDC than in NaDC. In this context the location of the drug molecules may be important in governing the observed photophysics. Upon addition of bile salt, an additional non-polarity is introduced in the system. It is possible that the neutral species of fluoroquinolone molecules are located in the hydrophobic side while the cationic species prefers hydrophilic side. The increase in non-polarity may be responsible for the observed quenching in this system. The Stern-Volmer constants were found to be almost same for NaDC and NaGDC but much lower in NaTC. According to hydrophobicity indices the order of hydrophobicity of NaDC, NaGDC and NaTC are reported to be 0.72, 0.65, 0.00 *[25]*. Thus NaDC and NaGDC are much more hydrophobic than NaTC. This confirms us that quenching processes is mostly governed by the hydrophobic interaction between fluoroquinolones and bile salt aggrgates.

We have estimated the association constant of NOR with bile salt using the method described by Singh et al. *[26]*. If 1:1 complex is formed between NOR and NaDC, the equilibrium constant can be written as

$$NOR + DC \underset{}{\overset{K_1}{\rightleftharpoons}} NOR - DC \qquad (3.2)$$

Here DC stands for NaDC. Therefore, the equilibrium constant is expressed as

$$K_1 = \frac{[NOR - DC]_{eq}}{[NOR]_{eq}[DC]_{eq}} \qquad (3.3)$$

Here $[NOR - DC]_{eq}$ is the concentration of this complex at equilibrium for 1:1 complex. As the concentration of bile salt is much higher than that of NOR, so the equation can be written as

$$K_1 = \frac{[NOR - DC]_{eq}}{([NOR]_0 - [NOR - DC]_{eq})[DC]_0} \qquad (3.4)$$

The Bensei-Hildebrand relation can be written as

$$\frac{1}{I_f - I_f{}^0} = \frac{1}{I_{NOR-DC} - I_f{}^0} + \frac{1}{I_{NOR-DC} - I_f{}^0}\left(\frac{1}{K_1[DC]_0}\right) \qquad (3.5)$$

Where $I_f{}^0$ is the fluorescence intensity of NOR in absence of bile salt and I_{NOR-DC} is the fluorescence intensity when all NOR molecules form complex with bile salt.

Now plot of $\frac{1}{I_f - I_f{}^0}$ vs. $\frac{1}{[DC]_0}$ should yield a straight line for 1:1 complex. However, nonlinear least square regression as described by Singh et al. is an alternative approach of data analysis *[26]*. For such analysis equation 3.5 can be rearranged to

$$I_f = \frac{I_f{}^0 + I_{NOR-DC}K_1[DC]_0}{1 + K_1[DC]_0} \qquad (3.6)$$

As $[DC]_0 >> [NOR]$, so it is likely that 1:2 complex might be formed. For the 1:2 complex formation between NOR and bile salt, the equilibrium constant can be written as

$$NOR\text{-}DC + DC \underset{}{\overset{K_2}{\rightleftharpoons}} NOR\text{-}(DC_2) \qquad (3.7)$$

The equilibrium process may be written as

$$I_f = \frac{I_f{}^0 + I_{NOR-DC} K_1 [DC]_0 + I_{NOR-DC_2} K_1 K_2 [DC]_0{}^2}{1 + K_1 [DC]_0 + K_1 K_2 [DC]_0{}^2} \qquad (3.8)$$

We have fitted integrated intensity of NOR and OFL following equation 3.8 to get the values for K_1 and K_2. The fitted graphs are shown for NaTC and NaDC in Figure 3.5. The estimated values of K_1 and K_2 for NaDC are 184 M^{-1} and 176 M^{-1}, for NaTC the values are 29^{-1}M and 100 M^{-1} and for NaGDC the values are 50^{-1}M and 135 M^{-1}. In case of OFL K_1 and K_2 values are 20^{-1}M and 80 M^{-1} for NaTC and 30^{-1}M and 51 M^{-1} for NaGDC. We cannot report the binding constant of OFL in NaDC because we did not observe any increase in the intensity of OFL in NaDC aggregates. The comparable values of K_1 and K_2 indicates that when bile salt concentration is low 1:1 complex is formed between fluoroqinolone and bile salt. But at relatively high concentration of bile salt 1:2 complex is formed between fluoroqinolone and bile salt.

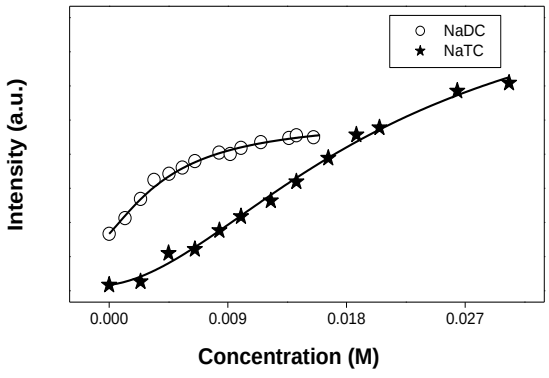

Figure 3.5. *The binding constant fitting curve for the integrated intensity of NOR assuming 1:1 and 1:2 complex following equation 3.8.*

3.2.2. Time Resolved Studies:

For the time resolved measurement, we excited NOR and OFL at 375 nm and decays were collected at the emission maxima. The corresponding decays were fitted to a bi-exponential function. The average lifetime of NOR in aqueous buffer solution at pH 7.40 is around 1.305 ns with time constants of 1.10 ns (94%) and 4.52 ns (6%). The average lifetime of OFL is around 4.11 ns with time constants of 0.400 ns (33%) and 5.97 ns (67%). The average lifetime values of NOR and OFL obtained in our experiment are in good agreement to that reported in the literature *[27]*. The representative decays of NOR in buffer solution and in different concentration of NaTC are shown in Figure 3.6. We calculated the radiative and non-radiative rate constants using the following equations.

$$\kappa_r = \frac{\phi_f}{\tau_{avg}} \tag{3.9}$$

$$\frac{1}{\tau_{avg}} = \kappa_r + \kappa_{nr} \tag{3.10}$$

where K_r and K_{nr} are the radiative and non-radiative rate constant and ϕ_f is the fluorescence quantum yield. The average lifetime constants, radiative and non-radiative rate constants are summarized in Table 3.1 (pp. 81). In buffer solution, a similar increase in lifetime takes place when the pH of the solution is changed from 7.40 to 3.50. We already mentioned in the previous section that at low pH range in aqueous buffer solution, fluoroquinolone mainly exist in a cationic form. Therefore, it is established that in bile salt aggregates NOR and OFL get protonated and are strongly bound to the hydrophilic surface of the bile salt aggregates.

One interesting feature revealed in Table 3.1(pp. 81) is that there is no significant change in the population (i.e. a_1 and a_2) of the fast (τ_1) and slow component (τ_2) on addition of bile salt to NOR solution.

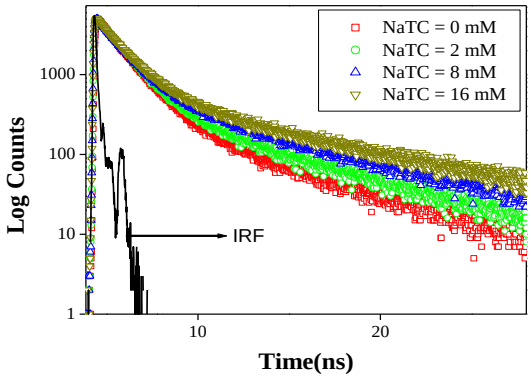

Figure 3.6. *Fluorescence decay curves of NOR in as a function of concentration of NaTC form 0 mM to 16 mM.*

However, considerable increment is found in the slow component i.e. in τ_2. We have plotted τ_2 and τ_1 values of NOR against the concentration of the bile salt in Figure 3.7a and Figure 3.7b respectively. It is seen that the fast time component i.e. τ_1 remains almost unchanged (around 1.00 ns) but τ_2 increases monotonously. At pH ~7.40 the τ_2 component of NOR is around 4.52 ns and in 40 mM NaDC, 40 mM NaTC and 40 mM NaGDC aggregates this becomes 6.84 ns, 7.81 ns and 8.48 ns respectively.

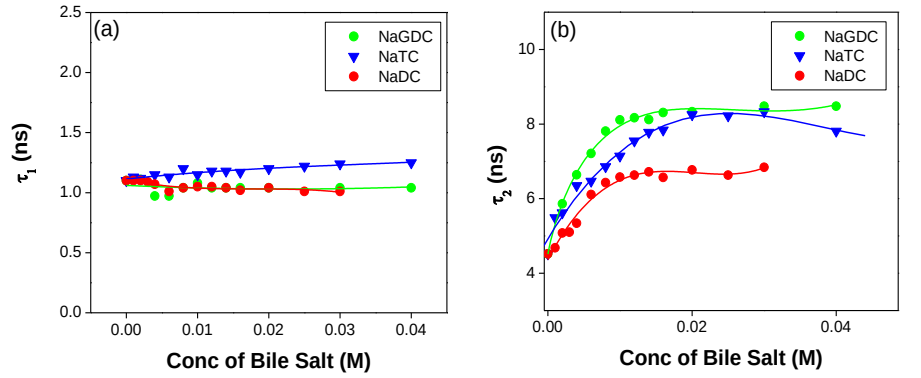

Figure 3.7 *Faster (τ_1) and slower (τ_2) lifetime component of NOR in presence of different bile salt concentration. A polynomial regression fit is drawn to show the change of measured values.*

Table 3.1: *Analytical parameters of lifetime, quantum yield and radiative rate constant for NOR and OFL in different pH and in NaDC, NaTC and NaGDC aggregates (Solution Prepared in Phosphate Buffer at pH 7.40).* [#]

System	a_1 (%)	a_2 (%)	τ_1 (ns)	τ_2 (ns)	$<\tau_{avg}>$ (ns)	Quantum yield	$K_r/s^{-1} \times 10^9$
NOR in buffer solution at pH 3.5	0.96	0.04	1.49	5.95	1.65	0.120	0.072
NOR in buffer solution at pH 7.40	0.94	0.06	1.10	4.52	1.305	0.075	0.053
NOR in 30 mM NaDC	0.90	0.10	1.01	6.84	1.59	0.095	0.060
NOR in 40 mM NaTC	0.92	0.08	1.25	7.81	1.77	0.150	0.084
NOR in 40 mM NaDGC	0.84	0.16	1.04	8.48	2.22	0.165	0.075
OFL in buffer solution at pH 3.50	0.11	0.89	3.37	7.70	7.23	0.253	0.034
OFL in buffer solution at pH 7.40	0.33	0.67	0.400	5.97	4.11	0.110	0.026
OFL in 40 mM NaDC	0.42	0.58	1.02	6.03	3.92	0.110	0.029
OFL in 40 mM NaTC	0.38	0.62	1.05	8.12	5.4	0.180	0.033
OFL in 40 mM NaGDC	0.34	0.66	1.83	9.83	7.10	0.270	0.038

[#] *The error in the measurement is about ± 10%*

This observation indicates that in bile salt aggregates cationic species of NOR are generated and strongly entrapped in the head group region. It is interesting to note that the rise in the slow time constant of NOR is in accordance with the order of enhancement in quantum yield in three bile salts i.e. NaGDC>NaTC>NaDC. We already mentioned that because of conjugated head groups, NaGDC and NaTC are more effective in converting neutral or zewitterionic species of fluoroquinolones into a cationic species than that of NaDC. Thus we observed a longer slower component in NaGDC and NaTC than that in NaDC.

In case of OFL the results were different than that of NOR. Surprisingly OFL does not show any increase in lifetime in NaDC aggregates. This is because of the fact that NaDC is more hydrophobic in character *[28]* and a weak proton donor than NaTC and NaGDC. However, in NaTC and NaGDC aggregates the life time of OFL increases significantly. We have plotted τ_1 and τ_2 as a function of concentration of bile salts in Figure 3.8.

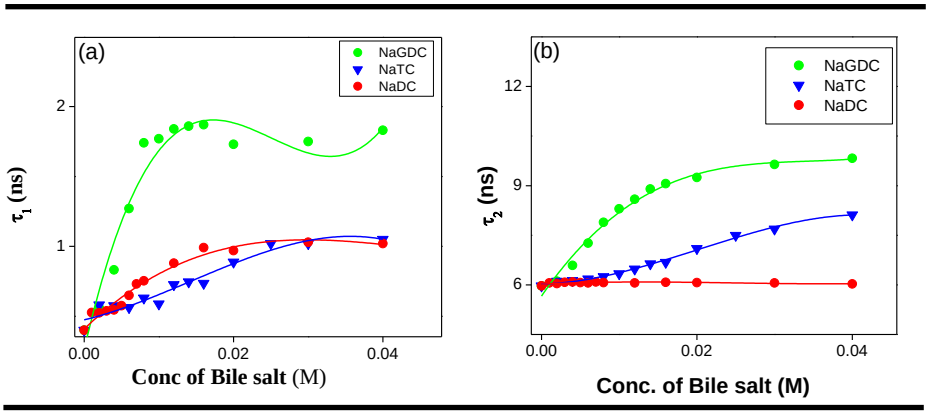

Figure 3.8. *Faster (τ_1) and slower (τ_2) lifetime component of OFL in presence of different bile salt concentration. A polynomial regression fit is drawn to show the change of measured values.*

It is seen that τ_1 increases appreciably in all the three bile salts while τ_2 values are increasing in NaTC and NaGDC and remains almost unchanged in NaDC.

Interestingly Table 3.1 reveals that the amplitude of fast component (a_1) increases significantly in NaDC and that of slow component decreases (a_2). This fact indicates that a substantial amount of OFL molecules are bound to hydrophobic pocket of NaDC. It could be due to the fact that OFL is more hydrophobic than NOR owing to a methyl group in piperazinyl ring. Due to increase in non-polarity upon addition of bile salt to aqueous buffer solution, a substantial amount OFL migrate from the aqueous phase to hydrophobic pocket of bile salt which may results in increase in the amplitude of fast component.

For better understanding regarding the binding of the drug molecules with the bile salts we carried out time resolved anisotropy

measurement of NOR and OFL in aqueous buffer and in bile salt aggregates. The representative anisotropy decays of OFL in aqueous buffer solution, in NaDC, NaTC and NaGDC aggregates are shown in Figure 3.9. The rotational relaxation of NOR and OFL in aqueous buffer solution was fitted to a single-exponential function, and the anisotropy decay time is 0.140 ns and 0.160 ns with finite accuracy. In NaDC, NaTC and NaGDC aggregates the rotational relaxation time follows a bi-exponential function and consists of a picosecond and a nanosecond components (Table 3.2 pp. 84). The average rotational relaxation time of OFL and NOR in NaDC and NaTC and NaGDC aggregates are longer compared to the rotational relaxation time of that in aqueous buffer solution. This fact strongly suggests that probe molecules are bound to the micellar surface. Table 3.2 reveals that average rotational relaxation time of both NOR and OFL are same in NaDC and NaGDC aggregates around 0.900 ns. However, the rotational relaxation time of both fluoroquinolone molecules are reduced in NaTC aggregates to around 0.600 ns. Figure 2.3 (pp. 52) reveals that the hydrophilic skeleton of NaDC and NaGDC salts have two hydroxyl groups. Thus nature of binding of NaDC and NaGDC to the fluoroquinolone molecules should be the similar.

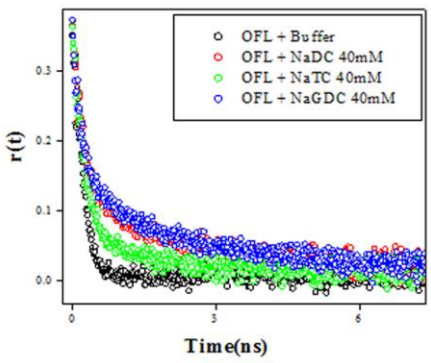

Figure 3.9. *Fluorescence anisotropy decay curves of OFL in aqueous buffer solution and in 40 mM NaDC, 40 mM NaTC, 40mM NaGDC aggregates.*

On the other hand NaTC is most hydrophilic among the three bile salts under this study because it has three hydroxyl group in the hydrophilic

surface which are capable of holding more number of water molecules in the hydrophilic surface through hydrogen bonding *[25,26]*. This factor can reduce the shear viscosity in the NaTC hydrophilic surface leading to a faster rotational relaxation for NOR and OFL compared to that in NaDC and NaGDC.

Table 3.2. *Analytical parameters of rotational relaxation times for NOR and OFL in NaDC, NaTC and NaGDC aggregates (Solution Prepared in Phosphate Buffer at pH 7.40).*[#]

System	r_0	a_{1r}	a_{2r}	τ_{1r} (ns)	τ_{2r} (ns)	$\langle\tau_r\rangle$ (ns)
NOR in buffer solution at pH 7.40	0.32	0.32			0.140	0.140
NOR in 30 mM NaDC	0.36	0.65	0.35	0.255	2.11	0.908
NOR in 30mM NaTC	0.35	0.72	0.28	0.271	1.643	0.655
NOR in 30mM NaGDC	0.35	0.64	0.36	0.250	2.2	0.952
OFL in buffer solution at pH 7.40	0.35	1		0.160		0.160
OFL in 30mM NaDC	0.36	0.54	0.46	0.178	1.6	0.840
OFL in 30mM NaTC	0.36	0.79	0.21	0.220	2.33	0.662
OFL in 30mM NaGDC	0.37	0.69	0.31	0.240	2.33	0.900

[#] *The error in the measurement is about ± 10%*

3.3. Conclusion:

It is evident from the present study that in presence of bile salt, Norfloxacin and Ofloxacin exhibit two opposite phenomena in emission properties upon excitation at shorter and longer wavelength. It is established from this study that with addition of bile salt at physiological pH (~ 7.40) the neutral and zwitterionic fluoroquinolone turns into a cationic species. The cationic species which is formed from neutral or zwitterionic species in presence of bile salt is selectively excited at longer wavelength and is entrapped by the hydrophilic face of bile salt. Consequently, the emission intensity increases upon excitation at longer wavelength. On the other hand zwitterionic/neutral species which decrease with addition of bile salt is excited at shorter wavelength and thus leads to quenching. We found that bile salts (NaTC and NaGDC) with the conjugated head group are more efficient in converting the neutral species into a cationic species than that (NaDC) with un-conjugated head group. The quenching occurs due to the non polarity introduced upon addition of bile salt to aqueous buffer solution. The quenching process in the present study is in accordance with the hydrophobic indices of NaDC, NaTC and NaGDC.

(B) Dynamics of Prototropic Species of an Anticancer Drug Ellipticine in Bile Salt Aggregates of Different Head Groups and Hydrophobic Skeleton: A Photophysical Study to Probe Bile Salt as Multisite Drug Carrier:

3.4. Perspective of the present study:

The self-assemblies of bile salts are of particular interest from the biological point of view because of their unique ability to solubilize various biologically active organic guests including many sparingly water-soluble drug molecules. Bile salt aggregates may be used as potential supramolecular host systems that can carry both hydrophobic and hydrophilic guest molecules of suitable size and shape because of the presence of both types of binding sites under varying experimental conditions, such as concentration, pH, and ionic strength of the surrounding medium *[21,22,29,30,31,32,33,34]*. This structure leads to a unique aggregation pattern, accounting for their solubilization of both hydrophobic and hydrophilic solutes *[35,36]*. Bohne and co-workers extensively carried out the study of host guest complexation of different probe molecules in bile salt aggregates *[37,38,39]*. Consequently bile salts have received much attention as drug delivery media. These bioactive molecules are synthesized in the liver from cholesterol and play an important role in the solubilization of lipids in the intestine, which allows them to be used as a potential drug delivery system *[40,41,42,43,44,45,46,47]*. Very recently, Miranda and co-workers demonstrated the existence of the two types of aggregates (primary/secondary) at different concentrations using fluorescent dansyl derivative of sodium cholate. It was shown that bile salt aggregates are suitable for carrying both hydrophobic and hydrophilic drug molecules due to the presence of these two different types of binding sites *[45,46,47]*. Miranda and co-workers showed that cholic acid aggregates can be used as effective drug carrier drug carriers. They have shown that hydrophobic drugs like naproxen and its methyl ester derivative can be entrapped in the hydrophobic pocket of bile salts *[47]*. Moreover, the formation of inclusion complexes in such

aggregates helps to control the selectivity of various chemical reactions such as photoinduced reactions, enzymatic reactions and complexation reactions. Due to presence of different tunable binding sites, bile salt aggregates are found to be interesting host systems capable of carrying both hydrophobic and hydrophilic guest molecules depending on the structure and size of the guests. Recently, Sarkar and co-workers have carried out extensive host guest interaction study in different bile slats *[41,48]*. This group reported photophysics of different molecules like curcumin, $BP(POH)_2$ and HAN in different bile salt systems. Collective and self-diffusion coefficients of sodium taurodeoxycholate and taurocholate in D_2O system have been reported as a function of ionic strength and bile salt concentration by quasielastic light scattering *[49]*. Bhattacharya and co-workers reported the dynamics of probe molecules in bile salt aggregates *[50,51]*.

In the study, we would like to report photophysical and photodynamical properties of different prototropic species of Ellipticine entrapped in the hydrophobic and hydrophilic sites of bile salts of different head groups and hydrophobic skeletons. The present study involves five different bile salts namely sodium salt of deoxycholate (NaDC), cholate (NaC), glycodeoxycholate (NaGDC), taurodeoxycholate (NaTDC) and taurocholate (NaTC). The structural formulae of bile salts are shown in Figure 2.3 (pp. 52). It is revealed from Figure 2.3 that the head groups of NaDC and NaC are akin but NaC contain an extra hydroxyl group in its hydrophilic surface. The hydroxyl groups make NaC less hydrophobic as compared to NaDC. Again NaDC, NaGDC and NaTDC have same number of hydroxyl groups in the hydrophilic surface but their head groups are different. While NaDC possesses an unconjugated head group (CH_2-COO^-), NaGDC and NaTDC have conjugated head groups -CO-NH-CH_2-CO_2^- and -CO-NH-CH_2-SO_3^- respectively. Owing to conjugation, head groups of NaTDC and NaGDC are supposed to be better proton donor than the head group of NaDC (i.e. the bile acids with conjugated head groups are stronger acid than bile acids with unconjugated head

groups.). On the other hand, head group of NaTC (-CO-NH-CH_2-SO_3^-) is same as that of NaTDC. However, extra hydroxyl group in their hydrophilic surface offers an additional hydrophilicity in NaTC as compared to that in NaTDC.

Because Ellipticine exists in protonated and deprotonated species in aqueous solution, therefore; by varying the head group and hydrophilic skeleton of bile salts, we tuned the photophysics and dynamics of the Ellipticine molecules as per our aspiration. In the present study we explored the entrapment of neutral and cationic species in hydrophobic and hydrophilic skeleton respectively and observed the effect of head groups as well as hydrophobic skeleton on the binding, partition and confinement of Ellipticine molecules.

3.5. Results and Discussion:

3.5.1. Steady state Absorption and Emission Spectra:

Elipticine exists in two prototropic species. The emission spectra of Ellipticine at different pH are shown in Figure 3.10a. The emission spectra of Ellipticine reveal that in acidic condition (pH~2) the emission maximum takes place at 535 nm. On the other hand at pH 12, an additional band appears around 450 nm with 535 nm band. The emission maxima at 450 and 535 nm are ascribed to the neutral species and cationic species respectively. Cationic species dominate at low pH due to protonation of the nitrogen atom on pyridine moiety and neutral species are prevalent at higher pH. Both the species simultaneously exist in physiological condition. Ellipticine shows two bands around 440 nm and 540 nm at physiological condition (pH~ 7.40). We assigned the bands at 440 and 540 nm wavelengths to neutral and cationic species respectively. Addition of bile salts to aqueous solution of Ellipticine enhances the intensity at 540 nm as well as at 440 nm (Figure 3.10b). The rise in intensity at 540 nm indicates the binding of cationic species with bile salts. On the other hand increase in intensity at 440 nm indicates that the neutral probe molecules are entrapped in the hydrophobic pocket of bile salt.

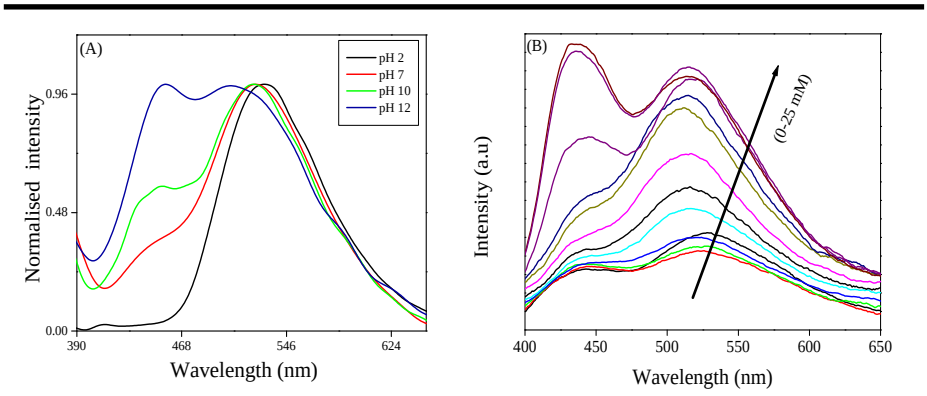

Figure 3.10. *(A) Normalized emission spectra of Ellipticine at different pH. (B)The emission spectra of Ellipticine at different concentration of NaDC (0-25 mM).*

The emission band of neutral species gradually shifts to the blue end. The extent of blue shift is greater in NaDC compared to other bile salts. This observation is consistent with earlier report that NaDC is more hydrophobic than other bile salts. The ratios of intensity of neutral species to that of cationic species (i.e. I_{440}/I_{540}) are 1.12, 1.81, 0.60, 0.48 and 0.42 for NaDC, NaC, NaTDC, NaGDC and NaTC respectively.

To gain an insight regarding the binding of neutral and cationic species with bile salts, we deconvoluted the emission spectrum into cationic species and neutral species by a combination of lognormal functions of the following form

$$I(\nu) = I \exp[-\ln 2(\frac{\ln[1+2b(\nu-\nu_p)/\Delta]}{b_1})^2] \qquad (3.11)$$

where ν_p, I, Δ, and b stand for peak frequency, peak height, width parameter and asymmetric parameters respectively. The deconvoluted spectra is shown in Figure 3.11a. The area under each of the curve corresponding to neutral and cationic species was used to estimate the quantum yield using the following equation:

$$\phi_S = \phi_R \left(\frac{n_S^2}{n_R^2} \right) \left(\frac{I_S}{I_R} \right) \left(\frac{1-10^{-0.5A_R}}{1-10^{-0.5A_S}} \right) \qquad (3.12)$$

We used Quinine sulphate dihydrate in 0·05 M H_2SO_4 as reference (ϕ_R = 0·508). The samples were excited at 325 nm. In equation 3.12, n_s and n_R represent refractive index of the sample (S) and reference solution (R) respectively, *I* is the integrated emission intensity, and *A* is the absorbance. The fluorescence quantum yield of cationic species of Ellipticine is calculated to be around 0.002 while the neutral species has a quantum yield around 0.0004. The plot of $\phi_{cationic}/\phi_{neutral}$ as a function of concentration of different bile salts (Figure 3.11b) reveals that $\phi_{cationic}/\phi_{neutral}$ initially decreases till 2-2.5 mM and then increases, reaches a maximum and then decreases for all the bile salts except NaTC. The initial decrement in $\phi_{cationic}/\phi_{neutral}$ may be attributed to the fact that very low concentration of bile salt increases the pH of the solution and this converts cationic species into the neutral species. This factor may be responsible for decrement in $\phi_{cationic}/\phi_{neutral}$ ratio in all bile salts. The rise in $\phi_{cationic}/\phi_{neutral}$ signifies that a strong interaction between Ellipticine and bile salt is dominated by electrostatic forces where the cationic Ellipticine species are anchored to the negatively charged head groups of bile salts. The electrostatic interaction dominates till a certain concentration of bile salts. The hydrophobic interaction dominates at higher concentration of bile salt due to formation of aggregates which results in entrapment of neutral Ellipticine in the hydrophobic cavity of aggregates. It is notable that aggregates of bile salts of non-conjugated head groups (for e.g. NaDC and NaC) display the drop in $\phi_{cationic}/\phi_{neutral}$ (i.e. dominance of hydrophobic force) at lower concentration than in bile salts having conjugated head groups. This observation indicates that unconjugated bile salts provide a more hydrophobic environment compared to conjugated bile salts.

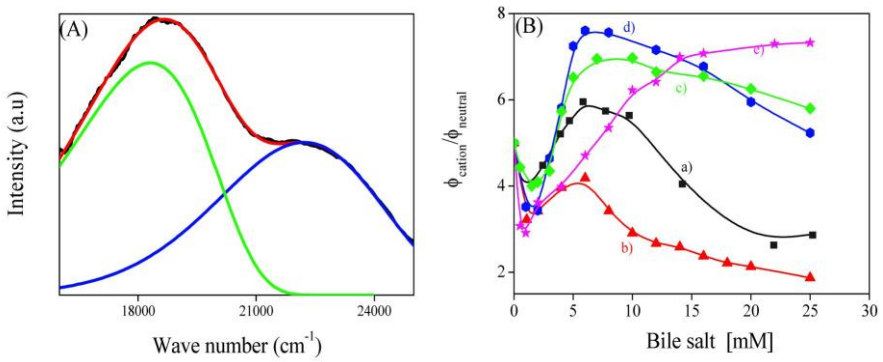

Figure 3.11. *(A) Deconvolution of emission spectrum of Ellipticine by a combination of lognormal functions. (B) The plot of* $\phi_{cationic}/\phi_{neutral}$ *as a function of different concentration (0-25 mM) of different bile salts (a) NaDC (b) NaC (c) NaGDC (d) NaTDC (e) NaTC.*

We interpreted the above findings in the light of structural difference of bile salts along with different parameters like hydrophobicity indices *[28,52]* and dissociation constant (pK_a) values of corresponding bile acids*[53,54]*.We shall start our discussion with photophysics of Ellipticine in three different bile salts namely NaDC, NaTDC and NaGDC. These three bile salts have same number of hydroxyl groups in their hydrophobic skeleton but differ in their head groups. NaDC possesses an unconjugated head group ($-CH_2-CH_2-COOH$) while NaTDC and NaGDC possess conjugated head groups $-CO-NH-CH_2-COOH$ and $-CO-NH-CH_2-SO_3H$ respectively. We listed the hydrophobicity indices of different bile salts and the pk_a of the corresponding acids in Table 3.3.

Table 3.3. *Hydrophobicity indices of different bile salts and* pK_a *of corresponding bile acids.*

System	No. of -OH groups in hydrophilic site	Hydrophobicity indices	Head groups	pK_a of corresponding bile acids
NaDC	2	0.72	$-CH_2-CH_2-CO_2^-$	6.20
NaGDC	2	0.65	$-CH_2-CO-NH-CO_2^-$	4.80
NaTDC	2	0.59	$-CH_2-CO-NH-SO_3^-$	<2
NaC	3	0.13	$-CH_2-CH_2-CO_2^-$	5.20
NaTC	3	0.00	$-CH_2-CO-NH-SO_3^-$	<2

It is revealed from Table 3.3 that conjugated head groups like –CO-NH-CH_2-COOH and –CO-NH-CH_2-SO_3H are stronger acid than unconjugated ones like –CH_2-CH_2-COOH. Thus it implies that head group of NaDC is less acidic compared to its analogous bile salts NaTDC and NaGDC although these three bile salts have same number of hydroxyl group in their hydrophobic moiety. The hydrophobicity indices in Table 3.3 reveal that NaDC is more hydrophobic as compared to NaTDC and NaGDC. Therefore NaTDC and NaGDC exhibit higher affinity towards cationic species of Ellipticine yielding higher $\phi_{cationic}/\phi_{neutral}$ as compared to NaDC.

Now we would like to compare entrapment of cationic and neutral species in NaGDC and NaTDC. Although NaGDC is more hydrophilic than NaTDC, Table 3.3 reveals that pK_a of Taurine group is less (< 2) than that of glycine (4.80). Therefore, due to taurine head group NaTDC is better candidate to capture the cationic Ellipticine and results in larger increment of $\phi_{cationic}/\phi_{neutral}$ values. Figure 3.11 reveals that $\phi_{cationic}/\phi_{neutral}$ values increases sharply in NaTC and does not decrease till 25 mM. This result is contradictory to that of NaTDC in which $\phi_{cationic}/\phi_{neutral}$ drops after a certain concentration. Although, these two bile salts have same head group, but NaTC possess an additional hydroxyl group in its hydrophilic skeleton and that makes NaTC more hydrophilic than NaTDC. The observation suggests that hydrophobic interaction between Ellipticine and NaTC aggregates is much weaker compared to that between Ellipticine and NaTDC. However, the above argument does not hold when we compare the results in NaDC and NaC aggregates. It is observed that Ellipticine exhibits a much smaller $\phi_{cationic}/\phi_{neutral}$ value in NaC as compared to that in NaDC aggregates although NaC is more hydrophillic than NaDC. We are not sure about the origin of this anomalous result. This anomalous result perhaps comes from the fact that NaC is less rigid compared to NaDC, thus allow more number of neutral Ellipticine molecules to penetrate inside NaC compared to that in NaDC.

Moreover, the critical micellear concentration of NaC is higher (16 mM) compared to that of NaDC (4 mM) which results in entrapment of more number of neutral Ellipticine. This could be the probable reason of observed anomalous result in NaC.

In the present perspective, the partition coefficient of the neutral species can be a measure of the hydrophobicity of different bile salts. We, therefore, estimated the partition coefficient of neutral Ellipticine using the following formulae (Figure 3.12) *[55]*.

$$\frac{1}{F} = \frac{55.6}{(K_P F_0 L)} + \frac{1}{F_0} \qquad (3.13)$$

where F_0 and F are fluorescence intensities of Ellipticine molecules in aqueous and in bile salts phase, respectively, L is the bile salt concentration and the molar concentration of water was considered to be 55.6 M.

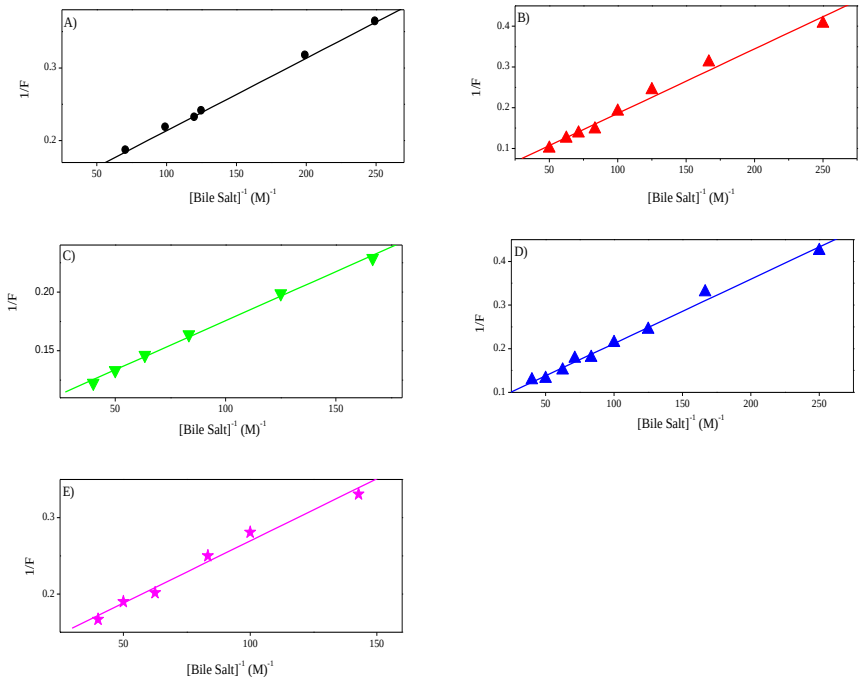

Figure 3.12. *Double reciprocal plot of the intensity of Ellipticine with respect to concentration of different bile salts.*

The partition coefficients of the neutral species in different bile salts are reported in Table 3.4.

Table 3.4: *Partition coefficient and free energy change of neutral species of Ellipticine in different bile salt aggregates.*

Bile salt	Partition coefficient, K_P (10^3)	Binding Enegry, -ΔG (kJ mol^{-1})
NaDC	7.50	22.10
NaTDC	5.90	21.50
NaGDC	3.60	20.30
NaC	2.50	19.30
NaTC	0.98	17.05

It is revealed that the partition coefficient between water and bile salt aggregates is highest in NaDC while the partition coefficient is lowest in NaTC. The order of the partition coefficient is in order of the hydrophobicity of bile salts. Therefore, it is conclusive that neutral species of Ellipticine is entrapped in the bile salt aggregates according to the hydrophobicity while the cationic species are attached to the head groups of bile salts according to number of hydroxyl group and acidity of the head group region. Figure 3.13 provides a cartoon representation indicating the solubilization of neutral Ellipticine in the hydrophobic pocket of micellar aggregates of bile salts and entrapment of cationic species in the hydrophilic surface.

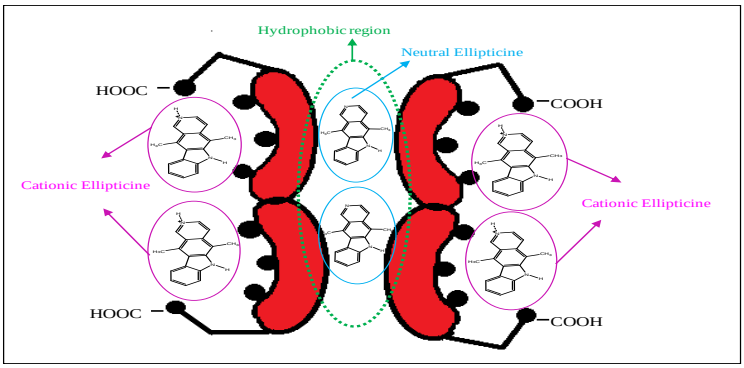

Figure 3.13. *Entrapment of neutral and cationic species of Ellipticine in hydrophobic and hydrophilic site of bile salt aggregates.*

3.5.2. <u>Time resolved studies:</u> We already mentioned that Ellipticine exists in cationic and neutral species in aqueous solution. Therefore, we took decays at 540 and 440 nm to measure the lifetime of cationic

species and neutral species respectively. The lifetime of Ellipticine at 540 nm consists of components around 1.80 (88%) and 5.94 ns (12%). The component around 1.80 ns was attributed to the cationic species of Ellipticine which is predominant at 540 nm emission band.

The other component perhaps comes from the zwitterionic species in the solution. Table 3.5 (pp. 97) reveals that, the shorter component i.e. τ_1 remains unchanged with addition of bile salts to aqueous solution of Ellipticine while a longer component (τ_2) is generated which increases with increasing concentration of bile salts. The increment in longer component is ascribed to the Ellipticine cation binding to head groups of bile salt and eventually formation of bile salt aggregates. We plotted τ_1 and τ_2 as a function of concentration of different bile salts (Figure 3.14). It is observed that the maximum increment in longer component takes place in NaTC while the least increment takes place in NaDC and NaC. The longer components were found to be 7.50, 12.95, 12.0, 7.50 and 8.9 ns in case of NaDC, NaTC, NaTDC, NaC and NaGDC respectively. Notably, τ_2 values are almost same in NaDC and NaC, although they are widely different in their hydrophobicity indices. Again a similar increment in τ_2 components is observed in NaTDC and NaTC aggregates despite of wide difference in the hydrophobicity indices of NaTDC and NaTC. Therefore, we conclude that the order of increment in the longer time component is not governed by the hydrophobicty indices of bile salts. It depends on the nature of the head groups of bile salt. Therefore, we have taken pK_a of bile salts into account for the interpretation of lifetime component. Table 3.3 reveals that NaDC and NaC possess same head groups which render similar pK_a for these two bile acids. Therefore, both NaDC and NaC offer similar environment in their head group region towards Ellipticine and results in similar changes in τ_2. On the other hand NaTC and NaTDC have same head group. Therefore, Ellipticine cation experiences similar binding in the head group region of these bile salts. Thus we observe a similar increment in τ_2 in these two bile salts. This assumption is further validated if we look at the amplitudes of τ_2

which, in the present case are found to be directly related to the pK_a values of bile acids. Bile acids with lower pK_a will be more dissociative and hence produce more number of anions which can bind with the cationic Ellipticine species. Table 3.5 (pp. 97) reveals that maximum change in population of the longer component takes place in NaTC (40%) while minimum takes place in case of NaDC (23%) and NaC (21%). The population of τ_2 depends directly on the pK_a of corresponding bile acids. It implies that higher the dissociation constant of bile acids higher would be the number of cations bound to head groups region. To illustrate this fact, we plotted a_2/a_1 as a function of concentration of different bile salts (Figure 3.14c).

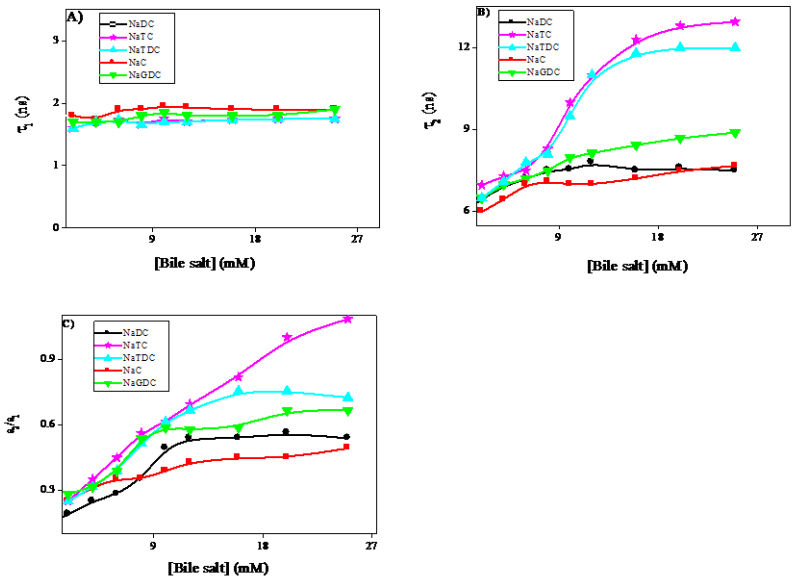

Figure 3. 14 *(A) Shorter (τ_1), (B) longer (τ_2) lifetime components and (C) ratio of population (a_2/a_1) of lifetime components of Ellipticine in presence of different bile salt concentration.*

The increment in a_2/a_1 values follows the same order of τ_2. In the earlier section, we already mentioned that binding of cationic species depends on the hydrophilicty of bile salts as well as the protonation ability of corresponding bile acids. Therefore, the lifetime components and amplitudes of the cationic species unambiguously establish this fact that entrapment of cationic species of Ellipticine takes place in bile salt according to the pK_a of corresponding bile acids.

Table 3.5. *The decay components of Ellipticine in presence of different bile salts at 540 nm.*[#]

System	a_1 (%)	a_2 (%)	τ_1 (ns)	τ_2 (ns)	$\langle\tau\rangle$ (ns)	χ^2
Conc. of NaDC						
0	0.88	0.12	1.80	5.94	2.30	1.20
2	0.84	0.16	1.79	6.45	2.53	1.21
4	0.80	0.20	1.79	6.95	2.82	1.20
6	0.78	0.22	1.8	7.20	2.99	1.15
8	0.74	0.26	1.650	7.50	3.17	1.16
10	0.67	0.33	1.720	7.53	3.63	1.23
12	0.65	0.35	1.75	7.80	3.87	1.10
16	0.65	0.35	1.75	7.50	3.76	1.05
20	0.64	0.36	1.70	7.60	3.82	1.20
25	0.65	0.35	1.78	7.50	3.782	1.10
Conc. of NaTC						
2	0.80	0.20	1.60	6.97	2.67	1.16
4	0.74	0.26	1.70	7.30	3.16	1.23
6	0.69	0.31	1.73	7.50	3.52	1.10
8	0.64	0.36	1.66	8.30	4.00	1.05
10	0.62	0.38	1.75	10.00	4.88	1.20
12	0.59	0.41	1.70	11.00	5.51	1.10
16	0.55	0.45	1.74	12.30	6.50	1.16
20	0.50	0.50	1.75	12.80	7.27	1.23
25	0.48	0.52	1.75	12.95	7.57	1.10
Conc. of NaTDC						
2	0.80	0.20	1.60	6.50	2.58	1.20
4	0.76	0.24	1.70	7.10	3.00	1.15
6	0.72	0.28	1.73	7.80	3.43	1.16
8	0.66	0.34	1.66	8.10	3.85	1.23
10	0.62	0.38	1.70	9.50	4.67	1.10
12	0.60	0.40	1.70	11.00	5.42	1.20

16	0.57	0.43	1.74	11.80	6.00	1.15
20	0.57	0.43	1.75	12.00	6.15	1.20
25	0.58	0.42	1.75	12.00	6.00	
Conc. of NaC						
2	0.80	0.20	1.8	6.00	2.64	1.20
4	0.76	0.24	1.73	6.44	2.86	1.10
6	0.74	0.26	1.90	7.00	3.23	1.16
8	0.74	0.26	1.90	7.10	3.25	1.23
10	0.72	0.28	2.00	7.00	3.40	1.10
12	0.70	0.30	1.932	7.00	3.45	1.10
16	0.69	0.31	1.90	7.20	3.54	1.19
20	0.69	0.31	1.9	7.50	3.64	1.25
25	0.67	0.33	1.9	7.68	3.81	1.30
Conc. of NaGDC						
2	0.78	0.22	1.70	6.50	2.75	1.23
4	0.76	0.24	1.70	7.0	2.97	1.48
6	0.72	0.28	1.70	7.20	3.24	1.45
8	0.65	0.35	1.80	7.50	3.79	1.19
10	0.63	0.37	1.85	8.0	4.12	1.25
12	0.65	0.35	1.75	8.15	3.99	1.20
16	0.63	0.37	1.56	8.44	4.10	1.23
20	0.60	0.40	1.68	8.70	4.49	1.10
25	0.60	0.40	1.9	8.90	4.70	1.10

[#] *The error in the measurement is ± 5%.*

Unlike lifetime components at 540 nm, life time components at 440 nm do not follow any particular trend of hydrophobicity of the bile salts. We summarized the lifetime components in Table 3.6. In aqueous solution the life time of Ellipticine at 440 nm consists of picosecond component around 0.400 ns (90%) and a longer component around 3.40 ns (10%). Addition of bile salts causes an enhancement in the picosecond component almost by two times along with an increase in

the nanosecond component. The decrease in the population of the picosecond component and subsequent increment in population of longer component indicate that neutral species are trapped in the hydrophobic site. However, we observe that the change in population follows the trend of the hydrophobicity of the bile salts.

Table 3.6. *The decay components of Ellipticine in presence of different bile salts at 440 nm.*[#]

System	a_1 (%)	a_2 (%)	τ_1 (ns)	τ_2 (ns)	$<\tau>$ (ns)	χ^2
Conc. of NaDC						
0	0.90	0.10	0.400	3.40	0.700	1.3
2	0.85	0.15	0.600	3.65	1.000	1.2
4	0.80	0.20	0.600	3.80	1.24	1.1
6	0.77	0.23	0.650	4.0	1.42	1.00
8	0.73	0.27	0.73	4.25	1.68	1.05
10	0.70	0.30	0.80	4.50	1.91	1.2
12	0.68	0.32	0.967	4.60	2.13	1.6
16	0.65	0.35	0.890	4.40	2.12	1.2
20	0.62	0.38	0.860	4.29	2.16	1.1
25	0.60	0.40	0.860	4.29	2.23	1.0
Conc. of NaTC						
2	0.88	0.12	0.587	2.45	0.81	1.2
4	0.89	0.11	0.717	3.380	1.00	1.4
6	0.85	0.15	0.600	3.63	1.00	1.4
8	0.82	0.18	0.670	4.00	1.27	1.3
10	0.80	0.20	0.75	4.50	1.50	1.2
12	0.78	0.22	0.830	5.62	1.88	1.1
16	0.75	0.25	0.815	6.166	2.15	1.1
20	0.76	0.24	0.871	6.535	2.23	1.3
25	0.76	0.24	0.871	6.535	2.23	1.3
Conc. of NaTDC						
2	0.88	0.12	0.7	2.5	0.92	1.4

4	0.89	0.11	0.77	3.2	1.00	1.2
6	0.85	0.15	0.600	3.4	1.00	1.4
8	0.82	0.18	0.780	3.8	1.32	1.3
10	0.80	0.20	0.80	4.5	1.54	1.1
12	0.78	0.22	0.83	5.00	1.74	1.1
16	0.75	0.25	0.86	5.4	1.99	1.2
20	0.76	0.24	0.85	5.6	1.99	1.2
25	0.76	0.24	0.85	5.6	1.99	1.1
Conc. of NaC						
2	0.86	0.14	0.6	3.5	1.0	1.3
4	0.80	0.20	0.650	3.86	1.29	1.3
6	0.80	0.20	0.72	4.0	1.38	1.4
8	0.80	0.20	0.75	4.26	1.45	1.2
12	0.76	0.24	0.715	4.26	1.56	1.4
16	0.75	0.25	0.85	4.76	1.83	1.5
20	0.73	0.27	.923	5.00	2.0	1.4
25	0.75	0.258	1.01	5.30	2.12	1.4
Conc. of NaGDC						
2	0.84	0.16	0.518	3.32	0.96632	1.2
4	0.77	0.23	0.861	4.53	1.70487	1.3
6	0.72	0.28	1.04	5.65	2.3308	1.3
8	0.69	0.31	1.06	5.77	2.5201	1.4
10	0.66	0.34	1.1	5.80	2.698	1.4
12	0.64	0.36	1.116	6.28	2.97504	1.2
16	0.62	0.38	1.20	6.40	3.176	1.2
20	0.65	0.35	1.20	6.35	3.0025	1.1
25	0.65	0.35	1.15	6.40	2.9875	1.1

[#] *The error in the measurement is ± 5%.*

We estimated the rotational relaxation of Ellipticine in different bile salts (Figure 3.15). The time resolved anisotropy was described with the following equation:

$$r(t) = r_0\left[\beta_{fast}\exp\left(-t/\phi_{fast}\right) + \beta_{slow}\exp\left(-t/\phi_{slow}\right)\right] \quad (3.14)$$

where $r(t)$ is the rotational relaxation correlation function. r_0 is the limiting anisotropy and ϕ_{fast} and ϕ_{slow} are the individual rotational relaxation time and β_{fast} and β_{slow} are the amplitude of rotational relaxation time.

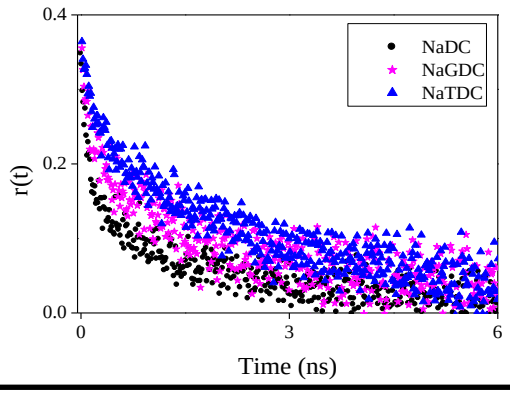

Figure 3.15. *Fluorescence anisotropy decays of Ellipticine in different bile salts.*

In aqueous solution Ellipticine exhibits a single exponential decay with rotational relaxation time around 180 ps. In bile salt aggregates, the rotational relaxation is found to be bi-exponential consisting of a picosecond component and a nanosecond components. The picosecond component originates from the Ellipticine molecules in aqueous phase while nanosecond component is attributed to the Ellipticine molecules held in the bile salt aggregates. The rotational relaxation parameters are summarized in Table 3.7. We have estimated the microviscosity of the hydrophilic region with the following equation considering the fact that ϕ_{slow} arises from the Ellipticine molecules bound to the head group region

$$\phi = \frac{\eta_m V}{kT} \quad (3.15)$$

Here, η_m is the microviscosity and V is the volume of the rotating molecular system. Hence, any change in ϕ could come from a change in either of the two factors (η, V). The molecular volume of Ellipticine is ~ 229.97 Å *[56]*. Table 3.7 reveals that the microviscosity is reasonably higher for conjugated head groups with less number of hydroxyl groups. This observation again corroborates well with the assumption that the bile salts having three hydroxyl groups can hold more number of water molecules which results in lower viscosity as compared to that in bile salts having two hydroxyl groups. We would like to start our discussion by comparing rotational relaxation in the bile salts which possess same head groups but differ in number of hydroxyl groups in their hydrophilic surface. It is revealed from Table 3.7 that ϕ_{slow} is higher in NaDC as compared to that in NaC. This may be attributed to the fact that NaDC possesses two hydroxyl groups in its steroidal moiety while NaC possesses three hydroxyl groups. Therefore, NaC can hold more number of water molecules.

Table 3.7. *Analytical parameters of rotational relaxation time of Ellipticine in different bile salt aggregates:*

Conc. of bile salts	r_0	β_{fast} **(%)**	β_{slow} **(%)**	ϕ_{fast} **(ns)**	ϕ_{slow} **(ns)**	χ^2	$<\eta_m>$ **(cP)**
0.00	0.30	1.00		0.180		1.0	
25 mM NaDC	0.38	0.66	0.33	0.160	1.54	1.1	30.00
25 mM NaTC	0.38	0.60	0.40	0.160	1.71	1.15	33.50
25 mM NaTDC	0.40	0.34	0.66	0.184	2.71	1.1	52.50
25 mM NaGDC	0.40	0.52	0.48	0.160	2.01	1.0	39.00
25 mM NaC	0.40	0.50	0.50	0.187	1.20	1.2	23.50

[#] *The error in the measurement is ± 5%.*

Thus the hydrophilic region of NaC is less vicous which reduce the frictional force as compared to that in NaDC. This perhaps results in faster rotational relaxation of Ellipticine in NaC as compared to that in NaDC. A similar conclusion can be drawn if we compare ϕ_{slow} in

NaTC and NaTDC. Ellipticine experiences less rigidity in NaTC due to an additional hydroxyl group as compared to that in NaTDC and hence exhibits faster rotational relaxation time.

Now we need to address the rotational relaxation in bile salts which have same number of hydroxyl group in the hydrophilic surface but differ in head groups. There are three bile salts namely NaDC, NaTDC and NaGDC which are same in number of hydroxyl groups in the hydrophilic site but differ in head groups. We found that Ellipticine exhibits faster rotational relaxation in NaDC compared to that in NaGDC and NaTDC. NaGDC and NaTDC possess unsaturated head groups which have lower pK_a hence higher dissociation constant than that of saturated head groups of NaDC. Thus NaTDC and NaGDC are capable of holding more number of Ellipticine cations leading to higher population of longer component. This fact may be responsible for the higher rotatioanl relaxation time in NaGDC and NaTDC. Interestingly, the longer component is higher in NaTDC than that in NaGDC. The taurine group is more acidic than glycine group. Therefore, NaTDC is better candidate to capture cationic species of Ellipticine. Thus higher partitioning of cationic Ellipticine takes place in NaTDC.

One inference can be drawn from the above discussion that partitioning of cationic species of drugs between aqueous phase and miceallar surface not only depends on the nature of the head groups but also on the number of hydroxyl group on the hydrophilic surface. Interestingly, we did not find any residual anisotropy which indicates absence of any restricted rotation in bile salt aggregates. In this context the comparison of global dynamics (i.e. rotation of the bile salt) and local dynamics (i.e. rotation of the probe molecules inside the bile salt aggregates) should be addressed. Maitra and co-workers reported that hydrodynamic radius of NaC is around 1.2 nm *[57]*. The the global rotational relaxation time was estimated to be around 1.2 ns obtained from the following equation

$$\phi_m = \frac{4\pi R_h^3 \eta_m}{3kT} \qquad (3.16)$$

This value is close in the range of the longer component (1.20 ns to 2.71 ns) of Ellipticine in bile salt aggregates. The observation implies that global rotational motion of bile salt aggregates has a significant contribution to the overall rotation of probe. Therefore, the rotational dynamics of Ellipticine is governed by the two factors (i) microvscosity felt by the Ellipticine and (ii) the global rotation of micellar aggregates.

Unlike cationic Ellipticine, when we measured rotational relaxation time at 440 nm, neutral Ellipticine molecules exhibit almost same rotational relaxation time in different bile salt aggregates (Figure 3.16). The fact implies that after intercalation, Ellipticine experiences a similar environment inside the hydrophobic pocket of bile salt. We have already shown in Figure 3.13 that neutral Ellipticine preferably form complexed to the hydrophobic region bile salt. One interesting point that Moitra et al. reported is DPH displays a single exponential correlation function which comes from the hydrophobic pocket of bile salts. It was reported that DPH being very hydrophobic mostly are entrapped in the hydrophobic pocket. In the present case, Figure 3.16 reveals a fast component (data are not shown) which is likely to be originated from neutral Ellipticine in the aqueous phase.

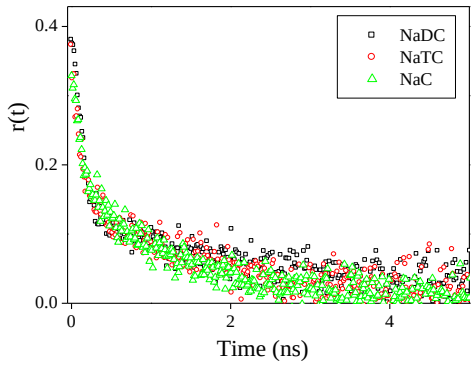

Figure 3.16. *Fluorescence anisotropy decays of Ellipticine in different bile salts aggregates at 440 nm.*

The observation implies partitioning of neutral Ellipticine in aqueous and hydrophobic phase. The full intercalation in the hydrophobic surface is not possible due formation of hydrogen bonding with water as well as bile salt head groups.

3.6. Conclusion:

In this chapter, we have shown the nanoconfinement of different prototropic species of anticancer drug Ellipticine in several bile salt aggregates through hydrophobic and hydrophilic interaction. The neutral species of the drug molecules were found to be partitioned according to the hydrophobicity indices of the bile salt. On the other hand, cationic species are attached to the head group region of the bile salt aggregates through electrostatic interaction. Our study revealed that initially bile salts acts like electrolytes and electrostatic interaction dominates over the hydrophobic interaction. The extent of binding of bile salt head group with the cationic species depends on the pK_a of the corresponding bile acids. Bile salts of conjugated head groups were found to be better candidates to capture the cationic species as compared to that of bile salts having non-conjugated head groups. The hydrophobic interaction dominates as aggregation of bile salts take place at higher concentration and results in the entrapment of the neutral species. The rotational relaxation of cationic species of Ellipticine was found to be higher in di-hydroxy bile salt aggregates compared to that in tri-hydroxy bile salt aggregates. However, rotational relaxation of rotational relaxation of neutral Ellipticine species is independent of the nature of bile salts.

3.7. References:

1. Hooper D. C. (1999), Mode of action of fluoroquinolones, *Drugs*, 58, 6-10 (10.2165/00003495-199958002-00002).
2. Zhang T., Li J. L., Ma X. C., Xin J., Tu Z. H. (2003), Reliability of phototoxic test of fluoroquinolones in vitro. *Acta Pharmacol. Sin.*, 24, 453–459.
3. Appelbaum P. C., Hunter P. A. (2000), The fluoroquinolone antibacterials: Past, present and future perspectives, *Int. J. Antimicrob. Agents*, 16, 5-15 (doi.org/10.1016/S0924-8579(00)00192-8).
4. Ball P. (2000), Quinolone generations: Natural history or natural selection? *J. Antimicrob. Chemother.*, 46, 17–24.
5. Stahlmann R., Lode H. (1999), Toxicity of quinolones, *Drugs*, 58, 37-42 (DOI:10.2165/00003495-199958002-00007).
6. Albini A., Monti S. (2003), Photophysics and photochemistry of fluoroquinolones, *Chem. Soc. Rev.*, 32, 238-250 (DOI: 10.1039/B209220B).
7. Monti S., Sortino S. (2002), Laser flash photolysis study of photoionization in fluoroquinolones, *Photochem. Photobiol. Sci.*, 1, 877-881 (DOI: 10.1039/B206750A).
8. Sortino S., Guidi G.D., Giuffrida S., Monti S.,Velardita A. (1998), Spectroscopic and photochemical behavior of Enoxacin: A steady-state and time-resolved study, *Photochem. Photobiol.*, 67, 167-173 (DOI: 10.1111/j.1751-1097.1998.tb05182.x.).
9. Sortino S. (2006), Selective entrapment of the cationic form of Norfloxacin within anionic sodium Dodecyl sulfate micelles at physiological pH and its effect on the drug photodecomposition, *Photochem. Photobiol.*, 82, 64-70 (DOI: 10.1562/2005-06-01-RA-560).

10. Sortino S., Guidi G. D., Giuffrida S. (2001), Drastic photochemical stabilization of Lomefloxacin through selective and efficient self-incorporation of its cationic form in anionic sodium dodecyl sulfate (SDS) micelles, *New. J. Chem.*, 25, 197-199 (DOI: 10.1039/B008257K).
11. Kratohvil J. P. (1986), Size of bile salt micelles: Techniques, problems and results, *Adv. Colloid Interface Sci.*, 26, 131-154 (DOI:0001868686800197).
12. Small D. M., Penkett S. A. Chapman D. (1969), Studies on simple and mixed bile salt micelles by nuclear magnetic resonance spectroscopy, *Biochim. Biophys. Acta*, 176, 178-189 (DOI:0005276069900861).
13. Small D. M. (1971), The Bile Acids: Chemistry, Physiology and Metabolism, Nair, P.P., Kritchevsky, D. (Eds.), vol. 1, Plenum Press, New York, pp. 249-356 (ISBN: 10: 0306371316).
14. Irwin Arias I., Wolkoff A., Boyer J., Shafritz D., Fausto N., Alter H., Cohen D. (2011), The Liver: Biology and Pathobiology, fifth ed. Wiley Blackwell, Hoboken U.S.A. (ASIN: B005UQLJCC)
15. Hjelm R. P., Schteingart C. D., Hofmann A. F., Thiyagarajan P. (2000), Structure of Conjugated bile salt-fatty acid-monoglyceride mixed colloids: studies by small-angle neutron scattering, *J. Phys. Chem. B*, 104, 197-211 (DOI: 10.1021/jp992157n).
16. Leng J., Egelhaaf S. U., Cates M. E. (2003), Kinetics of the Micelle-to-Vesicle Transition: Aqueous Lecithin-Bile Salt Mixtures, *Biophys. J.*, 85, 1624-1646 (doi.org/10.1016/S0006-3495(03)74593-7).
17. Mukhopadhyay, S., and U. Maitra (2004) Chemistry and biology of bile acids. *Current Sci.* 87 1666-1683.

18. Chakrabarty, D., Chakraborty A., Seth D., Sarkar N. (2005), Binding and relaxation behavior of Coumarin-153 in lecithin–taurocholate mixed micelles: A time resolved fluorescence spectroscopic study, *Chem. Phys. Lett.*, 412, 255-262 (http://dx.doi.org/10.1016/j.cplett.2005.06.098).
19. Sen S., Dutta P., Mukherjee S., Bhattacharyya K. (2002), Solvation dynamics in bile salt aggregates, *J. Phys. Chem. B*, 106, 7745 (DOI: 10.1021/jp0144799).
20. Chakraborty A., Chakrabarty D., Seth D., Sarkar N. (2006), Photo-induced intermolecular electron transfer from electron donating solvents to Coumarin dyes in bile salt aggregates: Role of diffusion in electron transfer reaction, *Spectrochimica Acta. Part A*, 63, 594-602 (http://dx.doi.org/10.1016/j.saa. 2005.06.006).
21. Li R., Carpentier E., Newell E. D., Olague L. M., Heafey E., Yihwa C., Bohne C. (2009), Effect of the Structure of Bile Salt Aggregates on the Binding of Aromatic Guests and the Accessibility of Anions, *Langmuir*, 25, 13800-13808 (DOI: 10.1021/la901826y).
22. Amundson L. L., Li R., Bohne C. (2008), Effect of the Guest Size and Shape on Its Binding Dynamics with Sodium Cholate Aggregates, *Langmuir*, 24, 8491-8500 (DOI: 10.1021/ la800439m).
23. Cuquerella M. C., Rohacova J., Marin M. L., Miranda M. A. (2010), Stereodifferentiation in fluorescence quenching within cholic acid aggregates, *Chem. Comm.*, 46, 4965-4967 (DOI: 10.1039/C0CC00176G).
24. Gomez-Mendoza M., Marin M. L., Miguel A. Miranda M. A. (2012), Dansyl-Labeled Cholic Acid as a Tool To Build Speciation Diagrams for the Aggregation of Bile Acids, *J. Phys. Chem. B*, 116, 14776-14780 (DOI: 10.1021/jp308624h).

25. Donovan J. M., Jackson, A. A., Carey M. C. (1993), Molecular species composition of inter-mixed micellar/vesicular bile salt concentrations in model bile: dependence upon hydrophilic-hydrophobic balance, *J. Lipid Res.,* 34, 1131-1141.
26. Singh M. K., Pal H., Koti A. S. R., Sapre A.V. (2004), Photophysical properties and rotational relaxation dynamics of neutral red bound to β-cyclodextrin, *J. Phys. Chem. A,* 108, 1465-1474 (DOI: 10.1021/jp035075e).
27. Bilski P., Martinez L. J., Koker E. B., Chingell C. F. (1996), Photosensitization by Norfloxacin is a function of pH, *Photochem. Photobiol.*, 64, 496–500 (DOI: 10.1111/j.1751-1097.1996.tb03096.x).
28. Mohapatra M., Mishra A. K. (2011), Effect of Submicellar Concentrations of Conjugated and Unconjugated Bile Salts on the Lipid Bilayer Membrane, *Langmuir,* 27, 13461-13467 (DOI**:** 10.1021/la203028s).
29. Garidel P., Hildebrand A., Neubert R., Blume A. (2000), Thermodynamic Characterization of Bile Salt Aggregation as a Function of Temperature and Ionic Strength Using Isothermal Titration Calorimetry, *Langmuir,* 16, 5267-5275 (DOI: 10.1021/la9912390).
30. Kawamura H., Murata Y., Amaguchi T., Igimi H., Tanaka H. M., Sugihara G., Kratohvil J. P. (1989), Spin-label studies of bile salt micelles, *J. Phys. Chem.,* 93, 3321-3326 (DOI: 10.1021/j100345a087).
31. Santhanlakshmi J., Shantha Lakshmi G., Aswal V. K., Goyal P. S. (2001), Small-angle neutron scattering study of sodium cholate and sodium deoxycholate interacting micelles in aqueous medium, *Proc. J. Indian Acad. Sci., Chem. Sci.,* 113, 55-62 (DOI:BF02708552).

32. Mazer N. A., Carey M. C., Kwasnick R. F., Benedek G. B. (1979), Quasielastic light scattering studies of aqueous biliary lipid systems. Size, shape, and thermodynamics of bile salt micelles, *Biochemistry* 18, 3064-3075 (DOI:10.1021/ bi00581a024).

33. Carey M. C., Small D. M. (1969), Micellar properties of dihydroxy and trihydroxy bile salts: Effects of counterion and temperature, *J. Colloid Interface Sci.,* 31, 382-396 (DOI: 0021979769901817).

34. Connor C. J. O., Wallace R. G. (1985), Physico-chemical behavior of bile salts, *Adv. Colloid Interface Sci.,* 22, 1-111 (DOI: 0001868685800026).

35. Kratohvil J. P. (1986), Size of bile salt micelles: Techniques, problems and results, *Adv. Colloid Interface Sci.,* 26, 131-154 (DOI: 0001868686800197).

36. Bohne C. (2011), Dynamics of Guest Binding to Supramolecular Assemblies. In: Ramamurthy V., Inoue Y. (eds), Supramolecular Photochemistry: Controlling Photochemical Process, John willey Wiley & Sons, New York chapter 1 (ASIN: B0092K3P8S).

37. Yihwa C., Quina F. H., Bohne C. (2004), Modulation with Acetonitrile of the Dynamics of Guest Binding to the Two Distinct Binding Sites of Cholate Aggregates, *Langmuir,* 20, 9983-9944 (DOI: 10.1021/la048943n).

38. Ju C., Bohne C. (1996), Dynamics of Probe Complexation to Bile Salt Aggregates, *J. Phys. Chem.,* 100, 3847-3854 (DOI: 10.1021/jp952657q).

39. Fuentelba D., Thurber K., Bovero E., Pace T. C. S., Bohne C. (2011), Effect of sodium chloride on the binding of polyaromatic hydrocarbon guests with sodium cholate aggregates, *Photochem. Photobiol. Sci.,* 10, 1420-1430 (DOI: 10.1039/C1PP05058C).

40. Wiedmann T. S., Liang W., Kamel L. (2002), Solubilization of Drugs by Physiological Mixtures of Bile Salts, *Pharm. Res.*, 19, 1203-1208 (DOI: 378047).

41. Mandal S., Ghosh S., Aggala H. K., Banerjee C., Govind Rao V., Sarkar N. (2013), Modulation of the Photophysical Properties of 2,2′-Bipyridine-3,3′-diol inside Bile Salt Aggregates: A Fluorescence-based Study for the Molecular Recognition of Bile Salts, *Langmuir*, 29, 133-143 (DOI: 10.1021/la304319r).

42. Cai X., Grant D. J., Wiedmann T.S. (1997), Analysis of the solubilization of steroids by bile salt micelles, *J. Pharm. Sci.*, 86, 372-377 (DOI: 10.1021/js9602148).

43. Zhong Z., Li X., Zhao Y. (2011), Enhancing Binding Affinity by the Cooperativity between Host Conformation and Host–Guest Interactions, *J. Am. Chem. Soc.*, 133, 8862-8865 (DOI: 10.1021/ja203117g).

44. Pattabiraman M., Kaanumalle L. S., Ramamurthy V. (2006), Photoproduct Selectivity in Reactions Involving Singlet and Triplet Excited States within Bile Salt Micelles, *Langmuir*, 22, 2185-2192 (DOI: 10.1021/la0528192).

45. Gomez-Mendoza M., Marin M. L., Miranda M. A. (2011), Dansyl Derivatives of Cholic Acid as Tools to Build Speciation Diagrams for Sodium Cholate Aggregation, *J. Phys. Chem. Lett.*, 2, 782-785 (DOI: 10.1021/jz200178r).

46. Rohacova J., Sastre G., Marin M. L., Miranda M. A. (2011), Dansyl Labeling To Modulate the Relative Affinity of Bile Acids for the Binding Sites of Human Serum Albumin, *J. Phys. Chem. B*, 115, 10518-10524 (DOI: 10.1021/jp201788d).

47. Gomez-Mendoza M., Nuin E., Andreu I., Marin M. L. Miranda M. A. (2012), Photophysical Probes To Assess the Potential of Cholic Acid Aggregates as Drug Carriers, *J. Phys. Chem. B*, 116, 10213-10218 (DOI: 10.1021/jp304708y).

48. Mandal S., Ghosh S., Banerjee C., Rao V. G., Sarkar N. (2012), Modulation of Photophysics and Photodynamics of 1′-Hydroxy-2′-acetonaphthone (HAN) in Bile Salt Aggregates: A Study of Polarity and Nanoconfinement Effects, *J. Phys. Chem. B,* 116, 8780-8792 (DOI**:** 10.1021/jp302435h).

49. Galantinia L., Pavel N. V. (2003), Collective diffusion and self-diffusion coefficients comparison to separate interactions and micellar size effects on ionic micelle diffusivities: Cylindrical micelles of sodium taurodeoxycholate, *J. Chem. Phys.,* 118, 2865-2872 (doi.org/10.1063/1.1536050).

50. Adhikari A., Dey S., Mandal U., Das D. K., Ghosh S., Bhattacharyya K. (2008), Femtosecond Solvation Dynamics in Different Regions of a Bile Salt Aggregate: Excitation Wavelength Dependence, *J. Phys. Chem. B,* 112, 3575-3580 (DOI**:** 10.1021/jp7106445).

51. Chowdhury A., Mojumdar S. S., Choudhury A., Banerjee R., Das K. P., Sasmal D. K., Bhattacharyya K. (2012), Deoxycholate induced tetramer of αA-crystallin and sites of phosphorylation: Fluorescence correlation spectroscopy and femtosecond solvation dynamics, *J. Chem. Phys.,* 136, 155101-155111 (doi.org/10.1063/1.3702810).

52. Carey M. C., Montet J. C., Phillips M. C., Armstrong M. J., Mazer N. A. (1981), Thermodynamic and molecular basis for dissimilar cholesterol-solubilizing capacities by micellar solutions of bile salts: cases of sodium chenodeoxycholate and sodium ursodeoxycholate and their glycine and taurine conjugates**,** *Biochemistry,* 20, 3637-3648 (DOI**:** 10.1021/ bi00515a052).

53. Jenkins G., Hardie L. J. (2008), Bile Acid: Toxicology and Bioactivity, Royal Society of Chemistry, Cambridge, UK (ISBN-10: 0854048464).

54. Hoffman A., Mysels K. J. (1992), Bile acid solubility and precipitation in vitro and in vivo: the role of conjugation, pH, and Ca2+ ions, *J. Lipid. Res.,* 33, 617-626.

55. Huang Z., Haugland R. P. (1991), Partition coefficients of fluorescent probes with phospholipid membranes, *Biochem. Biophys. Res. Commun.,* 181, 166-171 (DOI: S0006291X 0581396).

56. Das A., Thakur R., Dagar A., Chakraborty A. (2014), A spectroscopic investigation and molecular docking study on the interaction of hen egg white lysozyme with liposomes of saturated and unsaturated phosphocholines probed by an anticancer drug Ellipticine, *Phys. Chem. Chem. Phys.,* 16, 5368-5381 (DOI:10.1039/c3cp54247e).

57. Mukhopadhyay S., Krishnamoorthy I. G., Maitra U. (2003), Dynamics of Bound Dyes in a Nonpolymeric Aqueous Gel Derived from a Tripodal Bile Salt, *J. Phys. Chem B.,* 107, 2189-2192 (DOI: 10.1021/jp027079+).

Chapter 4

Fate of anticancer drug Ellipticine in reverse micelles in aqueous and methanolic environment: a photophysical approach.

In the present chapter, a detailed photophysics of an anticancer agent Ellipticine, in Sodium bis(2-ethylhexyl)sulfosuccinate (AOT) reverse micelle (RM) have been investigated using steady state and time resolved spectroscopy. We observed two opposite spectroscopic phenomena with addition of water and methanol to AOT/hydrocarbon system. Increase in water content in AOT/hydrocarbon system converts neutral Ellipticine into its cationic species while increase in methanol content causes Ellipticine to switch over to a neutral species. Unlike in pure methanol, we did not observe any solvent assisted proton transfer in AOT/hydrocarbon/methanol system. This unique observation was explained considering the inhomogeneity of methanol entrapped in AOT/hydrocarbon system.

4.1. Perspective of the Present Study:

Reverse micelle (RM) provides an attractive model for bio-systems since they can mimic several important and essential features of biological membranes. One of the significant features of RMs is the presence of highly structured and non-homogeneous water molecules, which represent an interesting model of water molecules present in biological systems such as membranes *[1,2,3,4,5]*. Enzyme-containing RMs may offer novel tools for biotechnology and for drug delivery through solubilization of lipophilic drugs *[6]*. In a recent publication, Levinger and co-workers defined AOT/hydrocarbon/methanol system as a microemulsion, as this is a continuous system *[7]*. However, in present study we would prefer the inhomogeneity of methanol in AOT/hydrocarbon/methanol system as reported by other groups *[3,4,5]*. The motivation of photophysical study of Ellipticine in reverse

micelles came from its role as photosensitizer of DNA cleavage *[8]*. It is already reported that in cytoplasm Ellipticine exists in both neutral and protonated forms but in nucleus it exist as only protonated species *[9]*.

Study of photophysical properties inside RM and its switchover from one species to another species will certainly help to understand the photophyscial behavior of Ellipticine inside biological membrane and its role as photosensitizer trigger of nuclease activity by enhancing DNA breakage inside tumor cell *[8]*. From the viewpoint of future biophysical applications, it seems interesting to make a vivid study of the photophysical processes of Ellipticine in Aerosol–OT (AOT) reverse micelles. The structure of AOT is shown in Figure 2.5 (pp. 53).

4.2. Results and Discussion:

4.2.1. Steady state absorption and emission spectra:

We took emission spectra of Ellipticine in aqueous medium at different pH. Since the solubility of Ellipticine in aqueous medium is very less ($<10^{-6}$ M) so; the change in the absorption spectra particularly at longer wavelength with change in pH is difficult of perception. Therefore, we would focus on excitation spectra of Ellipticine in aqueous solution rather than absorption spectra. The emission spectra of Ellipticine at different pH is already shown in previous chapter, still we are showing it for the convenience of the readers (Figure 4.1a). The emission spectra of Ellipticine reveal that in acidic condition (pH~2) the emission maximum takes place at 540 nm. On the other hand at pH 12, an additional band appears around 440 nm with 540 nm band (Figure 4.1a). The emission maxima at 440 and 540 nm are ascribed to the neutral species and cationic species respectively. The excitation spectra at pH~ 2 and pH ~ 12 monitored at 540 nm and 440 nm respectively are shown in Figure 4.1b. We provided the excitation spectra to understand the origin of emission of different species. The excitation spectra reveal that the absorption of neutral and cationic species takes place at 380 and 425 nm respectively (Figure 4.1b).

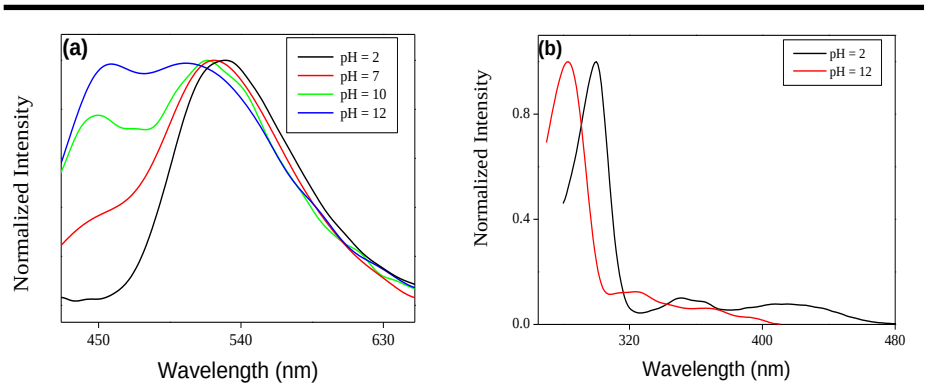

Figure 4.1. *(a) Normalized emission spectra of Ellipticine at different pH (b) Normalized excitation spectra of Ellipticine at pH = 2 and pH = 12.*

We took absorption and emission spectra in AOT/hydrocarbon system at different water and methanol content. In the non-polar solvent like hexane, the absorption band appears at 364 nm. Addition of 0.1 M AOT to n-hexane produces two major bands at 352 nm and 425 nm. The absorption band at 425 nm has a close resemblance with the excitation spectra at pH~2. Miskolczy et al. reported that 1,1,1,3,3,3-hexafluoro-2-propanol (HFIPA) in methanol produces a similar type of band at 425 nm *[10]*. Therefore, we conclude that in AOT reverse micelles, Ellipticine is trapped as cationic species. The absorbance was found to increase further with increase in w_0 value at 352 and 425 nm bands (Figure 4.2a). This fact indicates that with increase in w_0 values more number of Ellipticine molecules are entrapped in the interfacial region of aqueous AOT reverse micelles and are converted into the cationic species. It is observed that there is no change in the absorbance values beyond $w_0 = 8$.

Surprisingly, we observed a reverse trend i.e. decrease in absorbance at 425 nm in AOT/hydrocarbon/methanol system. Interestingly two isobestic points that appear at 297 nm and 409 nm implies that more than one kind of species exist in the ground state in AOT/hydrocarbon/methanol system (Figure 4.2b).

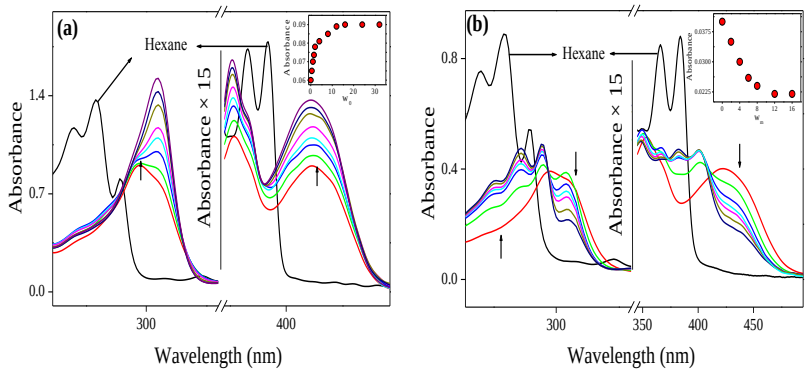

Figure 4.2. *Absorption spectra of Ellipticine in (a) n-hexane and in aqueous reverse micelles at different w_0 values (0-32). In the inset, the absorbance values at 425 nm at different w_0 are shown. (b) n-hexane and AOT/hexane/methanol system at different w_m values (0-16). In the inset, the absorbance values at 425 nm at different w_m are shown.*

We observed a steady decrease in absorbance at 425 nm this indicates that with addition of methanol to AOT/hydrocarbon system, cationic ellipticinium ions switch over to neutral forms and are removed from the head group region.

In this context the emission spectra could be more informative in understanding the observed switchover of Ellipticine from one species to other species. In hexane, the emission maximum appears at 385 nm. With addition of 0.1 M AOT to this solution the emission band shifts to 500 nm. The quantum yield increases from 0.15 to 0.28. The huge red shift and increase in the quantum yield in AOT/hydrocarbon system ensure the encapsulation of Ellipticines in AOT aggregates. With increase in the w_0 values, the emission spectra are found to be red shifted followed by a decrease in the quantum yield (Figure 4.3a). Figure 4.3a also reveals that there is an initial increment in quantum yield on going from w_0 =0 to w_0 = 0.5. The most plausible reason is that with increase in water content in reverse micelles neutral species are converted into the cationic species and at low water content these cationic species are bound to AOT head group region through electrostatic interaction.

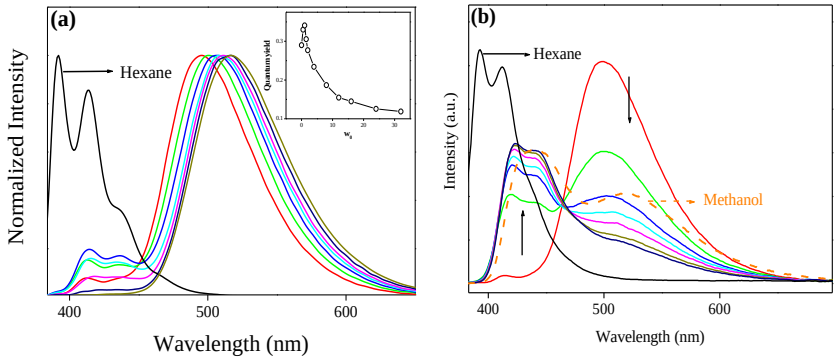

Figure 4.3. *(a) The normalized emission spectra of Ellipticine in aqueous reverse micelles at different w_0 values. In the inset the quantum yield versus w_0 plot is shown. (b) The emission spectra of Ellipticine in AOT/hydrocarbon/methanol system at different w_m values are shown. The dotted line indicates the emission of Ellipticine in pure methanol, which is normalized at 442 nm with respect to maximum w_m value. The quantum yield is not shown as there are two absorbing species in the ground state.*

One interesting finding is that initially, there is an increase in the intensity at 440 nm till w_0= 2. We ascribe the emission band at shorter wavelength region (around 440) nm to neutral species of Ellipticine which remain unbound in the interfacial region. This band continuously decreases with increase in the w_0 values due to conversion of neutral Ellipticines into cationic species. The quantum yield versus w_0 plot reveals that beyond w_0 = 12 there is no significant change in the quantum yield. In this context the photophysics in AOT-methanol microemulsion is more revealing. We observed that addition of methanol to AOT/hydrocarbon system diminishes the intensity at 500 nm band while another emission band grows up at 440 nm. Surprisingly, at highest methanol content the emission band at 500 nm almost disappears and the emission band at the shorter wavelength (440 nm) becomes the primary band. We observed an isoemissive point at around 466 nm in Figure 4.3b which indicates that more than one species take part in the excited state reaction. We assign the emission bands at 442 nm and 500 nm to neutral and cationic species

respectively. Here it is important to note that in pure methanol the Ellipticine exhibits two emission bands at 440 nm and at 520 nm. The band at 440 nm is attributed to the locally excited (LE) band and the second band (520 nm) is attributed to the excited state tautomerization through cyclic solvated species *[11]*. In the present study, the disappearance of longer wavelength emission band and the reappearance of shorter wavelength emission band indicate that cationic ellipticinium species are converted into the neutral species with addition of methanol to AOT/hydrocarbon/methanol system. This observation may be explained if we consider the inhomogeneity of methanol inside the reverse micelles *[3-5]*. It has been reported that four types of methanol molecules are present in AOT/hydrocarbon/ methanol system *[4]*. Among these the trapped methanol is defined as the methanol molecules which remain present in the long hydrocarbon tail of the AOT molecules. The other three types of methanol molecules are sulfonate bound, Na+ bound and bulk type. With increase in w_m values, sulfonate bound methanol molecules increase significantly but bulk type methanol remains constant. Venables et al. *[12]* reported long back that methanol molecules that are hydrogen bonded to the head groups of the surfactant cannot donate hydrogen bonds to other methanol molecules and the methyl groups would be directed towards the centre of reverse micelles, resulting in considerable steric congestion. Setua et al. *[13]* reported that with increasing w_m the area fraction of the bulk methanol remains practically constant. This observation is reasonable and concurrent with property that the reverse micellar size of the AOT/hydrocarbon/methanol system remains almost constant with increase in methanol content. Therefore, in the present study with increase in w_m values two phenomena take place. The first one is the switch over of cationic ellipticinium ions to the neutral species which is revealed by a decrease in intensity at 500 nm emission band. The second one is that the removed Ellipticines do not undergo any solvent assisted proton transfer reaction because in the interface methanol molecules are strongly bound to the AOT head groups and these

sulfonate bound molecules do not have any hydrogen bonding network. However, in case of aqueous reverse micelles free water content increases with increase in w_0 values. Thus in aqueous reverse micelles more number of Ellipticine molecules are converted into cationic species and migrate to water pool which is followed by a continuous red shift and decrease in the intensity.

4.2.2. Time Resolved Studies:

In this context the time resolved study might be more revealing in understanding the fate of Ellipticine with addition of water and methanol to AOT/hydrocarbon system. In the time resolved studies we shall first discuss the anisotropy of Ellipticine in reverse micelles at different water and methanol content (Figure 4.4). Ellipticine being very hydrophobic in nature is unlikely to penetrate deep inside the reverse micellar pool. The cationic species of Ellipticine prefer to bind with the negatively charged head groups of AOT. Table 4.1 reveals that the longer time constant (τ_{2r}) remains same with increasing w_0, till $w_0 = 16$.

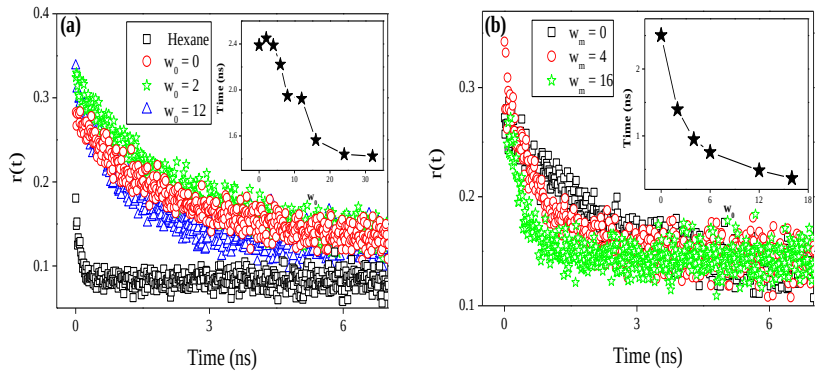

Figure 4.4. *Fluorescence anisotropy decays of Ellipticine in (a) aqueous reverse micelles at different w_0 values. In the inset the rotational relaxation time at different water content is shown. (b) AOT/hydrocarbon/methanol system at different w_m values. In the inset the rotational relaxation time at different methanol content is shown.*

We, therefore, ascribe the slower motion to be originating from the strong coupling between anionic head group of AOT and cationic Ellipticine. The shorter component (τ_{1r}) may originate from those

species which remain unbound in the interfacial region. The decrease in the time constant of shorter component from 1 ns to 0.644 ns and subsequent increase in its amplitude from 28% to 58% indicate that at higher w_0, a few Ellipticine molecules penetrate inside the reverse micelles leaving AOT interfacial region. A similar type of decrease in rotational relaxation is observed with addition of methanol to AOT/hydrocarbon system. We already mentioned that with addition of methanol to AOT/hydrocarbon system, cationic ellipticinium ions are converted into the neutral species. As bulk methanol does not increase with w_m values, so; the Ellipticine molecules which are removed from the interfacial region will remain unbound because methanol is single hydrogen bond donor and being bound to sulfonate group cannot offer any additional hydrogen bond towards Ellipticine.

Table 4.1: *Rotational relaxation data of Ellipticine in AOT/ hydrocarbon system as function of water (w_0) and methanol (w_m) contents.*[#]

AOT/hydrocarbon	a_{1r}(%)	a_{2r}(%)	τ_{1r} (ns)	τ_{2r} (ns)	$<\tau_r>$ (ns)	r_0
$w_0 = 0$	0.28	0.72	1.00	2.93	2.39	0.27
$w_{0=}2$	0.34	0.66	1.40	3.00	2.456	0.32
$w_{0=}4$	0.42	0.58	1.20	3.20	2.389	0.32
$w_{0=}6$	0.42	0.58	0.763	3.28	2.222	0.32
$w_{0=}8$	0.50	0.50	.891	3.05	1.949	0.32
$w_{0=}12$	0.54	0.46	0.882	3.126	1.924	0.32
$w_{0=}16$	0.62	0.38	0.738	3.00	1.564	0.29
$w_{0=}32$	0.58	0.42	0.644	2.44	1.424	0.30
$w_m = 0$	0.27	0.73	1.23	2.98	2.503	0.27
$w_m = 2$	0.81	0.19	1.126	2.553	1.395	0.32
$w_m = 4$	0.87	0.13	0.705	2.693	0.948	0.34
$w_m = 6$	0.86	0.14	0.464	2.527	0.755	0.29
$w_m = 12$	0.90	0.10	0.300	1.450	0.483	0.26
$w_m = 16$	1	-	0.367	-	0.367	0.25

 # Error in the measurement is around 5%

In this context the lifetime data may be more useful to interpret the observed photophysics. The ground state protonation corroborates well with the life time data. We have measured lifetime of Ellipticine at different pH. At pH 10, the lifetime of Ellipticine is bi-exponential and the time components are 0.282 ns (95%) and 5.6 ns (5%). At pH ~7, the lifetime is bi-exponential and consists of the components of 1.85 ns (88%) and 5.55 ns (12%). The lifetime did not change on decreasing the pH further from 7 to 2. The similar lifetime components at pH~2 and pH~7 confirm that at physiological pH Ellipticine remain as cationic species in aqueous solution. In bi-exponential decay, the shorter component may come from the neutral species and the longer component is attributed to the cationic species of Ellipticine. In hexane the lifetime was reported earlier *[14]*. We took decay at 505 nm at different w_0 and w_m values. In AOT/hydrocarbon reverse micelles the average lifetime becomes almost 22 ns. The corresponding components are 1.10 ns (14%) and 25.35 ns (86%). The results are summarized in Table 4.2. We assign that the shorter component to the neutral species while the longer component is coming from the cationic species which are bound to AOT head group owing to the electrostatic interaction. On addition of water to AOT/hexane system, there is a decrease in the lifetime. The longer component decreases from 25 ns to 9 ns while the shorter component decreases from 1 ns to 0.459 ns. Initially, it is observed that there is an increase in the shorter component from 1.10 ns to 1.60 ns with addition of water till $w_0 = 2$. This leads to conclusion, that at low water content, water molecules prefer to reside in the interfacial region. These water molecules are able to form bonds to the neutral Ellipticine molecules through hydrogen bonding which may enhance shorter component. The amplitude of the shorter component increases from 15% to 35%. The decrease in shorter component from nanosecond to a picosecond component and subsequent increase in its amplitude indicate that Ellipticine molecules gradually migrate to the reverse micellar pool leaving AOT interfacial region. We plotted the average lifetime against

the water content of reverse micelles (Figure 4.5a). This fact indicates that there is no change in the lifetime component beyond $w_0 = 12$.

***Table 4.2**: Lifetimes of Ellipticine in AOT/hydrocarbon system as function of water (w_0) and methanol (w_m) contents.*[#]

AOT/hydrocarbon	a_1 (%)	a_2 (%)	τ_1 (ns)	τ_2 (ns)	$\langle\tau\rangle$ (ns)	χ^2
$w_0 = 0$	0.14	0.86	1.1	25.35	22	1.07
$w_0 = 0.5$	0.17	0.83	1.20	22.50	19.25	1.15
$w_0 = 1$	0.20	0.80	1.40	21.50	17.50	1.10
$w_0 = 2$	0.27	0.73	1.63	18.37	13.89	1.16
$w_0 = 4$	0.31	0.69	0.91	16.03	11.32	1.17
$w_0 = 6$	0.34	0.66	0.624	14.21	9.65	1.17
$w_0 = 8$	0.34	0.66	0.546	12.99	8.77	1.14
$w_0 = 12$	0.36	0.64	0.491	11.548	7.589	1.21
$w_0 = 16$	0.35	0.65	0.488	10.76	7.174	1.21
$w_0 = 24$	0.36	0.64	0.438	9.886	6.47	1.19
$w_0 = 32$	0.35	0.65	0.459	9.479	6.33	1.15
$w_m = 0$	0.14	0.86	1.34	25.57	22.53	1.07
$w_m = 1$	0.13	0.87	1.60	20.00	17.60	1.10
$w_m = 2$	0.15	0.85	2.228	17.69	15.38	1.16
$w_m = 4$	0.17	0.83	1.79	13.96	11.94	1.17
$w_m = 6$	0.18	0.82	1.27	12.55	10.517	1.17
$w_m = 8$	0.20	0.80	1.04	11.86	9.74	1.14
$w_m = 12$	0.20	0.80	0.8169	11.36	9.213	1.21
$w_m = 16$	0.20	0.80	0.606	11.23	9.102	1.21

 # Error in the measurement is around 5%

It is interesting to note that there is an increase in the radiative rate constant with addition of water to AOT/hydrocarbon system till $w_0 = 10$ (Figure 4.5a). This fact unambiguously proves that with the addition

of water the neutral species are converted into cationic species and at low water content cationic Ellipticine molecules will be strongly attached to the head group region through electrostatic interaction.

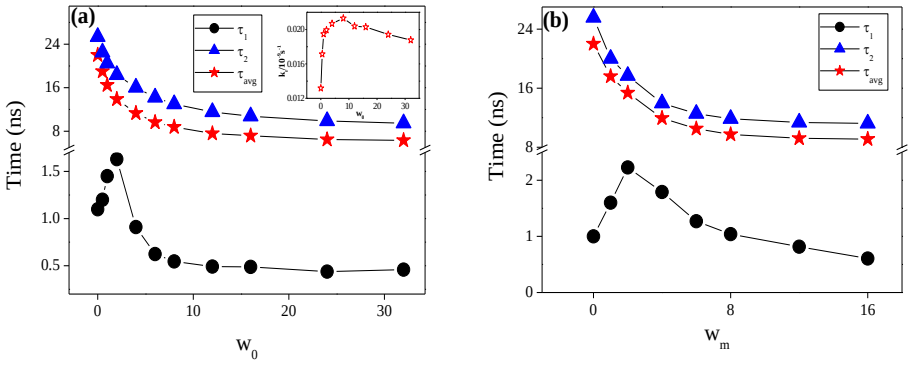

Figure 4.5. *The lifetime components τ_1, τ_2 and τ_{avg} of Ellipticine (a) at different w_0 values. In the inset the variation of radiative rate constant (kr) at different w_0 values are shown. (b) The same at different w_m values.*

In case of AOT/hydrocarbon/methanol system, we observed a similar trend in lifetime like AOT/hydrocarbon/water system. However, in AOT/hydrocarbon/methanol system, the increase in the amplitude of short component is around 6% compared to that (21%) in aqueous reverse micelles (Table 4.2). These results are in well agreement with the assumption that with increase in methanol content the sulfonate bound methanol increases but bulk methanol remains same. Moreover, size of AOT/hydrocarbon/methanol system does not increase significantly. Thus a less number of Ellipticine molecules would be moving towards bulk side. It has been reported earlier by Banerjee et al. *[11]* that Ellipticine undergoes a solvent assisted proton transfer in methanol. We measured lifetime at 560 nm in AOT/hydrocarbon/ methanol system. However, we did not observed any rise component even at highest methanol content. This fact also indicates that in reverse micelles bulk methanol does not increase with increase in w_m. Interestingly plot of average lifetime versus methanol content indicates no change in the photophysics beyond $w_m = 6$ (Figure 4.5b). In case of aqueous reverse micelles the photophysics did not change after w_0=10.

This fact confirms that AOT/hydrocarbon/methanol system gets saturated at lower solvent content than aqueous reverse micelles. However, in pure methanol we do not get any picosecond component. Since the neutral species are responsible for shorter component in AOT/hydrocarbon system, so; in the interfacial region neutral Ellipticine experiences an environment which is independent of the nature of solvent. We ascribe this Ellipticine devoid of any kind of bonding with the interfacial region.

4.3. Conclusion:

The present study reveals that in AOT/hydrocarbon system two contradictory phenomena take place upon addition of water and methanol. With increase in w_0 values, neutral Ellipticine is converted into cationic species while with increase in the w_m values, cationic Ellipticine is converted into neutral species. Interestingly, even at highest methanol content, we did not observe any solvent assisted proton transfer. We attribute this fact to the lack of bulk methanol in an AOT/hydrocarbon/methanol system. Moreover, methanol mostly binds to AOT head group region. Therefore, these methanol molecules are unable to donate a proton to Ellipticine as well as do not facilitate solvent assisted proton transfer. This fact is responsible for the observed decrease in fluorescence at longer wavelength in AOT/hydrocarbon/methanol system.

4.4. References:

1. Liu J., Xiao Y., Allen C. (2004), Polymer–drug compatibility: A guide to the development of delivery systems for the anticancer agent, Ellipticine, *J. Pharm. Sci*., 93, 132-143 (DOI: 10.1002/jps.10533).
2. El Mashak E. M., Paoletti C., Tocanne J. F. (1980), Interactions between Ellipticine and some derivatives and phospholipids in model membranes *FEBS Lett*., 107, 155-159 (http://dx.doi.org/10.1016/0014-5793(79)80485-80488).
3. Nandi N., Bhattacharyya K., Bagchi B. (2000), Dielectric Relaxation and Solvation Dynamics of Water in Complex Chemical and Biological Systems, *Chem. Rev*., 100, 2013–2046 (DOI: 10.1021/cr980127v).
4. Bhattacharyya K., Bagchi B. (2000), Slow Dynamics of Constrained Water in Complex Geometries, *J. Phys. Chem. A.* 104, 10603-10613 (DOI: 10.1021/jp001878f).
5. Bose D., Sarkar D., Girigoswami A., Mahata A., Ghosh D., Chattopadhyay N. (2009), Photophysics and rotational relaxation dynamics of cationic phenazinium dyes in anionic reverse micelles: Effect of methyl substitution, *J. Chem. Phys.,* 131, 114707-114715 (http://dx.doi.org/10.1063/1.3225476).
6. Biswas R., Pal S. K. (2004), Caging enzyme function: α-chymotrypsin in reverse micelle, *Chem. Phys. Lett.,* 387, 221-226 (http://dx.doi.org/10.1016/j.cplett.2004.02.018).
7. Correa N. M., Silber J. J., Riter R. E., Levinger N. E. (2012), Nonaqueous Polar Solvents in Reverse Micelle Systems, *Chem. Rev.,* 112, 4569-4602 (DOI: 10.1021/cr200254q).
8. Perrouault L., Asseline U., Rivalle C., Thuong N. T., Bisagn E. (1990), Sequence specific artificial photo induced endonucleases based on triple-helix forming oligonucleotide, *Nature*, 344, 358-360 (doi:10.1038/344358a0).

9. Schwaller M. A., Allard B., Sureau F., Moreau F. (1994), Protonation Equilibrium of Ellipticine Bound to the Energy-Transducing Membrane of Mitochondria, *J. Phys. Chem.*, 98, 4209-4211 (DOI: 10.1021/j100067a002).
10. Miskolczy Z., Biczok L., Jablonkai I. (2006), Effect of hydroxylic compounds on the photophysical properties of Ellipticine and its 6-methyl derivative: The origin of dual fluorescence, *Chem. Phys. Lett.*, 427, 76-81 (DOI: S0009261406008918).
11. Banerjee S., Pabbathi A., Chandra Sekhar M., Samanta A. (2011), Dual Fluorescence of Ellipticine: Excited State Proton Transfer from Solvent versus Solvent Mediated Intramolecular Proton Transfer, *J. Phys. Chem. A*, 115, 9217-9225 (DOI: 10.1021/jp206232b).
12. Venables D. S. , Huang K., Schmuttenmaer C. A. (2001), Effect of Reverse Micelle Size on the Librational Band of Confined Water and Methanol, *J. Phys. Chem. B*, 105, 9132-9138 (DOI: 10.1021/jp0112065).
13. Setua P., Seth D., Sarkar N. (2009), To probe the structure of methanol and Aerosol OT (AOT) in AOT reverse micelles by FTIR measurements, *Phys. Chem. Chem. Phys.*, 11, 8913-8922 (DOI: 10.1039/B818021K).
14. Fung S.Y., Duhamel J., Chen P. (2006), Solvent Effect on the Photophysical Properties of the Anticancer Agent Ellipticine, *J. Phys. Chem. A.*, 110, 11446-11454 (DOI: 10.1021/jp062778y).

Chapter 5

Photophysical and photodynamical study of Ellipticine: an anticancer drug molecule in bile salt modulated in vitro created liposome.

In the present chapter, entrapment of anticancer drug Ellipticine in *1,2-dipalmitoyl-sn-glycero-3-phosphocholine* (DPPC) liposome and its release by addition of three different bile salts namely Sodium deoxycholate (NaDC), cholate (NaC) and taurocholate (NaTC) have been studied by steady state and time resolved fluorescence spectroscopy. It was found that the release of the drug from liposome depends on the degree of penetration of bile salts. Among the three bile salts, deoxycholate was most effective in releasing the drug from hydrocarbon core of liposome because of its highest insertion ability owing to its maximum hydrophobicity.

5.1. Perspective of the Present Study:

Liposomes are small spherical vesicles which contain amphiphilic lipid enclosing an aqueous core *[1,2]*. Liposomes of desired size are used as biocompatible and protective vehicles, which encapsulate labile molecules such as drugs , proteins etc *[3]*. These systems serve as tools for understanding the permeability and physiology of transport of desired molecules *[4,5]*. The major functional characteristics of liposome that make them useful are, their ability to protect the reagents entrapped within them and to deliver those reagents at specific target site *[6-8]*. Physical characteristic of liposome are influenced by lipid composition and preparation method *[9]*. In present study, DPPC is used, because most saturated lipids are sphingolipids and DPPC exhibits properties very similar to those of sphingomyelin which is the most popular lipid in plasma membrane *[10]*. Natural eukaryotic plasma membranes contain cholesterol as a vital component, it is known to reduce the passive

permeability of membranes and increase membrane mechanical strength *[11]*. It is supposed to widen as well as often shifts the transition temperature, modifies the lateral bilayer organization *[12]*. DPPC is a saturated phospholipid and makes up to one third of total phospholipid present in the body and also accounts for 10-20 % of the phosphatidyl choline of brain myelin and erythrocyte membrane *[13]*. Appropriate amount of bio surfactants such as bile salts when added to the vesicle, it solubilize the vesicles and release the entrapped drug *[14]*. Liposomes after intake are solubilized under physiological conditions in the gastrointestinal tract by bile salts *[15]*. These surfactants induce membrane permeability which helps in drug release and its absorption *[16]*. Solubilization of liposome by surfactant is due to its insertion in the lipid shell of vesicle to form new aggregates *[17]*. The current study was designed to determine whether such liposomes incorporated with drug could be made to release the encapsulated drug upon contact with different bile salts. Usually vesicles are solubilized by bile salts in three stages. First is vesicular stage when the concentration of surfactant is low and surfactant is partitioned between aqueous solution and lipid bilayer. When the concentration of surfactant is further increased, vesicle micelle co-exist and solubilization starts taking place. In the last stage, surfactants are at their CMC and disrupt the bilayer into mixed micelles thus complete solubilization of vesicle takes place *[18,19,20]*. At physiological concentrations, the bile present in the gallbladder, bile ducts, and intestinal lumenis are associated with phospholipids and cholesterol in mixed micellar structures *[21]*. This suggests that the concentration of bile in gall bladder and the hepatic region can theoretically damage the membranes, thus liposome can be dissolved in vivo and can release the entrapped drug *[22,23,24,25,26]*.

Recently, some important photophysical, photodynamical and structural properties of lipid formed vesicles and vesicle-bile salt complexes have been reported. Hof and co-workers extensively studied many physical properties like polarity and viscosity inside the vesicle.

They also studied confinement of different probe molecules in lipid vesicles and in lipid-peptide system. *[27,28,29]*.Bhattacharyya and co-workers studied solvation dynamics and explored ultra slow dynamics inside the vesicle *[30]*. Egelhaaf and coworkers *[31,32]* have studied the structural properties of lecithin and bile salt mixed micelles using small angle neutron scattering study. Sarkar and co-workers *[33,34]* carried out energy transfer in lecithin vesicle and lecithin-bile salt mixed micelles. Recently, Mishra and co-workers reported the effect of submicellar concentration of different bile salts on liposome using the photophysical properties of Fisetin and 1-Napthol *[35,36]*. This group also reported the interaction of conjugated and unconjugated bile salts with DPPC and DMPC liposomes *[37]*.

In the present chapter we would like to report the entrapment of an anti-cancer drug Ellipticine in the DPPC vesicle and the release of this drug through penetration of bile salts into the vesicle. Ellipticine and its 9-methoxy analog have a net amphiphatic character, this structure gives ability to interact with the membrane *[38]*. Encapsulation within the liposomes increases the bioavailability of drug. Thus liposomes show potential as carrier systems for Ellipticine. This will enable one to monitor the uptake of Ellipticine by a given carrier and its release with addition of different bile salts (Deoxycholate, Cholate and Taurocholate) from the carrier to a target site by monitoring the change in absorption and emission spectra.

5.2. Results and Discussion:

5.2.1. Characterization of liposomes:

Before measuring the steady state absorption and emission spectra, we characterized the morphology of liposomes using TEM and AFM. Figure 5.1 shows TEM image of liposomes which were negatively stained with sodium phosphotungstate. Figure 5.2a and 5.2b are the AFM images of DPPC liposomes in two and three dimension respectively. We also provided the particle size distribution data as supporting information in Figure 5.3. The polydispersity factor was

around 0.33. The average diameter of liposomes was found to be around 43 nm.

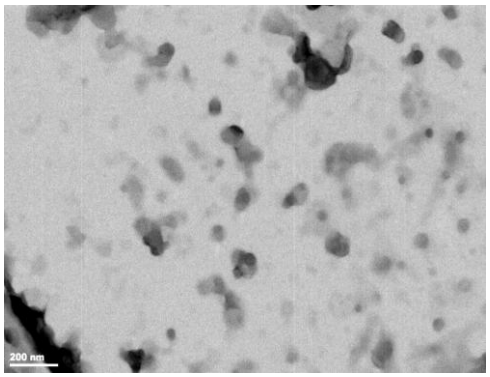

Figure 5.1. *TEM image of DPPC liposome negatively stained with sodium phosphotungstate.*

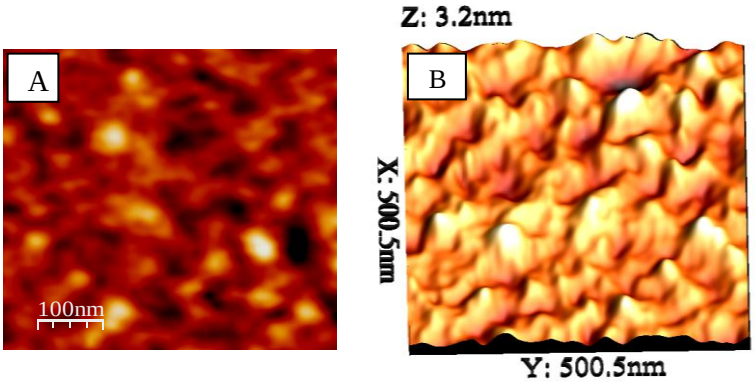

Figure 5.2. *AFM images of DPPC liposome (a) in two dimension (b) in three dimension.*

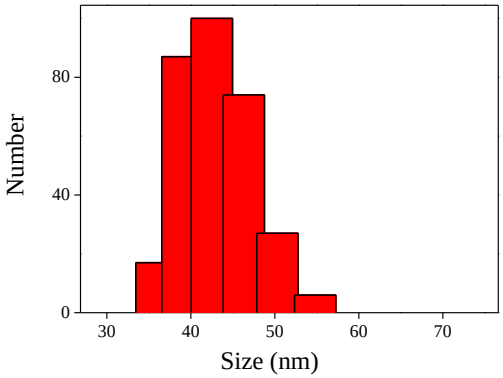

Figure 5.3. *Number (%) distribution of DPPC vesicle at room temperature.*

5.2.2. Steady state absorption and emission spectra:

Once the morphology of liposome was confirmed by different microscopic techniques, we examined the encapsulation of drug molecules into the liposome. Ellipticine is very hydrophobic and sparingly soluble in aqueous solution. The pK_a value of Ellipticine is reported to be 7.40 *[39]*. Therefore; at physiological pH both the neutral and protonated species will exist. The emission of Ellipticine is highly pH sensitive and arises from both protonated and deprotonated species. We took the emission spectra of Ellipticine in aqueous buffer solution at physiological pH (pH ~7.40). The emission maximum of Ellipticine in buffer solution appears at 535 nm. In liposome medium, the solubility of Ellipticine is enhanced more than ten times compared to that in aqueous solution. The emission maximum is shifted to 435 nm and the quantum yield of Ellipticine increases almost twenty five times as compared to that in aqueous buffer solution. To ensure the encapsulation of the drug molecules in the liposome, we took absorption and emission spectra of Ellipticine at several liposome concentrations. The corresponding absorption and emission spectra are shown in Figure 5.4. The partition coefficient between the lipid and aqueous phase was determined in order to quantify the extent of the interaction of the drug molecules with the liposome system using the following equation *[40,41]*.

$$I - I_w = \frac{(I_L - I_w)K_P \nu_L [L]}{1 + K_P \nu_L [L]} \qquad (5.1)$$

where, I_W and I_L are the limit fluorescence intensities with all the drug molecules in water and in water and in the lipid phase, respectively, ν_L is the molar volume of the phospholipid, and [L] is the lipid concentration. Plotting the values of $I - I_w$ obtained at different lipid concentrations versus [L], and performing a nonlinear regression, K_p and I_L are obtained. The corresponding fit is shown in Figure 5.5a. Thus the value of K_P was obtained 2×10^4 considering ν_L as 0.828 $dm^3\,mol^{-1}$.

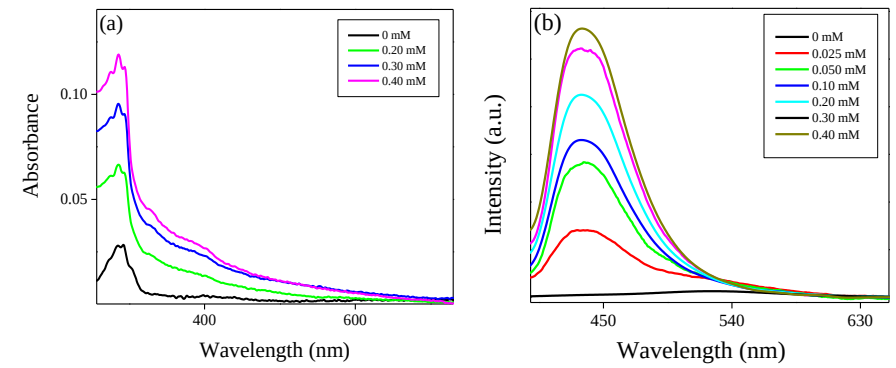

Figure 5.4. *Steady state spectra of Ellipticine at different lipid concentration (a) Absorption spectra (b) Emission spectra.*

However, the experimental data quality obtained using this methodology is not satisfactory due to difficulty in measuring precise intensity in the presence of significant light scattering caused by vesicles suspension. Therefore, we followed the methodology of Castanho and co-workers *[41]* based on the fluorescence lifetime measurement where this artifact is avoided. We discussed the results of partition coefficient using average lifetime in the next section of this chapter. The fitted figure for partition coefficient using average fluorescence lifetime is shown in Figure 5.5b.

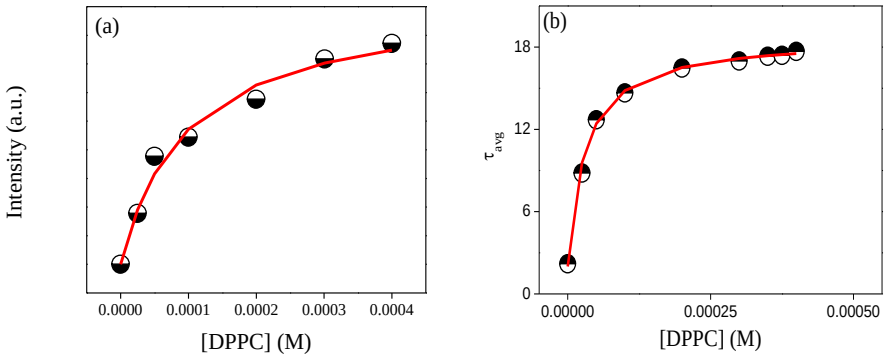

Figure 5.5. *Determination of the partition coefficient (K_p) of Ellipticine in the aqueous phase and DPPC liposome. (a) Fitting was done following equation 5.1 and (b) Fitting was done following equation 5.6.(pp.137)*

We calculated the quantum yield using the following equation:

$$\phi_S = \phi_R \left(\frac{n_S^2}{n_R^2} \right) \left(\frac{I_S}{I_R} \right) \left(\frac{1-10^{-0.5A_R}}{1-10^{-0.5A_S}} \right) \qquad (5.2)$$

We used Quinine sulphate dihydrate in 0·05 M H_2SO_4 as reference (ϕ_R = 0·508). The samples were excited at 325 nm.

In equation 5.2, n_S and n_R represent refractive index of the sample (S) and reference solution (R) respectively, I is the integrated emission intensity, and A the absorbance. The quantum yield is around 0.0020 in aqueous medium and in liposome it becomes around 0.020. The huge blue shift (from 535 nm to 435 nm) and simultaneous increase in the quantum yield of Ellipticine in liposome solution indicates the incorporation of drug in the liposome.

Fung et al. *[42]* suggested that dipole and quadruple moments of indole ring in Ellipticine are likely to interact with the charged polar groups of the phospholipid i.e. molecular internal energy conversion is responsible for observed blue shift in the emission spectra. We agreed with this fact, however; enormous increase in solubility in liposome indicates that substantial amount of Ellipticine will be entrapped inside the hydrophobic core of liposome. With addition of bile salt to liposome solution, the fluorescence intensity decreases at 435 nm and increases at 535 nm. The possible reasons for the decrease in the intensity could be due to the removal of drug molecules from liposomes as well as the change in the fludity of liposome due to the insertion of bile salt. The steady state emission spectra of Ellipticine in presence of different concentrations of bile salts are shown in Figure 5.6. We estimated the Stern-Volmer quenching constant for the same using following equation

$$\frac{I_0}{I} = 1 + K_{SV}[Q] \qquad (5.3)$$

The Stern-Volmer quenching constants obtained upon addition of NaDC, NaC and NaTC are 3300, 1200 and 550 M^{-1} respectively. The

emission intensity decreases around 73%, 65% and 45% for 2 mM concentration of NaDC, NaC and NaTC respectively. This order is in accordance with the hydrophobicity order of bile salt. NaDC possesses two hydroxyl groups and an unconjugated head group (-COOH). On the other hand NaC and NaTC both the bile salts contain three hydroxyl group but they are different in their head groups. NaC contains a -COOH head group like NaDC while NaTC has a conjugated head group (-CO-NH-SO_3Na). Structures are shown in Figure 2.3 (pp. 52). Thus NaDC will be most hydrophobic among three bile salts. The hydrophobicity indices of NaDC, NaC and NaTC are 0.72, 0.13 and 0.00 respectively *[35,36,37]*. Therefore; we expect that NaDC have higher penetrating ability than NaC and NaTC. So, NaDC will be more effective in removal of larger number of drug molecules. Moreover, because of higher insertion ability, NaDC causes hydration of liposome from membrane side to hydrocarbon core. This increases the fluidity in the membrane side and hydrocarbon core which is also partially responsible for the observed decrease in fluorescence intensity. Between cholate and taurocholate, the penetration of cholate would be more into the liposome than that of taurocholate.

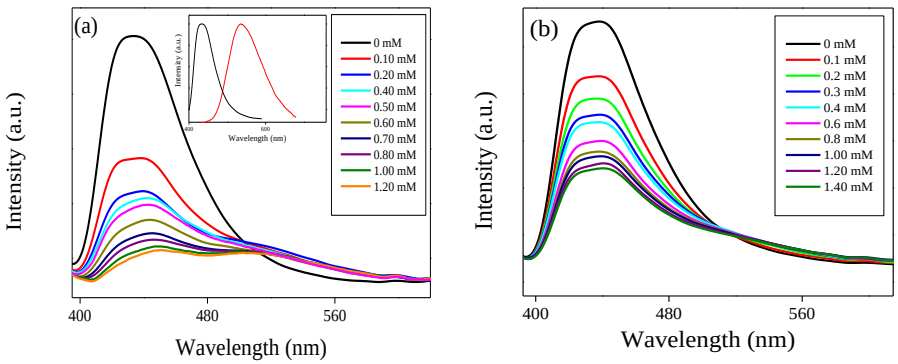

Figure 5.6. *The emission spectra of Ellipticine in liposome at different concentrations of bile salt (0-2 mM) (a) For NaDC, in the inset normalized spectra of Ellipticine in aqueous buffer (red spectrum) and in liposome (black spectrum) are shown (b) For NaC.*

Therefore, cholate would be more effective in penetration in the liposome than taudrocholate hence will quench the fluorescence more.

It is interesting to note that upon addition of bile salts there is a growth in intensity at 535 nm wavelengths.

We split the emission spectrum of Ellipticine at highest bile salt concentration using a combination of two lognormal functions. It is observed that the ratios of area under the two curves corresponding to the 535 and 435 nm wavelengths are 1.07 for NaDC, 0.65 for NaC and 0.55 for NaTC. This fact indicates that NaDC is much more efficient in releasing the drug molecules from the hydrocarbon core due to its high penetrating ability. Although steady state measurements revealed that addition of bile salts release the drug molecules from liposome core, however, it does not conclusively predict the location of Ellipticine after removal from the liposome. Our studies in chapter 3 indicates that in aqueous solution, Ellipticine binds strongly with the negatively charged head group of bile salt. Therefore, in the present study it is possible that Ellipticine molecules after removal from the liposome core are bound to the bile salt and liposome head group region. In this context the time resolved study might be more revealing in understanding the fate of Ellipticine upon addition of bile salt to liposome.

5.2.3 Time Resolved Studies:

Under time resolved studies, we shall first discuss the partition coefficient using average fluorescence lifetime. The relation between average lifetime and partition coefficient is

$$\langle\tau\rangle = \langle\tau\rangle_W \left(\langle\tau\rangle_L - \langle\tau\rangle_W\right) \frac{K_P \gamma_L [L]}{K_P \gamma_L [L] + \left(\varepsilon_W \phi_W / \varepsilon_L \phi_L\right)} \qquad (5.4)$$

The methodology requires the knowledge of ratio obtained by steady state fluorescence spectroscopy

$$\left(\varepsilon_W \phi_W / \varepsilon_L \phi_L\right) \qquad (5.5)$$

where ε is the molar absorptivity. To avoid the error associated with this determination the following equation was used.

$$\bar{\tau} = \frac{\bar{\tau}_W + \bar{\tau}_L K_P \gamma_L [L]}{1 + K_P \gamma_L [L]} \qquad (5.6)$$

where, $\bar{\tau}_W$ and $\bar{\tau}_L$ are the fluorescence lifetime in aqueous phase and in membrane respectively. By nonlinear fit of $\bar{\tau}$ versus $[L]$ data we obtained K_P and $\bar{\tau}_L$ as 4×10^4 and 18.60 ns.

We took fluorescence lifetime data to unravel the fate of Ellipticine drug molecules in the liposome and liposome-bile salt complex. Ellipticine in aqueous medium at pH 7.40 at 535 nm exhibits a bi-exponential decay. The shorter lifetime component (τ_1) and longer lifetime component (τ_2) are around 1.91 ns (90%) and 5 ns (10%). The average lifetime (τ) for Ellipticine at 535 nm is around 2.219 ns. Ellipticine when incorporated in liposome, exhibits emission maxima at 435 nm. The decay of Ellipticine in liposome at 435 nm is a bi-exponential function and consists of components around 1.210 ns (22.6%) and 25.03 ns (77.6%). Thus the average lifetime is around 20 ns. Upon addition of 2 mM NaDC, NaC and NaTC to liposome solution, average lifetime of Ellipticine is reduced from 20 ns to 11.64 ns, 13.7 ns and 16.52 ns respectively. The representative fluorescence decays of Ellipticine in liposome solution and at different concentration of NaDC are shown in Figure 5.7.

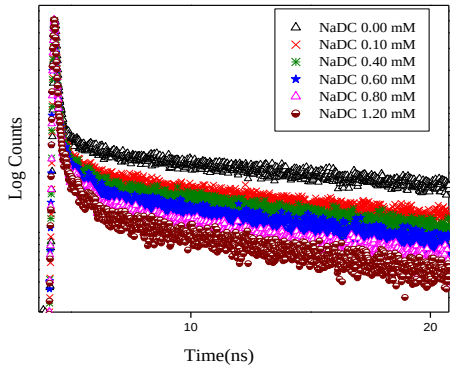

Figure 5.7. *Fluorescence decay curves of Ellipticine as a function of concentration of NaDC (0 mM to 1.2 mM) in liposome solution.*

This order is consistent with the order of decrease in the steady state intensity. It is important to note that decrement in average lifetime and longer time component values are in the order of NaDC>NaC>NaTC. We need to know the actual mechanism, which governs the fate of Ellipticine after removal from the liposome core upon addition of bile salts. It is already reported that bile salt can penetrate into the liposome depending upon their hydrophobicity *[37]*. The average lifetime at different concentrations of bile salts are shown in Figure 5.8. The penetration of bile salt may result in the removal of drug molecules from the hydrocarbon core and interfacial region. This also brings in hydration in the bi-layer as well as liposome core. Blume and co-workers *[43]* reported that addition of bile salt to vesicle, initially forms unstable mixed vesicles. Sometimes these mixed vesicles form larger aggregates.

To have a better knowledge regarding the fate of Ellipticine on addition of bile salt to Ellipticine embedded liposome, one should look into the details of lifetime components along with their relative amplitudes. In the following section, we are trying to discuss the change in lifetime components with the amplitudes and its implication on the fate of Ellipticine after addition of bile salt to liposome solution.

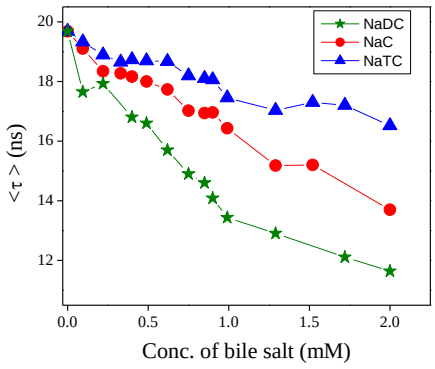

Figure 5.8. *The average lifetimes of Ellipticine in liposome solution with addition of NaDC (green), NaC (red) and NaTC (blue).*

It is revealed from the lifetime data that the shorter lifetime component (τ_1) and its amplitude (a_1) increase with the gradual addition of bile salt to liposome solution, while the longer component (τ_2) and its

amplitude (a_2) decrease. The change in τ_1 and τ_2 values with addition of bile salt to liposome solution are shown in Figure 5.9a and 5.9b. And the population of shorter and longer lifetime i.e. changes in a_1 and a_2 values at different concentration of bile salts are shown in Figure 5.10a and 5.10b. The increase in the a_1 and τ_1 values and subsequent decrease in the a_2 and τ_2 values raise several questions about the fate of the drug molecules after expulsion from liposome. If the simple migration of drug molecules takes place from liposome to aqueous phase then, there should be a major change in a_1 and a_2 values but τ_1 and τ_2 will remain unchanged. However, Figure 5.9 and Figure 5.10 reveal that τ_1 and a_1 are increasing, while τ_2 and a_2 are decreasing with addition of bile salts. Therefore, simple migration of drug molecules from the hydrocarbon core to aqueous phase does not merit in this case. The possibility of migration of the drug molecules from the interfacial region to aqueous phase is also ruled out in a similar argument. If the drug molecules are released from the interfacial region of the lipid membrane and migrates to aqueous phase, there would be no change in τ_1 values but the population should change. However**,** in Figure 5.9 we observe that τ_1 increases with the addition of bile salt. Therefore, migration of drug molecules from interfacial region to aqueous phase seems to be unlikely. Interestingly, we observed that maximum rise in τ_1 values takes place with addition of NaDC (from 1.2 ns to 4.50 ns) and least with addition of NaTC (1.21 ns to 1.58 ns). Therefore, we explain the change in the a_1 and τ_1 values and subsequent decrease in the a_2 and τ_2 values in the following way. It is reported *[36]* that because of one or more hydroxyl groups, hydrophilicity of bile salt is higher as compared to conventional surfactants. Bile salts are able to carry hydrogen-bonded water by polar hydroxyl groups, which causes wetness in membrane and hydrocarbon core region *[36]*.

This drops the τ_2 values of Ellipticine in the liposome. On the other hand due to insertion of bile salt, drug molecules are partially removed from the hydrocarbon core of liposome which results in decrement in the population (a_2) of τ_2.

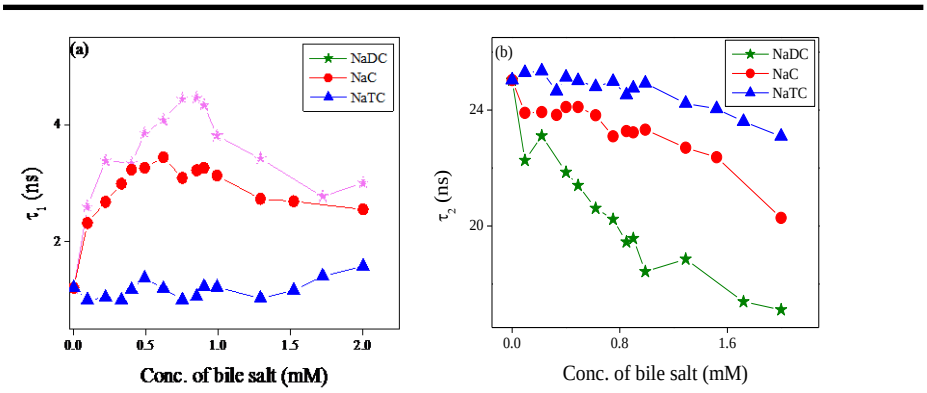

Figure 5.9. *The life time components of Ellipticine with addition of NaDC (green), NaC (red) and NaTC (blue), (a) shorter component (τ_1) and (b) longer component (τ_2).*

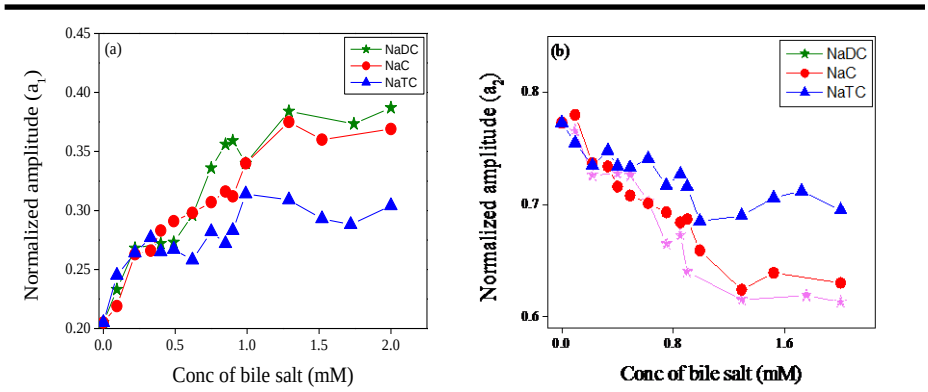

Figure 5.10. *The amplitudes of time constant of Ellipticine with addition of NaDC (green), NaC (red) and NaTC (blue) to liposome solution, (a) shorter component (a_1) and (b) longer component (a_2).*

The degree of removal of the drug molecules depends upon the degree of insertion in turn upon the hydrophobicity of the bile salt. It is noteworthy that among three bile salts, maximum changes in a_1 and a_2 values take place in case of NaDC and least for NaTC.

In this context study on binding of Ellipticine with different bile salts may be significant. We already stated in chapter 3 that, Ellipticine binds strongly with the head group of bile salt at physiological pH. The strong bonding between bile salt head group and Ellipticine is ascribed to the electrostatic interaction which causes an increase in the steady state intensity as well as average lifetime of Ellipticine. Ellipticine

perhaps are trapped as a cationic species in the interfacial region after removal from the liposome, which might be the reason for increasing the shorter component along with its amplitude.

One interesting observation in Figure 5.9a is that beyond 0.75 mM concentration of bile salts in liposome, the faster time constant i.e. τ_1 decreases for NaDC and NaTC. This is due to the fact that at higher concentration of bile salts, hydration takes place in the interfacial region significantly which is responsible for the decrease in the τ_1 values above 0.75 mM concentration of bile salts . However, steady increase in a_1 upon addition of bile salts to liposome indicates that the drug molecules remain in the bile salt-liposome complex even after expulsion from the liposome core.

5.3. Conclusion:

The present study revealed the entrapment of Ellipticine drug in DPPC liposome and its release by the addition of three different bile salts. We found that deoxycholate is more effective in releasing Ellipticine from liposome than cholate and taurocholate salts owing to its higher hydrophobic character. The decrease in the steady state fluorescence and average lifetime of Ellipticine with addition of bile salt were attributed to the release of drug molecules from the hydrocarbon core of liposome due to insertion of bile salts. It was found in the time resolved measurements that with addition of bile salt to liposome solution, the shorter lifetime component and its amplitude increase while longer component and its amplitude decrease. The drug molecules after removal from the liposomes are entrapped in the interfacial region due to the electrostatic interaction, which enhance the shorter lifetime and its amplitude. Bile salts also cause wetness in the membrane and in hydrocarbon core by carrying hydrogen-bonded water molecules which reduce the longer lifetime of Ellipticine in liposome.

5.4. References:

1. Bangham A. D., Standish M. M., Watkins J. C. (1965), Diffusion of univalent ions across the lamellae of swollen phospholipids, *J. Mol. Biol.,* 13, 238-242 (DOI: S0022283665800936).
2. Lichtenberg D., (1995), Liposomes as a model for solubilization and reconstitution of membranes, In: Lasic, D. D., Barenholz Y. (Eds.) Handbook of Nonmedical Applications of Liposomes-Models for Biological Phenomena, vol. 2, CRC Press, Boca Raton, pp. 199–218 (ISBN-10: 084934011X).
3. Lasic D.D. (1993), Liposomes: From Physics to Applications, Elsevier, Amesterdam, (ISBN-10:0444895485).
4. Widder K. J., Senyei A. E., Sears B. (1982), Experimental methods in cancer therapeutics, *J.P.S. Cancer Res.,* 71, 379-387 (doi.org/10.1002/jps.2600710403).
5. Bangham A. D. (1972), Lipid Bilayers and Biomembranes, *Ann. Rev. Biochem.,* 65, 59-64 (DOI: 10.1146/annurev.bi.41. 070172.003541).
6. Goyal P., Goyal K., Kuman V. S. G., Singh A., Katare O. P., Mishra D. N. (2005), Liposomal drug delivery systems-clinical applications, *Acta. Pharma.,* 55, 1-25.
7. Yanase M., Shinkai M., Honda H., Wakabayashi T., Yoshida J., Kobayashi T. (1998), Intracellular Hyperthermia for Cancer Using Magnetite Cationic Liposomes: An in vivo Study, *JPN.J. Cancer Res.,* 89, 463-470 (DOI: 10.1111/j.1349-7006.1998.tb00586.x).
8. Kamps J. D., Scherphof G. L. (2004), Biodistribution and Uptake of Liposomes In Vivo, *Method Enzymol.,* 387, 257-266 (http://dx.doi.org/10.1016/S0076-6879(04)87016-2).
9. Hope M. J., Bally M. B., Mayer L. D., Janoff A. S., Cullis P. R. (1986), Generation of multilamellar and unilamellar phospholipid vesicles, *Chem Phys Lipids,* 40, 89-107 (DOI: 0009308486900654).

10. Xu X., London E. (2000), The Effect of Sterol Structure on Membrane Lipid Domains Reveals How Cholesterol Can Induce Lipid Domain Formation, *Biochemistry*, 39, 843-849 (DOI: 10.1021/bi992543v).
11. Finegold L. X. (1993), Cholesterol in membrane models, CRC Press, London, pp. 4-8 (ISBN-10:0849342074).
12. Seddon A. M., Casey D., Law R.V., Gee A., Templer R. H., Ces O. (2009), Drug interactions with lipid membranes, *Chem Soc Rev*, 38, 2509-2519 (DOI: 10.1039/B813853M).
13. Sujatha J., Mishra A. K. (1998), Phase Transitions in Phospholipid Vesicles: Excited State Prototropism of 1-Naphthol as a Novel Probe Concept, *Langmuir*, 14, 2256-2262 (DOI: 10.1021/la9702749).
14. Fodor E., Jones R. H., Buda C., Kitazka K., Dey I., Farkas T. (1995), Molecular architecture and biophysical properties of phospholipids during thermal adaptation in fish: An experimental and model study, *Lipids*, 30, 1119-1126 (DOI: BF02536612).
15. Cabral D. J., Small D. M. (1989), Physical Chemistry of bile, In: Schultz S.G., Forte J. G., Rauner B. B. (Eds), Handbook of physiology: The gastrointestinal system, oxford university press, new York, , volume 3, section 6, pp. 621-622 (ISBN-10:0195207912).
16. Xia W. J., Onyuksen H. (2000), Mechanistic Studies on Surfactant-Induced Membrane Permeability Enhancement, *Pharma. Res.*, 17, 612-618 (DOI: 223205).
17. Ollivio M., Lesieur S., Madelmont C. G., Nostre M. P. (2000), Vesicle reconstitution from lipid–detergent mixed micelles, *Biochim. Biophys. Acta.*, 1508, 34-50 (DOI: S030441570000006X).
18. Jackson M. L., Schmidt C. F., Lichtenberg D., Litman B. J., Albert A. D. (1982), Solubilization of phosphatidylcholine bilayers by octyl glucoside, *Biochemistry*, 21, 4576-4582 (DOI:10.1021/bi00262a010).

19. Lichtenberg D., Robson R. J., Dennis E. A. (1983), Solubilization of phospholipids by detergents structural and kinetic aspects, *Biochem. Biophy. Acta.,* 737, 285-304 (DOI: 0304415783900047).
20. Hansen U. K., Marie M. le., Moller J. V. (1998), The Mechanism of Detergent Solubilization of Liposomes and Protein-Containing Membranes, *Biophys. J.,* 75, 2932-2946 (DOI: S0006349598777355).
21. Donovan J. M., Timofeyeva N., Carey C. M. (1991), Influence of total lipid concentration, bile salt:lecithin ratio, and cholesterol content on inter-mixed micellar/vesicular (non-lecithin-associated) bile salt concentrations in model bile, *J. Lipid Res.*, 32, 1501-1512.
22. Amigo L., Mendoza H., Zanlungo S., Miquel J. F., Rigotti A., Gonzaliz S., Nervi F. (1999), Enrichment of canalicular membrane with cholesterol and sphingomyelin prevents bile salt-induced hepatic damage, *J. Lipid Res.*, 40, 533-542.
23. Kremmer T., Wisher M. H., Evans W. H. (1976), The Lipid composition of plasma membrane subfractions originating from the three major functional domains of the rat hepatocyte cell surface, *Biochim. Biophys. Acta.,* 455, 655-664 (DOI: 0005273676900390).
24. Torchilin V., Weissig V. (2003), Liposome, a practicle approach, second ed., Oxford university Press, Newyork, pp. 77-89 (ISBN-10: 0199636540).
25. Fugler L., Clejan S., Bittman R. (1985), Movement of cholesterol between vesicles prepared with different phospholipids or sizes, *The J. Biol. Chem.,* 260, 4098-4102.
26. Paul B. K., Guchhait N. (2010), Modulated Photophysics of an ESIPT Probe 1-Hydroxy-2-naphthaldehyde within Motionally Restricted Environments of Liposome Membranes Having Varying Surface Charges, *J. Phys. Chem. B,* 114, 12528-12540 (DOI: 10.1021/jp1048138).

27. Sheynis T., Sykora J., Benda A., Kolusheva S., Hof M., Jelinek R. (2003), Bilayer Localization of Membrane-Active Peptides Studied in Biomimetic Vesicles by Visible and Fluorescence Spectroscopies, *Eur. J. Biochem.* 270, 4478-4487 (DOI: 10.1046/j.1432-1033.2003.03840.x).
28. Dertinger T., Von der Hocht I., Benda A., Hof M., Enderlein J. (2006), Surface sticking and lateral diffusion of lipids in supported bilayers, *Langmuir,* 22, 9339-9344 (DOI: 10.1021/la061389s).
29. Benda A., Beneš M., Mareček V., Lhotský A., Hermens W. Th., Hof M. (2003), How to Determine Diffusion Coefficients in Planar Phospholipid Systems by Confocal Fluorescence Correlation Spectroscopy, *Langmuir,* 19, 4120-4126 (DOI: 10.1021/la0270136).
30. Halder A., Sen S., Dasburman A., Patra A., Bhattacharya K. (2004), Solvation Dynamics in Dimyristoyl-Phosphatidylcholine Entrapped Inside a Sol-Gel Matrix, *J. Phy. Chem. B,* 108, 2390-2312 (DOI: 10.1021/jp035685e).
31. Leng J., Egelhaaf S. U., Cates M. E. (2003), Kinetics of the Micelle-to-Vesicle Transition: Aqueous Lecithin-Bile Salt Mixtures, *Biophysical J.,* 85, 1624-1646 (DOI: S0006349503745937).
32. Madenci D., Salonen A., Schurtenberger P., Pedersen J. S., Egelhaaf S.U. (2011), Simple model for the growth behaviour of mixed lecithin–bile salt micelles, *Phy. Chem. Chem. Phy.*, 13, 3171-3178 (DOI: 10.1039/C0CP01700K).
33. Seth D., Chakraborty A., Setua P., Chakrabarty D., Sarkar N. (2005), Study of Energy Transfer from 7-Amino Coumarin Donors to the Rhodamine 6G Acceptor in Lecithin Vesicles and Sodium Taurocholate−Lecithin Mixed Aggregates, *J. Phys. Chem. B.,* 109, 12080-12085 (DOI: 10.1021/jp050812n).

34. Ghatak C., Rao V. G., Pramanik R., Sarkar S., Sarkar N. (2011), The effect of membrane fluidity on FRET parameters: an energy transfer study inside small unilamellar vesicle, *Phys. Chem. Chem. Phys.*, 13, 3711-3720 (DOI: 10.1039/C0CP01925A).
35. Mohapatra M., Mishra A. K. (2011), Photophysical Behavior of Fisetin in Dimyristoylphosphatidylcholine Liposome Membrane, *J. Phys. Chem. B*, 115, 9962-9970 (DOI:10.1021/jp1123212).
36. Mohapatra M., Mishra A. K. (2010), 1-Naphthol as a Sensitive Fluorescent Molecular Probe for Monitoring the Interaction of Submicellar Concentration of Bile Salt with a Bilayer Membrane of DPPC, a Lung Surfactant, *J. Phys. Chem. B*, 114, 14934-14940 (DOI: 10.1021/jp103855q).
37. Mohapatra M., Mishra A. K. (2011), Effect of Submicellar Concentrations of Conjugated and Unconjugated Bile Salts on the Lipid Bilayer Membrane, *Langmuir*, 27, 13461-13467 (DOI: 10.1021/la203028s).
38. El Mashak E. M., Paoletti C., Tocanne J. F. (1980), Interactions between Ellipticine and some derivatives and phospholipids in model membranes, *FEBS Lett.*, 107, 155-159 (DOI: 0014579379804858).
39. Amman S. J. F., Marcia W. P., Osheroff N., Thompson R. B. (1995), Topoisomerase II Binds to Ellipticine in the Absence or Presence of DNA, *J. Biol. Chem.*, 270, 14998-15004 (doi.org/10.1074/jbc.270.25.14998).
40. Coutinho A., Prieto M. (1995), Self-association of the polyene antibiotic nystatin in dipalmitoylphosphatidylcholine vesicles: a time-resolved fluorescence study, *Biophys. J.*, 69, 2541-2557 (DOI: S0006349595801256).
41. Santos N. C., Prieto M., Castanho M. A. R. B.(1998), Interaction of the Major Epitope Region of HIV Protein gp41 with Membrane Model Systems. A Fluorescence Spectroscopy Study, *Biochemistry*, 37, 8674-8682 (DOI: 10.1021/bi9803933).

42. Fung S. Y., Duhamel J., Chen P. (2006), Solvent Effect on the Photophysical Properties of the Anticancer Agent Ellipticine, *J. Phys. Chem. A*, 110, 11446-11454 (DOI: 10.1021/jp062778y).

43. Hildebrand A., Beyer K., Neubert R., Garidel P., Blume A. (2004), Solubilization of negatively charged DPPC/DPPG liposomes by bile salts, *J. Colloid and Interface. Sci.*, 279, 559-571 (DOI: S0021979704006162).

Chapter 6

Binding of an anticancer alkaloid with HSA and IgG proteins: A spectroscopic and molecular modeling study:

Study of interaction of Ellipticine with various transport protein is essential to gain insight upon solubility and transport of Ellipticine in physiological conditions. Interactions of different prototropic species of Ellipticine with two prominent serum proteins i.e. Human Serum Albumin (HSA) and Immunoglobulin G (IgG) in their native and denatured states have been studied by molecular docking, circular dichroism (CD), steady state and time resolved fluorescence spectroscopy. Unlike, HSA, we found that IgG binds mostly with cationic species of Ellipticine in its native state. The fact implies that the hydrophobic pocket of IgG is inaccessible to drug molecules. However, being denatured by acid and heat treatment hydrophobic pockets were found to be exposed and capture the neutral Ellipticine molecules. The circular dichroism measurements reveal that upon interaction with heat and denatured HSA Ellipticine help in resuming α-helical content.

6.1. Perspective of the Present Study:

Binding of drugs with proteins in the blood stream is an important process in determining the eventual activity and fate of such drugs once they entered the circulation. Such interactions with several proteins control the rate of distribution excretion as well as toxicity of the drug *[1,2]*. These interactions are significant because drugs have maximum affinity towards serum proteins *[3,4,5]*. The major serum proteins are albumin and globulin, albumin mainly help in transport of various agents whereas globulins play role in inflammatory response *[6,7]*. Serum albumin is most abundant protein in circulatory system

accounting for 60% of the total serum proteins. Human Serum Albumin (HSA) is the major component of blood plasma and constitutes approximately half of the protein found in blood. It serves as transport protein for quite a lot of endogenous and exogenous ligands as well as for various drug molecules *[8,9,10]*. It also maintains the colloid osmotic pressure of the circulation, buffers the pH of plasma *[11,12]*. This protein of 585 residue is composed of a single polypeptide chain. It contains three α-helical domain I-III, each containing two subdomain *[13,14]*. The principle regions of ligand binding sites in albumin are located in hydrophobic cavities of sub domain IIA and IIIA. Nobleness of HSA lies in its interaction with various drugs and intracellular trafficking due to various binding sites on this protein *[15,16,17,18,19,20,21,22]*.

Along with albumin the major component of serum protein is globulin. The normal serum protein level is 6 to 8 gm/dl. Albumin makes up 3.5 to 5.0 gm/dl and the remainder is total globulin. Globulin constitute about 36% of plasma proteins. The serum globulins are classified as α , β and γ globulins, γ globulins are major among these and play crucial role in defense mechanism and are commonly known as immunoglobulin *[23,24]*. The major γ globulins in human blood are Immunoglobulin G (IgG). Antibodies principally IgG are intended by nature to defend against a variety of pathogens. This is the second most copious circulating protein and contains long-standing defensive antibodies against several infectious agents. IgG are serene of four polypeptide chains, two heavy and two light. These chains are cross linked by disulphide bonds in to the Y-shaped structure, which is characterized by three fragments (two F_{ab} and one F_c). Specific amino acid sequence in F_{ab} of an IgG determines its ability to selectively bind to a particular antigen *[25,26,27,28]*. These molecules have domains that are structurally independent. The typical IgG is highly soluble at physiological conditions. A prime attribute of these proteins is that non-polar residues are sequestered in a core, where they avoid contact

with water. The disclosure of these hydrophobic residue crop up upon heat and acid treatment *[29,30,31,32,33]*. It is anticipated that partial denaturation of IgG would lead to an increase in exposed hydrophobic surface which results in enhanced binding with 8-Anilinonaphthalene-1-sulfonic acid (ANS). It is believed that IgG acquire chemo attractant activity after exposure of hydrophobic sites. According to several reports hydrophobic domains are located at F_{ab} and F_c region of IgG. DSC measurements propose that F_{ab} domains are mostly affected by heating at 63º C due to lower melting temperature compared with Fc. IgG at low pH provides highly denatured and more hydrophobic conformation. Denaturation of F_c and F_{ab} is independent of each other, upon decreasing the pH F_c fragment is primarily affected and is denaturated *[34,35,36]*. Protein function is intimately linked to protein flexibility and any interaction between a protein and another molecule requires the protein to be able to change its conformation *[37,38]*.

In this chapter, we compared the binding of Ellipticine with IgG and HSA in their native states and various denatured conformations. The study of these proteins using Ellipticine the anti cancer drug as probe molecule will elaborate the possible transportation of drug through serum components in their native and denatured conformations. These results are likely to shed critical light on the fundamental understanding of binding of drug to native and denatured conformations of protein.

6.2. Results and Discussion:

6.2.1 Binding of Ellipticine with HSA:

6.2.1.1. Steady State Emission Spectra:

We already mentioned in our earlier chapter that at physiological pH, both the neutral and cationic species of Ellipticines co-exist. Gradual addition of HSA to aqueous solution of Ellipticine brings about drastic change in the emission spectra (Figure 6.1). We observe a significant increase in quantum yield at 440 nm. However, the intensity at 540 nm

remains almost unchanged. This fact indicates that cationic species of Ellipticine do not bind with HSA. The emission band at 440 nm in native HSA is ascribed to the neutral species of the Ellipticine which are entrapped in the hydrophobic pocket of HSA. For a quantitative estimation of the binding of drug molecules with HSA, we used Bensei-Hildebrand equation for 1:1 complex as shown in the previous chapter.

For such analysis we used the following equation

$$I_f = \frac{I_f^0 + I_{Ellp-HSA} K_1[HSA]}{1 + K_1[HSA]} \qquad (6.1)$$

The binding constant (K_1) obtained from this fitting (Figure 6.1) was around 2.5×10^5 M^{-1}.

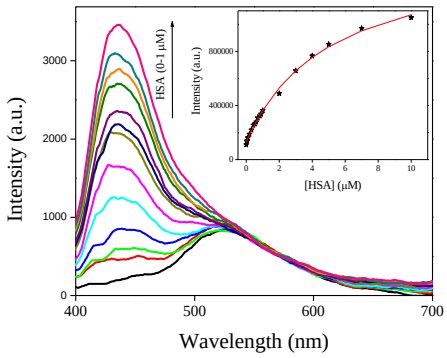

Figure 6.1. *The emission spectra of Ellipticine at different concentration of HSA (0-1 μM). The upward arrow indicates the increase in intensity with increasing concentration of HSA. In the inset, the binding curve of Ellipticine with HSA (0-10 μM) following equation 6.1 is shown.*

To understand the location of probe molecule in HSA, we carried out ANS and warfarin displacement experiments. When ANS is bound to HSA its quantum yield increases several folds and emission shifts to 470 nm. It is reported that Sudlow site I located at subdomain IIA of HSA has much more affinity (K_{as} = 0.87×10^6 M^{-1}) towards ANS

compared to that of Sudlow site II located at subdomain IIIA (K_{as} = 0.079×10^6 M^{-1}) *[39,40,41]*.

Titration of ANS bound to HSA against Ellipticine reveals that the intensity decreases continuously at 470 nm (Figure 6.2). Thus quenching in HSA bound ANS fluorescence proves that Ellipticine binds at a certain hydrophobic cavity, in the proximity of tryptophan 214 (Trp214). Since ANS binds to HSA at more than one site i.e. at subdomain IIA and at subdomain IIIA, *[41]* therefore, ANS displacement experiment cannot precisely judge the location of Ellipticine in HSA.

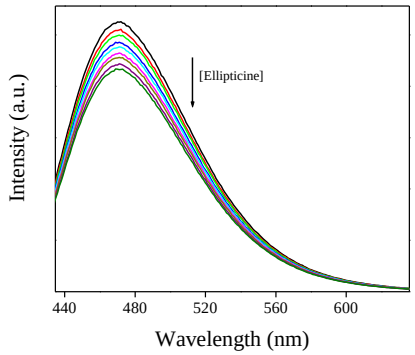

Figure 6.2. *Displacement of site markers from HSA by Ellipticine. Fluorescence emission spectra of HSA-ANS (λ_{ex} = 370) in the presence of increasing concentrations of Ellipticine (0-1 μM).*

So; we carried out warfarin displacement experiment with Ellipticine to find the exact binding site of drug molecules in HSA. The anticoagulant drug warfarin is well-known for binding with HSA at subdomain IIA as determined by X-ray crystallography *[42]*. The fluorescence intensity of warfarin bound to HSA is higher as compared to unbound warfarin. Similar to ANS displacement assay, Ellipticine was gradually added to warfarin bound HSA solution but it revealed no change in the intensity. This suggests that Ellipticine is not displacing the warfarin from Sudlow site I. Therefore, we conclude that Ellipticine mostly binds to hydrophobic cavity located in subdomain

IIIA. This site is already reported to have high binding affinity towards the molecules having carbazole moiety *[43]*.

In this context the energy transfer between Trp214 of HSA (5 μM) and Ellipticine may be useful to understand the binding of drug molecules with HSA. The distance between Trp214 and Ellipticine was estimated from the energy transfer efficiency expression:

$$E = 1 - \frac{I}{I_0} = \left(1 + \frac{R^6}{R_0^{\,6}}\right)^{-1} \qquad (6.2)$$

where I_0 and I are the intensities of Trp214 emission measured for the protein alone and for an Ellipticine-HSA complex, respectively. In the present work, the efficiency of energy transfer between Trp214 of HSA and Ellipticine was around 25%. In this equality, R is the distance between Trp214 and Ellipticine in Angstrom. R_0 is a characteristic distance for 50% energy transfer efficiency related to the properties of donor and acceptor, and can be calculated using following equation

$$R_0^{\,6} = 8.79 \times 10^{-5} n^{-4} \kappa^2 \phi_0 \int \varepsilon(\lambda) f(\lambda) \lambda^4 d\lambda \Big/ f(\lambda) \qquad (6.3)$$

where *n* is the refractive index of the medium, κ^2 is a geometric factor related to the relative orientation of the transition dipole moments of the donor and acceptor, $\varepsilon(\lambda)$ is the molar absorptivity of Ellipticine, and $f(\lambda)$ is the normalized fluorescence intensity of Trp214. Therefore, R_0 is calculated from equation 6.3 using geometrical parameter κ^2 as 2/3. These parameters yielded a value for R_0 of 25 Å, leading to an estimate for *R*, the apparent distance between Trp214 and Ellipticine of 31 Å. This distance is much higher compared to the distance of ligand that generally binds to Sudlow site I. Therefore, it is confirmed that Ellipticine primarily binds to Sudlow site II of subdomain IIIA. The emission spectra corresponding to energy transfer are shown in Figure 6.3.

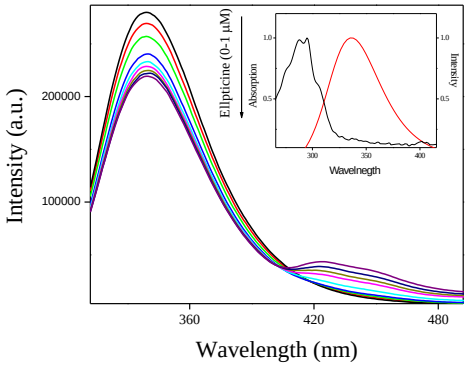

Figure 6.3. *Emission spectra of HSA (5 μM) in presence of different concentration of Ellipticine (0-1μM), λ_{ex} = 295 nm. The inset shows the overlap of absorption and emission spectra of Ellipticine and HSA respectively.*

However, unlike HSA different results are obtained when Ellipticine is treated with native IgG. It is observed that addition of IgG yields a three times rise in intensity at 540 nm while a marginal increment takes place in intensity at 440 nm (Figure 6.4). The significant increment in quantum yield at 540 nm implies that cationic species of Ellipticine binds with native IgG at physiological condition. It has already been reported that IgG has an isoelectric point around 5.80 *[26]*. This means that at pH 7.40, IgG is negatively charged. Therefore, cationic species of Ellipticine binds with native IgG through electrostatic interaction. The little increment in quantum yield at 440 nm indicates a less number of neutral species of Ellipticines bind with the hydrophobic pocket of IgG. This also implies that the hydrophobic pocket of IgG is inaccessible under native condition. The result was surprising when binding experiment was conducted with acid and thermally denatured IgG. Figure 6.4b and Figure 6.4c reveal that addition of heat and acid denatured IgG to aqueous solution of Ellipticine results in significant increment in intensity at 440 nm as compared to that at 540 nm. Since emission band at 440 nm corresponds to neutral species of Ellipticine, so; enhancement in fluorescence intensity at 440 nm implies that neutral species of Ellipticine binds with denatured IgG.

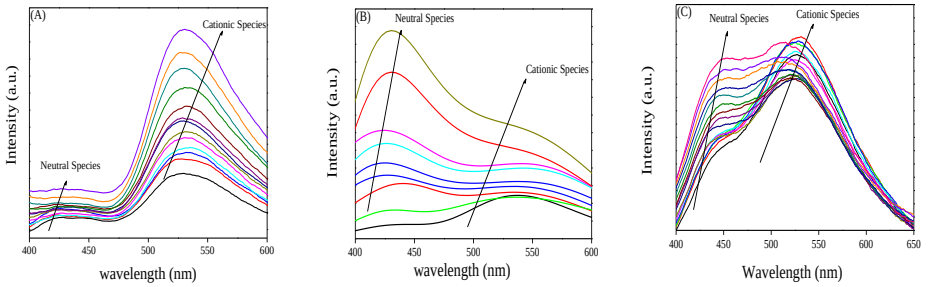

Figure 6.4. *(a) Steady state emission spectra of Ellipticine at different concentration of native IgG (0-3 μM) at pH~7.40 (b) Heat denatured IgG (0-3 μM) at pH~7.40 (c) Acid denatured IgG.*

Therefore, the boost in intensity at 440 nm with addition of denatured IgG may be attributed to the entrapment of Ellipticine in the hydrophobic pocket of IgG. We plotted I_{440}/I_{540} for native IgG and heat and acid denatured IgG (Figure 6.5). It is revealed that I_{440}/I_{540} decreases for native IgG indicating that cationic species primarily bind with native IgG. However, above concentration around 2 μM of IgG, all cationic species are grabbed by negatively charged IgG, the neutral species binds with hydrophobic pocket of native IgG resulting in an enhancement in I_{440}/I_{540}. On the other hand I_{440}/I_{540} from very beginning increases upon addition of denatured IgG leading to the fact that neutral species bind with denatured IgG.

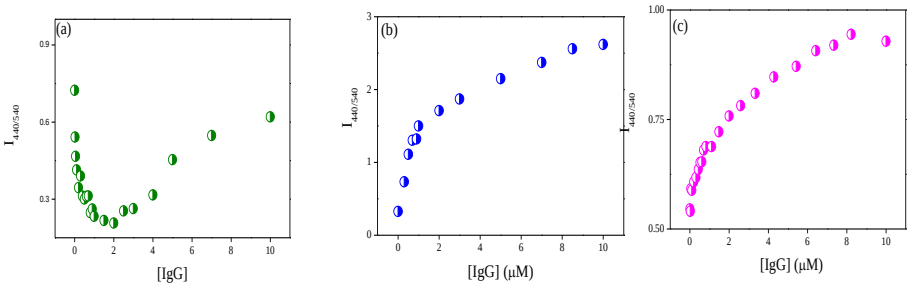

Figure 6.5. *I_{440}/ I_{540} plot of Ellipticine in (a) Native IgG (0-10 μM) at pH~7.40 (b) Heat denatured IgG at pH~7.40 (0-10 μM) and (c) acid denatured IgG at pH ~30 ((0-10 μM).*

It is reported that upon heat and acid treatment F_{ab} and F_c sites of IgG are exposed *[36]*. Therefore, it can be concluded that Ellipticine binds with F_{ab} site when IgG is thermally denatured and with F_c region when IgG is acid denatured. Unlike IgG, when binding studies were conducted with heat denatured HSA, the quantum yield at Sudlow site II was reduced. The similar observation was found when Ellipticine was treated with acid denatured HSA. To gain a more insight regarding the binding of Ellipticine to IgG and HSA, we plotted the quantum yield of Ellipticine at 440 nm at different concentration of native and denatured IgG and HSA (Figure 6.6).

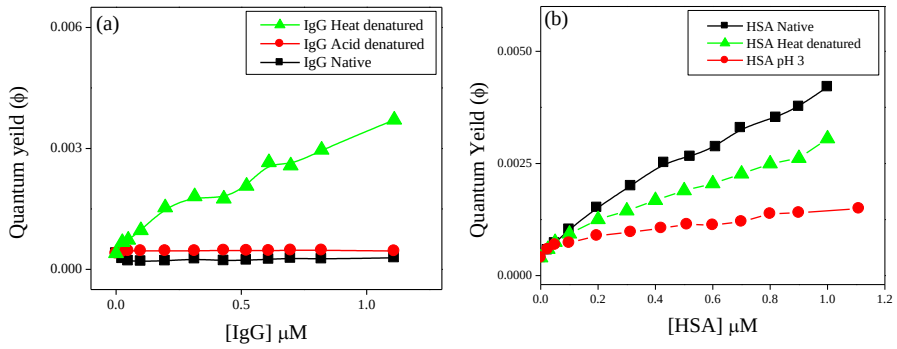

Figure 6.6. *Quantum yield plots of neutral species of Ellipticine at various concentration of native, heat denatured and acid denatured states of (a) IgG (b) HSA.*

It is revealed from Figure 6.6 that quantum yield of neutral species in presence of denatured IgG is much higher compared to that in presence of native IgG. This fact clearly supports the above finding that neutral species of Ellipticine is entrapped in the hydrophobic pocket of IgG. On the other hand the quantum yield was found to be higher in native HSA than that in denatured HSA.

6.2.1.2. <u>Molecular Docking Study:</u>

The interaction of Ellipticine with HSA and IgG were further probed by molecular docking study. In absence of a crystal structure of a protien-ligand complex, docking studies are generally carried out to obtain detailed information about the binding sites and the binding

interactions involved during complexation of ligand with the protein. Docking results can substantiate the experimental results to a large extent by finding preferred binding region of Ellipticine in the respective proteins.

The emission spectra of Ellipticine in (Figure 6.1) suggest that the ligand is going to a hydrophobic pocket of HSA. Subsequent experimentations suggest that the ligand is not interacting with site 1 (subdomain IIA), rather it is binding with other hydrophobic cavity (site II) present in subdomain IIIA. This binding site (site II) is composed of six helices from subdomain IIIA and has a preformed hydrophobic cavity with distinct polar features. The prominent polar region in site II is situated close to one side of the entrance to the binding pocket. These polar residues include Arg 410, Lys 414 and Ser 489. The distances between the interacting residues of HSA with the ligand are given in Table 6.1. It is evident from Table 6.1 that the polar nitrogen atoms of the ligand are in proximity to the polar residues like Arg 410, Lys 414 and Ser 489. The earlier report states that site II preferentially binds the drugs having peripherally located electronegative groups *[44]*. The compounds like difluisal, diazepam, ibuprofen, indoxyl sulphate etc., which bind specifically to site II in such a way that at least one oxygen atom is in vicinity of the polar patch of site II. A similar type of binding of the ligand with HSA is also observed in case of Ellipticine (Figure 6.7), which strongly supports and substantiates the experimental observations of binding of the ligand to site II.

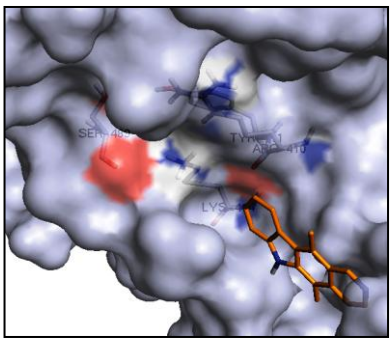

Figure 6.7. *Docked conformation of eppliticine with HSA.*

Table 6.1. *Distances (in Å) between the residues of HSA with the ligand*

HSA residue	Distance
Lys 414 N	6.25 (N_a)
Arg 410 N	10.72 (N_b)
Arg 410 Nδ	9.63 (N_a)
Lys 414 Nε	8.15 (N_a)
Ser 489 O	10.82 (N_a)

To identify the residues taking part in interaction, we have also calculated the Accessible Surface Area (ASA) of all the residues in free protein and in protein-Ellipticine complex. The changes in ASA of the interacting residues are given in Table 6.2. The major change in ASA was observed for the polar and charged residues like Arg 410, Lys 413, Lys 538, Lys 540. Most notably, the residues like Arg 410, Lys 414, which are accessible before interaction, become completely buried by the ligand.

Table 6.2. *Changes in accessible surface area of the amino acid residues of HSA on interaction with Ellipticine.*

HSA residue	ASA (uncomplexed) ($A°^2$)	ASA (protein-inhibitor complex) ($A°^2$)	ΔASA ($A°^2$)
Arg 410	71.25	50.09	21.16
Lys 413	42.62	1.72	40.9
Lys 414	13.38	6	7.38
Glu 492	120.56	100.64	19.92
Val 493	62.01	30.49	31.52
Lys 538	200.32	178.64	21.68
Thr 540	21.97	5.23	16.74
Lys 541	164.54	139.17	25.37

The distance from the ligand to Trp 214 (residue responsible for the intrinsic fluorescence of HSA in a major way) of site I was also measured and found that the ligand is 30.47 Å apart from Trp 214. This distance is very close to that one determined experimentally, which suggests a weak energy transfer between Trp 214 and the ligand.

To find preferred binding sites of Ellipticine within IgG, the ligand was docked individually with F_{ab} and F_c region of the protein (Fig. 6.8). In the docked structure of F_{ab} region with Ellipticine, it is found that the ligand is interacting with Phe 83, Ala 84, and Leu 85 residues through hydrophobic interaction and with Arg 106, Gln 166, Asp 167 and Ser 168 residues polar or charged interaction. CASTp (Computed Atlas of Surface Topography of proteins) program was also used to identify the surface accessible pockets as well as interior inaccessible cavities for proteins. Using CASTp, total 65 pockets have been found to be located in F_{ab} region of IgG, out of which the largest pocket have area 1316.1 $Å^2$. Interestingly, we have found that the residues having hydrophobic interaction Phe 83, Ala 84, Leu 85 and polar interaction Arg 106, Gln 166, Asp 167, Ser 168 are also included in this pocket.

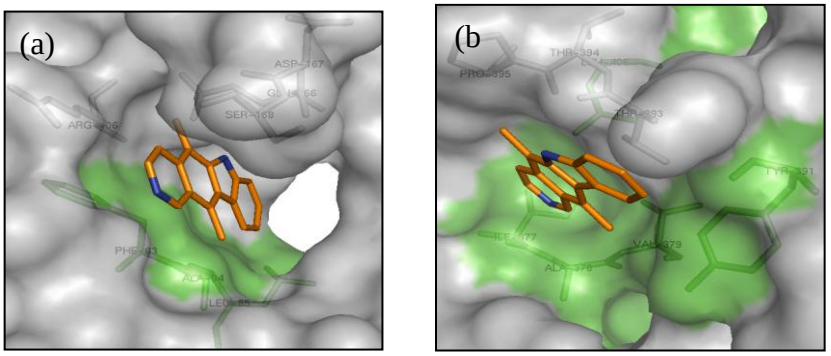

Figure 6.8. *Docked conformation of Ellipticine with (A) F_{ab} and (B) F_c regions of IgG protein.*

The hydrophobic residues are buried toward inside whereas polar residues are close to the entrance to the binding pocket. Whereas, in the docking of F_c region of IgG protein with Ellipticine, interaction with Ile 377, Ala 378, Val 379, Tyr 391, Leu 406 residues were found

through hydrophobic interaction and with Thr 393, Pro 395 residues through polar interaction. The distances between the interacting residues of F_{ab} and F_c regions of IgG protein with the ligand are given in Table 6.3 and Table 6.4. It is evident from these Tables that the hydrophobic atoms of the ligand are in close proximity to the hydrophobic residues like Phe 83, Ala 84, Leu 85 of F_{ab} region and the hydrophobic residues like Ile 377, Ala 378, Val 379, Tyr 391, Leu 406 of F_c region of IgG protein, whereas polar nitrogen atoms of the ligand are in close proximity to the polar residues like Arg 106, Gln 166, Asp 167, Ser 168 of F_{ab} region and Thr 393, Thr 394, Pro 395 of F_c region of IgG protein.

Table 6.3. *Distances (in Å) between the polar residues of F_{ab} and F_c regions of IgG protein with the polar atoms of Ellipticine.*

Polar residues of F_{ab} part	**Distances (Å)**	**Polar residues of F_c part**	**Distances (Å)**
Arg 106		**Thr 393**	
η^1N	4.64(N_b)	N	4.13(N_a)
N	4.69(N_a)	O	3.05(N_a)
		γO	5.12(N_a)
		γO	5.81(N_b)
Gln166		**Thr 394**	
ε^1O	2.69(N_a)	N	5.21(N_a)
ε^2N	4.76(N_a)	O	5.39(N_a)
N	4.81(N_a)	O	5.50(N_b)
O	4.10(N_a)		
Asp 167		**Pro 395**	
N	5.48(N_a)	N	5.75(N_a)
O	5.23(N_a)		
Ser 168			
O	4.23(N_b)		
γO	5.90(N_b)		

Within parenthesis the interacting atoms of the ligand are mentioned.

Table 6.4. *Distances (in Å) between the hydrophobic residues of Fab and Fc regions of IgG protein with the hydrophobic part of ellipticine.*

Hydrophobic residues of Fab part	**Distances (Å)**	**Hydrophobic residues of F_c part**	**Distances (Å)**
Phe 83	3.85(2C), 3.41(3C),	**Ile 377**	4.56(2′-C)
β-C	3.70(9C), 4.09(4C), 4.37(8C), 4.02(5′-CH_3), 3.96(7′-C), 4.31(8′-C), 3.52(5′-C), 4.71(6′-C), 4.25(4′-C)	β-C	
γ-C	4.50(2C), 4.44(3C), 4.92(9C), 4.49(4′-C), 4.50(5′-C), 4.51(7′-C), 4.52(8′-C)	γ^2-C	3.28(2′-C), 4.55(3′-C) 4.73(6′-C)
δ^1-C	4.97(2C), 4.96(3C), 4.68(5′-C), 4.60(4′-C), 4.30(7′-C), 4.27(8′-C), 4.59(3′-C), 4.88(2′-C), 4.59(6′-C)	**Ala 378** β-C	4.76(6′-C)
Ala 84 β-C	4.62(4C), 4.58(5C)	**Val 379** β-C	4.50(5′-CH_3), 4.04(6′-C), 4.87(7′-C)
Leu 85 β-C	5.96(5C)	γ^2-C	4.12(6′-C)
γ-C	5.51(5C) 5.63(6C)		
		Tyr 391	
		γ-C	4.78(4C), 4.76(5C)
		δ^1-C	3.59(4C), 3.86(5C), 4.73(9C), 4.68(5′-CH_3)
		ε^1-C	3.20(4C), 3.75(5C), 4.34(9C), 4.91(3C), 3.76(5′-CH_3), 4.77(5′-C)
		ζ-C	4.51(5′-CH_3), 4.19(4C) 4.58(5C)
		Leu 406 δ^2-C	3.65(2′-C), 4.11(3′-C), 4.88(8′-C), 4.74(6′-C)

Within parenthesis the interacting atoms of the ligand are mentioned.

To identify the residues taking part in interaction, we have also calculated the ASA of all the residues in F_{ab} and F_c regions of IgG protein and in protein-ligand complexes summarized in Table 6.5 and Table 6.6. From the comparison of ASA of free protein with protein-ligand complex, it was observed that for both the hydrophobic and polar residues ASA decreases significantly after protein-ligand interaction. Most notably, the residues like Phe 83, Ala 84 and Gln 166 of F_{ab} region of IgG protein which are accessible before interaction, become completely unaccessible due to ligand whereas residues like Ile 377, Ala 378, Val 379 and Leu 406 of F_c region of IgG protein become almost buried by the ligand.

Table 6.5. *Changes in accessible surface area of the amino acid residues of F_{ab} region of IgG protein on interaction with Ellipticine.*

Residues of F_{ab} part	**ASA of F_{ab} part residues in uncomplexed IgG ($Å^2$)**	**ASA of F_{ab} part residues in IgG-ligand complex ($Å^2$)**
Phe 83	34.5	0
Ala 84	9.75	0
Leu 85	48.58	21.39
Arg 106	89.27	39.37
Gln 166	36.22	0
Asp 167	50.58	4.69
Ser 168	101.71	10.9

Table 6.6. *Changes in accessible surface area of the amino acid residues of F_c region of IgG protein on interaction with Ellipticine.*

Residues of Fc region of IgG protein	**ASA (uncomplexed) ($A°^2$)**	**ASA (protein-ligand complex) ($A°^2$)**
Ile 377	16.76	1.93
Ala 378	9.04	0.3
Val 379	14.76	0.4
Tyr 391	57.05	20.27
Thr 393	53.81	6.38
Thr 394	61.88	24.55
Pro 395	51.46	16.22
Leu 406	3.68	0.02

6.2.1.3 Time Resolved Studies:

In the present study time resolved data will reveal the explicit binding of Ellipticine with proteins IgG and HSA. We measured lifetime of Ellipticine varying the concentration of IgG and HSA till 10 μM. Decays were collected at 440 nm as well as at 540 nm concurrently to supervise neutral as well as cationic species. However, in the steady state experiment of HSA we did not find any change at 540 nm upon addition of HSA. Therefore, in presence of HSA, lifetime was taken at 440 nm. However, significant changes were observed when decays were measured at 440 nm. The results are summarized in Table 6.7. It is observed that both the picosecond and nanosecond lifetime components increase upon addition of HSA to aqueous Ellipticine solution. In aqueous solution at physiological pH, Ellipticine exhibits bi-exponential decays at 440 nm. The lifetime components are 0.44 ns (87%) and 5.29 ns (13%) and the average lifetime is 1.07 ns. The fast component is attributed to the neutral species which are abundant at 440 nm emission band. On the other hand the slower component may come from any other prototropic species. Upon addition of HSA to aqueous solution of Ellipticine, we observed that the population of picosecond component decreases while a longer component is generated and monotonously increases with increasing concentration of HSA. At maximum concentration of HSA (5 μm), the components are 2.23 ns (61%) and 16.80 ns (39%). The depletion in the population of the picosecond component clearly indicates that neutral Ellipticine species bind with the hydrophobic pocket of HSA. The longer component suggests that Ellipticine is buried in the hydrophobic pocket of HSA. Since the pk_a of Ellipticine is less *[45]* in nonpolar solvent, therefore, it can be concluded the longer component is coming from the neutral Ellipticine species. It is worthy to mention here that lifetime of Ellipticine is very high. Again the other component in presence of HSA may come from the Ellipticine which are weekly bound in the surface of HSA.

We took lifetime of Ellipticine at 540 nm in presence of native and denatured IgG. The lifetime of Ellipticine in aqueous buffer solution at 540 nm consists of the components around 1.80 ns (84%) and 5.80 ns (16%). The component around 1.84 ns is ascribed to the cationic species which is dominated in the aqueous solution at physiological condition.

Table 6.7. *Fluorescence Decay Parameters of Ellipticine (λ_{ex} = 375 nm) at different concentration of HSA.*

System	a_1 (%)	a_2 (%)	τ_1 (ns)	τ_2 (ns)	$<\tau>$ (ns)	χ^2
Conc. HSA						
0	0.95	0.05	0.28	4.36	0.50	1.21
0.024	0.84	0.16	0.79	5.10	1.48	1.10
0.049	0.84	0.16	0.87	6.00	1.50	1.12
0.100	0.83	0.17	1.02	8.24	2.24	1.10
0.196	0.78	0.21	1.18	13.11	3.65	1.15
0.314	0.73	0.27	1.37	15.62	5.21	1.10
0.43	0.72	0.28	1.42	15.98	5.54	1.10
0.521	0.71	0.29	1.45	17.07	5.97	1.05
0.61	0.68	0.32	1.66	16.91	6.53	1.05
0.697	0.67	0.33	1.78	17.36	6.92	1.05
0.82	0.66	0.34	1.88	17.31	7.12	1.10
0.9	0.64	0.36	2.19	17.01	7.52	1.05
1.1	0.63	0.37	2.33	16.97	6.52	1.00
2	0.63	0.38	2.38	16.90	7.75	1.06
3	0.61	0.39	2.23	16.50	7.36	1.05
5	0.61	0.39	2.23	16.80	7.80	1.01

It is unlikely that at 540 nm wavelength, neutral species of Ellipticine has any contribution to the emission spectra. Therefore, the longer component may come from other prototropic species which are present in the solution in a little amount. Table 6.8 (λ_{em} = 540 nm) reveals that

a long component around 12.50 ns is generated at maximum concentration of IgG (10 μM). The population of this component monotonously increases till 54%. We, therefore, assign the longer component which increases with increasing the concentration of IgG as the cationic species bound to IgG. We already mentioned in the previous section that IgG remains negatively charged at physiological condition. The interaction between cationic species and native IgG is governed by electrostatic interaction. The depletion in the population of cationic species and subsequent increment in the longer component along with its population confirm that cationic species of Ellipticine bind with negatively charged IgG. A similar kind of increment in the longer component is observed when heat denatured IgG is added to aqueous Ellipticine solution. However, Table 6.8 and 6.9 reveals the population of the longer component in presence of native IgG is around 54% while in case of heat denatured IgG its is around 32% rendering a lower average lifetime values in denatured IgG as compared to that in native IgG. A plot of population of fast and slower component (a_2/a_1) corresponding to decays at 540 nm reveals much higher values for native IgG (Figure 6.9c). This may be attributed to the fact that upon heat treatment the hydrophobic pockets are exposed which may screen the native part of IgG and the interaction between cationic Ellipticine and IgG through electrostatic interaction.

In this context, the decays parameters at 440 nm corroborate well with the assumption that neutral species binds with the hydrophobic pocket of IgG. In case of HSA, we already mentioned that neutral Ellipticine binds with hydrophobic pocket of HSA, similar changes in the lifetime of Ellipticine upon addition of IgG to aqueous Ellipticine solution indicates that Ellipticine binds with the hydrophobic pocket of IgG. It is observed from Table 6.8 and 6.9 that addition of both native and heat denatured IgG, enhances both the pico and nanosecond components at 440 nm. At maximum concentration (10 μM) of native IgG, the picosecond component is found to be enhanced from 0.420 ns

to 1.20 ns while the nanosecond component increases up to 8.33 ns. The population of the nanosecond component increases while that of picosecond component decreases. Similar changes were obtained in case of HSA at 440 nm decays. Since picosecond component represents the neutral species, therefore, drop in population of picosecond component and subsequent increment in the population of nanosecond component indicates that neutral Ellipticine bind with the hydrophobic pocket of native IgG.

Table 6.8. *Lifetime components, normalized amplitudes of lifetime components and average lifetime of Ellipticine in IgG at 440 nm and 525 nm.*[#]

(λ_{em} = 440)					
Conc. Of IgG ($\times10^6$M)	**a_1 (%)**	**a_2 (%)**	**τ_1 (ns)**	**τ_2 (ns)**	**$<\tau>$ (ns)**
0	0.86	0.14	0.42	5.83	1.17
0.025	0.8	0.2	0.40	5.50	1.42
0.05	0.8	0.2	0.42	5.60	1.45
0.1	0.78	0.22	0.42	5.75	1.59
0.2	0.83	0.17	0.83	5.80	1.67
0.4	0.8	0.2	0.84	5.80	1.83
0.5	0.785	0.225	0.86	6.00	2.00
0.7	0.77	0.23	1.00	6.20	2.21
0.8	0.76	0.24	0.97	6.48	2.29
1	0.75	0.25	0.99	6.60	2.39
2	0.74	0.26	1.12	6.86	2.61
3	0.74	0.26	1.10	7.20	2.69
5	0.74	0.26	1.20	7.91	2.94
7	0.74	0.26	1.19	8.19	3.00
10	0.74	0.26	1.10	8.33	2.98
(λ_{em} = 540 nm)					
Conc. Of IgG ($\times10^6$M)	**a_1 (%)**	**a_2 (%)**	**τ_1 (ns)**	**τ_2 (ns)**	**$<\tau>$ (ns)**
0	0.84	0.16	1.80	5.80	2.44

0.025	0.82	0.18	1.81	6.00	2.56
0.05	0.85	0.15	1.80	6.20	2.46
0.1	0.82	0.18	1.81	6.62	2.67
0.2	0.79	0.21	1.81	7.73	3.00
0.3	0.78	0.22	1.82	8.00	3.19
0.4	0.76	0.24	1.80	9.40	3.62
0.5	0.74	0.26	1.83	9.40	3.80
0.6	0.7	0.3	1.81	9.93	4.25
0.7	0.7	0.3	1.84	10.12	4.32
0.8	0.66	0.34	1.81	10.83	4.88
0.9	0.65	0.35	1.85	11.11	5.1
1	0.6	0.4	1.84	11.39	5.66
2	0.58	0.42	1.84	11.87	6.00
3	0.5	0.5	1.86	12.08	6.97
4	0.48	0.52	1.86	12.63	7.46
5	0.46	0.54	1.86	12.25	7.47
7	0.46	0.54	1.87	12.45	7.58
10	0.46	0.54	1.87	12.50	7.58

[#]*Estimated error in the measurement is 5%.*

Table 6.9. *Lifetime components, normalized amplitudes of lifetime components and average lifetime of Ellipticine in heat denatured IgG at 440 nm and 540 nm.*[#]

(λ_{em} = 440)					
Conc. Of IgG ($\times 10^6$M)	**a_1 (%)**	**a_2 (%)**	**τ_1 (ns)**	**τ_2 (ns)**	**$\langle\tau\rangle$ (ns)**
0	0.86	0.14	0.42	5.83	1.17
0.025	0.80	0.20	0.55	5.97	1.64
0.05	0.78	0.22	0.64	6.00	1.83
0.1	0.77	0.23	0.64	6.44	1.97
0.2	0.76	0.24	0.76	6.66	2.17
0.4	0.76	0.24	0.833	6.94	2.30

0.6	0.75	0.25	0.97	7.64	2.64
0.8	0.73	0.27	1.11	8.00	2.98
1.0	0.71	0.29	1.25	8.47	3.34
2.0	0.68	0.32	1.38	8.75	3.74
3.0	0.67	0.33	1.52	9.00	3.99
5.0	0.66	0.34	1.59	9.00	4.12
7.0	0.65	0.35	1.66	9.1	4.26
10.0	0.63	0.37	1.66	9.50	4.56

(λ_{em} = 540 nm)

Conc. Of IgG ($\times 10^6$M)	**a_1 (%)**	**a_2 (%)**	**τ_1 (ns)**	**τ_2 (ns)**	**$<\tau>$ (ns)**
0	0.84	0.16	1.8	5.8	2.44
0.025	0.81	0.19	1.57	6.52	2.51
0.05	0.78	0.22	1.43	6.87	2.63
0.1	0.76	0.24	1.45	7.15	2.82
0.2	0.75	0.25	1.42	7.36	2.90
0.4	0.74	0.26	1.41	7.60	3.0
0.6	0.73	0.27	1.35	8.00	3.16
0.8	0.73	0.27	1.35	8.61	3.31
1.0	0.73	0.27	1.41	9.44	3.58
2.0	0.74	0.26	1.49	10.28	3.77
3.0	0.73	0.27	1.53	11.32	4.17
5.0	0.70	0.3	1.62	12.36	4.84
7.0	0.69	0.31	1.64	12.39	4.97
10.0	0.68	0.32	1.58	12.50	5.10

[#]*Estimated error in the measurement is 5%.*

This assumption is further supported when decays are measured in presence of heat denatured IgG. It is revealed that the addition of denatured IgG to aqueous solution of IgG causes an increment in the pico and nanosecond components quite similar to native IgG. Although the time constants of Ellipticine at 440 nm in denatured IgG remains same to that in native IgG, interestingly, decrement in the population

of picoseond component is from 86% to 63%. The plot of population of fast and slower component (a_2/a_1) corresponding to decays at 440 nm reveals much higher values for denatured IgG (Figure 6.9d).

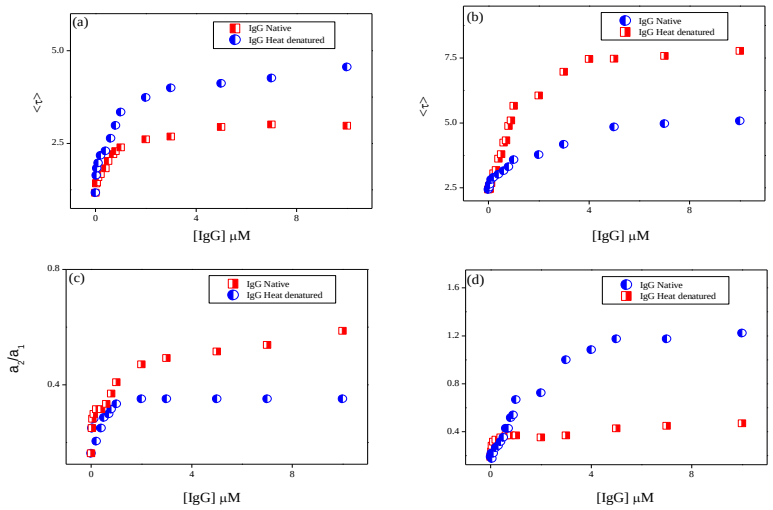

Figure 6.9. *Plot of average lifetime against concentration of native and heat denatured IgG (a) decay collected at 440 nm (b) decay collected at 540 nm (c) Ratio of a_2/a_1 at 540 nm(d) Ratio of a_2/a_1 at 440 nm .*

The higher decrement in the population of picosscond component substantiates the fact that more number of neutral species are entrapped in the hydrophobic pocket of IgG in its denatured state than in native state. We already mentioned that upon heat treatment, the hydrophbic pokets are exposed. These hydrophobic pockets enable denatured IgG to bind with more number of neutral species and results in higher depletion of picosecond component.

6.3. Circular Dichroism:

To gain a better insight on interaction of HSA and IgG with Ellipticine, CD measurements were performed using HSA and IgG in their native and denatured conformations at different concentration of Ellipticine. The CD spectra of native HSA exhibit two negative minima at 208 and 217 nm. The second one is typical characterization of α-helix structure of proteins (Figure 6.10) *[46]*.

Heat and acid denaturation cause reduction in the peak intensity at all wavelength. This reduction in the band intensity indicates conversion of α-helix in to other structures.

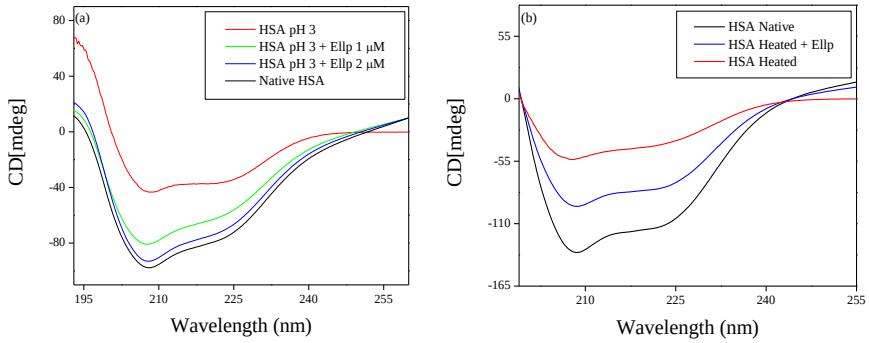

Figure 6.10*. Circular Dichroism spectra of Native and denatured HSA in presence of Ellipticine (A) CD spectra of HSA in acidic condition (B) CD spectra of heat denatured HSA.*

Quantitative analysis of protein secondary structure reveals that native HSA contains α-helical structures about 57.7 % (Table 6.10). The helical content was reduced up to 30.6 % upon treatment with acid (pH~ 3.50). However, we did not observe any significant shift of the peaks. Again addition of Ellipticine (2 μM Ellpticine) increases the band intensity at all wavelengths of the far UV CD and helical content was resumed up to 40 %. In a similar fashion the helical content was found to increase from 31.5% to 47.0% when heat denatured HSA is treated with Elliptcine. This observation confirms that ellipticne brings in stabilization of the secondary structure of protein *[46]*.

CD spectra of IgG exhibit a negative maximum at 217 nm and a positive maximum at 202 nm which is characteristic of β-sheets *[36,47]*. We found that intensity at 202 nm decreased in case of heat and acid denatured IgG without any significant shift and this signifies increase in random coil (Table 6.10). Analysis of secondary structure reveals that heat denaturation of IgG reduces the percentage of β-Sheet from 74% to 70% and and β-Turns from 12% to 9%. The probable

reason of this change may be the denaturation of IgG at higher temperature and conversion of β-sheets and βturns into α–helix and random coils. Addition of Ellipticine to heat denatured IgG helps in resuming β-sheets structure of IgG and also causes reduction in percentage of random coils, in turn, which may result in little binding of neutral species of Ellipticine to IgG in its denatured state. This assertion is also supported by the fact steady state emission spectra show a huge enhancement of peak at 440 nm upon interaction Ellipticine with IgG in denatured state. CD spectra of acid denatured IgG reveals a decrement in band intensity at 202 nm while the negative peak at 217 nm remains less affected. Quantitative analysis signifies that acid denaturation of IgG mainly increases the percentage of random coils (Table. 6.10). The decrease in ellipticity at 202 nm band signifies that F_c region of IgG is exposed due to acid denaturization *[48]*.

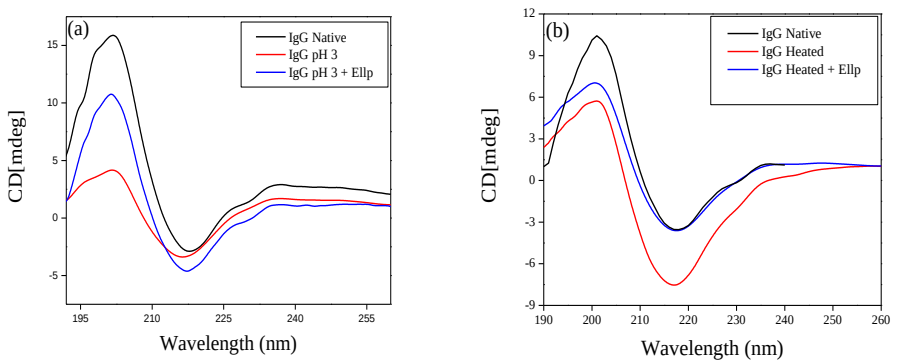

Figure 6.11. *Circular Dichroism spectra of Native and denatured IgG in presence of Ellipticine (A) CD spectra of IgG in acidic condition (B) CD spectra of heat denatured IgG.*

Addition of Ellipticine increase in band intensity at 202 nm along with reduction in the percentage of random coils and α-Helix. This signifies that in acid denatured state Ellipticine binds to Fc region of IgG and helps in resuming the ellipticity of IgG by increasing the intensity at 202 nm.

Table 6.10. *Secondary structure analysis of HSA and IgG at native and denatured states. (calculated by CDNN software).*

System	α-Helix (%)	β-Sheet (%)	β-Turns	Random coils
HSA				
Native	57.7 %	13.8 %	15.2 %	12.6 %
Heated	31.5 %	19.8 %	18.5 %	30.1 %
Heated + 1μM Ellp	47.0 %	19.1 %	15.8 %	17.9 %
pH 3.5	30.6 %	20.8 %	16.8 %	31.7 %
pH 3.5 + 1μM Ellp	33.2 %	24.1 %	18.6 %	24.0 %
pH 3.5 + 2 μM Ellp	40.1 %	18.8 %	17.9 %	23.0 %
IgG				
Native	3 %	74 %	12 %	11 %
Heated	7 %	70 %	9 %	14 %
Heated + 1μM Ellp	5 %	73.7 %	10 %	11.5 %
pH 3.5	2 %	72 %	7.3 %	18.7 %
pH 3 + 1μM Ellp	8.2 %	73.5 %	7.7 %	10.6 %

6.4. Conclusion:

The present study reveals comparative binding of Ellipticine with HSA and IgG. It was observed that neutral species of Ellipticine has more affinity towards native HSA in comparison with heat and acid denatured HSA. Unlike HSA, neutral Ellipticine has more affinity towards denatured IgG in comparision to native IgG. In native state of IgG there exist electrostatic attraction between negatively charged protein and cationic Ellipticine so we can conclude that cationic species of Ellipticine binds with native IgG whereas neutral species of Ellipticine binds with native HSA. Circular Dichroism measurements confirms renaturation of denatured protein by addition of Ellipticine. So; from the present study we can conclude that serum albumin is responsible for transport of neutral species of Ellipticine whereas serum globulin is responsible for transport of cationic Ellipticine.

6.5. References:

1. Lindup W. E. (1988), Progress in Drug Metabolism, Bridges J. W., Chasseaud L. F., Gibson G. G., (Eds.) Taylor & Francis: New York, Vol.10. (ISBN-10: 0850663725).
2. Wainer I. W. (1993), The impact of new liquid chromatography chiral stationary phase technology on the study of stereoselective pharmacokinetics, *Trends Anal. Chem., 12*, 153-158 (DOI: 016599369387017R).
3. Zou J., Taylor P., Dornan J., Robinson S. P., Walkinshaw M. D., Sadler P. J. (2000), First Crystal Structure of a Medicinally Relevant Gold Protein Complex: Unexpected Binding of [Au(PEt3)]+ to Histidine, *Angew. Chem. Int. Edit.***,** 39, 2931-2934 (DOI: 10.1002/1521-3773(20000818)39:16<2931::aid-anie2931>3.0.co;2-w).
4. Xie M., Long M., Liu Y., Qin C., Wang Y. (2006), Characterization of the interaction between human serum albumin and morin, *Biochim. Biophys. Acta***.,** 1760, 1184-1191 (DOI: S0304416506001231).
5. Shiwang L., Zhang L., Zhang X. (2006), Interaction between Fluoroquinolones and Bovine Serum Albumin Studied by Affinity Capillary Electrophoresis, *Anal. Sci.*, 22, 1515-1518 (doi.org/10.2116/analsci.22.1515).
6. Ramakrishnan S., Prasanna K. G., Rajan R. (2004), Chemistry of blood In. Textbook of Medical Biochemistry, Orient Longman Pvt. Ltd: Chennai, pp 155-158 (ISBN: 81 250 20713).
7. Schaller J., Gerber S., Kampfer U., Lejon S., Trachsel C. (2008), Human Blood Plasma Proteins:Structure and Function Jhon Willey & Sons: Hoboken (U.S.A.), pp 17-30 (ISBN-10: 0470016744).

8. Pedersen A. O., Mesenberg K. L., Kragh-Hansen U. (1995), Effects of ionic strength and pH on the binding of medium-chain fatty acids to human serum albumin, *Eur. J. Biochem.*, 233, 395-401 (10.1111/j.1432-1033.1995.395_2.x).
9. Carter D., Chang B., Ho J. X., Keeling K., Krishnasami Z., (1994), Preliminary Crystallographic Studies of Four Crystal forms of Serum Albumin, *Eur. J. Biochem.***,** 226, 1049-1052 (10.1111/j.1432-1033.1994.01049.x).
10. Tamm L. K. (2005), Protein-Lipid Interactions: From Membrane Domains to Cellular Networks, Wiley-VCH, Weinheim Germany, pp.103-114 (ISBN-10: 3527311513).
11. Carballal S., Radi R., Kirk M. C., Barnes S., Freeman B. A., Alvarez B. (2003), Sulfenic Acid Formation in Human Serum Albumin by Hydrogen Peroxide and Peroxynitrite, *Biochemistry***,** 42, 9906-9914 (DOI: 10.1021/bi027434m).
12. Bagatolli L. A., Kivatinitz S. C., Aguilar F., Soto M. A., Sotomayor P., Fidelio G. D. (1996), Two distinguishable fluorescent modes of 1-anilino-8-naphthalenesulfonate bound to human albumin, *J. Fluores.*, 6, 33-40 (DOI: BF00726724).
13. Peters, T. Jr. (1996.), All about Albumins: Biochemistry, Genetics, and Medical Applications; Academic Press: San Diego, (ISBN-10: 0123887232).
14. Zhong D., Douhal A., Zewail A. H. (2000), Femtosecond studies of protein-ligand hydrophobic binding and dynamics: Human serum albumin, *Proc. Natl. Acad. Sci. U. S. A.*, 97, 14056-14061 (doi.org/10.1073/pnas.250491297).
15. Sugio S., Kashima A., Mochizuki S., Noda M., Kobayashi K. (1999), Crystal structure of human serum albumin at 2.5 Å resolution, *Protein Engg*, 12, 439-446 (doi.org/10.1093/protein/12.6.439).

16. Carter D. C., Ho J. X. (1994), Structure of serum albumin, *Adv Protein Chem*, 45, 153-203 (doi.org/10.1016/s0065-3233(08)60640-3).
17. He X. M., Carter D. C. (1992), Atomic structure and chemistry of human serum albumin, *Nature*, 358, 209-215 (DOI: 358209a0).
18. Peters T. (1985), Serum albumin, *Adv. Protein Chem.*, 37, 161-245 (doi.org/10.1016/s0065-3233(08)60065-0).
19. Curry S., Brick P., Frank N. P. (1999), Fatty acid binding to human serum albumin: new insights from crystallographic studies, *Biochim. Biophys. Acta*, 1441, 131-140 (doi.org/10.1016/s1388-1981(99)00148-1).
20. Petitpas I., Grune T., Battacharya A. A., Curry S. (2001), Crystal structures of human serum albumin complexed with monounsaturated and polyunsaturated fatty acids, *J. Mol. Biol.*, 314, 955-960 (DOI: S0022283600952082).
21. Gelamo E. L., Silva C. H. T. P., Imasato H., Tabak M. (2002), Interaction of bovine (BSA) and human (HSA) serum albumins with ionic surfactants: spectroscopy and modeling, *Biochim. Biophys. Acta*, 1594 84-99 (doi.org/10.1016/s0167-4838(01)00287-4).
22. Chuang V. T. G., Otagiri M. (2001), Flunitrazepam, a 7-nitro-1,4-benzodiazepine that is unable to bind to the indole-benzodiazepine site of human serum albumin, *Biochim. Biophys. Acta*, 1546, 337-345 (DOI: S0167483801001510).
23. Busher J. T. (1990), Clinical Methods. In: Walker H. K., Hall W. D., Hurst J. W., The History, Physical, and Laboratory Examinations, third ed. Butterworths, Boston, pp 497-499 (ISBN-10: 040990077X).
24. Kindt T. J., Goldsby B. A., Osborne B. A., Kuby, J. (2007), Kuby Immunology, sixth ed. W. H. Freeman, New York, (ISBN-10: 1429202114).

25. Harris L. J., Skaletsky E., McPherson A., Larson S. B., Hasel K. W., Day J., Greenwood A. (1998), Crystallographic structure of an intact IgG1 monoclonal antibody, *J. Mol. Biol.,* 275, 861-872 (DOI: S0022283697915084).
26. Pilz I., Kratky O., Karush F. (1974), Changes of the Conformation of Rabbit IgG Antibody Caused by the Specific Binding of a Hapten. X-Ray Small-Angle Studies, *Eur. J. Biochem.,* 41, 91-96 (DOI: 10.1111/j.1432-1033.1974. tb03247.x).
27. Harris L. J., Larson S. B., Hasel K. W., Day J., Greenwood A., McPherson A (1992), The three-dimensional structure of an intact monoclonal antibody for canine lymphoma, *Nature,* 360, 369-372 (DOI: 360369a0).
28. Saphire E. O., (2001), Crystal Structure of a Neutralizing Human IgG Against HIV-1: A Template for Vaccine Design, *Science,* 293, 1155-1159 (doi.org/10.1126/science.1061692).
29. Chothia C. J., Novotny R. B., Karplus M. (1985), Domain association in immunoglobulin molecules, *J. Mol. Biol.,* 186, 651-653 (DOI: 0022283685901378).
30. Amzel L. M., Poljak R. J. (1979), Three-Dimensional Structure of Immunoglobulins, *Annu. Rev. Biochem.,* 48, 961-977 (DOI: 0.1146/annurev.bi.48.070179.004525).
31. Relkin P. (2000), Changes in Calorimetric Parameters and Solvent Accessibility of Hydrophobic Groups in Native and Chemically Modified Immunoglobulin G, *J. Phys. Chem. B,* 104, 4980-4985 (DOI: 10.1021/jp993350k).
32. Sompayrac L. M., (2012), How the Immune System Works, fourth ed. Wiley-Blackwell, Hoboken, pp.13-25 (ISBN-10: 0470657294).

33. Rispens T., Lakemond C. M. M., Derksen N. I. L., Aalberse, R. C. (2008), Detection of conformational changes in immunoglobulin G using isothermal titration calorimetry with low-molecular-weight probes, *Anal. Biochem.*, 380, 303-309 (DOI: S0003269708003734).
34. Parker C. W., Osterland C. K. (1970), Hydrophobic binding sites on immunoglobulins, *Biochemistry,* 9, 1074-1082 (DOI: 10.1021/bi00807a004).
35. Taves C. J., Kusumi A., Winkethake J. L. (1984), Human aglycosyl-IgG exhibits increased hydrophobicity, *Biochem. Biophysical. Res. Comm.,* 124, 605-613 (DOI: doi.org/10.1016/ 0006-291x(84)91597-3).
36. Vermeer A. W. P., Norde W. (2000), The Thermal Stability of Immunoglobulin: Unfolding and Aggregation of a Multi-Domain Protein,*Biophysical J.*, 78, 394-404 (DOI: S0006349500766021).
37. Kokkoli E., Mardilovich A., Wedekind A., Rexeisen E. L., Garg A., Craig J. A. (2006), Self-assembly and applications of biomimetic and bioactive peptideamphiphiles, *Soft Matter,* 2, 1015-1024 (DOI: 10.1039/b608929a).
38. Jaenicke R. (2000), Do ultrastable proteins from hyperthermophiles have high or low conformational rigidity, *Proc. Natl Acad. Sci. USA*, 97, 2962-2964 (DOI: 10.1073/pnas.97.7.2962).
39. Daniel E., Weber G. (1966), Cooperative effects in binding by bovine Serum albumin. I. The binding of 1-Anilino-8-naphthalenesulfonate. fluorimetric titrations, *Biochemistry,* 5, 1893-1900 (DOI: 10.1021/bi00870a016).
40. Turner D. C., Brand L. (1968), Quantitative estimation of protein binding site polarity: Fluorescence of N-arylaminonaphthalenesulfonates, *Biochemistry,* 7, 3381-3390 (DOI: 10.1021/bi00850a011).

41. Bagatolli L. A., Kivatinitz S. C., Anguilar F., Soto M. A., Patricio S., Fidelio G. D. (1996), Two Distinguishable Fluorescent Modes of 1-Anilino-8-Naphthalenesulfonate Bound to Human Albumin, *J. Fluorescence,* 6, 33-40 (DOI: BF00726724).

42. Petitpas I., Bhattacharya A. A., Twine S., East M., Curry S. (2001), Crystal Structure Analysis of Warfarin Binding to Human Serum Albumin: ANATOMY OF DRUG SITE I, *The J. Biol. Chem.,* 276, 22804-22809 (doi.org/10.1074/jbc. m100575200).

43. Kragh-Hansen U., Chuang V. T. G., Otagiri M. (2002), Practical Aspects of the Ligand-Binding and Enzymatic Properties of Human Serum Albumin, *Biol. Pharm. Bull.,* 25, 695-704 (doi.org/10.1074/jbc.m100575200).

44. Ghuman J., Zunszain P. A., Petitpas I., Bhattacharya A. A., Otagiri, M., Curry S. (2005), Structural basis of the drug-binding specificity of human serum albumin, *J. Mol. Biol.,* 353, 38-52 (DOI: S0022283605008855).

45. Sureau F., Moreau F., Millot J. M., Manfait M., Allard B., Aubard J., Marc-Antoine Schwaller M. A. (1993), Microspectrofluorometry of the Protonation State of Ellipticine, an Antitumor Alkaloid, in Single Cells, *Biophys. J.,* 65, 1767-1774 (DOI:10.1016/s0006-3495(93)81273-6).

46. Charbonneau D., M. Beauregard and H. A. Tajmir-Riahi, Structural Analysis of Human Serum Albumin Complexes with Cationic Lipids, *J. Phys. Chem. B,* 2009, 113, 1777-1784 (DOI: 10.1021/jp8092012).

47. Doi E., Jirgensons B. (1970), Circular dichroism studies on the acid denaturation of γ-immunoglobulin G and its fragments, *Biochemistry,* 9, 1066-1073 (DOI: 10.1021/bi00807a003).

Chapter 7

The fate of anticancer drug, Ellipticine in DPPC and DMPC liposomes upon interaction with HSA: A photophysical approach.

In this chapter, anticancer drug, Ellipticine is encapsulated within two liposomes namely 1,2-dipalmitoyl-*sn*-glycero-3-phosphocholine (DPPC) and 1,2-dimyristoyl-*sn*-glycero-3-phosphocholine (DMPC) and release of this encapsulated drug from these two liposomes upon addition of HSA have been studied by steady state and time resolved fluorescence spectroscopy. It was observed that HSA penetrates into the liposomes through hydrophobic interaction which reduces the packing order of the lipid bi-layer and leads to a quenching in fluorescence intensity of Ellipticine. DPPC is more dehydrated hence more hydrophobic due to its higher phase transition temperature (42^0 C) as compared to that of DMPC (23^0 C). Therefore, HSA exhibits more affinity towards DPPC than it does towards DMPC. The time resolved components revealed that penetration of HSA into liposomes results in migration of the drug molecules from liposomes to hydrophobic pocket of HSA. Incorporation of HSA in both the liposomes increases the rotational relaxation time of Ellipticine. The fact confirms that HSA penetrates into the liposome and forms bigger complex.

7.1. Perspective of the Present Study:

Vesicles serve as model systems for cell membranes and help in the study of basic mechanism and function of membranes *[1]*. Liposomes are artificial nanosized small spherical vesicles which contain amphiphilic lipid enclosing an aqueous core *[2]*. They are promising systems for drug delivery through the blood stream and are also known to be protein excipients *[3,4,5]*. If a substance entrapped in liposomes is injected intravenously, the substance may be rapidly lost

because of interaction of serum components with the liposomes *[6]*. Therefore, it is necessary to visualize the stability of liposomes in presence of serum proteins *[7]*. Human Serum Albumin (HSA) is the most prominent protein component of blood plasma. It serves as transport protein for several endogenous and exogenous ligands as well as for various drug molecules *[8]*. Its tertiary structure is composed of three domains I, II and III. Each of the domain contains two sub domains A and B. Various ligands bind to hydrophobic cavity in either sub domain IIA (Sudlow site I) or IIIA (Sudlow site II) *[9,10]*. Multiple binding sites in these domains on HSA make it a noble protein which interacts with drugs and regulates intracellular trafficking *[11,12,13,14,15,16,17,18]*. HSA also binds well with fatty acids *[19]*. It was reported that proteins partially penetrate and deform the lipid bi-layer *[20,21]*. HSA partially penetrates into the vesicle and gets adsorbed on the surface of vesicles to some extent. Packing of hydrophobic tails of the lipid is also disturbed in presence of HSA *[22]*. Charbonneau et al. suggested that both hydrophobic and hydrophilic interactions occur for lipid-HSA systems *[23]*. Various groups suggested that for prolonged circulation of liposomes in blood stream and to provide stability, cholesterol should be incorporated in the vesicle *[24,25,26,27]*.

In the present chapter, we would like to unravel the release of an anticancer drug Ellipticine from two different liposomes upon interaction with serum protein. We therefore tried to encapsulate the drug in two liposomes namely DPPC and DMPC and studied its release with addition of HSA. The lipids, DPPC and DMPC are chosen as they vary in their aliphatic chain length as well as in their phase transition temperatures. DPPC exhibits properties very similar to those of sphingomyelin which is the most predominant sphingolipid in plasma membrane. DPPC and DMPC both are zwitterionic lipids, thus there will be less electrostatic repulsion among lipid head groups which results in formation of more organized liposomes *[28]*. Ellipticine and its 9-methoxy analog have a net amphiphatic character

and this structure gives them ability to interact with the membranes *[29]*. The motivation for present study lies in fact that bio-availability of drug is increased by encapsulation within the liposomes, as these drug delivery vehicles easily deliver the drug to most prominent transport protein of blood plasma, which is mainly responsible for the transport of various drugs to their target. Thus present study gives a new insight for photophysics of liposome-HSA drug delivery system for drugs like Ellipticine.

In the previous chapters, we already studied the release of Ellipticine from DPPC liposomes upon addition of bile salts *[30]* and binding of Ellipticine with HSA. In the present chapter, we would like to reveal the photophysics of Ellipticine upon addition of HSA to the drug impregnated liposomes. This would enable us to understand the interaction between liposomes and HSA and fate of Ellipticine in liposomes-HSA system.

7.2. Results and discussion:

7.2.1. Steady state measurements:

After studying the interaction of Ellipticine with HSA in previous chapter, we precede to the study the encapsulation of Ellipticine in liposomes, we characterized the morphology of liposomes by AFM images (Figure 7.1). The size of the liposome was found to be around 100-120 nm.

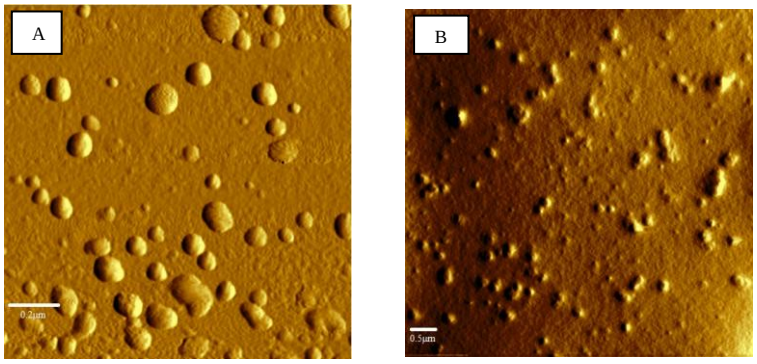

Figure 7.1. *AFM image of (a) DPPC liposomes and (b) DMPC liposomes.*

We have estimated the partition coefficient in DPPC and DMPC liposomes and compared these coefficients in the light of their phase transition temperature. We found that incorporation of Ellipticine in liposomes enhanced quantum yield of Ellipticine almost ten times as compared to that in aqueous buffer solution (Figure 7.2a). The normalized emission spectra of Ellipticine in DPPC and DMPC liposome are shown in Figure 7.2b. It is revealed that Ellipticine is little red shifted in DMPC liposome. The observation indicates that in DMPC liposomes, Ellipticine experiences a more polar environment than that in DPPC. This is because of the fact that DMPC (phase transition temperature 23°C) remains nearly in liquid crystalline phase at room temperature and is more hydrated than DPPC (phase transition temperature 43°C) as the latter remains in sol gel phase at room temperature. It is already reported that lipids having higher phase transition temperature are less hydrated than lipids with lower phase transition temperature *[31]*. We determined the partition coefficient of Ellipticine in liposomes to quantify the extent of interaction of the drug molecules with the liposomes system using the following equation *[32]*.

$$I - I_w = \frac{(I_L - I_w)K_P \nu_L [L]}{1 + K_P \nu_L [L]} \qquad (7.1)$$

where I_w and I_L are the limit fluorescence intensities with all the drug molecules in water and in the lipid phase, respectively, ν_L is the molar volume of the phospholipid, and $[L]$ is the lipid concentration. Plotting I as a function of $[L]$, and performing a nonlinear regression, K_P and I_L are obtained. The corresponding emission spectra and fit are shown in Fig. 7.2c. Thus the values of K_P were 1.1×10^4 and 2.1×10^4 for DPPC and DMPC respectively.

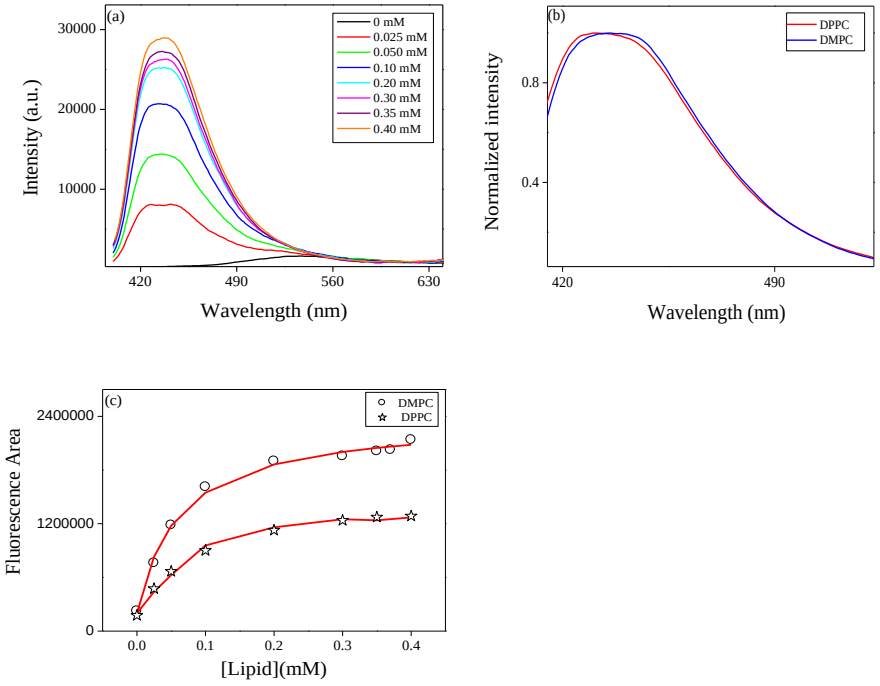

Figure 7.2. *(a) Emission Spectra of Ellipticine at different concentration of DMPC liposomes. (b) Normalized emission spectra of Ellipticine in DPPC and DMPC liposomes. (c) Determination of the partition coefficient (K_p) of Ellipticine in DPPC and DMPC liposomes. Data was fitted according to equation 7.1.*

The higher partition coefficient in DMPC stems from the fact that DMPC remain in nearly liquid crystalline phase while DPPC remains in sol gel phase at room temperature. Therefore, the interfacial region of DMPC is less packed compared to that in DPPC. This factor eases the penetration of Ellipticine in DMPC liposome and increases its encapsulation compared to that in DPPC liposome. As it is confirmed that the drug is incorporated in the liposomes, we studied HSA induced release mechanism of Ellipticine from liposomes. The gradual addition of HSA to Ellipticine loaded liposome solution drops down the intensity of drug molecules. We varied HSA concentration till 5 µM. Figure 7.3 depicts the steady state emission spectra of Ellipticine at different concentration of HSA in DPPC and DMPC liposomes.

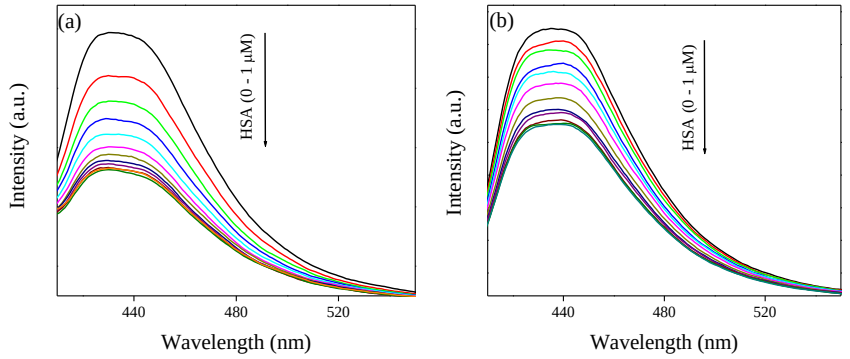

Figure 7.3. *Emission spectra of Ellipticine in (a) DPPC liposomes (b) DMPC liposomes varying the concentration of HSA from 0 to 1 μM. The samples were excited at 375 nm. Downward arrow indicates the decrease in intensity.*

The continuous decrease in the intensity with addition of HSA to Ellipticine impregnated liposomes implies that HSA interacts with the liposomes which may result in release of the drug molecules from vesicle *[33,34]*. The interaction of protein with the hydrocarbon core of liposomes and subsequently affecting the packing of hydrocarbon tails of the lipids has already been reported by Sabin et al *[22]*. This factor may be responsible for the observed quenching in the fluorescence intensity in liposomes. The interfacial tension measurement also supports that protein molecules intercalate between the hydrophobic tails of the lipids *[22]*.

We compared extent of quenching in DPPC and DMPC liposomes by plotting the quantum yield of Ellipticine as a function of the total concentration of HSA (Figure 7.4). The following equation was used to estimate the quantum yield in liposomes *[30]*.

$$\phi_S = \phi_R \left(\frac{n_S^2}{n_R^2} \right) \left(\frac{I_S}{I_R} \right) \left(\frac{1-10^{-0.5A_R}}{1-10^{-0.5A_S}} \right) \qquad (7.2)$$

We used Quinine sulphate dihydrate in 0·05 M H_2SO_4 as reference (ϕ_R = 0·508). The samples were excited at 325 nm. In equation 7.2, n_s and n_R represent refractive index of the sample (S) and reference

solution (R) respectively, *I* is the integrated emission intensity and *A* is the absorbance. It is revealed from Fig. 7.4 that quantum yield of Ellipticine decreases from 0.20 to 0.125 in DPPC-HSA system while the same decreases in DMPC-HSA system from 0.21 to 0.16. The higher decrement in quantum yield (Figure 7.4) in former system may be attributed to the prehydration level of these two liposomes.

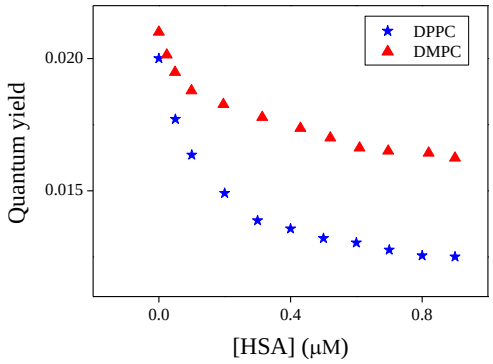

Figure 7.4. *Quantum yield of elliipticine in DPPC and DMPC liposomes at different concentration of HSA.*

At room temperature DMPC remains in nearly liquid crystalline phase (LC) phase while DPPC remains in sol gel (SG) phase. Because of LC phase, DMPC is much more hydrated and thus less hydrophobic compared to its analogue DPPC. Therefore, HSA is supposed to interact more with DPPC compared to that with DMPC due to hydrophobic interaction which results in higher quenching in DPPC compared to that in DMPC. Moreover, the aliphatic hydrophobic chain in DPPC is longer by two carbon atoms. It is already reported that saturated fatty acids bind with greater affinity to albumins as their chain length increases because of an increase in hydrophobic interaction *[35]*. One interesting observation is that although fluorescence intensity diminishes at 435 nm, but no enhancement takes place at 535 nm. The fact indicates that Ellipticine does not migrate to aqueous phase with addition of HSA to liposomes. This is also supported by the fact that no isoemissive point is obtained in Fig. 7.3. The migration from liposomes to hydrophobic pocket of HSA is possible if Ellipticine experiences a similar polarity in HSA and

liposomes. In support of the above statement, we have shown the normalized emission spectra of Ellipticine in 5 μM HSA and DPPC liposomes in Figure 7.5.

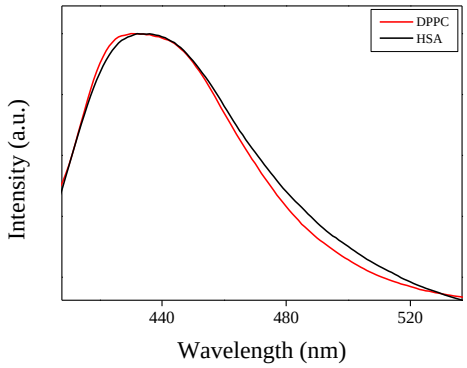

Figure 7.5. *Normalized emission spectra of Ellipticine in DPPC liposome and 5 μM HSA.*

The similar polarity experienced by Ellipticine in liposomes and HSA as revealed from Figure 7.5 may facilitate the migration from liposomes to hydrophobic pocket of HSA. However, from the steady state measurements we cannot get quantitative information regarding the release mechanism. Time resolved data may be more important to understand the release mechanism of Ellipticine from liposome upon addition of HSA. In the next section, we shall emphasize on the formation of liposomes-HSA complex due to partial penetration of HSA into liposomes and possible migration of Ellipticine from liposomes to HSA.

7.2.2 Time Resolved Studies:

In this section we shall first discuss time resolved anisotropy to probe interaction of DPPC and DMPC liposomes with HSA. The fitted anisotropy decays are shown in Figure 7.6. The rotational relaxation parameters are given in Table 7.1 In aqueous buffer solution at pH 7.40, Ellipticine exhibits a single exponential decay with a time constant of 150 ps. In liposomes, the rotational relaxation of Ellipticine is bi-exponential consisting of fast component (ϕ_{fast}) of 0.152 ns (65%) and slow component (ϕ_{slow}) of 2.181 ns (35%) in DPPC liposomes and

the same of 0.150 ns (75%) and 2.660 ns (25%) in DMPC liposomes respectively.

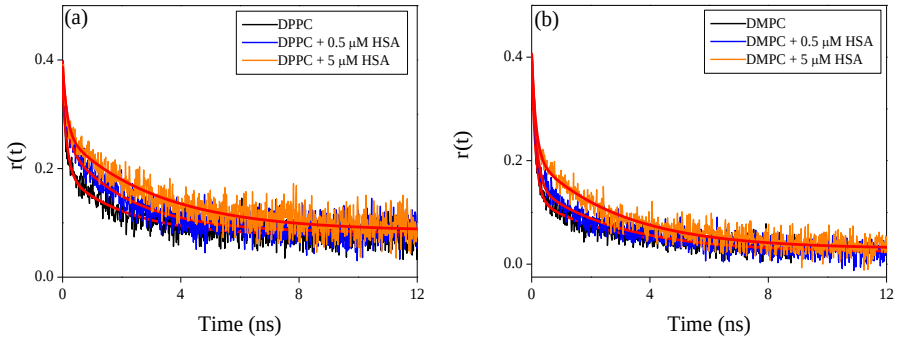

Figure 7.6. *Fitted fluorescence anisotropy decays of Ellipticine in (a) DPPC liposomes at different concentration of HSA (b) DMPC liposomes at different concentration of HSA.*

Table 7.1 reveals that incorporation of HSA causes an enhancement in the rotational relaxation time of Ellipticine in DPPC and DMPC liposomes. After addition of 5μM HSA the ϕ_{fast} and ϕ_{slow} are 0.150 (48%) and 3.145 ns (52%) respectively in DPPC liposome while for DMPC liposomes ϕ_{fast} and ϕ_{slow} are 0.160 (57%) and 2.923 ns (43%) respectively. The increase in the rotational relaxation time upon addition of HSA to liposomes confirms that the Ellipticine molecules do not migrate to aqueous phase. So; there is a possibility that incorporation of HSA into liposome results in the formation of a bigger complex.

The increase in size of liposome after incorporation of HSA has been reported earlier *[36]*. One interesting observation is that ϕ_{slow} as well as its amplitude [β_{slow} (%)] are enhanced with increase in HSA concentration. Since ϕ_{slow} is directly associated to the overall rotational motion of the complex, so; ϕ_{slow} may increase because of larger size of the liposomes–HSA complex.

Table 7.1. *Rotational relaxation parameters of Ellipticine in liposomes and liposome-HSA complex at λ_{em} = 435 nm[#]*

System	β_{fast}(%)	β_{slow}(%)	φ_{fast} (ns)	φ_{slow} (ns)	$\langle\varphi_r\rangle$ (ns)	r_0
Buffer solution, pH 7.4	1		0.150		0.150	0.35
DPPC	0.65	0.35	0.152	2.181	0.861	0.35
DPPC + 0.1 µM HSA	0.54	0.46	0.170	2.178	1.093	0.37
DPPC + 0.5 µM HSA	0.57	0.43	0.150	2.202	1.032	0.40
DPPC + 1 µM HSA	0.47	0.53	0.151	2.750	1.532	0.39
DPPC + 2 µM HSA	0.47	0.53	0.160	2.914	1.608	0.38
DPPC + 5 µM HSA	0.48	0.52	0.150	3.145	1.726	0.40
DMPC	0.75	0.25	0.150	2.660	0.774	0.38
DMPC + 0.1 µM HSA	0.74	0.26	0.141	2.810	0.859	0.38
DMPC + 0.5 µM HSA	0.69	0.31	0.151	2.880	0.996	0.39
DMPC + 1 µM HSA	0.64	0.37	0.150	2.924	1.147	0.40
DMPC + 2 µM HSA	0.61	0.39	0.160	3.086	1.300	0.40
DMPC + 5 µM HSA	0.57	0.43	0.160	2.923	1.350	0.39

 # The estimated error in the measurement is around 5%.

The formation of liposome-HSA complex also results in entrapment of larger number of drug molecules. This is revealed by increase in amplitude of slow component from 35% to 52% in DPPC-HSA complex and from 25% to 43% in DMPC-HSA complex. It is observed that the increment in ϕ_{slow} in DPPC-HSA complex is around 1 ns while the same is around 0.30 ns in DMPC-HSA complex. The higher increment in ϕ_{slow} in DPPC-HSA complex indicates that HSA penetrates more in DPPC than it does in DMPC. It is reasonable

because acyl chain in DMPC is shorter than that of DPPC. So; DMPC is supposed to be less hydrophobic than DPPC. This is also due to higher pre-hydration levels of DMPC vesicles at room temperature which in turn reduces its hydrophobicity. Therefore, hydrophobic interaction is stronger between DPPC and HSA compared to that between DMPC and HSA which leads to lesser penetration of HSA in DMPC vesicle.

In this context, lifetime data may be useful to unravel Ellipticine-HSA and liposomes-HSA interaction and fate of Ellipticine in liposomes. In the previous chapter, we already reported lifetime of Ellipticine at 440 nm varying the concentration of HSA. In absence of HSA, Ellipticine exhibits bi-exponential decay with the components of 0.446 (87%) and 5.29 ns (13%) respectively. With addition of HSA, both the picosecond and nanosecond components increase. The amplitude of picosecond component decreases while that of nanosecond component increases. At maximum concentration of HSA (5 μM), life time components are around 2.23 (61%) and 17 ns (39%) respectively. Thus the average lifetime of Ellipticine is around 7.91 ns at 435 nm at 5 μM HSA concentration. The average lifetime in DMPC liposomes is around 17.13 ns. In aqueous medium at 440 nm wavelength, Ellipticine does not exhibit any 2 ns component. The shorter component (τ_1) in DPPC and DMPC respectively corresponds to loosely bound Ellipticine molecule in the interfacial region and the longer component (τ_2) correspond to those Ellipticine molecules which are strongly held inside the liposomes.

Addition of HSA to liposomes diminishes the average lifetime of Ellipticine in liposomes. The fitted time resolved fluorescence decays of Ellipticine in liposomes upon addition of HSA are shown in Figure 7.7 and the results are summarized in Table 7.2.

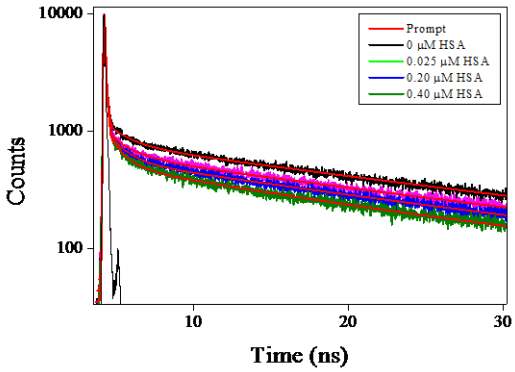

Figure 7.7. *Fitted time resolved fluorescence decays of Ellipticine in DPPC liposomes at different concentration of HSA.*

Table 7.2. *Fluorescence Decay Parameters of Ellipticine (λ_{ex} = 375 nm) in DPPC and DMPC liposome at different concentration of HSA at λ_{em} = 435 nm.*[#]

System	a_1 (%)	a_2 (%)	τ_1 (ns)	τ_2 (ns)	$\langle\tau\rangle$ (ns)	χ^2
DPPC liposome						
0 μM HSA	0.30	0.70	2.04	23.56	17.10	1.20
0.024 μM HSA	0.38	0.62	1.72	23.10	14.97	1.25
0.048 μM HSA	0.47	0.53	1.34	22.00	12.80	1.20
0.20 μM HSA	0.49	0.51	1.15	21.40	11.48	1.20
0.31 μM HSA	0.52	0.48	1.13	21.40	10.86	1.21
0.43 μM HSA	0.53	0.47	1.11	20.42	10.18	1.16
0.52 μM HSA	0.56	0.44	1.08	20.17	9.48	1.25
0.61 μM HSA	0.54	0.46	1.06	19.50	9.54	1.20
0.70 μM HSA	0.55	0.45	1.05	19.69	9.44	1.15
0.82 μM HSA	0.56	0.44	1.03	18.84	8.87	1.24
0.90 μM HSA	0.56	0.44	1.03	19.28	9.06	1.21
1.10 μM HSA	0.57	0.43	1.03	18.49	8.54	1.20
2 μM HSA	0.57	0.43	1.41	18.17	8.61	1.16
3 μM HSA	0.56	0.44	2.10	18.83	9.46	1.10
5 μM HSA	0.53	0.47	3.03	19.78	11.11	1.10

DMPC liposome						
0 μM HSA	0.31	0.69	2.18	24.12	17.13	1.11
0.024 μM HSA	0.36	0.64	1.87	24.00	16.03	1.14
0.048 μM HSA	0.37	0.63	1.76	24.09	15.82	1.12
0.099 μM HSA	0.39	0.61	1.61	23.25	14.80	1.15
0.20 μM HSA	0.39	0.61	1.52	22.98	14.60	1.10
0.31 μM HSA	0.41	0.59	1.38	22.84	14.04	1.14
0.43 μM HSA	0.44	0.56	1.18	22.36	13.04	1.13
0.52 μM HSA	0.47	0.53	1.11	22.36	12.37	1.14
0.61 μM HSA	0.48	0.52	1.04	22.41	12.15	1.15
0.70 μM HSA	0.50	0.50	1.04	22.42	11.73	1.13
0.82 μM HSA	0.48	0.52	1.04	21.96	11.91	1.16
0.9 μM HSA	0.49	0.50	1.11	21.89	11.48	1.17
1.10 μM HSA	0.49	0.50	1.11	21.64	11.36	1.15
2 μM HSA	0.50	0.50	1.63	22.56	12.09	1.10
3 μM HSA	0.48	0.52	2.57	23.22	13.72	1.12
5 μM HSA	0.48	0.52	3.38	23.57	13.87	1.10

 # The estimated error in the measurement is around 5%.

We plotted τ_1 and τ_2 values as a function of HSA in liposomes and in native HSA in Fig. 7.8 . The drop in τ_1 and τ_2 clearly indicates that the protein partially penetrates in the lipid bi-layer. Sabin et al. *[22]* reported that interfacial tension is decreased when protein is added to liposomes, which indicates that protein molecules intercalate between the hydrophobic tails of the lipid molecules. The DSC measurement revealed that due to penetration of HSA the phase transition temperature of lipid decreases and so the entropy change increases *[22]*. Thus the packing of the lipids is disturbed within the bi-layer i.e. their order is reduced. This may result in release of drug from the liposomes which drops the values of τ_1 and τ_2. Fig. 7.8 reveals that the decrease in lifetime τ_2 and $<\tau>$ is higher in DPPC compared to that in DMPC. Since DMPC liposomes remain in liquid crystalline phase at

room temperature owing to its lower phase transition temperature (23^0 C) and DPPC liposomes remain in sol gel phase because of its higher phase transition temperature (42^0 C) *[31]*, therefore, one should expect that HSA would penetrate deeper in DMPC than in DPPC liposomes.

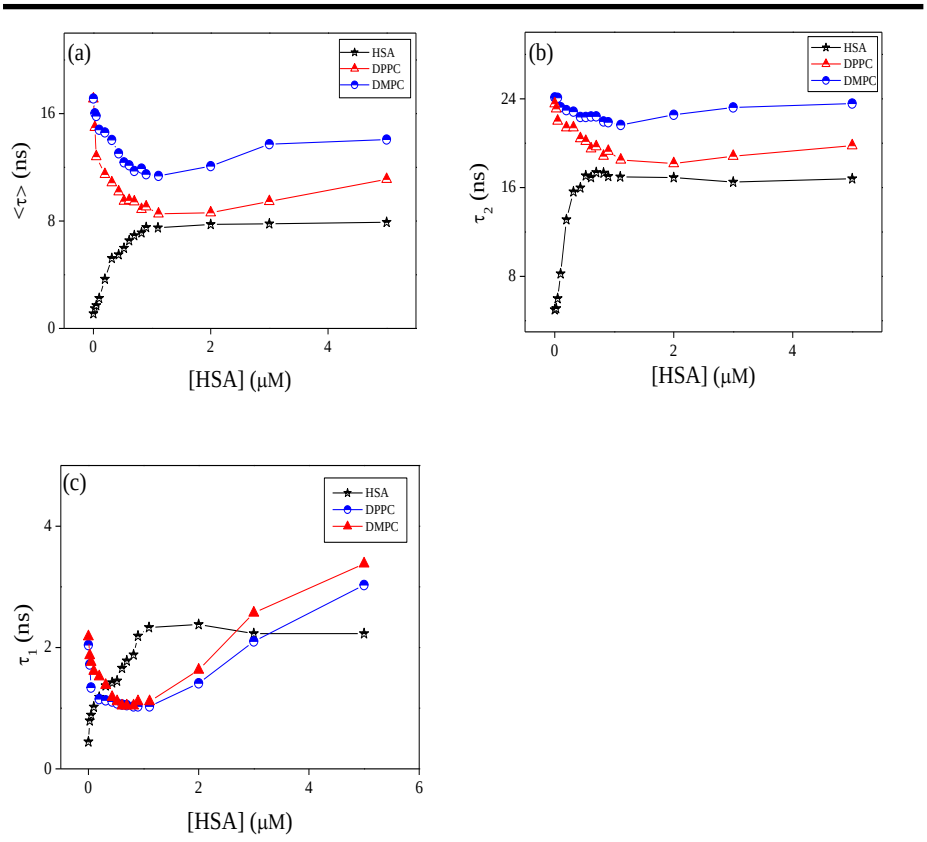

Figure 7.8. *The lifetime components of Ellipticine in HSA, DPPC and DMPC liposomes in presence of different concentration of HSA (a) <τ> (b) τ_2 (c) τ_1.*

However, because of liquid crystalline phase DMPC is much more hydrated compared to DPPC. So; DPPC being less hydrated is more hydrophobic which leads to a stronger hydrophobic interaction with HSA. One interesting observation revealed in Figure 7.8 is that lifetime components do not change beyond 1 μM concentration of native HSA and in liposome-HSA complex. The break point indicates that the Ellipticine could migrate from liposome to HSA.

This conjecture is validated by the increase in the amplitude of the shorter component (a_1) and decrease in the amplitude of longer

component (a_2). The change in the values of amplitudes (i.e. a_1 and a_2) may take place due to migration of Ellipticine from liposomes to hydrophobic pocket of HSA. To confirm this fact we plotted ratio of a_2 and a_1 as a function of HSA concentration (Fig. 7.9). It is revealed that like lifetime components (Figure 7.8), a very similar discontinuity in the amplitude is observed at 1 μM concentration of HSA in Figure 7.9. This fact confirms that Ellipticine migrate from liposome to hydrophobic pocket of HSA.

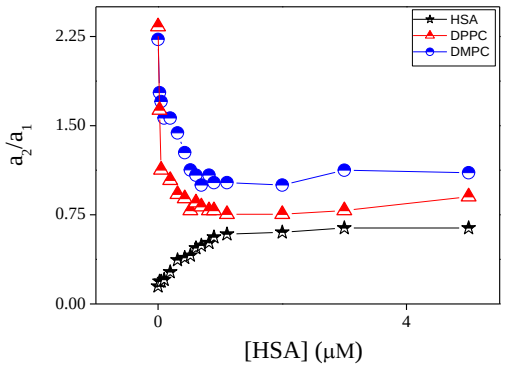

Figure 7.9. *The ratio of amplitudes of slow and fast components (a_2/a_1) of Ellipticine in native HSA, in DPPC and DMPC liposomes at different concentration of HSA.*

Ellipticine experiences almost similar polarity in liposomes and HSA which may facilitate the migration. One interesting observation is that at 1μM concentration of HSA, the lifetime parameters of Ellipticine in native HSA is in closer proximity to that in DPPC liposome compared to that in DMPC liposomes. This fact confirms that HSA has a stronger interaction with DPPC compared to that with DMPC.

7.3. Conclusion:

The present study revealed the release of encapsulated Ellipticine from DPPC and DMPC liposomes upon interaction with HSA. The entrapment of Ellipticine in liposome is confirmed by partition coefficient, huge increase in quantum yield and by significant blue shift. By addition of HSA to Ellipticine encapsulated liposome, HSA penetrates the liposome due to hydrophobic interaction and causes

migration of Ellipticine from liposome to HSA. Since DPPC is more hydrophobic and less prehydrated than DMPC, so; HSA exhibits deeper penetration in DPPC resulting in higher quenching and more decrement in average lifetime. The increment in rotational relaxation time with incorporation of HSA suggests the penetrative interaction as well as formation of a bigger complex.

7.4. References:

1. Lichtenberg D. (1996), In: Lasic D. D., Barenholz Y., (eds.), Liposomes as a model for solubilization and reconstitution of membranes. CRC Press, Boca Raton, 199-218 (ISBN-10: 084934011X).
2. Bangham A. D., Standish M. M., Watkins J.C. (1965), Diffusion of univalent ions across the lamellae of swollen phospholipids, *J. Mol. Biol.*, 13, 238-242 (DOI: S0022283665800936).
3. Sahoo S. K., Labhasetwar V. (2003), Nanotech approaches to drug delivery and imaging, *Drug Discovery Today*, 8, 1112-1120 (DOI: S1359644603029039).
4. Allen T. M., Cullis P. R. (2004), Drug delivery systems entering the mainstream, *Science*, 303, 1818-1822 (DOI: doi.org/10.1126/ science.1095833).
5. Hofheinz R. D., Grand-vogt U., Beyer U., Hochhaus A. (2005), Liposomal encapsulated anti-cancer drugs, *Anticancer Drugs*, 16, 691-707 (DOI: doi.org/10.1097/01.cad.0000167902.53039.5a).
6. Matos P. M., Freitas T., Castanho M. A. R. B., Santos N. C. (2010), The role of blood cell membrane lipids on the mode of action of HIV-1 fusion inhibitor sifuvirtide, *Biochem. Biophys. Res. Comm.*, 403, 270-274 (S0006291X10020619).
7. Chonn A., Semple S. C., Cullis P. R. (1992), Association of blood proteins with large unilamellar liposomes in vivo. Relation to circulation lifetimes, *J. Biol. Chem.*, 267, 18759-18765 (DOI: 0005273691901677).
8. Pedersen A. O., Mesenberg K. L., Kragh-Hansen U. (1995), Effects of ionic strength and pH on the binding of medium-chain fatty acids to human serum albumin, *Eur. J. Biochem.*, 233, 395-401 (10.1111/j.1432-1033.1995.395_2.x).
9. Peters T. Jr., (1977), Serum albumin: recent progress in the understanding of its structure and biosynthesis, *Clinical Chemistry*, 23, 15-12 (http://dx.doi.org/10.1016/S0065-2423(08) 60385-6).

10. Zhong D., Douhal A., Zewail A. H. (2000), Femtosecond studies of protein–ligand hydrophobic binding and dynamics: Human serum albumin, *Proc. Natl. Acad. Sci. U. S. A.*, 97, 14056-4061 (doi.org/10.1073/pnas.250491297).
11. Sugio S., Kashima A., Mochizuki S., Noda M., Kobayashi K. (1999), Crystal structure of human serum albumin at 2.5 Å resolution, *Protein Engg,* 12, 439-446 (doi.org/10.1093/protein/ 12.6.439).
12. Carter D. C., Ho J. X. (1994), Structure of serum albumin, *Adv Protein Chem,* 45, 153-203 (doi.org/10.1016/s0065-3233(08)60640-3).
13. He, X. M., Carter, D. C. (1992), Atomic structure and chemistry of human serum albumin, *Nature,* 358, 209-215 (DOI: 358209a0).
14. Peters T. (1985), Serum albumin, *AdV. Protein Chem.,* 37, 161-245 (doi.org/10.1016/s0065-3233(08)60065-0).
15. Curry S., Brick P., Frank N. P. (1999), Fatty acid binding to human serum albumin: new insights from crystallographic studies, *Biochim. Biophys. Acta,* 1441, 131-140 (doi.org/ 10.1016/s1388-1981(99)00148-1).
16. Petitpas I., Grune T., Battacharya A. A., Curry S. (2001), Crystal structures of human serum albumin complexed with monounsaturated and polyunsaturated fatty acids, *J. Mol. Biol.,* 314, 955-960 (DOI: S0022283600952082).
17. Gelamo E. L., Silva C. H. T. P., Imasato H., Tabak M. (2002), Interaction of bovine (BSA) and human (HSA) serum albumins with ionic surfactants: spectroscopy and modeling, *Biochim. Biophys. Acta,* 1594 84-99 (doi.org/10.1016/s0167-4838(01) 00287-4).
18. Chuang V.T.G., Otagiri M. (2001), Flunitrazepam, a 7-nitro-1,4-benzodiazepine that is unable to bind to the indole-benzodiazepine site of human serum albumin, *Biochim. Biophys. Acta,* 1546, 337-345 (DOI:S0167483801001510).

19. Bhattacharya A. A., Grune T., Curry, S. (2000), Crystallographic analysis reveals common modes of binding of medium and long-chain fatty acids to human serum albumin. *J. Mol. Biol.*, 303, 721–732 (DOI: S0022283600941585).
20. Toimila P., Prieto G., Mi˜nones J. Jr., Trillo J. M., Sarmientoa F. (2012), Monolayer and Brewster angle microscopy study of human serum albumin-Dipalmitoyl phosphatidyl choline mixtures at the air–water interface, *Colloids and Surfaces B: Biointerfaces,* 92, 64-73 (DOI: S0927776511006813).
21. Hoekstra D., Scherphoft G. (1979), Effect of fetal calf serum and serum protein fractions on the uptake of liposomal phosphatidylcholine by rat hepatocytes in primary monolayer culture, *Biochim. Biophys. Acta,* 551,109-121 (0005273679903572).
22. Sabin J., Prieto G., Ruso J. M., Messina P. V., Salgado F. J., Nogueira M., Miguel Costas M., Sarmiento F. (2009), Interactions between DMPC Liposomes and the Serum Blood Proteins HSA and IgG, *J. Phys. Chem. B,* 113, 1655-1661 (DOI: 10.1021/jp804641e).
23. Charbonneau D., Beauregard M., Tajmir-Riahi H. A. (2009), Structural analysis of human serum albumin complexes with cationic lipids, *J. Phys. Chem. B,* 113, 1777-1784 (DOI: 10.1021/jp8092012).
24. Tseng L. P., Liang H. J., Chung T. W., Huang Y. Y., Liu D. Z. (2007), Liposomes incorporated with cholesterol for drug Release triggered by magnetic Field, *J. Med. Biol. Engg*, 27 29-34.
25. Sikor M., Sabin J., Keyvanloo A., Schneider M. F., Thewalt J. L., Bailey A. E., Frisken B. J. (2010), Interaction of a Charged Polymer with Zwitterionic Lipid Vesicles, *Langmuir,* 26, 4095-4102 (DOI: 10.1021/la902831n).

26. Hernandez J., Estelrich J., Montero M. T., Valls O. (1989), Interaction between human serum albumin and liposomes: a monolayer and liposome study, *Int. J. Pharm.,* 57, 211-215 (DOI: 0378517389902093).
27. McMullen T. P. W., McElhaney R. N. (1996), Physical studies of cholesterol-phospholipid interactions, *Curr. Opin. Coll. Interf. Sci.,* 1, 83-90 (DOI: S1359029496800483).
28. Xu X., London E. (2000), The Effect of Sterol Structure on Membrane Lipid Domains Reveals How Cholesterol Can Induce Lipid Domain Formation, *Biochemistry,* 39, 843-849 (DOI: 10.1021/bi992543v).
29. Mashak E. M., Paoletti C., Tocanne J. F. (1980), interactions between Ellipticine and some derivatives and phospholipids in model membranes, *FEBS Lett.,* 107, 155-159 (DOI: 0014579379804858).
30. Thakur R., Das A., Chakraboty A. (2012), Photophysical and photodynamical study of Ellipticine: an anticancer drug molecule in bile salt modulated in vitro created liposome, *Phys. Chem. Chem. Phys.,* 14, 15369-15378 (DOI: 10.1039/C2CP41708A).
31. Horta B. A. C., Vries A. H., Hunenberger P. H. (2010), Simulating the transition between gel and liquid-crystal phases of lipid bi-layers: dependence of the transition temperature on the hydration level, *J. Chem. Theory Comput.,* 6, 2488-2500 (DOI: 10.1021/ct100200w).
32. Santos N. C., Prieto M., Catanho M. A. R. B. (1998), Interaction of the major epitope region of HIV protein gp41 with membrane model systems. A fluorescence spectroscopy study, *Biochemistry,* 37, 8674-8682 (DOI: 10.1021/bi9803933).
33. Dimitrova M. N., Matsumura H., Neitchev V., Furusawa K. (1998), Temperature dependence of protein-induced flocculation of phosphatidylcholine liposomes, *Langmuir*, 14, 5438-5445 (DOI: 10.1021/la980127q).

34. Dimitrova M. N., Matsumura H., Neitchev V. (1997), Kinetics of protein-induced flocculation of phosphatidylcholine liposomes, *Langmuir*, 13, 6516-6523 (DOI: 10.1021/la970378j).

35. Spector A. A. (1975), Fatty acid binding to plasma albumin, *J. Lipid Res.*, 16, 165-179 (doi.org/10.1016/0076-6879(86)28077-5).

36. Galantai R., Bardos-Nagy I. (2000), The interaction of human serum albumin and model membranes, *Int. J. Pharm.*, 195, 207-218 (DOI: S0378517399003993).

Chapter 8

Interaction of human serum albumin with liposomes of saturated and unsaturated lipids with different phase transition temperatures: a spectroscopic investigation by membrane probe PRODAN

The interaction of human serum albumin (HSA) with liposomes made of saturated and unsaturated phosphocholines having distinctly different phase transition temperatures has been studied using circular dichroism (CD), steady state and time resolved fluorescence spectroscopic techniques. We used 1,2-dipalmitoyl-sn-glycero-3-phosphocholine (DPPC), 1,2-dimyristoyl-sn-glycero-3-phosphocholine (DMPC) as the saturated lipid and 1,2-dioleoyl-sn-glycero-3-phosphocholine (DOPC), 2-oleoyl-1-palmitoyl-snglycero-3-phosphocholine (POPC) as the unsaturated lipid to prepare liposomes. The steady state and time resolved fluorescence spectra of PRODAN (6-propionyl 1,2-dimethylaminonaphthalene) were monitored to unravel the interaction between liposome and HSA.

8.1. Perspective of the Present Study:

Plasma membrane is a complicated assembly of lipids and proteins, organized into various specialized microdomains with versatile diversity *[1]*. To overcome the problems associated with this diversity it is worthwhile to use synthetic liposomes or vesicles which mimic the geometry and topology of cell membranes *[2,3]*. Phospholipids form the fundamental matrix of natural membranes and represent the environment in which many proteins and various macro molecules display their activity *[4]*. Therefore characterization of lipid membranes with sufficient selectivity will help to study the variation around its bulk properties *[5]*. Owing to their small size, amphiphilic character, and biocompatibility, liposomes or vesicles are promising

systems for drug delivery through the blood stream *[6,7]*. Therefore it is necessary to visualize the stability of liposomes in presence of serum proteins *[8]*. Human Serum Albumin (HSA) is the most prominent component of blood plasma. It serves as transport protein for several endogenous and exogenous ligands as well as for various drug molecules *[9,10,11,12,13,14,15,16,17]*. HSA also binds well with fatty acids *[18]*. It is reported that proteins partially penetrate and deform the lipid bi-layer *[19,20]*. HSA penetrates into the vesicle and gets adsorbed on the surface of vesicles to some extent. Packing of hydrophobic tails of the lipid is also disturbed in presence of HSA *[21,22,23]*. Charbonneau et al. suggested that both hydrophobic and hydrophilic interactions occur for liposome-HSA systems *[24]*. Various groups suggested that for prolonged circulation of liposomes in blood stream and to provide stability, cholesterol should be incorporated in the vesicle *[25,26,27,28]*.

Although there are a few reports regarding liposome-HSA system *[19,20,21,22,23,24]*, however, none of the studies addressed the nature of interaction between liposome and HSA by fluorescence spectroscopy using a polarity sensitive membrane probe. Moreover, it was not answered what will be fate of encapsulated molecules inside the liposome upon interaction with HSA. Therefore, it is desirable to undertake a study which involves different kind of liposomes. The present work has the novelty because it involves four different phosphatidylcholines lipids with zwitterionic head groups. These lipids are widely different in terms of their phase transition temperature and nature of their acyl chain. DPPC and DMPC are saturated phospholipids while DOPC and POPC contain unsaturation in their acyl chain (Figure 2.4 pp. 52). Phosphatidylcholines are dominant in eukaryotic membranes *[29]*. The lipids of more metabolically active membranes are considerably more unsaturated. POPC bilayers provide relevant models for the matrix of the endoplasmic reticulum *[30]*. DPPC exhibits properties very similar to those of sphingomyelin which

is the most abundant lipid in plasma membrane *[31]*. Hof and coworkers used PRODAN as probes within the lipid bilayer for studing solvation and photophysical properties within model membranes *[32,33]*. In our previous chapter, we encapsulated anticancer drug ellipticine in DPPC vesicles and studied its release by various bile salts *[34]*. The present study is done to reveal protein-liposome interaction and the transport of various drugs through lipid bilayers via Human Serum Albumin (HSA) with the help of fluorescence spectroscopy. Fluorescence spectroscopy has several advantages including a high sensitivity, a noninvasive nature, an intrinsic time scale and an excellent response to the physical properties of membrane *[35]*.For this purpose PRODAN (Figure 2.2 pp. 52) has been chosen as a probe molecule primarily to study the environment inside the liposomes and to reveal the liposome-HSA interaction. Photophysical properties of PRODAN has already been discussed in chapter 2.

HSA contains only one tryptophan residue at position 214 (Trp214) in domain II and one free cystine residue at position 34 in domain I, moreover it has 17 disulphide bonds *[36]*. The free thiol group allows site specific labeling of protein with chromophoric or fluorescent probes *[37,38]*. PRODAN binds with HSA within Sudlow site I i.e. on warfarin binding site *[39]*. So far, interaction of PRODAN with liposome and HSA is reported individually. But interaction of HSA and liposome is still unexplored using a membrane probe. Therefore, photophysics of PRODAN by steady state and time resolved spectroscopy will not only be able to reveal the environment inside the HSA, liposome and liposome-HSA complex but will also give a new insight regarding the interaction between liposomes and HSA. This study may further help in designing a novel drug delivery system for various drugs exhibiting properties very similar to PRODAN.

8.2. Results and Discussion:

We divided the results and discussion section in three tiers. At first we studied the interaction of PRODAN with HSA. In the second section we studied the interaction of PRODAN with Liposome. In the third section interaction between HSA and liposome has been studied.

8.2.1. Interaction of PRODAN with HSA:

PRODAN exhibits emission maxima at 520 nm in aqueous buffer solution. Addition of HSA to the buffer solution of PRODAN diminishes the intensity at 520 nm and additionally a band appears at 455 nm. The band at 455 nm is attributed to the LE state of HSA bound PRODAN. The appearance of LE state indicates that PRODAN experiences a less polar environment in HSA. With increase in HSA concentration, the contribution of TICT band decreases while that of LE band increases which implies that more number of PRODAN molecules bind with HSA. Interestingly, we obtained an isoemissive point at around 510 nm which implies that there are two emitting species in the excited state. The emission spectrum of PRODAN in presence of 20 μM of HSA was deconvoluted by a combination of the lognormal functions to show simultaneous existence of CT and LE species (Figure 8.1a) by taking the emission spectrum of PRODAN in aqueous buffer solution as reference. We estimated binding constant of PRODAN molecules with HSA using Bensei-Hildebrand equation as in the previous chapter for 1:1 complex as following.

$$I_f = \frac{I_f^0 + I_{PROD-HSA} K_1 [HSA]}{1 + K_1 [HSA]} \qquad (8.1)$$

where, I_f^0 is the fluorescence intensity of PRODAN in absence of HSA and $I_{PROD-HSA}$ is the fluorescence intensity when all PRODAN molecules form complex with HSA. The nonlinear regression analysis following equation 8.1 yields the binding constant (k_1)

around 7×10^5 M^{-1} (Figure 8.1b). The earlier report *[40]* states that PRODAN binds with HSA at Sudlow site I i.e. on warfarin binding site. This observation is consistent with our experimental result (The data are not shown). The formation of complex between PRODAN and HSA is exothermic with value of ΔH^o = -22.82 KJ mol^{-1} *[39]*. It was also reported that PRODAN does not bring about any conformational changes in HSA *[40]*.

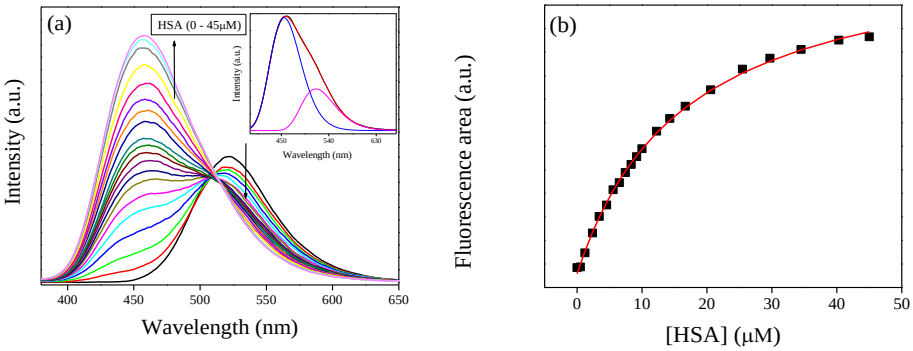

Figure 8.1. *(a) The emission spectra of PRODAN at different concentration of HSA. Inset is the emission spectrum of PRODAN in presence of 20 μM HSA that has been deconvoluted in LE and TICT state. (b) The fitted binding curve between PRODAN and HSA following equation 8.1.*

To gain more specific local information about the binding of PRODAN to HSA, we estimated the energy transfer efficiency between PRODAN and HSA by monitoring the emission spectra of Trp214 of HSA (Figure 8.2). The distance between Trp214 and PRODAN was estimated from the energy transfer efficiency expression:

$$E = 1 - \frac{I}{I_0} = \left(1 + \frac{R^6}{R_0^6}\right)^{-1} \qquad (8.2)$$

where I_0 and I are the intensities of Trp214 emission measured for the protein alone and for PRODAN-HSA complex, respectively. Figure 8.2 reveals that the efficiency of energy transfer between

Trp214 of HSA and PRODAN is around 43%. Such weak energy transfer indicates that PRODAN molecules bind at a location which is away from tryptophan. In the equality, R is the distance between Trp214 and PRODAN in Angstrom. R_0 is a characteristic Forster distance for 50% energy transfer efficiency related to the properties of donor and acceptor and can be calculated using following equation

$$R_0^{\,6} = 8.79\times10^{-5} n^{-4}\kappa^2\phi_0 \int \varepsilon(\lambda) f(\lambda)\lambda^4 d\lambda \Big/ \int f(\lambda) \qquad (8.3)$$

where, n is the refractive index of the medium, κ^2 is a geometric factor related to the relative orientation of the transition dipole moments of the donor and acceptor, $\varepsilon(\lambda)$ is the molar absorptivity of PRODAN, and $f(\lambda)$ is the normalized fluorescence intensity of Trp214. Therefore, R_0 is calculated from equation 8.3 using geometrical parameter κ^2 as 2/3. These parameters yielded a value for R_0 of 26 Å, leading to an estimate for R, the apparent distance between Trp214 and PRODAN being 24 Å. We fitted the quenching data with a modified Stern-Volmer equation as follows *[41]*:

$$\frac{I_0}{I} = \frac{1+K_{SV}[Q]_L}{(1+K_{SV}[Q]_L)(1-f_B)+f_B} \qquad (8.4)$$

In this equation I_0 is the intensity of HSA in absence of PRODAN. K_{SV} is the Stern-Volmer quenching constant and

$$f_B = \frac{I_{0,B}}{I_0} \qquad (8.5)$$

where $I_{0,B}$ is fluorescence intensity of the tryptophan accessible to quencher. Thus the estimated K_{SV} and f_B were around 1.77×10^6 M^{-1} and 0.54 respectively.

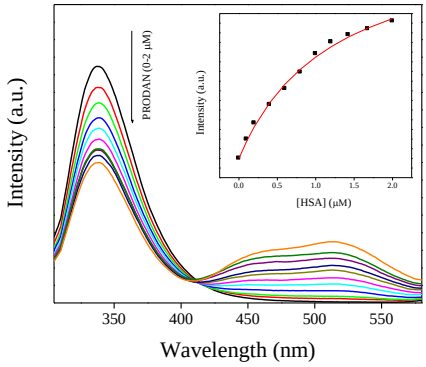

Figure 8.2. *Emission spectra of HSA (10 μM) in presence of different concentration of PRODAN (0-2 μM).*

We measured the fluorescence lifetime of PRODAN at 457 and 520 nm at different concentration of HSA (Table 8.1). The decay of PRODAN at 50 µM concentration of HSA at the 457 nm is comprised of 0.90 ns (33%) and 4.00 ns (67%) components with an average lifetime of 3.00 ns. We assign the time component of 4.00 ns to HSA bound PRODAN and the species with time component of 0.90 ns to the free PRODAN species in aqueous medium. Our result is consistent with the measurement made by Basak and co-workers *[42]*. The increase in fluorescent quantum yield and lifetime of PRODAN and its derivative when bound to protein is due to reduced conformational freedom of the amine and carbonyl groups because of the close packing of surrounding protein *[43]*. The significant increase in longer component from 45% to 67% upon addition of 50 µm HSA clearly indicates that PRODAN molecules are entrapped inside the hydrophobic pocket of HSA. Table 8.1 reveals a similar component at 520 nm when PRODAN binds with HSA. The lifetime at 520 nm was fitted with a bi-exponential function. The increase in nanosecond component which represents HSA bound PRODAN species from 26% to 45% confirms the binding of PRODAN molecules with HSA.

Table 8.1. *Lifetime components, normalized amplitudes of lifetime components and average lifetime of PRODAN in HSA at 520 nm and 457 nm.*[#]

Conc. Of HSA ($\times 10^{-6}$M)	**a_1 (%)**	**a_2 (%)**	**a_3 (%)**	**τ_1 (ns)**	**τ_2 (ns)**	**τ_3 (ns)**	**$\langle\tau\rangle$ (ns)**	**χ^2**
(λ_{em} = 520 nm)								
0	0.74	0.26		0.62	1.80		0.93	1.21
1	0.79	0.21		0.68	2.24		1.00	1.11
3	0.79	0.21		0.70	2.70		1.12	1.25
6	0.78	0.22		0.75	3.24		1.30	1.06
10	0.74	0.26		0.76	3.52		1.48	1.20
16	0.68	0.32		0.75	3.71		1.69	1.11
20	0.66	0.34		0.76	3.83		1.80	1.03
25	0.63	0.37		0.75	3.89		1.91	1.20
30	0.61	0.39		0.78	3.97		2.00	1.11
40	0.57	0.43		0.74	3.96		2.12	1.05
50	0.55	0.45		0.73	4.03		2.20	1.12
(λ_{em} = 457 nm)								
1	0.55	0.45		0.73	3.60		2.00	1.19
2	0.46	0.54		0.80	3.65		2.34	1.21
3	0.43	0.57		0.79	3.68		2.44	1.05
4	0.40	0.60		0.74	3.66		2.49	1.11
6	0.36	0.64		0.81	3.70		2.66	1.21
10	0.34	0.66		0.85	3.75		2.76	1.27
16	0.34	0.66		0.87	3.78		2.79	1.08
20	0.33	0.67		0.82	3.80		2.81	1.11
25	0.33	0.67		0.79	3.80		2.80	1.20
30	0.33	0.67		0.80	3.85		2.84	1.15
40	0.33	0.67		0.80	3.95		2.91	1.07
50	0.33	0.67		0.90	4.00		3.00	1.11

[#]*Estimated error in the measurement is around ± 5%*

8.2.2. Interaction of PRODAN with Liposomes:

In this section we first encapsulate PRODAN in different liposomes. Addition of liposomes to aqueous solution of PRODAN causes a blue shift in emission spectra followed by a new band at 435 nm. This band is assigned as LE state of PRODAN. The appearance of LE band indicates that PRODAN molecules are encapsulated inside the liposomes. Interestingly, we observed an isoemissive point in DPPC and DMPC liposomes which indicates the existence of two emissive species in these two liposomes (Figure 8.3). On the other hand isoemissive point was not observed when PRODAN is incorporated into DOPC and POPC liposomes.

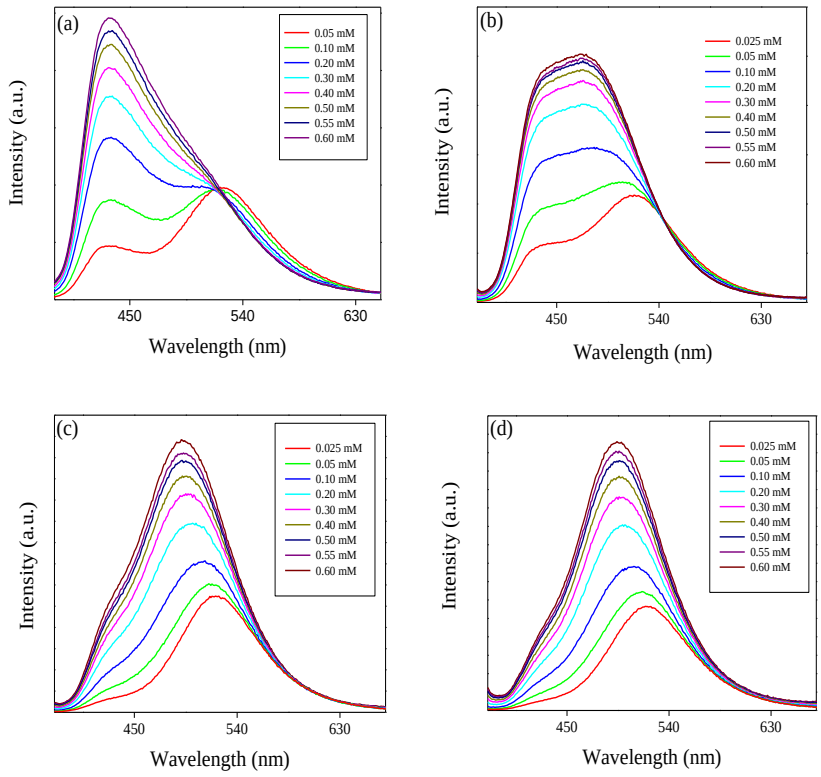

Figure 8.3. *The emission spectra of PRODAN at different concentration of liposomes (a) DPPC (b) DMPC (c) DOPC and (d) POPC liposomes.*

A similar observation was reported by Correa and co-workers in case of DOPC liposomes *[44]*. They explained this observation with the model proposed by Chong and co-workers *[45]*. The lack

of isoemissive point in POPC and DOPC liposomes may be due to absence of a prominent LE state in DOPC and POPC liposomes. To explain this observation we consider the differences in the hydration level which depends on the phase transition temperature of the lipids. DPPC and DMPC have phase transition temperatures around 43°C and 23°C respectively while POPC and DOPC have phase transition temperature around - 2°C and - 20°C respectively. It is reported by Horta and co-workers *[46]* that the liposomes having lower phase transition temperature is more hydrated than liposomes having higher phase transition temperature. Again because of much lower phase transition temperature, DOPC and POPC are significantly much more hydrated and are much softer than DPPC and DMPC at room temperature. PRODAN molecules are mostly encapsulated in the interfacial region of DOPC and POPC. Since DOPC and POPC exist in the liquid crystalline phase at room temperature, the non polar region is less motionally restricted compared to that in interfacial region. Thus lack of a prominent LE state may be responsible for absence of an isoemissive point. The normalized emission spectra of PRODAN (Figure 8.4) in different liposomes at room temperature reveal that maximum blue shift takes place in DPPC liposomes.

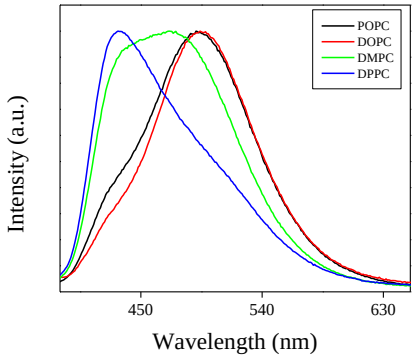

Figure 8.4. *Normalized emission spectra of PRODAN in different liposomes.*

This fact also indicates that DPPC and DMPC are more hydrophobic as compared to DOPC and POPC due to their higher

phase transition temperature and due to difference in their prehydration levels.

Correa and co-workers correlated the maximum emission band energy of PRODAN ($E_{em\text{-}PRODAN}$) with $E_{T(30)}$ polarity scale for different solvents by the following equation *[44]*.

$$E_{T(30)} = 147 \pm 5 - (1.62 \pm .02) E_{em-PRODAN} \qquad (8.6)$$
$$n = 23, r = 0.98$$

Following this equation $E_{T(30)}$ values as obtained for DPPC, DMPC, POPC and DOPC liposomes are 41.7, 47, 52 and 54 Kcal/mol respectively. The different micropolarity as experienced by PRODAN in different liposomes could be attributed to the difference in their prehydration levels which further depends on phase transition temperatures. At room temperature DPPC vesicles remain in sol gel phase (SG) and DMPC vesicles remain in nearly liquid crystalline (LC) phase. As, torsion of the $-N(CH_3)_2$ are more restricted in SG phase of the phospholipid bilayer than that in LC phase, LE band has less contribution in LC phase compared to that in sol gel phase. DOPC and POPC liposomes exist completely in LC phase at room temperature. Thus they have similar emission spectra for PRODAN at room temperature which is clear from Figure 8.4.

We estimated the partition coefficient of PRODAN in different liposomes using the following equation *[47]*.

$$\frac{1}{F} = \frac{55.6}{(K_P F_0 L)} + \frac{1}{F_0} \qquad (8.7)$$

where F_0 and F are fluorescence intensities of PRODAN molecules in aqueous and in lipid phase, respectively, L is the lipid concentration and the molar concentration of water was considered to be 55.6 M. Thus using equation 8.7 and the slopes from Figure 8.5, the calculated K_P values are 1.0×10^5, 5.8×10^5,

2.8×10^5, 2.6×10^5 for DPPC, DMPC, POPC and DOPC liposomes respectively. Notably the lower partition coefficient in DPPC liposomes compared to that in other liposomes stems from the fact that the interfacial region of DPPC is much more rigid due to its sol gel phase and this rigidity hinders the encapsulation of more number of PRODAN molecules. The liposomes like DMPC, DOPC and POPC remain in liquid crystalline phase at room temperature and they allow PRODAN to penetrate in the interfacial region.

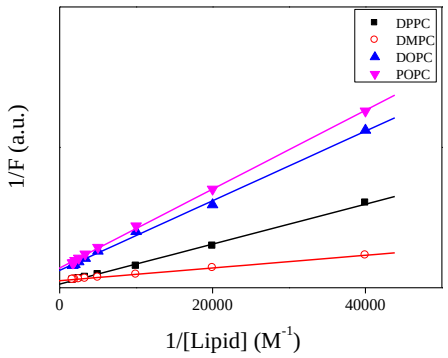

Figure 8.5. *Double reciprocal plot of the intensity of PRODAN with respect to concentration different liposomes.*

We estimated the lifetime of PRODAN at various concentrations of liposomes at 440 and 520 nm. The values of lifetime for different vesicles are summarized in Table 8.2a and Table 8.2b and the representative decays are shown in Figure 8.6. PRODAN exhibits a bi-exponential decay in aqueous buffer solution at 520 nm with the lifetime components 0.62 ns (τ_1) and 1.8 ns (τ_2) with a population of 74% and 26% respectively.

Table 8.2a. *Lifetime components, normalized amplitudes and average lifetime of PRODAN at different concentration of liposomes at 520 nm.*[#]

	a_1 (%)	a_2 (%)	a_3 (%)	τ_1 (ns)	τ_2 (ns)	τ_3 (ns)	$<\tau>$ (ns)	χ^2
Conc. Of DPPC ($\times10^{-3}$M) (λ_{em} = 520 nm)								
0	0.74	0.26		0.60	1.8		0.95	1.1
0.05	0.82	0.18		0.69	2.60		1.00	1.43
0.10	0.63	0.28	0.09	0.57	1.48	4.47	1.16	1.09
0.20	0.55	0.31	0.14	0.52	1.36	4.73	1.37	1.04
0.30	0.59	0.22	0.18	0.58	1.61	4.97	1.62	1.07
0.40	0.59	0.19	0.22	0.61	1.90	5.16	1.84	1.02
0.50	0.58	0.17	0.25	0.63	2.11	5.23	2.00	1.04
0.60	0.53	0.16	0.31	0.64	2.17	5.19	2.28	1.06
Conc. Of DMPC ($\times10^{-3}$M) (λ_{em} = 520 nm)								
0.025	0.41	0.46	0.14	0.412	1.00	4.09	1.18	1.06
0.05	0.51	0.28	0.22	0.524	1.13	4.75	1.60	1.08
0.10	0.59	0.41		0.605	4.92		2.36	1.12
0.20	0.29	0.71		0.583	4.55		3.40	1.02
0.30	0.20	0.80		0.577	4.65		3.83	1.05
0.40	1	-		-	4.50		4.50	1.20
0.50	-0.20	0.80		1.20	4.50		5.16	1.16
0.60	-0.31	0.69		1.65	4.50		5.40	1.12
Conc. Of DOPC ($\times10^{-3}$M) (λ_{em} = 520 nm)								
0.025	0.76	0.24		0.668	2.69		1.15	1.33
0.05	0.71	0.29		0.685	3.12		1.40	1.27
0.10	0.57	0.43		0.670	3.42		1.87	1.07
0.20	0.33	0.67		0.568	3.59		2.58	1.02
0.30	0.21	0.79		0.631	3.6		2.98	1.00
0.40	0.16	0.84		0.879	3.6		3.16	1.02
0.50	-	1.00		-	3.6		3.60	1.10
0.60	-	1.00		-	3.52		3.52	1.20
Conc. Of POPC ($\times10^{-3}$M) (λ_{em} = 520 nm)								
0.025	0.78	0.22		0.674	2.64		1.11	1.2

0.05	0.75	0.25	0.698	3.14	1.31	1.21
0.10	0.66	0.34	0.676	3.56	1.66	1.06
0.20	0.46	0.54	0.603	3.81	2.32	1.06
0.30	0.33	0.67	0.641	3.78	2.74	1.12
0.40	0.31	0.69	0.746	3.83	2.87	1.00
0.50	0.28	0.72	0.834	3.83	2.99	1.05
0.60	-	1.00	-	3.38	3.38	1.25

[#]*Estimated error in the measurement is around ± 5%.*

Table 8.2b. *Lifetime components, normalized amplitudes of lifetime components and average lifetime of PRODAN at different concentration of liposomes at 435 nm.*[#]

	a_1 (%)	a_2 (%)	a_3 (%)	τ_1 (ns)	τ_2 (ns)	τ_3 (ns)	$\langle\tau\rangle$ (ns)	χ^2
Conc. Of DPPC ($\times10^{-3}$M) (λ_{em} = 435 nm)								
0								
0.05	0.40	0.60		1.19	6.08			1.31
0.10	0.18	0.30	0.52	0.45	2.26	6.47	4.11	1.25
0.20	0.16	0.30	0.53	0.45	2.26	6.47	4.19	1.30
0.30	0.17	0.31	0.53	0.47	2.45	6.53	4.27	1.17
0.40	0.15	0.31	0.54	0.48	2.42	6.48	4.34	1.21
0.50	0.16	0.31	0.52	0.62	2.73	6.61	4.41	1.10
0.60	0.17	0.31	0.52	0.62	2.73	6.57	4.39	1.20
Conc. Of DMPC ($\times10^{-3}$M) (λ_{em} = 435 nm)								
0.025	0.18	0.34	0.48	0.59	1.89	4.51	2.91	1.28
0.05	0.19	0.31	0.49	0.72	2.03	4.47	2.98	1.22
0.10	0.15	0.30	0.55	0.75	1.78	4.33	3.00	1.30
0.20	0.25	0.25	0.50	1.03	2.36	4.43	3.00	1.09
0.30	0.16	0.27	0.57	0.85	1.80	4.26	3.00	1.17
0.40	0.19	0.29	0.52	0.85	2.04	4.35	3.00	1.25
0.50	0.18	0.28	0.54	0.90	1.99	4.31	3.00	1.11
0.60	0.14	0.31	0.55	0.74	1.77	4.25	3.00	1.09
Conc. Of DOPC ($\times10^{-3}$M) (λ_{em} = 435 nm)								

0.025	0.70	0.30	0.84	2.62	1.37	1.25
0.05	0.69	0.31	0.83	2.57	1.37	1.29
0.10	0.69	0.31	0.87	2.63	1.42	1.21
0.20	0.68	0.32	0.87	2.61	1.43	1.10
0.30	0.68	0.32	0.87	2.62	1.43	1.20
0.40	0.68	0.32	0.88	2.63	1.44	1.05
0.50	0.69	0.31	0.88	2.65	1.43	1.13
0.60	0.69	0.31	0.86	2.69	1.43	1.23
Conc. Of POPC ($\times 10^{-3}$M) (λ_{em} = 435 nm)						
0.025	0.61	0.39	0.84	2.59	1.52	1.31
0.05	0.60	.40	0.84	2.59	1.54	1.28
0.10	0.61	0.39	0.87	2.64	1.56	1.21
0.20	0.59	0.41	0.86	2.63	1.58	1.24
0.30	0.60	0.40	0.87	2.64	1.58	1.19
0.40	0.61	0.39	0.87	2.65	1.56	1.07
0.50	0.60	0.40	0.86	2.63	1.57	1.11
0.60	0.60	0.40	0.86	2.62	1.56	1.10

[#]*Estimated error in the measurement is around ± 5%*

Thus the average lifetime of PRODAN at 520 nm is around 0.95 ns. In DPPC liposome, at 520 nm, where the emission spectra is predominantly from TICT state of PRODAN has conspicuously dependence on the concentration of lipid and is well described by a tri-exponential function. The picosecond component i.e. τ_1 remains same throughout the concentration of DPPC and the nanosecond component i.e. τ_2 increased up to around 2.17 ns. A third component of around 5.19 ns (τ_3) with a population of 31% appeared at higher concentration of DPPC (Table 8.2a). We, therefore, assign τ_1 component to the PRODAN molecules remaining in the aqueous phase which drops from 74% to 53% upon increasing the concentration of DPPC from 0 to 0.6 mM. The 2.17 ns component i.e. τ_2 may be ascribed to the PRODAN

molecules in aqueous phase or loosely bound in the interfacial region and the longest component i.e. 5.20 ns (τ_3) component may come from the PRODAN molecules strongly held inside the liposome. Interestingly, PRODAN at 435 nm in 0.6 mM DPPC liposome where emission mainly comes from LE state exhibits a tri-exponential decay. The components are 0.62 ns (17%), 2.73 ns (31%) and 6.57 ns (52%). We already assigned these components to different locations in liposomes.

In DMPC liposome, the decays at 520 nm were fitted to a bi-exponential function with a picosecond and a nanosecond component. As the liposome concentration increases and incorporate more number of PRODAN molecules, the picosecond component disappeared leading to a rise component around 1.65 ns (31%) and a nanoscecond component around 4.72 ns (69%). The decay proceeds with a rise component indicates that solvation takes place. Surprisingly, in case of DPPC liposomes, we did not observe any rise component which could be because of the fact that the aliphatic tail region of DPPC is more dehydrated than that of DMPC. Table 8.2b reveals that the decay of PRODAN in DMPC liposomes at 435 nm is tri-exponential with picosecond component (τ_1) and two nanosecond components (τ_2 and τ_3). The components are 0.59 ns (18%), 1.89 ns (34%) and 4.51 ns (59%). It is noteworthy that τ_3 is significantly less in DMPC liposomes compared to that in DPPC liposomes. The probable reason is that DMPC remains in nearly liquid crystalline phase at room temperature while DPPC remains in sol-gel phase which brings in additional rigidity in DPPC compared to that in DMPC. This may be responsible for higher time component in DPPC compared to that in DMPC. In DOPC and POPC liposomes initially decay at 520 nm was bi-exponential with a picosecond component (~670 ps) originating from the PRODAN molecules in the aqueous phase and a nanosecond component around 2.65 to 2.69 ns.

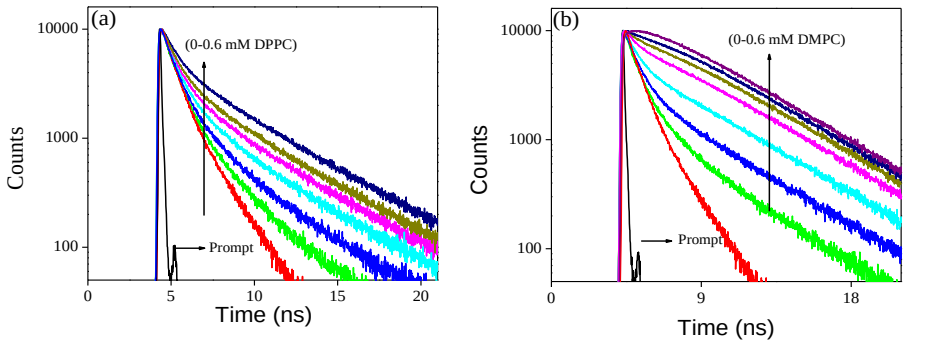

Figure 8.6. *Decay of PRODAN at different concentration of liposomes (a) DPPC liposome (b) DMPC liposome*

Due to low concentration of lipid two components are observed picosecond component in aqueous phase and the other nanosecond component in lipid phase. However, at higher concentration the decay becomes single exponential with time constant around 3.52 ns and 3.38 ns for DOPC and POPC liposomes respectively. These results are in accordance with that reported by Correa and co-workers *[44]*. At 435 nm the decays in DOPC and POPC were fitted to a biexponential function having a picosecond component around 0.840 ns and a nanosecond component around 2.60 to 2.70 ns. Notably, the longer components in POPC and DOPC liposomes at 520 and 435 nm are significantly smaller compared to longer component of DPPC and DMPC liposomes at the same wavelength. This observation may be explained by considering the fact that at room temperature both DOPC and POPC remain in liquid crystalline phase due to significant lower phase transition temperature compared to DPPC and DMPC. Therefore, PRODAN experiences a less constrained environment in DOPC and POPC liposomes giving rise to a shorter lifetime component as compared to DPPC and DMPC liposomes.

8.2.2. Interaction between liposomes and HSA:

8.2.2.1. CD Measurements:

To gain a better insight into interaction of HSA with various liposomes CD measurements were performed using HSA, DPPC liposomes and POPC liposomes at various concentrations of these lipids. The CD spectra of HSA exhibit two negative minima at 208 and 217 nm, which is typical characterization of α-helix structure of proteins *[48]*. Interaction between DPPC-HSA and POPC-HSA caused an increase in band intensity at all wavelengths of the far UV CD without any significant shift of the peaks (Figure 8.7). This indicates that both DPPC liposomes and POPC liposomes causes a slight increase in the α-helical structure of HSA. While heating HSA till 90°C and addition of 8M urea causes decrease in the band intensity at all the wavelengths (Figure 8.7c). This signifies decrease in α-helical content upon denaturation of HSA *[49]*. Thus we conclude that both the lipid upon interaction with HSA cause perturbation in the secondary structure of HSA but increase in α-helical content suggest that HSA is not denatured or unfolded during the interaction *[24]*.

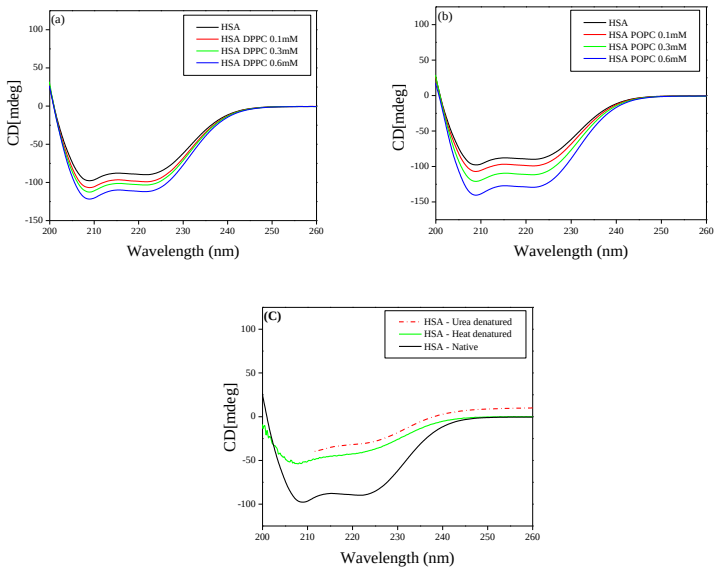

Figure 8.7. *CD spectra of (a) HSA and DPPC liposomes (b) HSA and POPC liposomes (c) Native HSA and denatured HSA.*

8.2.2.2 Steady state and Time resolved measurement:

Addition of HSA to PRODAN impregnated liposomes causes a quenching in the fluorescence intensity of PRODAN. The continuous decrease in the intensity with addition of HSA to PRODAN impregnated liposomes indicates that HSA interacts with the liposomes. Interestingly, we observe a red shift in the emission spectra of PRODAN in DPPC liposomes (from 435 to 460 nm) while a blue shift is observed in DMPC (from 460 to 455 nm), DOPC (from 497 to 471 nm), and POPC (from 490 to 467 nm) liposomes (Figure 8.8). There are two reasons that may be accounted for the observed quenching in liposomes. The first one is the penetration of HSA into liposomes and the second is the release of PRODAN molecules from liposome and subsequent migration to hydrophobic core of the HSA.

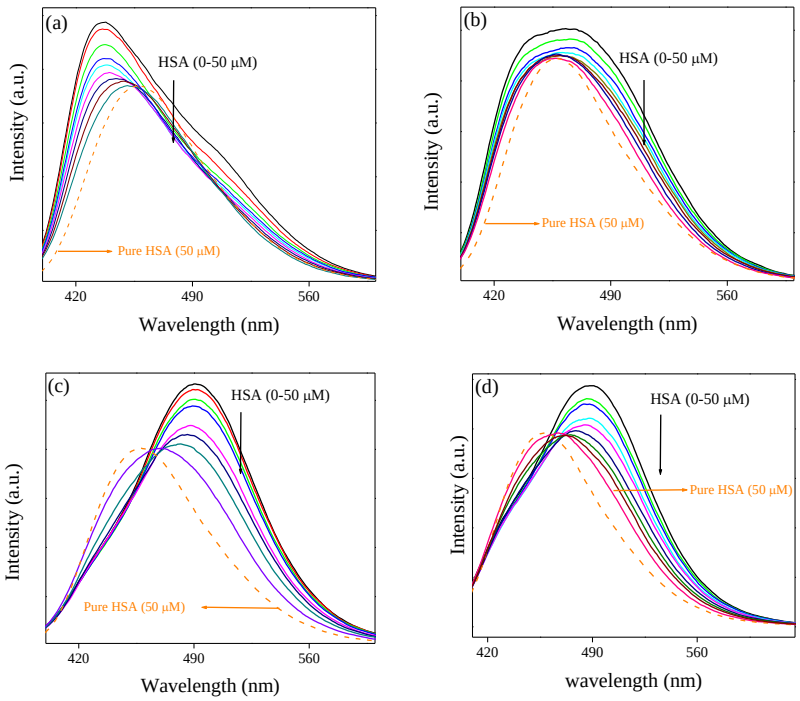

Figure 8.8. *The steady state emission spectra of PRODAN in different liposomes as a function of HSA concentration. (a) DPPC, (b) DMPC, (c) DOPC and (d) POPC. The dashed graph represents emission spectra of PRODAN in native HSA which is normalized with respect to highest concentration of HSA in liposomes.*

Sabin et al. *[21]* reported that the forces which are involved in the interaction between liposomes and HSA are of electrostatic and hydrophobic in nature. Primarily HSA interacts with the liposome through electrostatic interaction to form HSA liposome complex and destabilize the packing of lipid within bilayer and the order of acyl chain is reduced. The zeta potential (ξ) was used to monitor the electrostatic interaction between liposomes and HSA *[21]*. It was found that ξ decreases exponentially with the protein concentration. The strong dependence of ξ was reported as a patent evidence that the attractive electrostatic contribution has a major role in the formation of liposome-HSA complex. A similar type of electrostatic interaction has been invoked by Charbonneau et al. *[24]*. Sabin et al. *[21]* also reported the protein penetration inside the liposome. DSC measurement by them reveal that pretransition temperature of DMPC liposomes decreases by more than one degree at the same time the enthalpy change (ΔH) increases. A similar type of results were reported by Gatlantai and co-workers *[22,23]*. The effect of HSA over DMPC and DPPC liposomes indicates that protein penetrates into hydrophobic bilayer affecting the packing of the hydrocarbon tails of lipids. Therefore, there is contribution of hydrophobic forces in formation of liposome HSA-complexes. The contribution comes from interaction between the lipid tails and parts of HSA that penetrate into the lipid bilayer.

The decrease in the interfacial tension indicates that protein molecules intercalate between the hydrophobic tails of the lipid. This intercalation causes the leakage in the interfacial region which facilitates the migration of the probe molecules from liposome to either aqueous phase or hydrophobic pocket of HSA. Notably, upon addition of HSA to PRODAN impregnated liposomes, the emission maxima are shifted towards the emission maximum of native HSA (Figure 8.8). This observation led to the conclusion that PRODAN molecules being

released from the liposome are trapped in the hydrophobic pocket of HSA.

We compared the extent of quenching from Figure 8.9 in different liposomes by plotting ϕ_0/ϕ as a function of concentration of HSA. Since we cannot calculate the local concentration of HSA, so; we did not estimate Stern-Volmer quenching constant from this plot. It is observed from Figure 8.9 that among the un-conjugated lipids, quenching is higher in DPPC liposome compared to that in DMPC liposomes. On the other hand in case of conjugated lipids, the quenching is little higher in POPC liposomes compared to that in DOPC liposomes. The extent of quenching depends upon the extent of perturbation of lipid bilayer by HSA. The significant difference in quenching in DPPC and DMPC liposomes and little difference in DOPC and POPC liposomes may be explained by considering the structural differences of different lipids, phase transition temperature and prehydration level.

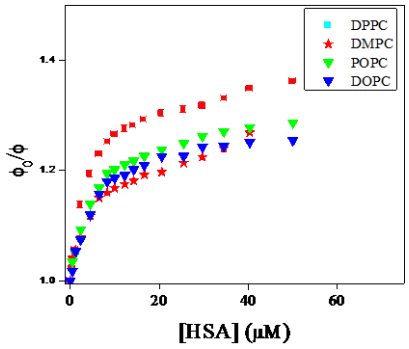

Figure 8.9. *ϕ_0/ϕ Plot as a function of concentration of HSA (0-50 μM) in different liposomes.*

In the present study, all the four lipids are zwitterionic and they possess similar head groups but differ in their acyl chains. While DPPC and DMPC contain saturated acyl chain with different chain length, POPC and DOPC contain unsaturated acyl chain with different number of carbon atoms. As the length of hydrophobic acyl chain is the measure of hydrophobicity and it is already reported that saturated

fatty acids bind with greater affinity to albumins due to increase in hydrophobic interaction, *[50]* in that sense the order of quenching follows the right trend. DPPC has higher phase transition temperature than DMPC. The liposomes with lower phase transition temperature remains more hydrated as compared to liposome with higher phase transition temperature. Therefore DPPC is less hydrated as compared to DMPC. So; higher quenching is observed in DPPC as compared to DMPC. Among POPC and DOPC bilayers, POPC is monounsaturated while DOPC is bi-unsaturated with CH=CH in *cis* position. The unsaturated fatty acids with a *cis* double bond, faces little steric restriction on binding to various sites on protein *[51]*. Therefore perturbation of lipid bilayer by HSA will be more pronounced in POPC bilayers as compared to DOPC bilayers. Along with this phase transition temperature of POPC is higher than DOPC. The DOPC bilayers will remain in a more prehydrated state as compared to POPC. Thus lower quenching is observed in DOPC as compared to POPC.

In this context the lifetime data may be helpful to unravel the dynamics of PRODAN inside the liposome. We already mentioned that the fluorescence decay of PRODAN in aqueous buffer solution is adequately fitted to a bi-exponential function with time constant 0.60 ns (74%) and 1.80 ns (26%). The lifetime of PRODAN is significantly enhanced when encapsulated in liposomes. This is already discussed in the previous section. Table 8.2a reveals that PRODAN exhibits a tri-exponential decay with time components of 0.62 ns (15%), 2.73 ns (31%) and 6.57 ns (54%) in DPPC liposomes. We already assigned that the picosecond component corresponds to the PRODAN molecules in the aqueous phase, 2.73 ns component is attributed to the PRODAN molecules loosely bound in the interfacial region and third component i.e. 6.57 ns component perhaps comes from those PRODAN molecules which are strongly held inside the liposome. Addition of HSA to PRODAN impregnated DPPC liposomes causes quenching in the lifetime components of PRODAN (Figure 8.10).

After addition of 2 μM HSA, the decays became bi-exponential and at 50 μM HSA the decay is comprised of the components of 1.48 (40%) and 4.60 ns (60%). The significant quenching in the longer component (from 6.48 ns to 4.60 ns) implies the penetration of HSA into liposome. The striking observation is that the lifetime components of PRODAN in presence of 50 μM HSA in DPPC liposomes (1.48 and 4.60 ns) are very similar to that in pure HSA (1.49 ns and 4.0 ns, Table 8.1) which indicates that PRODAN molecules upon interaction with HSA are released from liposome and migrate to the hydrophobic pocket of HSA. Had the PRODAN molecules migrated to aqueous phase, we would have obtained a picosecond component. We already mentioned that a shift is observed in the steady state emission spectra of PRODAN upon addition of HSA which indicates that PRODAN is migrating to the hydrophobic pocket of HSA. Thus this fact is supported by the lifetime data.

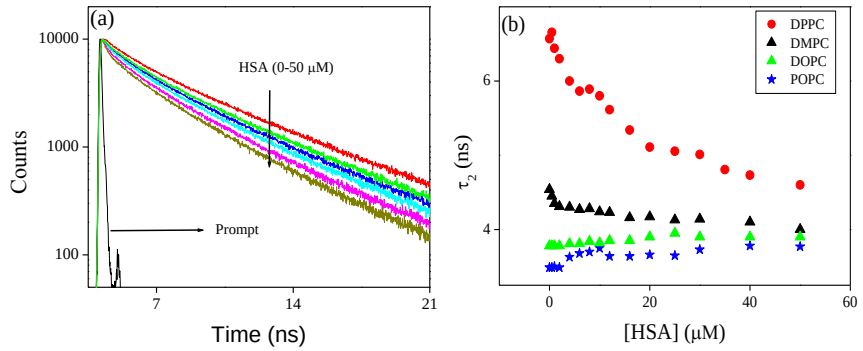

Figure 8.10. *(a) Time resolved decays of PRODAN at different concentration of HSA in DPPC liposome. (b) Longer component of PRODAN in liposomes at different concentration of HSA.*

However, a different result is obtained in DMPC-HSA system. It is revealed that unlike in DPPC system, DMPC offers only little decrement in lifetime components in presence of HSA. Addition of HSA causes a little quenching in the longer component from 4.55 to 4.10 ns while the shorter component decreases from 2.2 ns to 1 ns. The little quenching in the longer component indicates that, HSA has a less penetration in DMPC liposomes. The less penetration stems from the

fact that DMPC because of its low phase transition temperature (23^0 C) remains nearly in liquid crystalline phase at room temperature and is much more hydrated than DPPC. As the hydrophobic interaction is responsible for the penetration of HSA into liposomes, therefore, HSA prefers DPPC over DMPC as former is more dehydrated hence is more hydrophobic compared to the latter. Although one should expect that DMPC is loosely packed and thus eases HSA to penetrate inside the liposome. However, higher quenching of the longer component in DPPC liposomes made it clear that hydrophobic interaction dominates over the other factors. On the other hand significant decrement in the shorter time component in DMPC liposomes indicates that HSA destabilize the interfacial region leaving the liposome core intact. Therefore, from the above results, we may conclude that the changes in the shorter component takes place when HSA destabilizes the interfacial region and the change in longer component in liposomes takes place when HSA affects the core of the liposomes due to penetration by hydrophobic interaction *[21]*. The latter process depends on prehydration level of liposomes.

The above finding is again supported by the time resolved data in conjugated liposomes (Table 8.3b). In case of DOPC and POPC liposomes, we observe that the lifetime of PRODAN is single exponential with a component around 3.49 ns and 3.77 ns respectively. Addition of HSA results in quenching and time resolved decay becomes bi-exponential. Surprisingly we observe a marginal increment in the longer component in POPC (from 3.77 to 3.90 ns) and DOPC liposomes (3.40 to 3.77 ns). The observation in these two liposomes clearly indicates the HSA does not penetrate in these two liposomes.

Table 8.3b. *Lifetime components, normalized amplitudes of lifetime components and average lifetime of PRODAN in POPC and DOPC liposomes as a function of concentration of HSA. The decays were measured at the emission maxima following Figure 8.7.*[#]

[HSA] (μM)	a_1 (%)	a_2 (%)	a_3 (%)	τ_1 (ns)	τ_2 (ns)	τ_3(ns)	$<\tau>$(ns)	χ^2
POPC liposomes								
0	1			3.77			3.70	1.1
0.5	1			3.77			3.70	1.12
1	1			3.77			3.70	1.12
2	1			3.750			3.75	1.16
4	1			3.80			3.80	1.2
6	0.06	0.94		0.86	3.81		3.63	1.22
8	0.081	0.92		0.93	3.84		3.61	1.20
10	0.14	0.86		1.00	3.82		3.43	1.19
12	0.18	0.82		0.86	3.85		3.31	1.21
16	0.25	0.75		0.79	3.85		3.10	1.25
20	0.29	0.71		0.80	3.90		3.00	1.24
25	0.33	0.67		0.79	3.95		2.90	1.20
30	0.34	0.66		0.85	3.90		2.92	1.25
40	0.32	0.68		0.75	3.90		2.90	1.27
50	0.35	0.65		0.95	3.90		2.93	1.26
DOPC liposomes								
0	1.00			3.49			3.49	1.16
0.5	1.00			3.49			3.49	1.20
1	1.00			3.45			3.49	1.22
2	1.00			3.49			3.50	1.21
4	0.11	0.89		1.92	3.63		3.44	1.20
6	0.16	0.84		1.72	3.68		3.37	1.25
8	0.20	0.80		1.68	3.70		3.30	1.24
10	0.22	0.78		1.68	3.75		3.29	1.29
12	0.19	0.81		1.00	3.64		3.15	1.30

16	0.22	0.76	0.89	3.64	2.96	1.35
20	0.27	0.73	0.82	3.66	2.89	1.30
25	0.30	0.70	0.75	3.65	2.78	1.27
30	0.31	0.69	0.75	3.73	2.80	1.29
40	0.35	0.65	0.75	3.78	2.72	1.29
50	0.35	0.65	0.75	3.77	2.71	1.31

[#]*Estimated error in the measurement is around ± 5%.*

On the other hand appearance of picosecond component (0.86 to 0.95 ns) and increment in its amplitude up to 35-40% in both the liposomes indicates the leakage of PRODAN molecules and confirms the fact that HSA destabilize the interfacial region of these liposome and core of the interfacial region remains intact. It is noteworthy that in case of DPPC liposome similar kind of changes in the population of shorter and longer components was observed. Therefore, it may unambiguously be concluded that the leakage of PRODAN molecules takes place due to destabilization of interfacial region of liposomes.

We carried out time resolved anisotropy measurements to probe interaction of liposomes with HSA. The anisotropy decays are shown in Figure 8.11 and the results are summarized in Table 8.4. PRODAN exhibits a single exponential decay with a time constant of 0.170 ns at 520 nm in aqueous buffer solution at pH 7.40. In liposomes and liposomes-HSA complex the anisotropy was measured at 450 nm. PRODAN exhibits bi-exponential anisotropy decays consisting of a picosecond and a nanosecond component in all liposomes. The fast components (ϕ_{fast}) are around 0.47 (44%), 0.50 (45%), 0.40 (32%) and 0.416 ns (37%) in DPPC, DMPC, DOPC and POPC liposomes respectively. On the other hand the slow components (ϕ_{slow}) are 2.77 (56%), 2.93 (55%), 2.25 (68%), and 2.20 ns (63%) in DPPC, DMPC, DOPC and POPC liposomes respectively. It is revealed that addition of HSA to PRODAN loaded liposomes causes a significant increment in ϕ_{slow}. Thus in presence 15 μM HSA, ϕ_{slow} were found to be 3.5 (60%),

3.90 ns (56%), 3.75 (40%), 3.60 (53%) in DPPC, DMPC, DOPC and POPC liposomes respectively. Since liposomes and liposomes-HSA complex are big in the size, the motion of liposome and liposome-HSA is too slow to impact on the overall rotational relaxation of PRODAN. The increment in ϕ_{slow} may be due to the fact that the interfacial region of liposome becomes compact due to electrostatic interaction between liposomes and HSA. It is revealed from above mentioned result that the increment in ϕ_{slow} in DPPC and DMPC liposomes is less compared to that in DOPC and POPC liposomes.

The higher increment in ϕ_{slow} in DOPC and POPC liposomes may be attributed to the fact that the interfacial region of DOPC and POPC becomes more compact due to adsorption of HSA. The other explanation is that possibly lipid packing order of DPPC and DMPC are much more affected by higher penetration of HSA in these liposomes as compared to that in DOPC and POPC liposomes. This prevents the increment in ϕ_{slow} in DPPC and DMPC liposomes. A similar conclusion was drawn in the discussion of quenching in the time resolved data. Interestingly, we observed a decrement in the population of ϕ_{slow} in case of DOPC and POPC liposomes. However, we do not observe any increment in the population of slower component (β_{slow}).

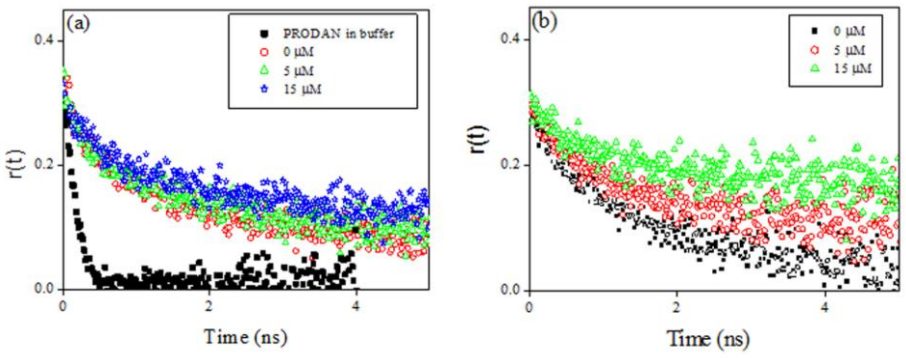

Figure 8.11. *Fluorescence anisotropy decays of PRODAN at different concentration of HSA (a) DMPC liposomes (b) DOPC liposomes.*

Since these two liposomes are soft in the interfacial region, there is possibility that these two liposomes can accommodate more number of HSA molecules which causes a significant leakage. Moreover, HSA penetrates deeper in DPPC and DMPC liposomes, so; for these liposomes PRODAN can migrate to hydrophobic pocket of HSA.

Table 8.4. *Rotational relaxation parameters of PRODAN in different liposomes and liposome-HSA complex at* λ_{em} *= 450 nm*[#]

System	β_{fast} (%)	β_{slow} (%)	φ_{fast} (ns)	φ_{slow} (ns)	r_0
PRODAN in Buffer solution, pH 7.4	1		0.17	-	0.29
DPPC	0.44	0.56	0.47	2.77	0.32
DPPC + 5 µM HSA	0.40	0.60	0.60	3.20	0.32
DPPC + 15 µM HSA	0.40	0.60	0.57	3.50	0.33
DMPC	0.45	0.55	0.50	2.93	0.35
DMPC + 5 µM HSA	0.42	0.58	0.39	3.46	0.35
DMPC + 15 µM HSA	0.45	0.55	0.37	3.90	0.33
DOPC	0.32	0.68	0.40	2.25	0.31
DOPC + 5 µM HSA	0.42	0.58	0.62	3.51	0.32
DOPC + 15 µM HSA	0.60	0.40	0.57	3.75	0.31
POPC	0.37	0.63	0.42	2.20	0.32
POPC + 5 µM HSA	0.39	0.61	0.45	2.99	0.33
POPC + 15 µM HSA	0.46	0.54	0.40	3.60	0.33

[#]*Estimated error in the measurement is around ± 5%*

8.3. Conclusion:

The present study reveals a clear understanding of how HSA interacts with liposomes of saturated and unsaturated lipids having different phase transition temperature. The CD measurement indicates that HSA is stabilized upon interaction with liposomes. Steady state and time resolved fluorescence analysis reveal that HSA alters the packing order

of liposome through penetration and releases the encapsulated probe molecules from liposome, which simultaneously migrates in the hydrophobic pocket of HSA. The penetration is apparently caused by hydrophobic interaction between liposomes and HSA. The extent of penetration depends on the prehydration level of liposomes. The liposomes of saturated lipids (DPPC and DMPC) having higher phase transition temperature are less prehydrated at room temperature and hence have stronger affinity towards HSA than that of liposomes of unsaturated lipids. The penetration caused by hydrophobic interaction is revealed also in anisotropy measurement.

8.4. References:

1. Pike L. J. (2003), Lipid rafts: bringing order to chaos, *J. Lipid Res.,* 44, 655-667 (doi.org/10.1194/jlr.r200021-jlr200).
2. Ashgarian N., Schelly Z. A. (1999), Electric field-induced transient birefringence and light scattering of synthetic liposomes, *Biochim. Biopys. Acta,* 1418, 295-306 (DOI: S0005273699000425).
3. Correa N. M., Schelly Z. A., Zhang H. (2000), Preparation of AgBr Quantum Dots via Electroporation of Vesicles, *J. Am. Chem. Soc.,* 122, 6432-6434 (DOI: 10.1021/ja000073i).
4. Parassasi T., Satasio G. D., Ubaldo A., Gratton E. (1990), Phase fluctuation in phospholipid membranes revealed by Laurdan fluorescence, *Biophys J.,* 57, 1179-1186 (DOI: S0006349590826370).
5. Klymchenko A. S., Demchenko A. P. (2002), Probing AOT Reverse Micelles with Two-Color Fluorescence Dyes Based on 3-Hydroxychromone, *Langmuir,* 18, 5637-5639 (DOI: 10.1021/la025760x).
6. Sytnik A., Litvinyuk I. (1996), Energy transfer to a proton-transfer fluorescence probe: Tryptophan to a flavonol in human serum albumin, *Proc. Natl. Acad. Sci. U.S.A.,* 93, 12959-12963 (doi.org/10.1073/pnas.93.23.12959).
7. Sahoo S. K., Labhasetwar V. (2003), Nanotech approaches to drug delivery and imaging, *Drug Discovery Today,* 8, 1112-1120 (DOI: S1359644603029039).
8. Chonn A., Semple S. C., Cullis P. R. (1992), Association of blood proteins with large unilamellar liposomes in vivo. Relation to circulation lifetimes, *J. Biol. Chem.,* 267, 18759-18765 (DOI: 0005273691901677).

9. Pedersen A. O., Mesenberg K. L., Kragh-Hansen U. (1995), Effects of ionic strength and pH on the binding of medium-chain fatty acids to human serum albumin, *Eur. J. Biochem.*, 233, 395-401 (10.1111/j.1432-1033.1995.395_2.x).

10. Sugio S., Kashima A., Mochizuki S., Noda M., Kobayashi K. (1999), Crystal structure of human serum albumin at 2.5 Å resolution, *Protein Engg,* 12, 439-446 (doi.org/10.1093/protein/ 12.6.439).

11. Carter D. C., Ho J. X. (1994), Structure of serum albumin, *Adv Protein Chem,* 45, 153-203 (doi.org/10.1016/s0065-3233(08)60640-3).

12. He X. M., Carter D. C. (1992), Atomic structure and chemistry of human serum albumin, *Nature,* 358, 209-215 (DOI: 358209a0).

13. Peters T. (1985), Serum albumin, *AdV. Protein Chem.*, 37, 161-245 (doi.org/10.1016/s0065-3233(08)60065-0).

14. Curry S., Brick P., Frank N. P. (1999), Fatty acid binding to human serum albumin: new insights from crystallographic studies, *Biochim. Biophys. Acta,* 1441, 131-140 (doi.org/10.1016/s1388-1981(99)00148-1).

15. Petitpas I., Grune T., Battacharya A. A., Curry S. (2001), Crystal structures of human serum albumin complexed with monounsaturated and polyunsaturated fatty acids, *J. Mol. Biol.*, 314, 955-960 (DOI: S0022283600952082).

16. Gelamo E. L., Silva C. H. T. P., Imasato H., Tabak M. (2002), Interaction of bovine (BSA) and human (HSA) serum albumins with ionic surfactants: spectroscopy and modeling, *Biochim. Biophys. Acta,* 1594 84-99 (doi.org/10.1016/s0167-4838(01) 00287-4).

17. Chuang V. T. G., Otagiri M. (2001), Flunitrazepam, a 7-nitro-1,4-benzodiazepine that is unable to bind to the indole-benzodiazepine site of human serum albumin, *Biochim. Biophys. Acta*, 1546, 337-345 (DOI: S0167483801001510).
18. Bhattacharya A. A., Grune T., Curry S. (2000), Crystallographic analysis reveals common modes of binding of medium and long-chain fatty acids to human serum albumin, *J. Mol. Biol.*, 303, 721–732 (DOI: S0022283600941585).
19. Lis L. J., Kauffman J. W., Shriver D. F. (1976), Raman spectroscopic detection and examination of the interaction of amino acids, polypeptides and proteins with the phosphatidylcholine lamellar structure, *Biochim. Biophys. Acta*, 436, 513-522 (DOI: 0005273676904375).
20. Hoekstra D., Scherphoft G. (1979), Effect of fetal calf serum and serum protein fractions on the uptake of liposomal phosphatidylcholine by rat hepatocytes in primary monolayer culture, *Biochim. Biophys. Acta*, 551,109-121 (DOI: 0005273679903572).
21. Sabin J., Prieto G., Ruso J. M., Messina P. V., Salgado F. J., Nogueira M., Miguel Costas M., Sarmiento F. (2009), Interactions between DMPC Liposomes and the Serum Blood Proteins HSA and IgG, *J. Phys. Chem. B*, 113, 1655-1661 (DOI: 10.1021/jp804641e).
22. Galantai R., Bardos-Nagy I. (2000), The interaction of human serum albumin and model membranes, *Int. J. Pharm.*, 195, 207-218 (DOI: S0378517399003993).
23. Bardos-Nagy I., Galantai R., Laberg M., Fidy J. (2013), Effect of Trehalose on the Nonbond Associative Interactions between Small Unilamellar Vesicles and Human Serum Albumin and on the Aging Process, *Langmuir*, 19,146-153 (DOI: 10.1021/ la026166q).

24. Charbonneau D., Beauregard M., Tajmir-Riahi H. A. (2009), Structural analysis of human serum albumin complexes with cationic lipids, *J. Phys. Chem. B,* 113, 1777-1784 (DOI: 10.1021/jp8092012).

25. Tseng L. P., Liang H. J., Chung T. W., Huang Y. Y., Liu D. Z. (2007), Liposomes incorporated with cholesterol for drug Release triggered by magnetic Field, *J.Med. Biol. Engg.*, 27, 29-34.

26. Kim C. K., Park D. K. (1987), Stability and drug release properties of liposomes containing cytarabine as a drug carrier, *Arch. Pharm. Res.*, 10, 75-79 (DOI: BF02857770).

27. Hernandez J., Estelrich J., Montero M. T., Valls O. (1989), Interaction between human serum albumin and liposomes: a monolayer and liposome study, *Int. J. Pharm.,* 57, 211-215 (DOI: 0378517389902093).

28. McMullen T. P. W., McElhaney R. N. (1996), Physical studies of cholesterol-phospholipid interactions, *Curr. Opin. Coll. Interf. Sci.*, 1, 83-90 (DOI: S1359029496800483).

29. Vance D. E., Vance J. E., (1995) Biochemistry of lipids, Lipoproteins and membranes, Elsevier Science: Vancouver, B. C. Canada, pp. 1-38 (ISBN-10: 0444532196).

30. Arbuzova A.L., Koeppe R.E. (2007), Bilayer Thickness and Membrane Protein Function: An Energetic Perspective, Annu. Rev. Biophys. Biomol. Struct., 37, 107-130 (10.1146/annurev. biophys.36.040306.132643).

31. Nelson D. L., Cox M. M. (2008), Principles of Biochemistry, fourth ed, W. H. Freeman and company, U. S. A, New York, pp. 343-370 (ISBN-10: 071677108X).

32. Sÿachl R., Sÿtepanek M., Prochazka K., Humpolíčková J., Hof M. (2008), Fluorescence Study of the Solvation of Fluorescent Probes Prodan and Laurdan in Poly (E-caprolactone)-block-poly(ethylene oxide) Vesicles in Aqueous Solutions with Tetrahydrofurane, *Langmuir,* 24, 288-295 (DOI:10.1021/ la702277t).

33. Cwiklik L., Aquino A. J. A.,Vazdar M., Jurkiewicz P., Pittner J., Hof M., Lischka H. (2011), Absorption and Fluorescence of PRODAN in Phospholipid Bilayers: A Combined Quantum Mechanics and Classical Molecular Dynamics Study, *J. Phys. Chem. A,* 115, 11428-11437 (DOI:10.1021/jp205966b).

34. Thakur R., Das A., Chakraboty A. (2012), Photophysical and photodynamical study of ellipticine: an anticancer drug molecule in bile salt modulated in vitro created liposome, *Phys. Chem. Chem. Phys.,* 14, 15369-15378 (DOI: 10.1039/C2CP41708A).

35. Lakowicz J. R. (2006), Principles of Fluorescence Spectroscopy, third ed. Kluwer Academic Plenum Publisher, New York , pp. 3-23 (ISBN-10: 0387312781).

36. Peters T. Jr. (1995), All about Albumins: Biochemistry, Genetics, and Medical Applications, Academic Press, San Diego, pp. 9-54 (ISBN-10: 0123887232).

37. Farruggia B., Garcia F., Pico G. (1995), Structural features of the hydroxy- and keto-disubstituted bile salts: human serum albumin binding, *Biochim. Biophys. Acta,* 1252, 59-68 (DOI: 016748389500110G).

38. Nerli B., Romanini D., Pico G. (1997), Structural specificity requirements in the binding of beta lactam antibiotics to human serum albumin, *Chem. Biol. Interact.,* 104, 179-202 (DOI: S0009279797000240).

39. Moreno F., Cortijo M., Jimenez J. G. (1999), The Fluorescent Probe Prodan Characterizes the Warfarin Binding Site on Human Serum Albumin, *Photochem. Photobiol.*, 69, 8-15 (DOI:10.1111/j.1751-1097.1999.tb05299.x).

40. Krishnakumar S. S., Panda D. (2002),Spatial Relationship between the Prodan Site, Trp-214, and Cys-34 Residues in Human Serum Albumin and Loss of Structure through Incremental Unfolding, *Biochemistry,* 41, 7443-7452 (DOI: 10.1021/bi025699v).

41. Santos N. C., Prieto M., Castanho M. A. R. B. (1998), Interaction of the Major Epitope Region of HIV Protein gp41 with Membrane Model Systems. A Fluorescence Spectroscopy Study, *Biochemistry,* 37, 8674-8682 (DOI: 10.1021/bi9803933).

42. Basak S., Debnath D., Haque H., Ray S., Chakrabarti A., Structural perturbation of proteins in low denaturant concentration, *Indian J. Biochem. Biophys.*, 2001, 38, 84-89.

43. Zhong D., Douhal A., Zewail A. H. (2000), Femtosecond studies of protein–ligand hydrophobic binding and dynamics: Human serum albumin, *Proc. Natl. Acad. Sci. U. S. A.,* 97, 14056-14061 (doiy10.1073ypnas.250491297).

44. Moyano F., Biasutti M. A., Silber J. J., Correa N. M. (2006), New Insights on the Behavior of PRODAN in Homogeneous Media and in Large Unilamellar Vesicles, *J. Phys. Chem. B,* 110, 11838-11846 (DOI: 10.1021/jp057208x).

45. Chong P. L. G. (1988), Effects of hydrostatic pressure on the location of PRODAN in lipid bilayers and cellular membranes, *Biochemistry,* 27, 399-404 (DOI: 10.1021/bi00401a060).

46. Horta B. A. C., De Vries A. H., Heunenberger P. H. (2010), Simulating the Transition between Gel and Liquid-Crystal Phases of Lipid Bilayers: Dependence of the Transition Temperature on the Hydration Level, *J. Chem. Theory Comput.*, 6, 2488-2500 (DOI: 10.1021/ct100200w).

47. Huang Z., Haugland R. P. (1991), Partition coefficients of fluorescent probes with phospholipid membranes, *Biochem. Biophys. Res. Commun.,* 181, 166-171 (DOI: S0006291X 05813968).

48. Gerbanowski A., Malabat C., Rabiller C., Gueguen J. (1999), Grafting of Aliphatic and Aromatic Probes on Rapeseed 2S and 12S Proteins: Influence on Their Structural and Physicochemical Properties, *J. Agric. Food Chem.,* 47**,** 5218-5226 (DOI: 10.1021/jf990226p).

49. Moriyama Y., Takeda K. (1999), Re-formation of the Helical Structure of Human Serum Albumin by the Addition of Small Amounts of Sodium Dodecyl Sulfate after the Disruption of the Structure by Urea. A Comparison with Bovine Serum Albumin, *Langmuir,* 15, 2003-2008 (DOI: 10.1021/la981442f).

50. Spector A. A. (1975), Fatty acid binding to plasma albumin, *J. Lipid Res.,* 16, 165-179.

51. Parks J. S., Cistola D. P., Small D. M., Hamilton J. A. (1983), Interactions of the Carboxyl Group of Oleic Acid with Bovine Serum Albumin: A 13C NMR Study, *The J. Biol Chem.,* 258, 9262-9269.

Appendix I

Chapter 2: Instrumentation and Materials

Introduction to FRET analysis:

Förster resonance energy transfer or fluorescence resonance energy transfer (FRET) is a technique in fluorescence spectroscopy that supplies accurate spatial measurements and detects molecular complexes over distances from 10 to 100 A° *[1]*. FRET depends on the distance dependent transfer of energy from donor fluorophore to an acceptor fluorophore. This method is well established for studying various biological systems like protein folding, antibody-antigen binding etc. *[2,3,4]*.

According to Förster resonance energy transfer (FRET), the rate of transfer for a donor and acceptor separated by a distance *r* is given by

$$k_T(r) = \frac{Q_D k^2}{\tau_D r^6}\left(\frac{9000(In10)}{128\pi^5 N n^4}\right)\int_0^\infty F_D(\lambda)\varepsilon_D(\lambda)\lambda^4 d\lambda \quad \text{.....(1)}$$

where Q_D is the quantum yield of the donor in the absence of acceptor, N is Avogadro's number, *n* is the refractive index of the medium between donor and acceptor, τ_D is the lifetime of the donor in the absence of acceptor; $F_D(\lambda)$ is the corrected fluorescence intensity of the donor in the wavelength range λ to $\lambda+\Delta\lambda$, with the total intensity normalized to unity; $\varepsilon_A(\lambda)$ is the extinction coefficient of the acceptor at λ, which is typically in units of M^{-1} cm^{-1}; k^2 is the well-known orientation factor of two dipoles interacting and is usually assumed to be equal to 2/3 which is appropriate for dynamic random averaging of the donor and acceptor.

The overlap integral $J(\lambda)$ express the degree of spectral overlap between the donor emission and the acceptor absorption,

$$J(\lambda)=\frac{\int_0^{\infty} F_D(\lambda)\varepsilon_A(\lambda)\lambda^4 d\lambda}{\int_0^{\infty} F_D(\lambda)d\lambda} \quad \text{.....(2)}$$

$F_D(\lambda)$ is dimensionless. If $\varepsilon_A(\lambda)$is expressed in units of M^{-1} cm^{-1} and λ is in nanometer, then $J(\lambda)$ is in units of M^{-1} cm^{-1} nm^{-4}. Eq. (1) can be expressed as

$$k_T(r)=\frac{1}{\tau_D}\left(\frac{R_0}{r}\right)^6 \quad \text{.....(3)}$$

Where R_0 is defined as

$$R_0^6=\frac{9000(In10)k^2Q_D}{128\pi^5 Nn^4}\int_{\circ}^{\infty} F_D(\lambda)\varepsilon_A(\lambda)\lambda^4 d\lambda$$

The above equation is reduced to

$$R_0=9.78\times10^3\left[k^2n^{-4}Q_D J(\lambda)\right]^{1/6} \quad \text{.....(4)}$$

R_0 (in Å) is known as Förster distance and it is the distance at which the transfer rate (k_T(r)) is equal to the decay rate of the donor in the absence of acceptor (τ_D^{-1}). That is the separation distance that yields 50% of energy transfer efficiency.

The efficiency of energy transfer (E) is the fraction of photons absorbed by the donor that are transferred to the acceptor. This fraction is given by

$$E=\frac{k_T}{\tau_D^{-1}+k_T} \quad \text{.....(5)}$$

which is the ratio of the transfer rate to the total decay rate of the donor. Recalling that $k_{ET}=\tau_D^{-1}(R_0/r)^6$, one can easily rearrange Eq. (5) to yield

$$E=\frac{R_0^6}{R_0^6+r^6} \quad \text{.....(6)}$$

References:

1. Lakowicz J. R., (1999), Principles of Fluorescence Spectroscopy, second ed. Plenum Press, New York, pp. 103-154 (ISBN:978-1-4757-3063-0).
2. Stryer L. (1978), Fluorescence Energy Transfer as a Spectroscopic Ruler, *Annu. Rev. Biochem.*, 47, 819-846 (DOI: 10.1146/annurev.bi.47.070178.004131).
3. Dale R. E., Eisinger J., Blumberg W. E. (1979), The orientational freedom of molecular probes. The orientation factor in intramolecular energy transfer, *Biophy. J.*, 26, 161-193.
4. Domanov Y. A., Gorbenko G. P. (2002), Analysis of resonance energy transfer in model membranes: role of orientational effects, *Biophys. Chem.*, 99, 143-154.

Appendix II

Chapter 3: Photophysical and Photodynamical Study of Fluoroquinolone and Ellipticine Drug Molecules in Bile Salt Aggregates

---

Different prototropic forms of the various drugs used:

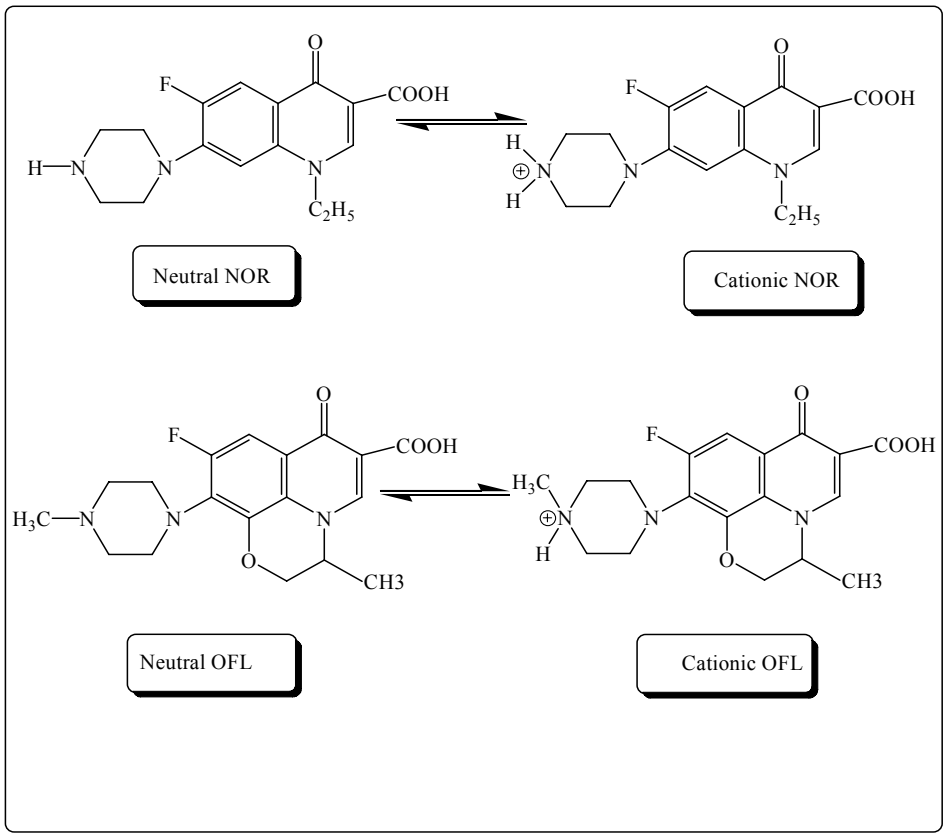

Figure 2A.1 Prototropic forms of Norfloxacin and ofloxacin

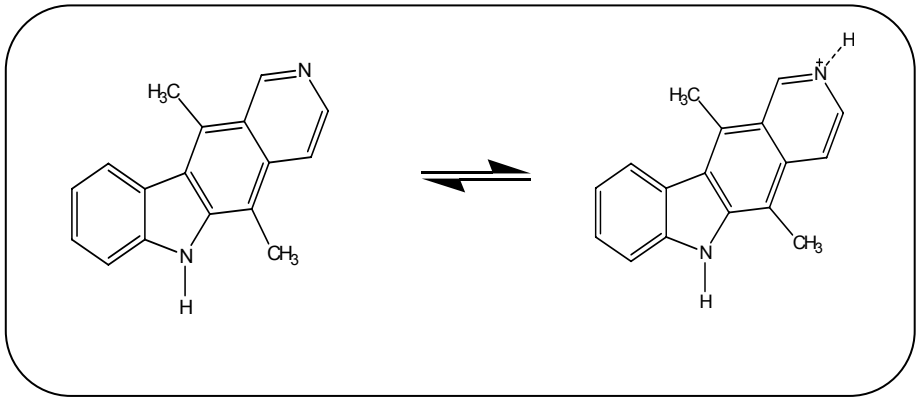

Figure 2A.2 Prototropic forms of Ellipticine .

Appendix III

Chapter 5: Photophysical and photodynamical study of Ellipticine: an anticancer drug molecule in bile salt modulated in vitro created liposome.

Anisotropy Measurements:

After the incorporation of ellipticine in liposome is confirmed, we underwent the study of time resolved anisotropy. Rotational relaxation of ellipticine in aqueous medium (at pH ~ 7.40) is single-exponential and average rotational relaxation time is around 0.150 ns. In liposome, the rotational relaxation of ellipticine is bi-exponential consisting of fast time constant (τ_{r1}) around 0.170 ns (74%) and slow time constant (τ_{r2}) 2.525 ns (26%) respectively. The average rotational relaxation time in lipid is around 0.785 ns. The significant increase in the rotational relaxation time in liposome indicates that ellipticine molecules are strongly bound to the liposome. In the bi-modal rotational relaxation, the fast component originates from the free ellipticine molecules and slow component is attributed to the ellipticine bound to liposome. The addition of bile salt to the liposome solution increases the rotational relaxation time. We measured anisotropy decays in liposome solution upon addition 0.5 and 1.5 mM bile salt concentrations. The fitted anisotropy decays of ellipticine in pure water, in liposome and bile salt-liposome complex are shown in Figure A3**.** The results are summarized in Table A3. It is revealed that addition of 0.5 mM and 1.5 mM NaDC to liposome solution cause an enhancement in the rotational relaxation time from 0.785 to 0.950 and 1.850 ns with an experimental error of ± 5%. A similar increase in the rotational relaxation time is observed when NaC is added to liposome. Interestingly, no significant change takes place in the rotational relaxation time upon addition of NaTC to liposome solution. The increase in rotational relaxation time with different bile salt concentration is in the order of the insertion ability of bile salts in

liposome. It is noteworthy that our results are different from the earlier report of Sarkar and co-workers *[1]*. Sarkar and co-workers *[1]* reported that incorporation of the bile salt inside the liposome reduces the rotational relaxation time of Coumarin 151 and Coumarin 153. In table A3 we observe that the amplitude (a_{r2}) of the slow component is found to increase from liposome to liposome-bile salt complex. In the liposome solution the slow component is around 2.5 ns with amplitude around 26%. Interestingly with addition of 1.5 mM NaDC, NaTC and NaC to liposome solution the slow components have become around 2 ns (90%), 2.25 ns (74 %), and 2.20 ns (35%) respectively. Though the average rotational relaxation time increases but the time constants of slow and fast component did not increase. The most plausible reason is that insertion of bile salt can induce permeation of water into the bi-layer membrane, which may be responsible for not increasing the rotational relaxation time even after bigger complex is formed. Increase in the slower component also implies that ellipticine molecules remain in the complex after being removed from the liposome hydrocarbon core. The order of increase in slow component is in accordance to the insertion ability of bile salts in the liposome. It is expected that due to more penetration, NaDC will form a bigger complex compared to NaC and NaTC. Hence the liposome-NaDC complex will entrap a larger number of ellipticine molecules and will have the slowest relaxation time which is in accordance with Table A3. According to Blume et al. addition of bile salt to vesicle, initially forms unstable mixed vesicles *[2]*. Sometimes these mixed vesicles form larger aggregates. In the present study submicellar concentration of bile salt is used, which will not completely solubilize the vesicle but may form mixed vesicle, which are larger aggregates than initial vesicle. This results in larger anisotropy.

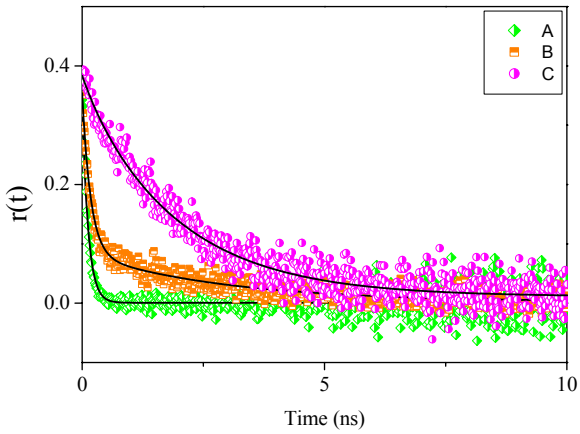

Figure A3. *Fluorescence anisotropy decays of ellipticine in different systems (A) In buffer solution (B) In DPPC liposome (C) In DPPC liposome with addition of 1.5 mMNaDC.*

Table A3: *Rotational relaxation parameters of ellipticine in different system*

System	r_0	a_1 (%)	a_2 (%)	τ_1 (ns)	τ_2 (ns)	$\langle\tau_r\rangle^{\#}$ (ns)
Ellipticine in buffer solution, pH~ 7.4	0.35	1		0.150		0.150
Ellipticine + DPPC liposome	0.35	0.74	0.26	0.170	2.525	0.785
Ellipticine in DPPC liposome + 0.50 mM NaDC	0.38	0.70	0.30	0.170	2.620	0.950
Ellipticine in DPPC liposome + 1.50 mM NaDC	0.38	0.10	0.90	0.200	2.00	1.850
Ellipticine in DPPC liposome + 0.50 mM NaC	0.37	0.55	0.45	0.173	2.313	1.126
Ellipticine in DPPC liposome + 1.50 mM NaC	0.39	0.29	0.71	0.157	2.230	1.600
Ellipticine in DPPC liposome + 0.50 mM NaTC	0.39	0.61	0.39	0.200	2.25	0.975
Ellipticine in DPPC liposome + 1.50 mM NaTC	0.39	0.65	0.35	0.200	2.20	0.900

$^{\#}$ The error in the measurement is about ± 5%

References:

1. Seth D., Chakraborty A., Setua P., Chakrabarty D., Sarkar N. (2005), Study of Energy Transfer from 7-Amino Coumarin Donors to the Rhodamine 6G Acceptor in Lecithin Vesicles and Sodium Taurocholate−Lecithin Mixed Aggregates, *J. Phys. Chem. B.,* 109, 12080-12085 (DOI: 10.1021/jp050812n).
2. Hildebrand A., Beyer K., Neubert R., Garidel P., Blume A. (2004), Solubilization of negatively charged DPPC/DPPG liposomes by bile salts, *J. Colloid and Interface. Sci.,* 279, 559-571 (DOI: S0021979704006162).